Susana Xavier Coentro

Mestre em Conservação e Restauro

An Iberian Heritage: Hispano-Moresque architectural tiles in Portuguese and Spanish collections

Dissertação para obtenção do Grau de Doutor em Conservação e Restauro do Património

Especialidade em Teoria, História e Técnicas

Orientador:	Rui C. da Silva, Investigador Principal, IST-UL; Professor Convidado, FCT-UNL
Co-orientadores:	Rui André Alves Trindade, Conservador do MNAA; Investigador Integrado do VICARTE, FCT-UNL
	Vânia Solange F. Muralha, Investigadora Pós-Doc, VICARTE, FCT-UNL

Júri:

Presidente:	Prof. Doutora Maria Adelaide de Almeida Pedro de Jesus
Arguentes:	Prof. Doutora Trinitat Pradell
	Prof. Doutor João Paulo Pereira de Freitas Coroado
Vogais:	Doutor Alexandre Manuel Nobre da Silva Pais
	Prof. Doutora Márcia Gomes Vilarigues

FACULDADE DE CIÊNCIAS E TECNOLOGIA
UNIVERSIDADE NOVA DE LISBOA

Março 2017

An Iberian Heritage: Hispano-Moresque architectural tiles in Portuguese and Spanish collections

ACKNOWLEDGEMENTS

I want to start by thanking my supervisors, Solange Muralha, Rui da Silva and Rui Trindade, for the constant support, teaching and advice, as well as their friendship throughout these years. A special and deeply felt acknowledgement to the late Solange Muralha, who first introduced me to this project and sadly could not be here today to see its completion.

To Márcia Vilarigues, Director of the Research Unit VICARTE, I would like to thank all the support as well, especially after Solange's departure.

To Luís C. Alves, a big Thank You! for the help with μ-PIXE, which was essential for this work. His positivity and availability to help and to teach were constant during the endless hours of analyses and interpretation of the results.

To Trinitat Pradell and Judit Molera, thank you for the opportunity to perform the SR-*μ*-XRD analyses and all the help with the results. Most of all, thank you for taking an interest in this project early on, for all the shared knowledge, and for providing the contact with the Instituto Valencia de Don Juan (Madrid), which opened the door for the study of Spanish collections as well.

I would also like to thank Bernard Gratuze for kindly performing the LA-ICP-MS analyses and for all the precious help in interpreting the results.

To the researchers at HERCULES Laboratory, in Évora, who contributed to this work – Dr António Candeias, Luís Dias, Margarida Nunes, and especially Cátia Relvas, Dr Teresa Ferreira and Dr José Mirão – thank you all for your help with the SEM-EDS and μ-XRD analyses.

I am very grateful for the collaboration and interest of several people and institutions, without whom this project would not have been possible:

- Parques de Sintra, Monte da Lua, namely the Director of the National Palace of Sintra, Dra. Inês Ferro, and the former and current Conservators of the palace, Dra. Rita Dargent and Dra. Joana Amaral, respectively;
- Mosteiro de Santa Clara-a-Velha (Coimbra), namely the former Directors, Dr Artur Côrte-Real and Dra. Lígia Gambini, and the Conservator Catarina Leal;
- Instituto Valencia de Don Juan (Madrid), in particular Dr Elisa Ramiro and Dr Cristina Partearroyo;
- Museo Nacional de Cerámica y Artes Suntuarias "González Martí" (Valencia), namely its Director, Dr Jaume Coll Conesa;
- Museo Municipal de Cerámica de Manises, in particular, its former and current Directors, Dr Josep Pérez Camps and Dra. Sara Blanes, respectively;
- Fundación Casa de Medinaceli (Casa de Pilatos, Seville), in particular, its Director, Sr. Dn. Juan Manuel Albendea;
- Dr. Tânia Casimiro, for kindly granting access to the tiles from Santo António da Charneca's kiln.

To Professor Alfonso Pleguezuelo, I thank the support and encouragement for this project, as well as for establishing contact with Fundación Casa de Medinaceli, making it possible to study the tiles from Casa de Pilatos.

To João Manuel Mimoso, my first mentor in this journey through the Portuguese tile heritage research (which started in 2009 at LNEC), thank you for the constant support and availability to share your impressive knowledge in this field. To Dr Sílvia Pereira and Dr Dória Costa, also from LNEC, I am also grateful for the support and collaboration throughout these years.

To Dr Michael Tite and Dr João Coroado, as members of my Thesis Advisory Committee, and, again, to Dr Trinitat Pradell, Dr João Coroado, Dr Alexandre Pais, and Dr Márcia Vilarigues, as members of the Thesis Jury, I wish to express my gratitude for the insightful and challenging comments that contributed to a better final version of this thesis.

To my colleagues and friends, Andreia Machado, Inês Coutinho, Joana Delgado, Alexandra Rodrigues, Hélia Marçal, Teresa Palomar, Fernanda Barroso, Francisca Pulido Valente, Amanda Pinto, and Vanessa Otero, a very special thank you! It has been a pleasure working with you! Also, to Mathilda Coutinho and Augusta Lima, thank you as well for all the insightful conversations and ideas on glazed tiles.

To Ana Maria Martins and Cremilde Cascalheira, thank you for your kindness and constant availability to guide us throughout the world of bureaucracy.

To all my friends and family – especially to my parents, to my husband Tiago, and to my baby Bernardo – a sincerely huge thank you for always believing in me and for always being there during the best and worst times of this journey.

A final acknowledgement to everyone who somehow contributed to this work and was not named here.

This PhD project was funded by Fundação para a Ciência e Tecnologia (SFRH/BD/73007/2010).

In loving memory of my supervisor,
Solange Muralha (1978-2015)

ABSTRACT

This is the first archaeometric study comparing Hispano-Moresque tiles from different Portuguese and Spanish collections, no other published one being known at the time of writing. Despite the increasing interest in the Iberian ceramic cultural heritage, a specific study dedicated to architectural tiles was lacking. With this in mind, this thesis offers a first approach on the technological features of these impressive – although somehow undervalued – architectural tiles.

With this work, important Portuguese and Spanish Hispano-Moresque tile collections are characterised, compared and studied: National Palace of Sintra (Portugal) (PNS), Monastery of Santa Clara-a-Velha (Coimbra, Portugal) (SCV), archaeological site of Santo António da Charneca (Barreiro, Portugal) (SAC), Instituto Valencia de Don Juan (Madrid, Spain) (IVDJ), Casa de Pilatos (Seville, Spain) (CPS) and Museo de Cerámica y Artes Sumtuarias "González Marti" (Valencia, Spain) (MCV). The aim is to provide a physicochemical characterisation of both the glazes and the ceramic bodies of the tiles to better understand the production technology.

The methodology proposed for this study had the main purpose of developing a minimally invasive and essentially non-destructive approach with complementary analytical techniques that will allow for replication in future studies with other Hispano-Moresque tile collections. The techniques chosen were: Micro-Particle Induced X-Ray Emission (μ-PIXE), Laser Ablation Inductively Coupled Plasma Mass Spectrometry (LA-ICP-MS), Scanning Electron Microscopy with X-ray Microanalysis (SEM-EDS), μ-Raman spectroscopy, Micro-X-ray diffraction (μ-XRD) and Synchrotron Radiation Micro-X-ray diffraction (SR-μ-XRD).

The archaeometric study concluded that calcareous clays were the standard material used for the ceramic bodies of the tiles. Lime content is frequently higher than 20 wt.%, which is a high value among the typical calcareous clays analysed in the literature, although within the expected results for tin-opacified ceramic bodies.

The glaze technology employed in Hispano-Moresque tiles followed the Islamic tradition that was introduced in the Iberian Peninsula from the 8th century onwards. High-lead glazes (ca. 30-50 wt.% PbO) were identified in all analysed samples. Two types of high-lead glazes were identified: "transparent" and tin-opacified. Besides the disparity in tin contents, the two glaze types also evidence differences in sodium and lead values. A sodium compound (most likely NaCl) may have been added to compensate the lower PbO content in tin-opacified glazes. The pictorial layer is composed of five colours: white (SnO_2), blue (SnO_2 + CoO), green (CuO), amber (Fe_2O_3) and brown (MnO). These colours exhibit different shades depending on the glaze recipe, its thickness and the influence of the underlying ceramic body. White and blue are consistently tin-opacified, whereas most green, amber and brown glazes are transparent.

The results of the archaeometric study identify a widespread ceramic technology. Nevertheless, it is still visible a higher proximity between the CPS, IVDJ-Seville, SCV and PNS collections – although with differences among them – whereas the MCV and IVDJ-Toledo groups display distinct features that attest for their different provenance.

Keywords: Glazed tiles; Azulejo; Hispano-Moresque; Lead-tin glazes; Archaeometry; Ceramic tiles

PUBLICATIONS

Coentro, S., Alves, L.C., Mirão, J., Trindade, R., da Silva, R.C., Muralha, V. (2017). Hispano-Moresque tiles in Portugal: The collections of Palácio Nacional de Sintra and Mosteiro de Santa Clara-a-Velha in Coimbra, *Medieval Ceramics* [accepted]

Coentro, S., Alves, L.C., Relvas, C., Ferreira, T., Mirão, J., Molera, J., Pradell, T., Trindade, R., da Silva, R.C., Muralha, V. (2017). Glaze Technology of Hispano-Moresque Ceramic Tiles: A Comparison Between Portuguese and Spanish Collections, *Archaeometry* [online]. DOI: 10.1111/arcm.12280

Coentro, S., Trindade, R., Mirão, J., Candeias, A., Alves, L.C., Silva, R.C. da, Muralha, V. (2014), Hispano-Moresque ceramic tiles from the Monastery of Santa Clara-a-Velha (Coimbra, Portugal), *Journal of Archaeological Science*, 41, 21-28. DOI: http://dx.doi.org/10.1016/j.jas.2013.07.031

RESUMO

Este trabalho apresenta o primeiro estudo arqueométrico comparativo entre colecções portuguesas e espanholas de azulejaria Hispano-Mourisca, considerando as publicações conhecidas à data de escrita. Apesar do interesse crescente no património cultural ibérico, faltava um estudo especificamente dedicado à azulejaria. Assim, esta dissertação oferece uma primeira abordagem ao estudo da tecnologia destes impressionantes – ainda que algo subvalorizados – azulejos.

Importantes colecções portuguesas e espanholas são caracterizadas e comparadas: Palácio Nacional de Sintra (Portugal) (PNS), Mosteiro de Santa Clara-a-Velha (Coimbra, Portugal) (SCV), colecção arqueológica de Santo António da Charneca (Barreiro, Portugal) (SAC); Instituto Valencia de Don Juan (Madrid, Espanha) (IVDJ), Casa de Pilatos (Sevilha, Espanha) (CPS) e Museo de Cerámica y Artes Sumtuarias "González Marti" (Valência, Espanha) (MCV).

A metodologia proposta teve como principal objectivo o desenvolvimento de uma abordagem minimamente invasiva e essencialmente não destrutiva que permita a continuação e replicação da mesma em estudos futuros de outras colecções. As técnicas analíticas utilizadas foram: Micro-Particle Induced X-Ray Emission (μ-PIXE), Laser Ablation Inductively Coupled Plasma Mass Spectrometry (LA-ICP-MS), Scanning Electron Microscopy with X-ray Microanalysis (SEM-EDS), μ-Raman spectroscopy, Micro-X-ray diffraction (μ-XRD) and Synchrotron Radiation Micro-X-ray diffraction (SR-μ-XRD).

O estudo arqueométrico concluiu que as chacotas dos azulejos eram produzidas na sua grande maioria com pastas cálcicas. Estas apresentam frequentemente um teor de CaO acima de 20 % (m/m), considerado elevado quando comparado com os teores referidos na literatura, ainda que dentro dos expectáveis para cerâmicas decoradas com vidrados estaníferos.

A tecnologia do vidrado empregue nos azulejos hispano-mourisco, em análise neste trabalho, seguiu a tradição da cerâmica islâmica introduzida na Península após a ocupação no século VIII. Todas as amostras analisadas contêm vidrados de chumbo (ca. 30-50 wt.% PbO). Estes podem dividir-se em dois tipos: "transparentes" e opacos. Além da marcada diferença no teor de estanho, os dois tipos de vidrado também apresentam diferenças nos teores de sódio e chumbo, sendo que um composto rico em sódio poderá ter sido intencionalmente adicionado aos vidrados opacos para compensar os teores inferiores de chumbo nos mesmos. Cinco cores foram identificadas – branco (SnO_2), azul (SnO_2 + CoO), verde (CuO), âmbar (Fe_2O_3) e castanho (MnO) – exibindo diferentes tonalidades dependendo da receita do vidrado, da sua espessura e da influência da chacota. Os vidrados brancos e azuis são sempre opacos, enquanto que a maioria dos verdes, âmbar e castanhos é transparente.

Os resultados identificaram uma tecnologia cerâmica disseminada pelos vários centros produtores. No entanto, é ainda possível identificar uma maior proximidade entre os resultados das colecções CPS, IVDJ-Sevilha, SCV e PNS – ainda que com diferenças entre si – enquanto que os conjuntos MCV e IVDJ-Toledo evidenciam características que reforçam uma proveniência distinta.

Palavras-chave: Azulejo; Hispano-Mourisco; Vidrados de chumbo e estanho; Arqueometria; Cerâmica

CONTENTS

LIST OF FIGURES

CHAPTER 1

CHAPTER 2

CHAPTER 4

CHAPTER 5

LIST OF TABLES

CHAPTER 4

CHAPTER 5

SYMBOLS AND NOTATIONS

μ-PIXE – micro-Particle Induced X-ray Emission

μ-XRD – micro X-Ray Diffraction

CPS – Casa de Pilatos, Seville, Spain

IVDJ-S – Instituto Valencia de Don Juan, Madrid, Spain – tiles attributed to Seville

IVDJ-T – Instituto Valencia de Don Juan, Madrid, Spain – tiles attributed to Toledo

LA-ICP-MS – Laser Ablation Inductively Coupled Plasma Mass Spectrometry

MCV – *Museo* Nacional de *Cerámica* y de las Artes Suntuarias González Martí, Valencia, Spain

n.d. – not detected

PNS – National Palace of Sintra, Portugal

SAC – Santo António da Charneca, Barreiro, Portugal

SCV – Monastery of Santa Clara-a-Velha, Coimbra, Portugal

SR-μ-XRD – Synchrotron micro X-Ray Diffraction

REE – Rare Earth Elements

INTRODUCTION

Of all manifestations of Portuguese ceramics, the most beautiful, most characteristic and most varied is, without a doubt, the ceramic tile.

The ceramic tile is an expression of the Portuguese soul.

Conde de Sabugosa in *O Paço de Cintra,* 1903 (p. 206)

The ceramic tile has become an intrinsic part of Portuguese architectural heritage. For more than five centuries, this decorative art has been used uninterruptedly and has known to adapt throughout artistic movements, cultural influences and historical events. Ceramic tile panels are present in centuries-old churches and palaces, as well as in contemporary buildings and subway stations. They decorate walls, ceilings, gardens, murals, altar frontals and every visible architectural detail one can imagine. While this thesis is being written, several work groups are preparing a candidacy for the Portuguese tile to join the UNESCO World Heritage list.

The earliest use of decorative glazed ceramic tiles in Portugal is believed to date back to the 13th century. They are the medieval pavements of the Abbey of Santa Maria de Alcobaça, the Castle of Leiria or the Lisbon's Cathedral (Sé de Lisboa) (Trindade, 2007). These are monochromatic flat tiles in various geometric shapes representing a Christian pavement tradition which was widespread in Northern Europe at the time. It is possible that the use of these tiles was widespread in medieval constructions in Portugal as well, although only a few examples are still visible today. During the 13th century, these medieval tiles already incorporated a combination of the Christian and Islamic ceramic traditions, as attested by the opaque tin-glazed tiles in Alcobaça (Carvalho et al., 2016; Trindade, 2007).

The Islamic influence was decisive on the incorporation of the ceramic tile in the Portuguese culture, with its colourful palette and the integral coating of the walls. The Islamic presence in the Iberian Peninsula is

connected with the development of important ceramic production centres that continued their production throughout the Christian Reconquest. The ceramic technology, including the glazes, was transferred from the Muslims to the Christians and, for decades, both worked side by side (Martinez, 1991; Trindade, 2007). The most important innovations brought by the Islamic potters were the tin-opacified glazes – which provided a white brilliant coating to the ceramic objects – the cobalt blue pigment – which became inseparable from the architectural tile until our days – and the lustre decorations that resulted in layers with a metallic shine with shades from gold to copper, depending on their composition. During the 14th and 15th centuries, cobalt and lustre-decorated ceramics were traded as highly regarded luxury goods and they were exported from the Iberian Peninsula to all of Europe (Martinez, 1991).

The term "Hispano-Moresque" comes from the particular political and cultural context of the Iberian Peninsula during the Christian Reconquest. Hispano-Moresque ceramics are the result of the work of Moresque (Moorish) and Christian potters, with both Moorish and Christian stylistic features, in (today's) Spanish and Portuguese territories. The Hispano-Moresque tile is, therefore, included in the group of pre-majolica tile techniques, such as the *alicatado*, the *cuerda seca* and the *arista*, which will be further explained in Chapter 1 (Martínez, 1991). In Portuguese literature, the term *archaic* has also been used for pre-majolica tiles (Meco, 1985; Santos Simões, 1945, 1990) which include the above-mentioned 13th-century pavements. Recently, these tiles have also been named as *medieval*, with focus on their production chronology and discarding the somehow undermining term "archaic", as well as the geographically-limited term "Hispano" (Trindade, 2007). In this study, however, the choice for using the nomenclature "Hispano-Moresque" instead of "Medieval" aims at reaching the most consensual denomination in international literature and at the same time to avoid confusion with earlier medieval tiles.

Despite the written sources on Portuguese production of "Malaga and Valença ware" (*louça de Malaga e Valença* – ancient Portuguese terms for tin-glazed ceramics), which attest knowledge of the technology used for making Hispano-Moresque tiles, there has been an established idea of the non-existence of the production of decorative glazed tiles in Portugal until the mid-16th century, when the production of the first majolica tiles was documented in Portuguese territory (Trindade, 2007). Until then, Hispano-Moresque tiles are essentially considered as imports from Seville (Meco, 1985; Santos Simões, 1945, 1990, Macedo, 2006 and others). This is explained by the existing documentation referring the trade of tiles between Seville and Portugal, along with the inexistent written documentation on Portuguese tile production (Gestoso, 1903). Recently, the work of Rui Trindade (2007) brought together several documents that attest how there was not an absence of the mention of tiles ("azulejos") during the 15th century but, instead, that the Portuguese word used for tile was different: "ladrilho". Furthermore, *arista* tiles were found in an early 16th-century kiln in Barreiro, an area once known as an important ceramic production centre in Portugal (Barros et al., 2003; Meco, 2003; Trindade, 2007).

The established idea of a non-existing Portuguese tile production until the second half of the 16th century makes this subject somewhat controversial but interesting and important to study. Santos Simões, an important author on Portuguese tile heritage, wrote that: "The main historical document for the study of Portuguese tile heritage is the tile itself" (Santos Simões, 1990). Hispano-Moresque tiles have been

studied from an art historical point of view, but – to our knowledge – there were no known studies on the materials and production techniques when this work began. This applies both to Portugal and Spain.

With this work, important Portuguese and Spanish Hispano-Moresque tile collections dated between the late 15th century and the first half of the 16th century are studied and compared: National Palace of Sintra (Portugal), Monastery of Santa Clara-a-Velha (Coimbra, Portugal), archaeological site of Santo António da Charneca (Barreiro, Portugal), Instituto Valencia de Don Juan (Madrid, Spain), Casa de Pilatos (Seville, Spain) and Museo de Cerámica y Artes Suntuarias "González Martí" (Valencia, Spain). The aim is to chemically characterise both glazes and the ceramic body of the tiles to better understand the production technology. Several questions are meant to be addressed:

- What is the chemical composition of different coloured glazes?
- Are there differences in the chemical composition of the glazes that characterise specific groups of tiles with different chronologies or provenances, whether known or assigned?
- Is the technology used in Hispano-Moresque tiles identical to other coeval Iberian ceramics?
- What types of clays were used for the ceramic body of the tiles?
- Are there technological differences that relate to the evolution of the decorative techniques (*alicatado*, *cuerda* seca, *arista*)?

The methodology proposed for this study had the main purpose of developing a non-destructive, minimally invasive approach with complementary analytical techniques that will allow for replication in future studies with other Hispano-Moresque tile collections. Archaeometric studies have developed in the last decades side by side with the development of analytical techniques that allow the characterisation of cultural artefacts with minimal or no sampling requirements. This is fundamental when analysing large numbers of samples and using simultaneously different analytical techniques. Hence, it is possible to gain important knowledge on the material nature of our cultural heritage with a minimally invasive approach.

This work is structured in five chapters:

Chapter 1 offers a summarised historical and artistic contextualisation on the subject. The evolution of the decoration techniques and iconography is explained so that the reader understands the complexity and variety of techniques and motifs that make up the Hispano-Moresque tile heritage. The controversy regarding the provenance topic is also explained. Finally, a brief state-of-the-art on the most relevant scientific literature on coeval ceramics is presented.

Chapter 2 contextualises the collection studied in this work. The historical context of these collections is sometimes different than the original context of the tiles. There are museum collections and archaeological ones.

Chapter 3 explains the methodology used in this study, including the sampling process, the chosen criteria, and the analytical techniques.

Chapter 4 and Chapter 5 include the results and discussion. Chapter 4 focuses on the ceramic body of the tiles, whereas Chapter 5 is dedicated to the glaze technology. The different nature of these two components of the tile was the basis for separating the results into two Chapters.

In Chapter 5, the results are presented according to typology: *cuerda seca* and *arista*, flat, underglaze decorated tiles, and reliefs. This structure allows the discussion of the results according to the glaze technology and comparison among tiles with the same technology from different collections. A final sub-chapter deals with the results obtained from the LA-ICP-MS analysis since, in this case, it is important to compare all the tiles at the same time to tackle the provenance issue.

Finally, the main conclusions are presented along with questions that remain and suggestions on how to answer them in the future.

This work is the first large archaeometric study on Hispano-Moresque tiles. However, many other important collections remain unstudied that could provide precious knowledge on the production and trade of these important architectural ceramics. This study intends to be the first step in understanding the production technology of these amazing tiles that have been, somehow, neglected until recently.

CHAPTER 1

MEDIEVAL CERAMIC TILES: HISTORICAL AND ARTISTIC CONTEXT

1.1. GLAZED CERAMIC TILES: A MEDITERRANEAN TRADITION

The ceramic tile became an important architectural decorative element in the Iberian Peninsula with the Islamic presence from the 8th century onwards. Glazed tiles were widely used in the Middle East thousands of years before and their impact on architecture was already impressive. Eight centuries of Islamic presence left an incredible influence in the Spanish and Portuguese cultures, in particular, the Mediterranean coast.

The Muslims introduced in the Iberian Peninsula the technologies that made it the main ceramic production centre in Europe for centuries: the lead-tin glazes (opaque white glazes which centuries later evolved to the majolica technique), the use of cobalt oxide (to achieve the blue colour) and the lustre-decorated ceramics (with metallic shine) (Malo, 2001; Martínez, 1991). Blue and white ceramics are known since the early Abbasid period. They became almost timeless since their influence extended from Orient to the West and from the 8th century until nowadays. The blue and white Ming porcelain was influenced by this "Muslim blue" as the Chinese called it (Martínez, 1991), and so was the Delft ceramics and the so-called "golden" period of Portuguese tiles – the 18th century Masters' Cycle, also known as "the blue-and-white period".

Medieval Iberia is linked with the Christian Reconquest and a mixture of cultures that coexisted for centuries. One of the first examples of Portuguese use of ceramic tiles in architecture is the pavement of the Cistercian Abbey of Alcobaça. The glaze technology was adopted from Islamic knowledge – lead-tin glazes were already used and it is known that Muslim tillers from Spanish kingdoms were hired to produce this type of pavements in Cistercian churches in France, at least since the last decade of the 13th century.

Despite the opposing cultures, Christian and Muslim artists and craftsmen worked side by side after the Christian conquest at least until the 16th century (Carvalho *et al*., 2016; Norton, 1984; Trindade, 2007).

Granada, the last Muslim kingdom in the Iberian Peninsula, fell in 1492 into the hands of the Catholic Monarchs, Isabel I of Castile and Fernando II of Aragon. The King and Queen had established the Tribunal of the Holy Office of the Inquisition in 1478, which led to the expulsion of thousands of Jews and Muslims from Spanish lands or their mandatory conversion to Christianity. Many fled to Portugal and other European countries to escape the severity of the Inquisition and their procedures. In addition, the confiscation of properties of those accused of heresy helped to finance the war and finally making the Iberian Peninsula a totally Christian territory by the end of the 15th century (Bernal, 2011). However, the admiration the Christian monarchs felt for Islamic architecture and decorative arts is well imprinted in their palaces, such as *Real Alcazar* in Seville and the *Palacio Real* in Tordesillas (Martínez, 1991).

The visit of Portuguese king D. Manuel I to Granada and Seville also influenced what is now called the *Manuelino* style. Hispano-Moresque tiles were profusely used in Portuguese architecture during the reign of Manuel I (1495-1521). There are many important surviving examples of this fashion in Portugal, with Lisbon, Coimbra, Évora and Beja as main centres. The existence of numerous medieval tiles in churches throughout the country and continuously appearing in archaeological excavations are, nevertheless, the strongest suggestion that this was a widespread decorative art in Portuguese architecture during the first half of the 16th century (Trindade, 2007).

The Hispano-Moresque tile represents a period of great transformations from the 14th century to the first half of the 16th century. Throughout the period of the Reconquest, the Islamic technology is progressively adopted and developed by Christian potters. Christian influences from Northern Europe become more visible in the decoration techniques and iconography. Throughout a series of historical events and cultural changes, the Hispano-Moresque tile suffered several technological evolutions and became a large-scale production up until the mid-16th century, when the new majolica technique and its new pictorial potential surpassed the demand for *arista* tiles.

1.2. Evolution of decorative techniques

The evolution of the Hispano-Moresque tile may be summarised from the Islamic *alicatado* mosaic to the *cuerda seca* tile and finally to the *arista* technique, which is explained below. This evolution made the tiles easier to produce and to install, drastically reducing the need for specialised craftsmanship and, thus, the production costs. Nevertheless, the three techniques coexisted in time and with other techniques as well, such as the relief tiles and Valencian *rajolas*.

1.2.1. *ALICATADO*

The alicatado is composed by small ceramic pieces of different coloured glazes, forming together complex geometric patterns. Its production starts with large ceramic glazed plates that are cut into geometric shapes and put together on the wall or floor – only then the final result can be seen. Therefore, the artisans that applied the ceramic pieces on the wall were as skilled and important as the ceramists who produced those plates. The final result was a flat, colourful and brilliant surface, both durable and with high decorative value, which complied with the non-figurative norms of the Muslim art (Pleguezuelo, 2011; Trindade, 2007) (*Figure 1.1*).

The height of the *alicatado* technique in the Iberian Peninsula occurred in the 14th and 15th centuries, mainly in Granada and later in Seville. Examples of surviving *alicatado* panels can still be seen in the *Alhambra* (Granada) and in the *Real Alcázares* (Seville). In Portugal, the pavement of Palatina Chapel in Sintra's National Palace is the oldest surviving example (Santos Simões, 1945).

Figure 1.1. Alicatado pavement in the Palatina Chapel, National Palace of Sintra, Portugal. (Photograph taken by the author in 2011)

In the 15th century, the use of *alicatados* declined, being replaced by *cuerda seca* tiles. In Seville, the last examples of that technique showed larger pieces and simpler geometric compositions, eventually causing a loss of technical knowledge and influences from gothic mural painting (Pleguezuelo, 2011). Chromatic changes also took place between the 14th and the 16th centuries. In the 14th century, black, green, turquoise and white prevail, but later other colours are progressively included, such as amber and

shades of brown, warming up the palette. During the transition to the 16th century, the colours were the same as the ones used in *cuerda seca* and *arista* tiles – white, black or dark brown, amber, blue and green (Pleguezuelo 2011).

In the Middles Ages, *alicatado* tiles were produced in Andalusia, Aragon, Valencia, Cataluña and Toledo, but no workshops were found with this type of production in Castile, León or the Portuguese territory so far. Malo Cerro (2001) suggests that tiles found in Castile and León were probably imported from the production centres mentioned above. The pavement in the National Palace of Sintra, however, has been considered a possible local production manufactured by Islamic ceramists that were brought by the king D. Afonso V from Northern Africa to Sintra in the late 15th century (Trindade, 2007).

1.2.2. *CUERDA SECA*

The *cuerda seca* technique was used at least since the Caliphal period. It was certainly used to decorate the most elaborate ceramic objects during Almohad period (12th-13th century) and later until the 15th century, already under Christian rule. However, the transition between the Islamic and the Hispano-Moresque productions are not well known. The *cuerda seca* technique is used in architectural ceramics at least since the 14th century in Nazarí art, as observed in *Puerta del Vino* in Alhambra Palace (Martínez, 1991; Pleguezuelo, 2011).

The expression *cuerda seca* was published for the first time by Gestoso y Pérez (1903), citing a Sevillian document from 1558 where *azulejos de cuerda seca* are mentioned. Despite the questionable attribution of the terminology to this specific technique which, among other arguments, was probably already out of use in 1558, the term has been adopted by following scholars and it is now generally accepted to designate this technique.

The *cuerda seca* technique made it possible to use different coloured glazes on the same tile or ceramic object. It is possible because an oily substance (linseed oil is the most referred to in the literature), mixed with manganese oxide, is applied on the surface of the tile, marking the contours. The grease keeps the different glazes separated, and the manganese results in a dark line after firing (*Figure 1.2*). It is possible that the contours were first marked on the surface of the object or tile through a stencil process, and then the greasy mixture was applied with a pencil (González 1944; Martínez, 1991, Trindade, 2007).

The composition of the contours has been under debate among scholars. It has not been possible to identify the exact oily compound because it burns during the firing of the ceramic object and the existence of the oily substance has even been challenged (o'Kane, 2011). As for the manganese contour, it has been suggested that it was applied as an impure manganese oxide without fluxes or as manganese sulphur, or even as a mixture of manganese oxide and a lead silicate (Sosa, 2007). The double firing of *cuerda seca* Islamic ceramics was demonstrated in the archaeological excavation of San Pablo workshop (11th century), in Zaragoza, where fired ceramic objects were found with the black outline but without the glaze decoration (Chapoulie *et al.,* 2005).

Pleguezuelo (2011) differentiates two types of *cuerda seca* in ceramic tiles: flat (*cuerda seca plana*) and mixed (*cuerda seca mixta*). Other names are found in Spanish and Portuguese literature, such as *cuerda seca hendida* ("sprung") or *de refuerzo* ("reinforced"), the latter for the transition to the *arista* technique, explained ahead (Sosa, 2007).

Simple or flat *cuerda seca* used the manganese oxide-bearing contour directly applied on the ceramic surface. The coloured glazed areas are separated by this dark contour and appear as low reliefs once the tile is fired.

Mixed *cuerda seca* is believed to have appeared in Seville at the end of the 15th century (Pleguezuelo, 2011). It replaced the *alicatados* and their need of highly specialized workmanship in the final work stage – placing the tiles on the walls. Consequently, *cuerda seca* tiles were less expensive and easier to export. Mixed *cuerda seca* contains the same dark contours, but applied on previously marked grooves on the surface of the tiles. The grooves were made by pressing a mould with protuberant contours of the motif onto the fresh clay. The use of moulds simplified the production process and made it possible to easily achieve more complex patterns and different decorative motifs.

A "hybrid technique" is also mentioned by Martínez Caviró (1991), the same as the "reinforced" *cuerda seca*, where the grooves are defined by two protuberant "walls" – a transition to the *arista* technique.

Figure 1.2. Examples of *cuerda seca* tiles from the Monastery of Santa Clara-a-Velha (Coimbra): **(a)** tiles *in situ* in the cloister; **(b)** a detail of a tile where the dark contour is still visible. (Photographs taken by the author in 2011)

The oldest known *cuerda seca* tiles are the ones called "Niebla tiles" or "tiles from Niebla's castle". This designation comes from the idea among collectors that these tiles were originally from a town called Niebla, which was a capital in a Taifa kingdom for three periods between the 11th and the 13th centuries. Pleguezuelo (2011) suggests they were produced between the 12th-13th centuries, making them the "first and only Islamic tiles in western Andalusia". Niebla tiles are decorated with very thick black/dark brown, amber, white and turquoise green glazes, corresponding to the usual Taifa and Almohade palette. The ceramic body has a more reddish tone than most Sevillian tiles, and it is very thick with originally canted

sides. They are also smaller than the most common Hispano-Moresque tiles, measuring usually ca. 110 mm *versus* the more standard 135 mm of the usual *cuerda seca* tile. Only Hispano-Muslim *lacería* motifs are known in Niebla tiles (Pleguezuelo 2011).

One of the oldest examples of *cuerda seca* tiles in Portuguese territory exists in the pavement of the prison-room of king D. Afonso V, in the National Palace of Sintra (*Figure 1.3*). This pavement combines *cuerda seca*, *alicatado* and Cistercian mosaic tiles (Trindade, 2007).

Figure 1.3. Detail of the pavement in the prison-room of king D. Afonso V in the National Palace of Sintra, showing some of the oldest *cuerda seca* tiles in Portugal. © Parques de Sintra

In the 15th century, the production of *cuerda seca* tiles in Seville suffered a major development and increase. The chromatic palette was the same as the one from the then new *arista* tiles: white, blue, amber, green and brown/black (Pleguezuelo 2011). However, judging by the few tiles visible today, the production was probably not that abundant, certainly not as great as the *arista* tile production that later developed (Martínez, 1991).

Lacería stars and so called "rooster's paw" are among the most common motifs in *cuerda seca* tiles. Figurative subjects are also present, such as animals and people. Another important part of tile production in the 15th century were coats of arms. According to Pleguezuelo (2011), the most important *cuerda seca* tile sets *in situ* are in the chapel of the *Casa de Pilatos* and the small cloister in *Cartuja de las Cuevas,* both in Seville, the cloister in Santa Clara's Convent (Carmona, Spain), the Church of *Santa Maria* in Abrantes Castle (Portugal) and in the National Palace of Sintra (Portugal).

1.2.3. *ARISTA* OR *CUENCA*

Between the end of the 15th century and the beginning of the 16th century, a new method gradually replaced the *cuerda seca* technique: it was called *arista* or *cuenca* (from the Spanish *concavidad* – concavity) (Martínez, 1991; Pleguezuelo, 2011; Trindade, 2007). In this method, a wood or plaster mould was used, where the contours of the motif were carved in, and the clay was pressed onto it. The drawing in the tile appeared as ridged edges that would separate the different coloured glazes and, at the same time, eliminate the need for manually drawing the contours with a brush (as in *cuerda seca*) (*Figure 1.4*). This technical innovation allowed for a semi-industrial large scale production – it was faster and cheaper to produce – and so it largely surpassed *cuerda seca* and *alicatado* productions (Martínez, 1991; Pleguezuelo, 2011; Trindade, 2007).

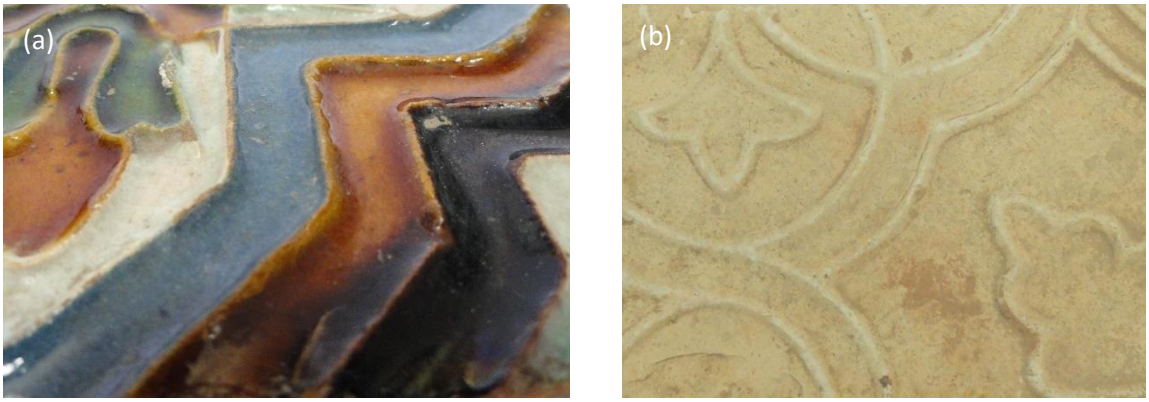

Figure 1.4. Arista tiles from the Monastery of Santa Clara-a-Velha, Coimbra: (a) detail of the *arista* separating different coloured glazes; (b) unglazed *arista* tile.

The most ancient use of a technique similar to *arista* is already observed in the 5th century BC in the Frieze of the Archers (Susa, Persia; today in Louvre Museum, France). The fabric in the archers' clothes shows a pattern with flowers whose glazes of different colours are separated in the same way as in 16th-century *arista* tiles (*Figure 1.5*). Nonetheless, the closest influence for the Hispano-Moresque *arista* tiles were the 14th-century line-impressed tiles profusely used in monasteries (namely in pavements) in France and the United Kingdom, as pointed out by Trindade (2007) (*Figure 1.6*). The great innovation was the use of the impressed protuberant lines to separate different coloured glazes, whereas the tiles from Northern Europe were monochromatic.

Furthermore, several Gothic patterns were also adopted and reproduced in polychrome patterns, along with Renaissance *arista* tiles. *Figure 1.6* illustrates a pattern found both in pavement monochromatic tiles from Northern Europe and in Hispano-Moresque tiles. This represents a proximity with Christian techniques and iconography, as well as a progressive disengagement from the Muslim ones. Hence, the *arista* technique emerges as the final stage of Hispano-Moresque tile production, still using Islamic geometric patterns, but also Gothic and Renaissance motifs, becoming a representation of the social and political transformations of the early 16th century, when Christian potters already surpassed Muslim and Moresque ones (Trindade, 2007).

Figure 1.5. Detail of the Frieze of the Archers, Louvre Museum, France (AA VV., 2013)

Figure 1.6. Line-impressed tile with oak leaf motif, 14th century, Acton Burnell parish church, Shropshire, UK (Eames, 1992).

Either way, the *arista* technique suffered a rapid expansion. It was so easy to produce that other workshops could have easily copied both the technique and patterns. The *arista* technique completely changed the commercial panorama of 16th-century tiles: it became almost a pre-industrial standardized process, where no special craftsmanship was needed (Pleguezuelo, 2011). Tiles were moulded and then coloured – the worker only had to fill the concave spaces with the coloured glazes and then the tile was fired. It was easy, fast and consequently cheaper than it had ever been before. It also made it an easy technique to copy and probably the rise in production was due to more workshops producing these tiles, not only to the fact that it was faster to produce. This could also explain why it took decades to be replaced by the majolica technique, which was hand painted and thus much more expensive (Martínez Caviró, 1991).

Sancho Corbacho (1948) was the first author to try a systematic approach to a stylistic evolution in *arista* tiles. He divided the patterns in Mudéjar, Isabelino and Renaissance themes. The three styles co-existed ever since the first years of the 16th century. There are no known dated panels prior to the year 1500 and the first *arista* panels show the three styles together. Martínez (1991) prefers the terms Moorish (as in late Mudéjar with Islamic inspiration), late Gothic and Renaissance. The author explains that the name "Isabelino" has been replaced by "Hispano-Flemish", as it generated some confusion between the Queen Isabel the Catholic, Queen Elisabeth I of England and Queen Elizabeth II (Martínez, 1991).

In 1509, it was ordered in Seville for the rich embroideries in churches' altars to be copied in tiles, which multiplied the fabric-inspired patterns in *arista* tiles for the first half of the 16th century. However, such patterns were already produced before in *cuerda seca* technique, as Damask and brocade *cuerda seca* patterns attest (Pleguezuelo, 2011).

A document from 1518 stipulates an order of 6000 tiles *de labores* to be produced by Niculoso Pisano for the *Convento de San Pablo* in Seville. If Niculoso could not fulfil this order, he would have to order the missing tiles to another tiler. Gestoso (1903) considers this document as a strong indication of this referring to *arista* tiles, since there is no other evidence of another tiler in Seville that could make majolica tiles – hence, this order must have been for *arista* (Gestoso 1903; Pleguezuelo 1992). Among the

archaeological findings in *calle Pureza*, there are similar *arista* motifs to the ones that Pisano surely painted in majolica technique (Pleguezuelo 1992), which partially supports Gestoso's thesis. Also, several Pisano's works contain both majolica and *arista* tiles. On the other hand, Pleguezuelo (1992) suggests that the expression *de labores* should be interpreted as "decorated tiles", regardless of the decoration technique.

1.2.4. Reliefs

Monochromatic glazed relief tiles were used in pavements in England since the 12th century (Eames, 1992). Relief tiles were produced with moulds in Seville and Valencia since the end of 13th century, before the implementation of mixed *cuerda seca* and *arista* techniques. Mostly heraldic tiles were produced in relief. It was not such a popular technique in Hispano-Moresque ceramics because of their connection to masonry, and it was mostly used for decorating baptismal fonts, as well as exterior walls and large ceramic jars (Martínez, 1991; Trindade, 2007).

The collection of relief tiles in Sintra's National Palace is, therefore, an exceptional set of this technique because it is not only the largest collection known today, but the technology and iconography used are also remarkably different from other tiles produced in medieval Europe, including the Iberian Peninsula. The attribution of these tiles to a specific production centre has always been controversial, either being considered the first Portuguese production or a special order made in Sevillian workshops specifically for Sintra's Palace. However, Trindade (2007) demonstrated the connection between these reliefs and the identical iconography observed in the masonry work in the Monastery of Batalha (Portugal), attesting for their Portuguese provenance.

The relief tile is obtained in a similar way to the *arista*'s, as the clay is pressed into a mould with the motif. However, relief tiles were essentially monochromatic, the exception being the ones in Sintra's National Palace, a few examples of blue and white reliefs produced in the region of Valencia and the star-shaped motifs that exist in Seville and in the Monastery of Santa Clara-a-Velha, in Coimbra. In Sintra, an evolution is well marked as the relief becomes more pronounced and the separation of the colours becomes more successful, suggesting a process of trial and error that culminates with high-relief tiles that resemble stonework (Trindade, 2007) (Figure 1.7). Some tiles exhibit evidence of having been fired upside down (with the glaze facing downwards), which also shows a technical innovation in the process of avoiding the spreading of the colours (Trindade, 2007). The combination of the relief with polychrome glazes and the *cuerda seca* technique makes this set unique in the world.

Figure 1.7. Relief polychrome tiles with wine leaves from the National Palace of Sintra: **(a)** the less pronounced relief; **(b)** relief with *cuerda seca*; **(c)** high relief showing the spreading of the copper green colour. Images: © Parques de Sintra

1.2.5. LUSTRE TILES

Lustre pottery was the highlight of the Hispano-Moresque ceramic production. It is characterised by the metallic shine with colours ranging from golden to copper shades, depending on their chemical composition. It was applied on white tin glazes, mostly combined with cobalt blue decorations. These lustre decorations were mostly applied on *arista* tiles and rarely on flat ones (Martínez, 1991).

The process to produce lustre ceramics was difficult and fallible and, thus, expensive. The lustre "paint" was made with a mixture of copper and silver compounds to which were added other substances to aid the obtainment of the metallic effect, such as vinegar or sulphur, and iron oxides. The lustre decoration was applied on a tin-glazed tile which was then fired for the third time. This third and last firing was performed under a reducing atmosphere and with a lower temperature (ca. 600-700 °C) than the previous two firings (ca. 900-1000 °C), just enough to soften the glaze in order to allow for the copper and silver ions to enter the glaze matrix without it melting completely. The reducing atmosphere "steals" oxygen from the silver and the copper oxides at the same time as an ionic exchange mechanism takes place between the metallic ions (Cu^{+}, Cu^{2+}, Ag^{+} and $(Ag_n^{0})^{+}$) and the alkali ions from the glaze (Pradell *et al*., 2008).

Manises was the main Iberian centre of lustre pottery. However, lustre-decorated tiles were also produced in Seville between the late 15th century and the beginning of the 16th, although the scarce number that survived leads to the supposition that it was an occasional production. It was an expensive technique, probably reserved for exceptional works. Fernán Martínez Guijarro had *tiendas de dorado* ("stores of golden"), according to a document from 1507, which was likely referring to lustre ceramics. Also, the Polido workshop used lustre-decorated tiles in Casa de Pilatos in the 1530s (Martínez, 1991). Floral and brocade decorations (*Figures 1.8* and *1.9*) were the most abundant, but there are also late Mudéjar, late Gothic and Renaissance themes, as well as coats of arms. They were used in wainscots and ceilings, and rarely in pavements, since the lustre layer would easily wear out (Martínez, 1991).

Figure 1.8. Hispano-Moresque tile panel with a brocade pattern painted in cobalt blue and lustre (Martínez Caviró, 1991).

Figure 1.9. Detail of the pattern in *Figure 1.8*, illustrating the *arista* contours, the metallic shine and differences in the lustre colours. (Picture taken by the author in the Instituto Valencia Don Juan, Madrid).

1.2.6. VALENCIAN PAINTED TILES (*RAJOLAS*)

Brush-painted tiles were the highlight of Valencian tile production, being so distinct from the coeval *cuerda seca* and *arista* tiles that were massively produced in other ceramic centres in the Iberian Peninsula. *Cuerda seca* and *arista* tiles were also imported from Andalusian workshops to Valencia, where they were later produced but never gained the importance of the blue-and-white painted tile (Martínez, 1991).

Flat white tin-glazed tiles were decorated in green and brown since the late 13th century, but the arrival of cobalt to the Iberian Peninsula in the 14th century completely surpassed the green and brown decorations. Cobalt blue was then the main colour in Valencian ceramics, sometimes used with manganese brown or copper green, but mostly used with lustre decoration. The decorations followed the Mediterranean tradition, highly influenced by Islamic iconography with vegetal and geometric motifs, but also included anthropomorphic themes and Christian inscriptions. Heraldic decorations were also very important (Coll Conesa, 2009; Martínez, 1991).

During the 14th and 15th centuries, *rajola* was the common word for tile in the region of Valencia. When referring to decorated tiles, sometimes appears *rajoles pintades* (painted tiles) or *rajoletes de Manises* (tiles from Manises). By the end of the 15th century, tiles were also called *taullels* (Coll Conesa, 2009). *Figure 1.10* illustrates a typical Valencian pavement used in the 15th century.

Figure 1.10. Valencian pavement (reconstitution), 15th century. (Picture taken by the author in the Museo de Cerámica y Artes Suntuarias, Valencia, Spain.)

In Valencian blue-and-white or blue-and-lustre ceramics, the cobalt pigment was applied onto the raw ceramic object, which was then fired for the first time. The tin glaze frit was applied afterwards and the ceramic object was fired a second time. This process was first described by González Martí in 1908 upon observing the (then) recently discovered ceramic wastes of medieval workshops in Paterna. Fragments of biscuit-fired ceramics decorated with dark lines were found with drops of tin-glaze in which the blue pigment emerged. This proved the underglaze decoration and that both biscuit-firing and second firing were made simultaneously. More recently, unfired decorated fragments were discovered in Paterna, confirming that the cobalt painting was made previously to the biscuit firing (Coll Conesa, 2009a). Along with Valencian ceramics, also in Teruel an under-glazed cobalt decoration was observed (Roldán *et al*., 2004; Perez-Arantegui *et al*., 2009).

The beginnings for the underglaze decoration technique are believed to have taken place in 12th century Syria – the so-called *laqabi* ware (Shovelton, 2016). It was the first time that pigments were applied directly on the ceramic body and covered with an alkali or lead-alkali transparent glaze frit previously to firing. Before, only slip-based mixtures had been used. From Syria, underglaze painting expanded to Persia (Iran) and then to China, where it was used mainly in blue-and-white porcelain (Mason *et al*., 2001). Considering that previously referenced literature only mentions transparent glazes, Valencian underglaze decoration using a tin-opacified white glaze represents – so far – a technological innovation. The closest parallel seems to be Iznik ceramics, where a lead-alkali glaze with a considerable amount of tin oxide (ca. 3-8.5 wt.%) was used over the colourful decorations. However, most of the tin oxide in Iznik ware is in solution in the glaze, making it basically transparent (Paynter et al., 2004; Tite, 1989). Contrarily to what was believed, this transparency is not essential to reveal the underglaze decoration – at least in what regards blue and manganese-brown pigments – as the Valencian underglaze-decorated tin-opacified ceramics attest.

1.3. PORTUGUESE *VERSUS* SPANISH PRODUCTION: THE CONTROVERSY

The existence of written documentation mentioning Sevillian exports of tiles to Portugal, together with the absence of known documents that confirm a Portuguese production, have been the basis for attributing all Hispano-Moresque tile collections in Portugal to a Sevillian origin. This idea still prevails despite new defying studies that have been published (Barros *et al*., 2003; Trindade, 2007). Furthermore, only recently a kiln with such tiles was discovered in Portuguese territory – contrasting with the well-documented archaeological sources in Seville, Toledo and Valencia regions – which resulted in decades of published literature always mentioning a Sevillian origin for the Portuguese tiles.

The work of the Sevillian historian José Gestoso y Pérez – *Historia de los barros vidriados sevillanos*, 1903 ("History of Sevillian Clays") – was decisive for the studies that followed. Not only did he study both Sevillian tiles and Portuguese ones – when he visited Portugal in 1900 –, but he also published important documents[1] referring the export of Sevillian tiles to Portugal (Gestoso, 1903):

1479 A letter referring Fernán Martínez Guijarro, a potter from Triana, as "a great master of tiles and all things related to his craft, like there is no other in the kingdom". According to the document, the quality of his work was such that orders came from all over, including Portugal.

1502 A debt note from a shipowner from Sesimbra, Portugal, who owed 400 *maravedís* for 200 tiles.

1503 An order of tiles from Olivier de Gand, a sculptor from Toledo who was working at the time in the Coimbra's Cathedral (now *Sé Velha* of Coimbra). Olivier de Gand ordered tiles (*azulejos de labores*) in the amount of 20000 *maravedís* to Fernán Martínez Guijarro and his son Pedro de Herrera.

The records from 1479 and 1503 are very important to document the activity of the workshop of Fernán Martinez Guijarro and the commercial relationship it had with Portugal. Although it does not mention any specific destiny for the exported tiles, Reynaldo dos Santos (1957) considers that the document from 1479 can only refer to the oldest tiles in Sintra's Palace: the pavement in Palatina's Chapel, the pavement in the room of D. Afonso VI and the *sgrafitto* and *alicatado* set that frames the door of the Mermaids' room, since the rest of the tiles would belong to a later period than 1479.

Santos Simões (1945) suggested that the order from 1502 could have been destined for Bacalhoa's Palace, in Azeitão, since Sesimbra is the nearest port and the Palace has a very important collection of *arista* tiles. The author considers, however, the tiles from Bacalhoa to be a lesser work than the ones of Guijarro's workshop.

[1] Gestoso (1903) lists in fact four documents. One of them, from 1501, describes a debt from Alfon Álvarez to Pedro de Herrera for "some work from his craft" (*cierto labor de su officio*), a debt which he must pay by buying a slave in Portugal and bringing him to Seville. However, this document does not specify which product Alfon Álvarez had bought; therefore, it cannot be listed as a proof of export of Sevillian tiles to Portugal (Trindade, 2007).

Finally, the order from 1503 documents the commercial connections between Coimbra and Seville. From the previous document, where a sum of 400 *maravedís* was owed for 200 tiles, it was estimated that a total of circa 10000 tiles were delivered in Coimbra. This is a very low number for covering the walls of Coimbra's Old Cathedral (*Sé Velha*), which original tile decoration has been estimated at ca. 37000 tiles (Gomes, 2011). Thus, it could be one of several orders where the others were lost, or it could be a group of tiles destined to a different location than the Old Cathedral, as it has been pointed out by several authors (Santos Simões, 1945; Trindade, 2007). The use of Hispano-Moresque tiles was particularly abundant in Coimbra and other important Hispano-Moresque tile collections are known today, such as the old Episcopal Palace (today Machado de Castro Museum) or the impressive collection of the Monastery of Santa Clara-a-Velha, here under study (Trindade, 2007). Santos Simões (1945) also advanced the hypothesis that these tiles were in fact destined to the church of Santa Maria in the Castle of Abrantes, considering that by 1503 they were most likely *cuerda seca* tiles and this church hosted the most important set of *cuerda seca* tiles in Portugal, whereas in Coimbra mostly *arista* tiles had been used. This idea is however challenged by the numerous *cuerda seca* tiles that have been found in the archaeological excavations of the Monastery of Santa Clara-a-Velha.

Nonetheless, both Portuguese and Spanish authors have had doubts regarding such unconditional attributions of Portuguese Hispano-Moresque tile collections to Seville and several hypotheses of Portuguese productions have been drawn in major studies of Hispano-Moresque tiles. The "first hypotheses of a national production in the 16th century" were drawn by Joaquim Rasteiro, who wrote a very important work on Bacalhoa's Palace, in Azeitão (Rasteiro, 1895), and Gestoso (1903), according to Reynaldo dos Santos (1957). In his monograph, Rasteiro compares some Mudéjar tiles to others from Beja (Convent of Conceição), suggesting a Portuguese production on the basis of the orange/red clay in both sets of tiles. Gestoso (1903) points out the wine leaf reliefs in the National Palace of Sintra, as well as the flower-de-lis reliefs, as possible Portuguese production. In 1945, Santos Simões groups three sets of tiles from the National Palace of Sintra and separates them from the rest as a local production made by Islamic tilers who were brought to Portugal right after the first conquests in the Northern Africa during the mid-15th century. The three sets that Santos Simões (1945) considers as a local production are the *alicatado* pavement in the chapel, the pavement in D. Afonso VI's bedroom, which is a combination of *alicatado* and *cuerda seca* tiles, and the *esgrafitado* tiles on the door of the Mermaids' Room. According to the author, the details of the *alicatado* work would imply a local production and highly specialized craftsmanship to put it in place.

According to José Meco (1985), the high-relief tiles with corn and flower-de-lis motifs remember the Della Robbia technique combined with Sevillian *arista* and *cuerda seca.* When considering possible local productions, Meco (1985) refers a group of "rough" mid-16th century relief tiles in the Chapel of Santo Amaro (Lisbon), a group of *arista* tiles from the same Chapel and also a group of plaques, glazed only in green or beige, in the altar of the Chapel of Santa Marta, in Tomar. The same author published in 2003, along with the archaeology team that worked on the site, a report on the discovery of *arista* tiles found inside a 16th-century kiln in Santo António da Charneca, Portugal. He considered these tiles as the first secure Portuguese production of *arista* tiles (Meco, 2003).

The threshold in Art History has been established by the work of Rui Trindade (2007), who challenged the theory of a "production desert" in what regards the Portuguese tile production before the mid-16th century, stating that the thousands of Hispano-Moresque tiles in Portuguese collections cannot be explained by three Sevillian documents alone. Trindade (2007) demonstrates that there is not an absence of documentation on tiles previous to that date, but that the word by which we know tiles today (*azulejo*) was only progressively introduced in the Portuguese language during the 15th century. Before that, another word (*ladrilho*) was used. During the 15th century, there was a transition period in which the word "ladrilho" appears simultaneously with the term "azulejo" in several documents. Two documents of the set studied by Trindade (2007) are especially important. One is a contract from 1498 (corrected in 1501) that contains the name *Alle Azulejo*, a Muslim who benefitted from the protection of Queen Leonor and was allowed to stay in Portugal after the expulsion in 1496 of all non-Christians. Considering that it was usual at that time to use the profession and ethnic origin after the person's name, Trindade (2007) states that *Alle Azulejo* is the first documented tile maker in Portugal from the late 15th century. Another document thought to be dated from 1519 contains an instruction for buying tiles – "the best ones you find for sale and not the ones from Seville"[2] –, implying that lesser tiles were sold in Lisbon, perhaps copies, and that there is a need to choose the high-quality ones (Trindade, 2007).

More recently, the research undertaken by Patrícia Alho *et al*. (2015a; 2015b) demonstrated that ceramic objects were ordered from Lisbon to the workshops in the south bay of the Tagus river. When studying 15th-16th-century documents from the Chelas Convent (Lisbon), Alho *et al*. (2015a; 2015b) found out that several contracts were made between the Convent and pottery workshops from Coina (Barreiro). The Barreiro area is where the only archaeological evidence of the production of *arista* tiles in Portugal in a kiln context was found, as will be further discussed (Meco, 2003).

Still, there is an absence of known documents explicitly mentioning the production of tiles in Portugal or the commercialization by Portuguese workshops. A problem concerning Portuguese historiography has been the treatment of the tile as a distinct craft from pottery because it is known today that tiles were made in pottery workshops along with other ceramic objects (Trindade, 2007; Barros *et al*., 2003). Even in Seville, Fernán Martínez Guijarro is acknowledged as a *"great master of tiles and (baptismal?) fonts and all things of his craft*"[3] (Trindade, 2007). Thus, the study of documents on pottery, in general, will likely prove to be a valuable source of information on tiles as well. Taking this into consideration, the study of Hispano-Moresque pottery for comparison purposes is likewise an important source of information on the production techniques and materials used to produce tiles.

[2] " (…) *forar os assentos dazulejos que ficaram por acabar destes mjlhores que achardes a vender e nam dos ujeram de sevilha que trouve ho monte negro* (…)" (Trindade, 2007, p. 55)
[3] "(…) *ferrant martines Guijarro vezino de triana […] es muy grand maestro de azulejos e pilas [baptismais?] e de todas las cosas de su oficio (…)"* (Trindade, 2007, p. 43)

1.4. ARCHAEOMETRY STUDIES ON HISPANO-MORESQUE CERAMICS

The technological aspects of Hispano-Moresque ceramics have been the subject of important archaeometric studies (Garcia Iñañez, 2007; Molera *et al*., 1996, 1997a, 1997b, 2001b, 2009, 2013; Ortega *et al*., 2012; Pérez-Arantegui *et al*., 2005, 2009a, 2009b; Polvorinos *et al*., 2011; Roldán *et al*., 2006; Vendrell-Saz *et al*., 2006; Zuluaga *et al*., 2012). However, only a small number of analytical studies was specifically dedicated to Hispano-Moresque tiles (Coentro *et al*., 2014; Leal, 2014; Vieira Ferreira *et al*., 2014) and all of them were led by Portuguese researchers, which is probably a consequence of the increasing interest that the Portuguese tile heritage has been the subject of during the last decade. Nevertheless, most of the knowledge on the production techniques of Hispano-Moresque ceramics was centred on the research performed by Spanish teams, in particular with the analytical studies on archaeological finds from important Iberian ceramic centres, such as the Valencian, Sevillian and Zaragoza regions.

Archaeometry studies of ceramics generally consider that the finished ceramic objects may be traded among different locations, whereas the clays and tempers are not (Hall *et al*, 1999). Therefore, the chemistry of the ceramic objects is a consequence of the chemistry of the local geological environment together with the treatments suffered by the raw materials until the finished product. This reflects the technology of a specific production area or pottery workshop (Hall *et al*., 1999). In agreement with these assumptions, medieval documents found in Valencia indicate that the clay was extracted from the same area where the ceramic workshop was placed. There were contracts demanding that the holes on the ground would be filled with the slags and ashes, leaving the soil suitable for later cultivation. Several silos filled with ceramic fragments were found in Paterna, providing archaeological evidence that sustains these documents (Coll Conesa & Pérez, 1993; Coll Conesa, 2009b).

Lead glazes were identified in all the above-mentioned studies on Islamic and Hispano-Moresque ceramics from the Iberian Peninsula. Lead glazes were already known from Roman times, but the great innovation brought by the Muslim occupation was the white tin glaze that made the Iberian Peninsula an important ceramic production centre from – at least – the 13th century onwards (Tite *et al*., 2008). The mechanism by which tin oxide acts as an opacifier was described by Molera *et al*. (1999): in lead glazes, lead oxide (PbO) reacts with silica (SiO_2) to form lead silicate ($PbSiO_3$) at ca. 550 °C and with tin to form lead stannate (Pb_2SnO_4) at ca. 600 °C. At a temperature range between 650 °C and 750 °C, depending on glaze recipe, tin starts to precipitate in the form of cassiterite (SnO_2) and remain as such once the glaze melt starts to cool down because then there is no longer enough PbO available to once again form the lead stannate. The SnO_2 particles have diameters of few hundred nanometres, similar to the wavelengths of visible light, scattering it and rendering the glaze opaque (Vendrel *et al*., 2000).

Archaeological evidence from a 13th-century ceramic workshop in Paterna (Valencia) has shed an invaluable light on the knowledge of the recipes for making tin-opacified glazes. The study by Molera *et al*. (2009) analysed several frits that were found inside crucibles and the results indicated that a mixture of lead, tin and sand was used to produce the tin-opacified glazes. There was no evidence of lead and tin being previously fired prior to the mixture with the sand, as described in the Persian treatise from 1301 by

Abu l'Qasim (Allan, 1973) or in the Italian treatise on majolica by Cipriano Piccolpasso (ca. 1557) (Piccolpasso, 1980). Abu l'Qasim describes how the lead was put first in the kiln, and then the tin was immediately added. The mixture stayed in the kiln for half a day, while an earthy substance was forming on the surface, which was removed with a large iron shovel. The lead-tin calcined mixture was added to other mixtures that would include calcite and sodium carbonate (Allan, 1973; Molera *et al*, 1997a). The analysis of glass wastes from a 16th century Iznik pottery production site corroborates Abu l'Qasim's recipe, since the glass lumps found at the site were a mixture of silica, soda, lead oxide and tin oxide (Paynter *et al*., 2004; Tite *et al*., 2008). González Martí (1952) explains a similar fritting process used in Valencia. It also starts with calcining lead (first) and tin (added right afterwards), which was then cooled and mixed with salt and sand. The final mixture was put in a ceramic kiln and fired along with the ceramic objects, and then again cooled and ground (Molera *et al*, 1997a).

The analyses of Hispano-Moresque tin-opacified glazes have quantified most SnO_2 contents between 6 and 10 wt.%, with variable degrees of homogeneity. The data from the literature regarding quantification analysis of Islamic and Hispano-Moresque tin-glazed ceramics has been gathered in Appendix I.

The colours used for decorating Hispano-Moresque pottery followed the artistic tradition of Islamic ceramics and exhibit differences among different Iberian pottery centres. With exception of blue, all colours observed in Hispano-Moresque glazes (white, green, amber and brown) were inherited from the Islamic technology used for *cuerda seca* ceramic objects. Copper, iron and manganese were commonly mined in the Iberian Peninsula, but cobalt and tin were not and mostly relied on imported raw materials (McSweeney, 2011).

The most used colours were the green and the brown, which were obtained from copper and from manganese oxides, respectively (*Figure 1.11*). Transparent – usually dark – green and brown colours resulted from copper and manganese being added to high lead glazes, whereas opaque lighter shades were obtained when the metallic oxides used were added to tin-opacified glazes. Depending on the copper content and the alkaline content of the tin-opacified glaze, green shades could vary from a "bottle green" to a light turquoise (Chapoulie *et al*., 2005). Tin glazes were also used as a white background for painting directly with a brush, as in the so called "green and brown" ceramics produced in Teruel or Paterna (Pérez-Arantegui *et al*., 2005). An important study on the manganese brown decorations in Iberian glazes from different chronologies was published by Molera *et al*. (2013), identifying the manganese compounds in glazes with different types of decoration (underglaze, over glaze and frit). Amber-coloured glazes were obtained from iron oxide, which could arise from the reaction with the ceramic body of the object and could easily be obtained by adding iron-rich clay to the glaze mixture. Iron has also been identified in green Hispano-Moresque glazes, resulting from reducing atmosphere conditions that reduced the Fe^{3+} (yellow – amber) to Fe^{2+} (green) (Molera *et al*., 1996).

Cobalt blue has been the subject of many research papers, due to its significance in decorated ceramics (Coll Conesa, 2009a; Fares *et al*., 2012; Pappalardo *et al*., 2004; Pérez-Arantegui *et al*., 2009b; Resano *et al*., 2005; Roldán *et al*, 2006; Trindade, 2009, Zucchiatti *et al*., 2006, among others). It is believed that this pigment arrived in the Iberian Peninsula during the 13th century and came from Islamic lands, where it was used since ca. 2000 BC (Trindade, 2009). During the 9th century, the cobalt blue became profusely

used by Muslim ceramists, who had the raw materials available "nearby" in one of the most important cobalt deposits in the world – Qamsar, in today's Iran. By the 13th century, both the Middle Eastern and the European cobalt mines were known in the Muslim Kingdom, as referred by Abu l'Qasim's ceramic treatise (Kessler, 2012).

The earliest known written source referring the cobalt blue pigment in the Iberian Peninsula is Valencian and dates from 1333. It uses the term *safra* (Coll Conesa, 2009a, 2009b), which is still used in the Portuguese language (*zafre* in Castillian) to refer to a yellow cobalt-rich powder used as a blue pigment in glass. The word is believed to have been originated from the Arabic *s'afra* or *s'oufr,* also related to yellow and golden colours (Coll Conesa, 2009a, 2009b).

Figure 1.11. Decorative dish with green and brown decorations over a lead-tin glaze, Paterna, 14th century, Ø 25 cm (Martínez, 1991)

The cobalt mines in the Freiberg-Erzgebirge region (today's Germany) were explored since the 12th century and became the main European source for cobalt (Gratuze *et al*., 1996). The rise of the cobalt demand in this region is linked to the establishment of the Venetian glass industry and the development of majolica during the Renaissance (Zucchiatti *et al*., 2006). Cobalt was exported in the form of zaffre, which was prepared from roasting different cobalt mineral ores, such as cobaltite (CoAsS), erythrite ($Co_3(AsO_4)_2 \cdot 8H2O$ and skutterudite (Co,Ni,Fe)As_3. Elemental associations for cobalt imported from the Freiberg-Erzgebirge region are Fe-Co-Ni and, from the early 16th century onwards, Fe-Co-Ni-As. Trace amounts of Bi, Mo and Zn are also mentioned (Gratuze *et al*., 1996; Zucchiatti *et al*., 2006).

Chemical analysis of cobalt blue decorated glasses and glazes have been conducted with the aim of identifying characteristic elemental combinations that would be associated with a specific cobalt ore from a designated source (Coll Conesa, 2009a; Gratuze *et al*., 1997, Pappalardo *et al*., 2004; Pérez-Arantegui *et al*., 2009b; Roldan *et al*., 2006; Zucchiati *et al*., 2006, Fares *et al*., 2012). In particular, the

presence of arsenic has been appointed as a possible chronological marker when associated with cobalt (Pappalardo *et al*., 2004). Studies on terracotta sculptures from Della Robbia's workshop revealed that arsenic is only present in the blue glaze in pieces dated from 1520 onwards. The authors suggest that a change in the treatment of the raw materials in the region of Saxony is the reason for the presence of arsenic, instead of a different source (Pappalardo *et al*., 2004; Zucchiatti *et al*., 2006).

The study and analysis of ceramic shards from several Islamic and Hispano-Moresque archaeological contexts has concluded that different types of clays or clay mixtures were used depending on the type and function of the ceramic object. Therefore, provenance studies must take into account ceramic typologies when comparing the chemical composition of shards from different locations. The use of calcareous clays has been reported for tin-glazed Islamic and Hispano-Moresque ceramics in several studies concerning the Iberian Peninsula, such as Paterna and Manises (Valencia) (Molera *et al*. 1997a), Muel and Teruel (Zaragoza) (Pérez-Arantegui *et al*., 2009a, 2009b). The analysis of archaeological findings in Islamic (Murcia, 10th century; Denia, 13th century) and Hispano-Moresque (Paterna) workshops have identified that calcareous clays (*ca.* 20 wt.%) were used for tin-glazed ceramics (Molera *et al*., 1997, 2009). In Teruel, two different clay bodies were identified: a red-coloured one, with CaO content ca. 7.4 wt.% used for green-and-brown-decorated ceramics, and a white-buff-coloured one, with CaO content ca. 13.5 wt.%, used for cobalt blue decorated ceramics. The red paste continued to be used alongside with the buff one, even though both were covered with tin glaze (Pérez-Arantegui *et al*., 2009b).

In a general way, calcareous clays were preferred for decorative tin-glazed ceramic objects, although non-calcareous clays were also used in tin-opacified ceramics. Utilitarian glazed objects were mostly made with non-calcareous clays, but no mention was made regarding architectural tiles (Molera *et al*., 1997a; Pérez-Arantegui *et al*., 2005). A selection of the composition of calcareous clays from the literature on Hispano-Moresque tin-glazed ceramics is presented in Appendix I.

The only secure archaeological evidence of Portuguese production of Hispano-Moresque tiles is the kiln from Santo António da Charneca, in Barreiro, located on the south margin of the Tagus river and a known ceramic production centre throughout several centuries (Meco, 2003; Trindade, 2007; Vieira Ferreira *et al*., 2014). The results of the multi-analytical study of two tiles from this kiln (Vieira Ferreira *et al*., 2014) identified high-silica ceramic bodies with only a very small CaO content (<1.5 wt.%), a different clay mixture from the commonly used calcareous clay. Tiles identical to the ones from Santo António da Charnerca's kiln are believed to exist in a church from a nearby town – Alhos Vedros – but the chemical analysis to confirm this has not been published so far (Vieira Ferreira *et al*., 2015).

Hispano-Moresque ceramics represent a time of great technological, cultural and artistic changes, as previously stated. The above-mentioned literature confirms a continuity in the ceramic technology from the Islamic to the Christian workshops. Therefore, analytical studies focusing Islamic ceramics in the Iberian Peninsula, as well as the first examples of majolica in Renaissance ceramic centres, are also an invaluable source of information for comparison purposes and will be considered in this study (e.g.: Chapoulie *et al*., 2005; Garofano *et al*., 2015; Guirao *et al*., 2014; Lapuente & Pérez-Arantegui, 1999; Molera *et al*., 1997a, 2001b; Ortega *et al*., 2012; Pérez-Arantegui *et al*, 1999; Polvorinos del Rio & Castaing, 2010).

CHAPTER 2

GLAZED TILE COLLECTIONS

The glazed tiles considered for this study were selected among some of the most important collections in the Iberian Peninsula: the Monastery of Santa Clara-a-Velha, Coimbra, Portugal (SCV), the National Palace of Sintra, Portugal (PNS), the archaeological site of Santo António da Charneca, Barreiro, Portugal (SAC), the Instituto Valencia de Don Juan, Madrid, Spain (IVDJ), the Casa de Pilatos, Seville, Spain (CPS) and the Museu de Cerámica y Artes Suntuarias González Martí, Valencia, Spain (MCV).

Figure 2.1. Map of the Iberian Peninsula illustrating the location of the collections under study and other reference points. IVDJ-S and IVDJ-T have attributed provenances since the collection is in Madrid.

In this chapter, a brief contextualization of the collections is given. Their geographical location is indicated in *Figure 2.1*. Scaled photographs of all the tiles under study can be observed in Appendix II.

2.1. Monastery of Santa Clara-a-Velha, Coimbra, Portugal

The history of Santa Clara-a-Velha is intrinsically connected with the Mondego river. Today a beautiful ruin, the Monastery of Santa Clara-a-Velha (SCV) was once a rich property occupied by a community of Clarisse nuns. The monastery's location right next to the south margin of the Mondego river resulted in many floods throughout the centuries (*Figure 2.2*). Construction works and several adaptations were not enough to endure the damage from constant floods, which eventually led to the definitive abandonment of the property in the 17th century. The nuns moved to a new monastery built in a nearby upper location – a new Santa Clara's monastery, which named as such – Santa Clara-a-Nova (Saint Claire-the-New), in opposition to the old monastery, which was now called Santa Clara-a-Velha (Saint Claire-the-Old) (Trindade and Gambini, 2009).

The history of the Monastery of Santa Clara-a-Velha begins in the 13th century, when a strong-willed noble lady decided to build a new monastery dedicated to the Order of Saint Claire and to Saint Elizabeth of Hungary. This lady was Dona Mor Dias, a wealthy woman from the Nobility that was living in another feminine monastery in Coimbra (Mosteiro de S. João das Donas, which belonged to Mosteiro de Santa Cruz) since 1250. Her will to build another convent resulted in strong opposition from the Santa Cruz's monks, as they feared to be deprived of the rights to D. Mor Dias' heritage. Despite this opposition, the authorization to start the construction was granted in 1283. The foundation of the Monastery of Santa Clara-a-Velha – the cornerstone ceremony – is described in a document from 1286 (Trindade and Gambini, 2009).

The fight between D. Mor and the Santa Cruz's monks continued until after her death, in 1302. Despite the intervention of the King D. Dinis and the Queen D. Isabel themselves, the dispute for D. Mor's fortune went on until 1316, when D. João de Soalhães (by then the Lisbon's bishop) and the Santa Cruz's Prior achieved an agreement where all D. Mor's assets were then property of the Monastery of Santa Cruz. Against her dying wishes, D. Mor's fortune was taken from the Monastery of Santa Clara-a-Velha and, with that, the monastery was closed (Trindade & Gambini, 2009).

Queen Isabel of Aragon, wife of the King D. Dinis, continued to fight for D. Mor's wish to found a Clarisse community and intervened with the Pope. The authorization finally arrived from Rome – a letter dated from April 10th 1314 – and, thanks to the Queen's efforts and donations, a new bigger monastery was built. The Queen bought properties which she later added to the monastery, including a small palace where she lived after the death of King D. Dinis in 1325. She also created a hospital and sponsored the first modifications to the church in 1331, just one year after its inauguration, because of the floods that submerged great part of the building. Queen Isabel transformed a small church and few adjacent

buildings into a great monastic complex surrounded by a community of workers, the construction site where they worked and their homes (Trindade & Gambini, 2009).

Figure 2.2. View of Coimbra in 1669 with the Monastery of Santa Clara-a-Velha in the foreground (Magalotti, 1933).

But the Queen's role in Santa Clara-a-Velha's history extends beyond that: she wore the habit of Santa Clara's rule and decided to be buried in the monastery, for that ordering a tomb that was placed in a lateral nave of the church. Soon after the Queen's death in 1336, a process of canonization begun and two miracles were registered. She was called Isabel, the "Saint Queen" (Rainha Santa). The monastery was ever since connected with the cult of the Saint Queen, which attracted many donations and the presence of nuns from the most important and richest families. In 1625, Isabel, the Saint Queen, was finally canonized by the Pope Urban VIII (Trindade and Gambini, 2009).

The Monastery of Santa Clara-a-Velha suffered several transformations throughout the centuries, most of them structural changes essential for the day-to-day life of the nuns. The Mondego river kept invading the area of the monastery, so a new floor was built half-height of the church, where the religious celebrations were performed from then on. The cloister was also elevated and a side door was open in the church for a direct access. However, the constant floods made life too hard in the monastery and in 1647 the King D. João IV authorized the construction of a new Santa Clara monastery on a nearby hill. In 1677, the nuns were living in the new monastery, now called Santa Clara-a-Nova. The old monastery was definitely abandoned and entered a period of decadence (*Figure 2.3*). It stood there as a ruin, partially submerged, until the last decade of the 20th century, when major rehabilitation works started to rescue the monastery from the water (Trindade and Gambini, 2009).

In 1995, the cloister was rediscovered during the drainage works and soon it became obvious that these ruins extended to a much larger area than it was initially thought. The archaeological findings were incredibly rich, revealing a lot about the life in the monastery. Luxury glass and ceramic objects were retrieved from the mud, agreeing with the social and economic status of the nuns. In 2009, the recovered monastery was open to the public, along with a museum where the archaeological findings are exhibited (Trindade and Gambini, 2009) (*Figure 2.4*).

Figure 2.3. The ruin of the Monastery of Santa Clara-a-Velha with the church partially submerged (date unknown) (Côrte-Real, 2003).

Figure 2.4. The Monastery of Santa Clara-a-Velha after the rehabilitation works. (Picture taken by the author in 2012)

During the archaeological excavations and rehabilitation works in the monastery, thousands of Hispano-Moresque glazed tiles were found (Macedo, 2006). The specimens that are still preserved *in situ* give just a slight idea of what the monastery must have looked like with the apse covered with tiles, including the ceiling of its chapels, as well as several rooms around the cloisters and the fountains in their centre. The

diversity of patterns is astonishing: from the oldest *cuerda seca* Islamic patterns to the latest Renaissance *arista* ones, there are many varied motifs, either geometric, vegetal or even anthropomorphic. The diversity of techniques and iconography suggest the employment of such tiles over several decades, mostly between the late 15th century and the first half of the 16th century.

Although a large part of the collection was submerged for centuries, most tiles have their original glaze in a fairly good conservation state, except for the obvious weathering due to burial conditions that caused a loss of the original surface. It is surprising that glaze detachment is a minor conservation problem in this collection regarding the conditions in which it was preserved for so many centuries.

The placing of the tiles coincided with the elevation of the pavement in the apse in the first decades of the 16th century. The massive use of Hispano-Moresque tiles in Coimbra is associated with the bishopric of D. Jorge de Almeida (1482-1543), who was responsible for major works of art in the city and its surroundings and became associated with the import of Sevillian tiles for Coimbra's cathedral (see *Chapter 1.3*) (Macedo, 2006). Either from Seville or a local production, the artistic scheme must have been similar to the tiles in the cathedral and in the church of the Monastery of Santa Clara-a-Velha, as *Figures 2.5* and *2.6* illustrate.

Figure 2.5. The interior of the Coimbra's Cathedral (*Sé Velha*) before the restoration works in the 1940s (Meco, 1985).

Figure 2.6. Detail of a column with its based covered with tiles, suggesting a similar decoration as the one in *Figure 2.5.* (Picture taken by the author in 2012)

Along with the tiles, many production markers were found during the excavations, such as tripods, unglazed tiles and ceramic residues (*Figure 2.7*), suggesting the existence of a ceramic workshop in the proximities. Unfortunately, no kiln was discovered. There is no question that Coimbra had pottery production in the 15th and 16th centuries because there are documents that prove it. An example was a request made by a potter named Braz Eanes to the King Afonso V to explore a lead mine (near Coimbra) which was abandoned, as it was rich in *alcanfor.* This was a Medieval term for galena (lead(II) sulphide, PbS), a substance that could be used as a raw material for glazes (Trindade, 2007). Nevertheless, no known documents mention the specific production of ceramic tiles.

Figure 2.7. Production markers found in the Monastery of Santa Clara-a-Velha: (a) unglazed *arista* tile; (b) tripods; (c) a rest of biscuit clay with pressed fingerprints (Sebastian, 2010).

2.2. National Palace of Sintra

> *Indeed, it may be said that tile work is the most characteristic feature of Portuguese buildings, and that to it many a church, otherwise poor and even mean, owes whatever interest or beauty it possesses. Without tiles, rooms like the* Sala das Sereias *or the* Sala dos Arabes *would be plain whitewashed featureless apartments, with them they have a charm and a romance not easy to find anywhere but in the East.*
>
> Walter Crum Watson, 1908 (p. 29)

Described in the 16th century as *magnificent* by Damião de Gois, the National Palace of Sintra (*Palácio Nacional de Sintra*) has been the subject of many literary works (Góis, 1926). The beauty of the location and its surroundings, the proximity to Lisbon, the perfect conditions for hunting, made this palace one of the favourites of the Portuguese nobility. Despite the transformations over the centuries, it is the only Portuguese palace that conserved his original medieval essence and its tile collection is considered the largest *in situ* in Europe (Silva, 1995).

The pavement of the *Palatina* Chapel, in *alicatado* technique, is one of the oldest surviving examples of Hispano-Moresque tiles in Portugal. According to Santos Simões (1945), this pavement has been considered by some authors as an original Islamic pavement from a mosque that previously existed in that location. This fed the idea of the Palace having been built over an Islamic construction (either a palace or a mosque, or both) after the conquest of Lisbon by D. Afonso Henriques (the first King of

Portugal) in 1147. At least two Muslim castles existed in Sintra prior to the Christian Conquest, according to Al-Bakrî, an Arab geographer from the 11th century. However, there is no indication (only suppositions) that one of them would be the actual Sintra's National Palace and, therefore, there is no historical proof of the Islamic origin of the Palace (Lino, 1948; Santos, 1957; Silva, 1995).

Figure 2.8. The National Palace of Sintra. ©Parques de Sintra

The oldest known documents are dated from 1281 and refer to construction works for the enlargement of the Palace during the reign of King D. Dinis (1261-1325). The presence of Moorish craftsmen is documented, as the King granted them privileges for working on the conservation and renovation of the Palace (Trindade, 2007). The construction of the *Palatina* Chapel and the prison-room of D. Afonso VI took place during the transformations by D. Dinis (Silva, 1995).

D. João I (1357-1433) started a major construction campaign in the first quarter of the 15th century, adding new chambers and the famous chimneys that became the symbol of the palace. The King hired João Garcia de Toledo as foreman and decorated the palace in *Mudéjar* style (Silva, 1995).

In April 2002, when maintenance works to replace the sewage system of the Palace were taking place, a ceramic kiln was found under the Queen D. Amélia's Yard, located right next to the main entrance of the Palace. Works were suspended and a team from IPPAR (*Instituto Português do Património Arquitectónico* – Portuguese Institute for the Architectural Heritage) was called for the documentation and conservation of the archaeological findings. The date of the kiln is not clear because the findings only include architectural ceramics without any particular characteristics that could be associated with a specific chronology. However, there are glazed tiles in its structure, like the ones in Palatina's Chapel's pavement, and the kiln is located next to D. João I's façade, so there is a possibility that this kiln was used during the construction works that this King implemented in the Palace from 1415 onwards and that the kiln was shut down after that. The kiln has an oval structure and the furnace is still in its place, as well as a part of the (cooking) chamber and an access hall. The kiln was consolidated and protected, and finally, it was covered again. This was considered the best option for the conservation of the structure (Sabrosa et al, 2003).

The decoration of the walls with the Hispano-Moresque tiles that still characterise the palace today took place during the Kingdom of D. Manuel I (1469-1521). The tiles were likely installed between 1497 and 1510, corresponding to the first phase of the transformations the King performed in the palace. Afterwards, he built the Oriental wing of the palace and the tower, hiring João Rodrigues as his foreman (Silva, 1995).

Figure 2.9. Hispano-Moresque tiles in the National Palace of Sintra. (Picture taken by the author in 2011.)

The tiles from Sintra's National Palace include geometric *cuerda-seca* and *arista* patterns that are commonly observed in Hispano-Moresque tile decorations, but the importance of this collection is focused on the relief patterns. The palace contains several different relief patterns which do not have a parallel in the Iberian ceramic production (Trindade, 2007) and are addressed in this work.

The great earthquake of 1755 caused major destructions to the Palace. Some work was done under the rule of Marquês de Pombal to consolidate the most part, but this intervention is considered by Sabugosa (1903) as "deplorable". In the 19th century, King D. Fernando lived in this palace at the same time that he

supervised the construction of Pena's Palace. The Count of Sabugosa, in 1903, published an important work on Sintra's National Palace (Sabugosa, 1903) – describing the tiles and including important drawings that are now a valuable testimony of the Palace's architecture and decoration in the first years of the 1900s.

2.3. Santo António da Charneca, Barreiro

In 1997, during the construction of a housing development in Santo António da Charneca (Barreiro, Portugal), large amounts of ceramic fragments and ashes were found. An emergency archaeological excavation took place before the construction works proceeded and the shards were collected. According to the population, other findings such as this one were discovered before in the area: ceramic shards, charcoal, ashes, bricks and even a circular structure that could be an old ceramic kiln. This area was completely urbanised. The specific location of the ceramic fragments is today a school playground (Barros et al., 2003).

The excavation occurred in two separate zones. In both of them, abundant ceramic shards were found, both biscuit-fired and glazed. The most common types were sugar bread forms (very common in this area), kitchen and table utensils, personal hygiene utensils, biscuit forms, construction materials and tripods. Also, six tiles were found (Barros et al., 2003).

Some biscuit fired shards have some glaze residues, which probably fell from objects that were second fired at the same time as these were firing for the first time in a lower part of the kiln. All findings were dated between the end of 15th century and the first half of the 16th, according to the ceramic typologies. Due to a number of imperfections, they were considered as a set of rejected objects from a nearby kiln (Barros et al., 2003).

Six tiles were among the findings: five arista tiles and one flat tile. The flat tile has a white matte glaze with some rough drawings in light blue, yellow, brown and green. Barros et al. (2003) suggest this could be an experiment to test the behaviour of the different coloured glazes in the tiles. There are two different patterns in arista tiles and these are very common patterns in other collections as well. The tiles measure between 13,2 cm and 13,9 cm on the side and were fired in oxidizing kilns piled with tripods between them (Barros et al., 2003). These tiles have been considered the first known specimens of decorated tiles certainly produced in Portugal (Meco, 2003).

2.4. Instituto Valencia de Don Juan, Madrid

The Instituto Valencia de Don Juan (IVDJ) is located in Madrid, Spain. It was founded in 1916 to host the collection of decorative arts and documents that comprises an impressive set of Hispano-Moresque ceramics, including tiles from Seville, Toledo and Valencia (Martínez, 1978).

Don Guillermo de Osma y Scull and his wife Doña Adelaida Crooke y Guzmán (XIII Condesa de Valencia de Don Juan) founded the Instituto with their own private collections, as well as the collection of Don Juan Crooke y Navarrat (Doña Adelaida's father) and of the Counts of Oñate. The Instituto displays paintings and sculptures, as well as glass and ivory objects, embroideries and armours. But the most remarkable set of objects within these collections is the ceramics group, which includes one of the most important sets of lustre-decorated ceramics in the world (Martínez, 1978).

The ceramics collection of Instituto Valencia de Don Juan comprises glazed tiles from the 13th to the 16th century, mostly Islamic and Hispano-Moresque tiles with a few examples of early majolica tiles. The collection is rich in cuerda seca and arista tiles from Toledo, Andalusia and the Valencia region (Martínez, 1978). There are also lustre-decorated tiles that form part of this study.

2.5. Museo Nacional de Ceramica y Artes Suntuarias "González Martí"

The Museo Nacional de Cerámica ("National Ceramic Museum") was founded in 1947, when Manuel González Martí (1877-1972) donated his impressive ceramic collection to the Spanish government with the condition that the collection would never leave Valencia. He was then designated lifelong director of the museum (Museo, 2013).

Manuel González Martí began collecting ceramics in 1895, at the age of 18. He studied Law and Fine Arts, but his true passion was the study of ceramics. He was a professor of Technical and Artistic Evolution of Ceramics at the School of Ceramics of Manises, becoming the school director from 1922 to 1936, and from 1939 to 1947, when he retired. He also discovered the medieval ceramic workshops in Paterna in 1907 and participated in the first archaeological excavations. Between 1944 and 1952, he published one of the most important works on Valencian ceramics, the three volumes of Cerámica del Levante Español (1944-52) ("Ceramics from Eastern Spain") (Museo, 2013).

By the 1920s, the ceramic collection of González Martí and his wife Amelia Cuñat was already impressive. They borrowed objects for exhibitions and were constantly asked to show their collection, which they obliged. During the Civil War (1936-1939), their home, library and collections were confiscated and many art works were unfortunately lost forever. However, González Martí continued to fight for his dream of creating a Valencian Ceramic Museum. Once he achieved his gold, in 1947, he continued to improve the collections through donations and publications, and finally, in 1954, he managed to convince the Spanish Ministry of Education to purchase the Palacio del Marqués de Dos Águas to be the Ceramics Museum's headquarters (Museo, 2013).

The Museo Nacional de Cerámica y Artes Suntuárias "González Martí" exhibits major ceramic art works from the medieval period to the present day. The tile collection includes seven complete pavements and many medieval works from archaeological excavations in Paterna and Manises, including lustre-decorated tiles. Other collections donated by González Martí and his wife also belong to the museum, such as paintings, textiles and their bibliographical collection (Museo, 2013).

2.6. Casa de Pilatos, Sevilla

> *But the greatest and richest tile collection is, without a doubt, the one that adorns the Palace of the Dukes of Medinaceli* […]*. The Casa de Pilatos is the richest museum, the most outstanding collection* [of tiles] *there is for its incalculable number, for the diversity of motifs and for the artistic and orderly combinations they present* […]. (Gestoso, 1903, p. 145)

The Casa de Pilatos (House of Pilatos) was built by one of the most influent Sevillian families, the Enríquez de Ribera, between the late 15th century and the first half of the 16th. Catalina de Ribera bought the first property in 1483 for 320000 maravedis, a house which belonged to Pedro Lopez, a *converso*[1] Jew who (along with many other *conversos*) had his properties confiscated by the Spanish Inquisition. Other properties were bought and added to the house in 1487 (Bernal, 2011).

The new house of the Enríquez de Ribera family should reflect their economic and social status in the Sevillian society. Don Pedro Enríquez de Quiñones was one of the last medieval cavalrymen and his sons belonged to the first generation of Humanists in Seville. It was a time of transitions. The Sevillian architecture was a mixture of gothic constructions and Muslim buildings still in use, but the Mudéjar style was the preferred one. Also, Muslim slaves were taken upon the winnings of the war against the Kingdom of Granada and their knowledge and expertise were used in architectural construction and decorations. Thus, the Casa de Pilatos reflects the perfect integration of Almohade, gothic, mudéjar, Nazarí and Renaissance architectural models and decorations (Bernal, 2011).

Don Pedro Enríquez died in 1491 and Doña Catalina in 1505. Their oldest son, Fadrique Enríquez de Ribera, I Marquis of Tarifa, inherits their estate and becomes one of the most important figures in introducing the Renaissance style in Seville through the decorative transformations he endured in Casa de Pilatos upon returning from a two-year travel through the Holy Land and Italy. Don Fadrique was marvelled by the Renaissance style and, when returned, he started a major expansion and refurbishment of his palace, redesigning the traditional Sevillian noble house. Italian marble columns and statues were ordered and soon influenced the Sevillian architectural taste (Bernal, 2011).

In the last years of his life, Don Fadrique (m. 1544) continued his transformation of the palace with a major order of arista tiles, with which he covered most walls of the palace's first floor in a "colourful explosion". This major work was ordered in 1536-38 to the workshop of Diego and Juan Pulido (or Polido), who had also worked for the Alhambra Palace and the *Pabellón* Carlos V in the Sevillian Alcázar (Martínez, 1991). The contract implied the delivery of 2000 tiles per week, otherwise, the workshop of the Pulidos would have to pay a fine of 1000 *maravedíes*. Don Fadrique wanted to make sure the work was finished before he died.

[1] A *converso* was a former Jew who converted to Catholicism, also called "New Christian". In the last decades of the 15th century, the Spanish Inquisition condemned many Sevillian *conversos* for allegedly continuing to practice their former religion, many of them rich prominent figures in Sevillian society. Their assets were confiscated and sold, which guaranteed considerable profits for the city of Seville and helped funding the Granada War (Bernal, 2011).

The Casa de Pilatos was built over a period of great transformations and it fuses the Moresque and gothic styles with the Renaissance. It hosts the most impressive set of arista tiles, a true corpus of this technique, according to several Spanish scholars (Gestoso, 1903; Martínez, 1991; Sancho Corbacho, 1978).

CHAPTER 3

METHODOLOGY

The study of cultural heritage objects implies specific limitations and challenges. The great intrinsic value of the artefacts as unique testimonies of our collective past makes their study surrounded with added care in terms of manipulation of the objects, sampling and their conservation. As such, the analytical techniques chosen in cultural heritage studies must whenever possible be non-destructive or, at most, micro-destructive.

Sampling is then a delicate process that must be minimal or preferably non-existent, although minimal sampling that does not aesthetically alter the object is sometimes preferable to avoid excessive manipulation and transportation, which would probably increase the risks of damage.

Major advances in analytical techniques during the last decades have made possible to chemically characterise our works of art with minimal or no sampling necessary. In a general point of view, one can say that the evolution of the analytical methods for studying works of art is pointed towards the minimization of the sample and of the increasing sensitivity of the available techniques, as well as their detection power and spatial resolution (Janssens & van Grieken, 2004).

The study of historic glazed tiles implies analysing two chemically and morphologically different components: the glaze and the ceramic body. These two components interact with each other with different results depending on their chemical composition and firing conditions and, therefore, the analysis of the glaze-ceramic interface was also considered since it is a source of information on the production technology (Molera *et al.*, 2001a).

A multi-analytical, non- or micro-destructive approach was chosen in order to leave the samples visually unaltered. The analytical methods that were used allowed for the chemical and mineralogical

characterization of both the glaze and the ceramic body of the tile, as well as the study of the morphology of the glaze and glaze-ceramic interface.

The samples under study represent some of the most important collections of Hispano-Moresque tiles in Portugal and Spain. All the tiles are illustrated in Appendix II.

3.1. Sampling procedure

Sampling was performed with the same procedure for every collection under study. Very small samples (ca. 2-3 mm of glaze and ca. 3-5 mm of ceramic paste) were collected from fractured areas in the tiles, always with the aim that this sampling would be visually imperceptible.

Samples were then mounted as cross-sections in epoxy resin (Araldite® 2020). They were polished in Micro-Mesh® sheets up to grit 8000. μ-PIXE, LA-ICP-MS, μ-Raman and SEM-EDS analyses were performed on these polished cross-section samples. μ-XRD analyses required samples which were not mounted in resin, as it would interfere with the analysis. SR-μ-XRD required thin-cut polished cross-sections, as explained below.

This sampling procedure allowed the study of important collections without the need for transporting the tiles to the laboratory. The principal aim is to open other possibilities to continue this study even further and allow more samples to be collected from other collections. Also, the non-/micro-destructive techniques used make it possible for the same samples to be analysed again in the future.

3.2. Analytical techniques

Micro-Particle Induced X-Ray Emission (μ-PIXE)

PIXE is the most well-known analytical method within the group of ion-beam techniques and its use has become widespread among provenance studies and materials characterisation of cultural artefacts (Coutinho *et al.*, 2016b; Pappalardo *et al.*, 2004; Vilarigues *et al.*, 2011). There are several reasons for this: PIXE allows for detection of elements as light as sodium, which is very important in glass and ceramics' studies; by combining beam focusing with raster scanning, its mapping capabilities allow for selection of a specific area to analyse, avoiding large inclusions, gas bubbles, as well as the glaze-ceramic interface and the weathered surface; most importantly, it is considered a non-destructive technique, as the damage induced by the particle beam is nearly negligible (Calligaro, 2008; Šmit, 2013).

The principle behind PIXE is the detection of characteristic X-rays that are excited through irradiation with protons or other light ions (Šmit, 2013). The low sensitivity for trace and REE elements is a disadvantage of the PIXE technique when these are necessary for provenance studies. This happens due to the low production yield of their K lines, which are masked by overlapping with K and L lines of other elements (Calligaro, 2008). For detection and quantification of trace and REE elements, a complementary technique with higher sensitivity was used – LA-ICP-MS – with demonstrated comparable measurements for the major elements (Coutinho *et al.*, 2016). The fact that PIXE is not a portable technique may arise as a disadvantage when comparing to other X-ray based techniques such as X-ray Fluorescence Spectrometry (XRF) (Calligaro, 2008).

Particle Induced X-Ray Emission with micrometre lateral resolution (μ-PIXE) was performed using an Oxford Microbeams OM150 type scanning microprobe capable both of focusing down to 3 x 4 μm^2 the used 1 MeV proton beam and scanning a sample surface area as large as 3730 x3730 μm^2. The sample fragments were irradiated in a vacuum and a 30 mm^2 Bruker SDD X-ray detector with 145 eV energy resolution (at the energy of the Mn Kα line, 5.9 keV) was used for X-ray collection. Equipped with an 8 μm thick Be window, it allows detecting X-ray energies as low as the ones of Na while preventing most of the protons from entering and damaging the detector crystal. From the initially obtained 2D elemental distribution maps (with typical dimensions of 750 x 750 μm^2), the glaze and the ceramic body of the tiles could be properly identified and a representative region of interest selected for quantitative analysis. Operation and basic data manipulation were achieved through the OMDAQ software code (Grime and Dawson, 1995), while quantitative analysis was performed with the GUPIX code (Campbell *et al.*, 2010).

In order to validate the results, two glass reference standards (Corning B and Corning C) were also analysed (*Table III.1* – Appendix III).

The equipment used belongs to Instituto Superior Técnico (IST), University of Lisbon, Portugal, and the analyses were performed by Luís C. Alves.

Laser Ablation Inductively Coupled Plasma Mass Spectrometry (LA-ICP-MS)

Laser Ablation Inductively Coupled Plasma Mass Spectrometry has become one of the most important techniques used for studying glass and glazes, as it allows for a fast and complete elemental characterisation of inorganic materials with lowest detection limits in the range of 0.1-1 μg/g (Giussani *et al.*, 2009; Gratuze, 2013; Resano *et al.*, 2005; Wedepohl *et al.*, 2011). It is especially useful to address questions regarding raw materials, as REE and trace elements are detected and quantified, and consequently, provenances may be determined.

The sample is placed under a laser beam that ablates a very small quantity of material, which is then transported through a flow of argon or helium into the plasma torch. The plasma decomposes the ablated material, ionises the elements and then the mass spectrometer separates the ions according to their mass. The laser used leaves behind a small crater with a diameter of ca. 100 μm, which is considered

a small disadvantage of this technique. However, it is hardly detectable to the naked eye and, therefore, LA-ICP-MS is considered as a practically non-destructive technique (Giussani *et al.*, 2009; Gratuze, 2013).

The LA-ICP-MS analysis was carried out on the cross-section samples mounted in epoxy resin. The ablation system used in this study is located at the National Centre for Scientific Research (CNRS) in Orleans, France. It consists of a Neodyme:YAG laser working at 266 nm (quadrupled frequency) operating at a maximum energy of 2 mJ and at a maximum pulse frequency of 15 Hz. The beam diameter can be adjusted from 20 μm to 100 μm. The glass analysis was performed at 8 Hz with a beam diameter of 80 μm. A pre-ablation time of 20 s is set in order to eliminate the transient part of the signal which is then acquired for 55 s corresponding to 20 mass scans from lithium to uranium (the signal in count/second is measured in the low-resolution mode for 58 different isotopes). Glass calibration was undertaken by employing NIST610, and Corning Museum of Glass (CMoG) B, C, and D glass reference material (Gratuze, 2013). The detection limits range from 0.1 to 0.01 wt.% for major elements and from 20 to 500 μg/g for others.

In order to validate the obtained concentration results, glass reference standards CMoG A and NIST610 are also analysed as an unknown sample. Those values are presented in Table III.2 – Appendix III and shown to agree within 5 to 10% with the certified ones.

In this work, LA-ICP-MS was used in complement to μ-PIXE to chemically characterise the glazes of the tiles. The analyses were undertaken on the same cross-section samples mounted in resin that were analysed by μ-PIXE.

Scanning Electron Microscope with X-ray Microanalysis (SEM-EDS)

Electron microscopy was considered a fundamental technique for this study, providing invaluable information on the morphology of the glazes and glaze-ceramic interfaces of the tiles. SEM allows for high magnifications, showing the glaze in great detail and, at the same time, it provides information on the elemental composition of the sample due to the X-ray analysis component of the method.

The images provided by the SEM-EDS equipment may result from two different methods: backscattered electron images (BSE) and secondary electron images (SE). BSE results from the scattering of the irradiating electrons by the atoms in the sample – the heavier the atoms, the stronger is the scattering effect. Therefore, the grayscale of the BSE image reflects the elemental composition of the sample, with brighter areas corresponding to heavier elements (Janssens, 2013b). For the study of glazed tiles, this is especially important because the high lead glaze appears in high contrast with the ceramic body in the polished cross-section samples mounted in epoxy resin, as well as most mineral inclusions. SE images, on the other hand, provide information on the surface of the sample, as the electrons are emitted from the surface according to the angle of the sample. Thus, non-flat surfaces show up as darker areas than the flat ones (Janssens, 2013b).

The equipment used for the analyses was a variable pressure scanning electron microscope HITACHI S-3700N coupled with a Bruker Xflash 5010 SDD energy dispersive X-ray spectrometer. Samples were

analysed either in a vacuum (in which case, the samples were coated with a thin, conductive film of carbon), or under an air pressure of 20 Pa or 40 Pa (with uncoated samples). The backscattering mode was used for SEM imaging. The resolution of the EDS detector is 123 eV at the Mn Kα line energy. The system allows reliable elemental point analysis and mapping from Na Kα X-ray emission energy up to the L emissions of the heaviest elements. In order to collect X-ray emissions from heavier elements like Pb, an acceleration voltage of 20 kV was chosen. The EDS tasks and the quantification were achieved through the Esprit1.9 software from Bruker Corporation.

The SEM-EDS analyses were performed in the HERCULES Laboratory, in Évora, Portugal, by Cátia Relvas, Teresa Alexandra Ferreira, José Mirão, Luís Dias, Margarida Nunes and the author.

Micro-Raman spectroscopy (μ-Raman)

μ-Raman spectroscopy identifies compounds on a molecular level. This technique has gained importance over the last decades in the identification of pigments and minerals in cultural artefacts (Buzgar *et al.*, 2013; Coentro *et al.*, 2012; Colomban, 2013a, 2013b; Mwenesongole, 2008). In the study of ceramic tiles, μ-Raman was especially useful for the identification of mineral inclusions in the glaze and the glaze-ceramic interface. Equipped with a microscope, μ-Raman allows focusing on a specific inclusion and, depending on its size, also allowing for analysing different points on the same inclusion.

In the μ-Raman analysis, an intense monochromatic light (i.e. a laser) is focused on a sample and the scattered light is measured. Part of this scattered light is of a different energy than that of the laser, due to the interaction with the molecules. The shift in energy is related to the characteristic vibration modes of the molecules (bending or stretching modes) (Colomban, 2013).

μ-Raman offers several important advantages in cultural heritage studies, such as minimal or no sample preparation and the analysis of very small samples with detection of crystals with only a few micrometres. One of the great advantages when comparing to X-ray diffraction is the identification of amorphous compounds and intermediate phases. However, the laser operating at a high power may induce thermal changes in iron oxides and therefore it is important to reduce it with the use of filters (Colomban, 2013a, 2013b).

Analyses were performed on polished cross-sections of the tiles with a Labram 300 Jobin Yvon spectrometer, equipped with a He-Ne laser of 17 mW power operating at 633 nm and a solid-state laser of 500 mW power operating at 532 nm. The laser beam was focused either with 50x or 100x Olympus objective lenses. The laser power was filtered to 10% incident power using a neutral density filter for all analyses. Analyses were performed both on the surface of the glazes and on polished cross-sections. Spectra were recorded as an extended scan. A mixed Gaussian-Lorentzian curve-fit provided by the LabSpec software (v 5.15.25) was used to determine the exact peak wavenumbers. The attribution of the Raman spectra was made using the RRUFF database project on minerals (RRUFF, 2014). The equipment was operated by the author.

MICRO-X-RAY DIFFRACTION (μ-XRD)

X-ray diffraction is one of the most used analytical techniques in the study of ceramics because it provides a complete information on the mineralogical composition of the sample (Janssens, 2013a). With the identification and semi-quantification of the crystalline phases, one can compare different ceramic objects and address the questions regarding the raw materials, firing temperatures and alteration phenomena in archaeological shards.

The analysis of the samples is performed under an incident X-ray beam. This technique relies on the principle that each crystalline compound diffracts the incident X-rays in specific angles, resulting in a specific pattern of diffraction peaks – the diffractogram. Most samples are a mixture of different crystalline phases, which appear simultaneously in the diffractogram and are compared with databases in order to be identified (Janssens, 2013a).

The samples used in this study were very small due to restrictions related to the fact that these are historic ceramic tiles. Samples with ca. 5 mm^3 were collected from the interior area of the ceramic body of the tile (in already existent fractured zones) in order to avoid the presence of mortar from the back of the tile, as well as the contamination by lead from the glaze.

The μ-XRD analyses were performed directly on the samples, without previous preparation, using a Brüker AXS D8 Advance diffractometer with a DAVINCI design, equipped with a Cu Kα radiation source, a Göbel mirror assembly and a LynxEye 1D detector, and operating with a DIFFRAC.COMMANDER (Copyrigh©Bruker, AXS 2009-2013, v. 3.0) software package. The analyses were carried out with a 0.3 mm diameter pinhole collimator. The diffraction patterns were collected from 3º to 75º 2θ at a step size of 0.05º 2θ, with a time per step of 1 s, with a working voltage and current of 40 kV and 40 mA, respectively. The identification was performed with DIFFRAC.EVA (v. 3.0, Copyright© Bruker AXS 2010-2013) software package using the ICDD PDF X-ray pattern database. To ensure reproducibility, at least two analyses were done for each sample.

The equipment used belongs to the HERCULES Laboratory in Évora, Portugal. The analyses were performed by Cátias Relvas, Margarida Nunes, Teresa Alexandra Ferreira and José Mirão.

SYNCHROTRON RADIATION MICRO-X-RAY DIFFRACTION (SR-μ-XRD)

The analysis of a small set of samples was undertaken by SR-μ-XRD. This technique follows the same chemical principles of μ-XRD, but it offers other possibilities for studying glazes: it allows the detection of very small crystallites and polymorphs down to 0.5 μm, as well as to determine their spatial distribution. This is possible due to the very small probe size and high brilliance of the method (Pradell *et al.*, 2010, 2013).

Analyses were performed in the Material Science Powder Diffraction (MSPD) beamline at the Spanish synchrotron ALBA-CELLS by Judit Molera and Trinitat Pradell. Small fragments (a few millimetres) of 8 samples from PNS, SCV and IVDJ collections were embedded in an epoxy resin and fixed onto a glass

microscope slide. Thin sections 30 µm thick were obtained by grinding by hand and samples were polished with 1-micron diamond paste in order to be studied under the petrographic microscope. Using a polished thin cut, it is possible to study the nature and spatial distribution of the crystalline compounds by microscopy and the same thin section is used for µ-Diffraction analyses. Micro-X-ray diffraction with synchrotron radiation (SR-µ-XRD) was performed using 0.0413 nm wavelength (30 keV), spot size of 20 µm × 20 µm and recorded using an SX165 Rayonix CCD detector.

CHAPTER 4

THE CERAMIC BODY

The ceramic body represents the first stage to produce architectural tiles. The preparation of the clay included soaking it in water, letting it settle and then leaving it maturing to gain plasticity. Archaeological findings in the Valencian region uncovered what it looks like soaking tanks. Clays would be used "pure" or mixed with other clays (Coll & Pérez, 1993).

In flat tiles, the ceramic body acts as a base on which the pictorial layer is applied and painted. In *arista*, *cuerda seca* and relief tiles, however, the ceramic body plays a fundamental role in the aesthetics of the pictorial layer, since the separation of the coloured glazes and the definition of the motifs is directly related to the quality of the mould print.

The ceramic body of Hispano-Moresque tiles measures between approximately 19 mm and 25 mm. In relief tiles from PNS collection, the thickness can be measured up to 35 mm. These tiles show two types of canted sides: one type which was made by hand after the final firing, characterised by an irregular surface; and another type with regular surfaces obtained directly from the mould. The latter often contains glaze run-offs, attesting that the ceramic body of the tile was moulded into its final shape before the glaze had been applied.

The tile sets under study exhibit some colour-related differences obvious to the naked eye, as *Figure 4.1* illustrates. In these Hispano-Moresque tiles, a range of colours can be observed, from light yellow to strong red. Other terms such as *cream* or *buff* have also been used in the literature to describe these light pink-yellow hues (Molera *et al*., 1996, 1997, 2001b; Pérez-Arantegui *et al*., 2005, 2009a; Tite, 2008), which represent the vast majority of the studied tiles.

PNS, SCV and IVDJ-S samples are mostly buff to light pink-coloured. In some samples, areas of both orange and light yellow coexist in the same tile and, if generally, a yellow area is present near the surface,

there are yellow areas also in the interior of the ceramic body. This is especially visible in MCV samples, although it can be observed in SCV and PNS tiles as well.

The colour of the ceramic body has been used as a macroscopic method for distinguishing between Sevillian and Toledan tiles, where light-coloured pastes are considered Sevillian and orange-coloured ones are attributed to Toledo. There are, however, 3 samples (IVDJ-S 3794, IVDJ-S 3919 and IVDJ-S 3601) that are attributed to Seville and exhibit a dark pink ceramic body. The differences observed in the colour of the ceramic bodies will be studied in this chapter.

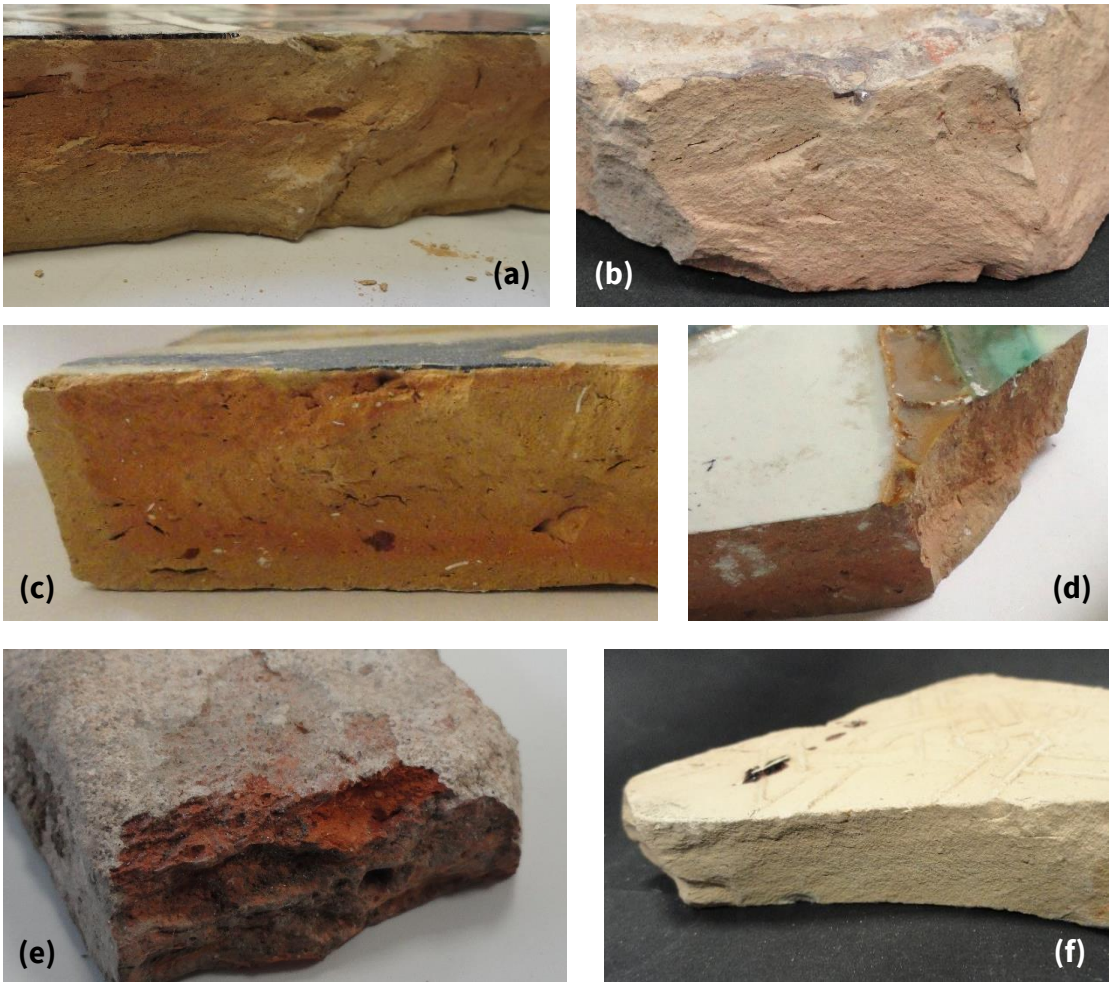

Figure 4.1. Ceramic bodies of samples **(a)** IVDJ-S SN, **(b)** PNS 31, **(c)** MCV 5.1R, **(d)** IVDJ-T 3683, **(e)** PNS 04, **(f)** SCV SPF8435

4.1. CHEMICAL CHARACTERISATION BY μ-PIXE

The results of the quantitative analysis performed by μ-PIXE on the ceramic body of the studied tiles are shown in *Table IV.1* (Appendix IV). Results indicate that calcareous[1] clays were the most used among the analysed tiles, which agrees with the literature on Islamic and Hispano-Moresque ceramics decorated with tin-opacified glazes (Coll & Pérez, 1993; Molera *et al*., 1996, 1997, 2001b; Pérez-Arantegui *et al*., 2005, 2009a; Polvorinos *et al*., 2011, among others). Calcareous clays were preferred for tin-glazed ceramics for several reasons: a) they provide a light-coloured background for the glaze, reducing the amount of tin necessary to achieve a white colour (tin was a relatively expensive material); b) the thermal expansion is compatible with the glaze, reducing production-related defects, such as crazing or shivering (Mason & Tite, 1997; Molera *et al*., 1998).

Figure 4.2 illustrates the average chemical composition obtained by μ-PIXE for the types of clays identified. Clays are considered as calcareous (C) when they contain more than 10 wt.% CaO and as non-calcareous (NC) when their CaO content is inferior to 5 wt.% (Tite 2008). Less calcareous clays (< 10 wt.% CaO – LC) were identified in four IVDJ tiles and non-calcareous clays (< 2 wt.% CaO) were found in two PNS samples and the two SAC tiles.

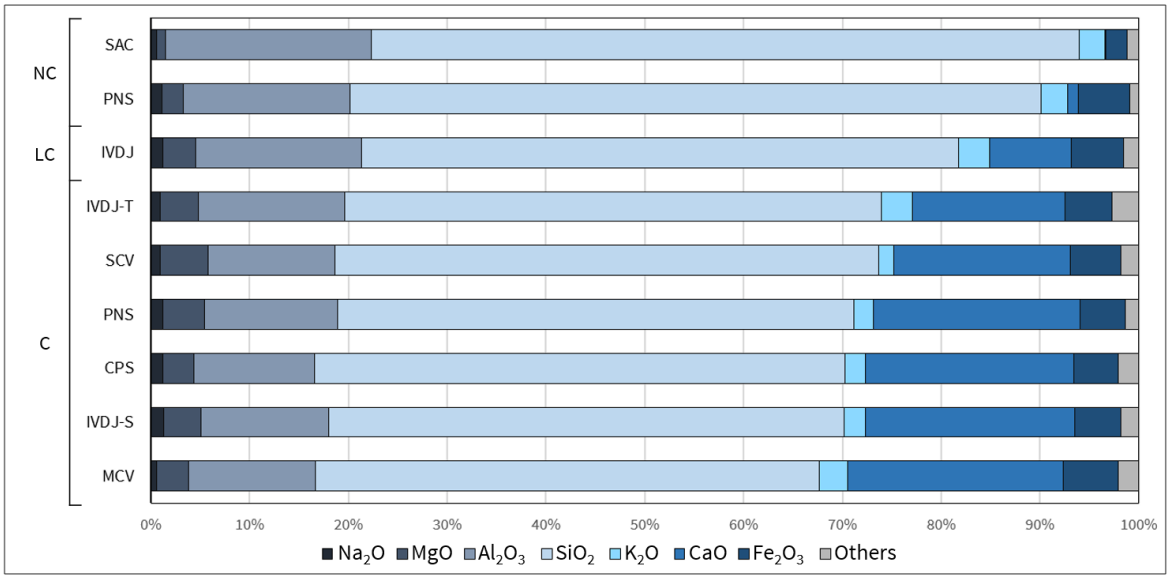

Figure 4.2. Average chemical composition of the ceramic body obtained by μ-PIXE. Results are divided by groups: *NC* non-calcareous, *LC* less calcareous, *C* calcareous. (MCV 10-3 was removed from the average for the MCV set due to its specific composition.)

The four non-calcareous shards show the highest SiO_2 contents (68-74 wt.%) and alumina contents higher than in most of the other tiles (15-23 wt.%), but they also show very different characteristics among

[1] In the English dictionary, the word for calcium-containing clays is *calciferous.* However, *calcareous* is the term currently used in the literature for clays with a CaO content above 5-10 wt.%. The term was introduced by Prof Michael Tite to distinguish ceramic bodies with fine and evenly-distributed $CaCO_3$ particles from other ceramic bodies with large $CaCO_3$ particles (> 2 mm) in the form of, i.e., limestone or shell. (Tite, personal communication)

themselves. PNS samples (PNS 03 and PNS 04) have a red ceramic body, whereas SAC01 and SAC02 exhibit a very light buff colour. The major difference contributing to the colour is the Fe_2O_3 content, which is considerably higher in the two PNS samples (> 4.5 wt.%) than in the SAC set (< 2.5 wt.%), as shown in *Figures 4.2* to *4.4*. Red-coloured ceramic bodies can be observed *in situ* in the National Palace of Sintra, e.g. in the *Sala das Pegas*, in several wall tiles where the glaze has detached.

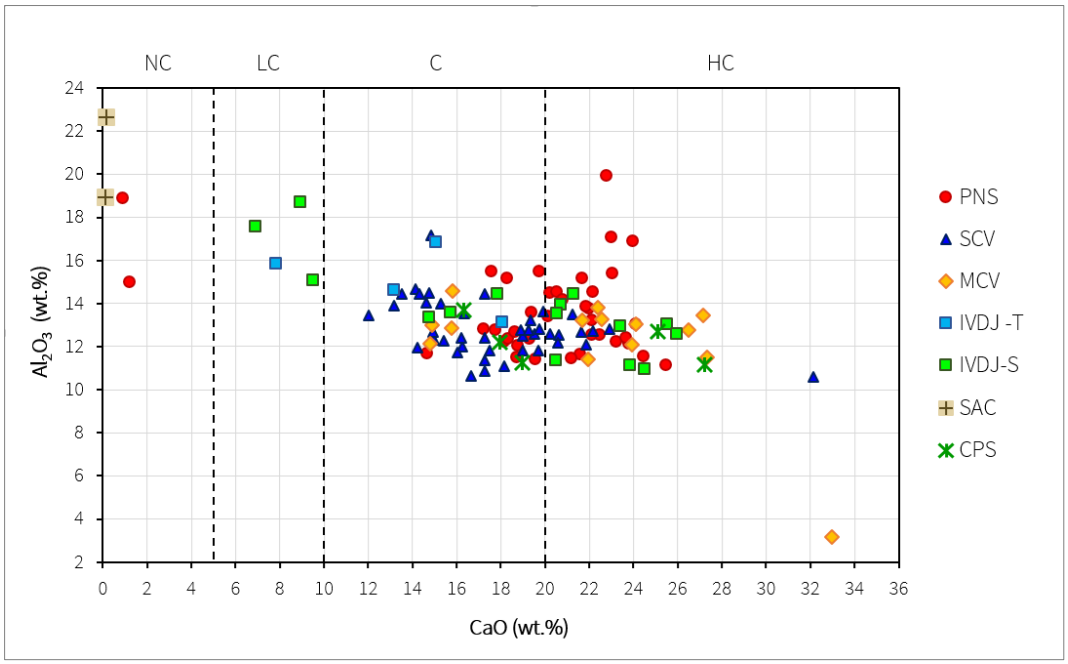

Figure 4.3. Plot CaO *vs* Al_2O_3 obtained from the µ-PIXE results. Classification of the ceramic body according to its CaO content: *NC* non-calcareous, *LC* less calcareous, *C* calcareous, *HC* high-calcareous.

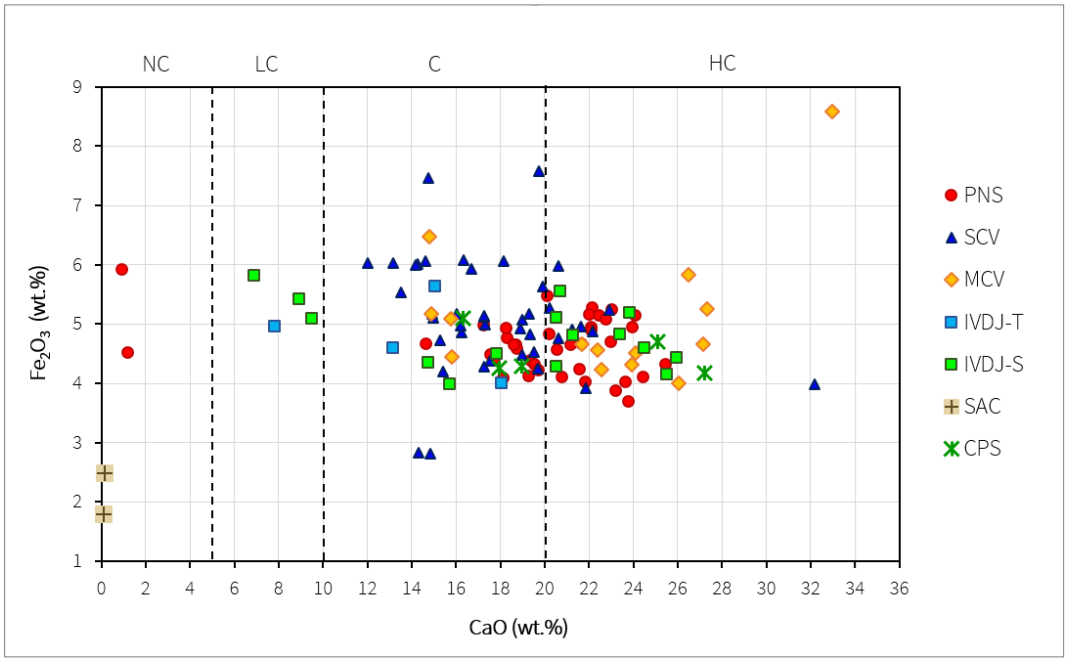

Figure 4.4. Plot CaO *vs* Fe_2O_3 obtained from the µ-PIXE results. Classification of the ceramic body according to its CaO content: *NC* non-calcareous, *LC* less calcareous, *C* calcareous, *HC* high-calcareous.

SAC samples are also very different in other aspects, and they exemplify a completely different production. Their lime content is almost null (< 0.20 wt.% CaO) and their SiO_2 and Al_2O_3 contents are the highest among all the studied samples. These results agree with the already published ones by Vieira Ferreira *et al*. (2014), who concluded that the ceramic body of the SAC tiles corresponds to the same clay used for the other lead-glazed ceramic shards found in the same kiln. It is not clear whether these tiles were a one-off manufacture for a specific location or a broader production. Identical tiles have been identified *in situ* in a church in Alhos Vedros, a town near the kiln site (Vieira Ferreira *et al*., 2014, 2015) and in another church in Azeitão (*ca*. 15 km away from the site) (Barros *et al.*, 2003). More differences concerning the glaze technology of the SAC tiles are discussed in *Chapter 5.2*.

The less-calcareous group is composed of three IVDJ-S and one IVDJ-T samples (*Figures 4.3* and *4.4*). All of them are red-coloured. Like the non-calcareous group, these four samples also show higher alumina and silica contents when compared to the majority of the tiles (15-19 wt.% Al_2O_3 and 56-62 wt.% SiO_2). Iron contents are also slightly higher (≥ 5 wt.%), although they fit well among the values for all the other samples. Sample IVDJ-S 3601 stands out for its higher magnesium content (5.7 wt.% MgO) and a lower value for silica (56 wt.% SiO_2) when compared with the other three tiles in this group.

The vast majority of the samples have calcareous bodies, with an average CaO content of 20 ± 4 wt.%. There is an apparently slightly negative correlation between the lime and the silica contents that is consistent with these compounds coming from different mineral phases – lime from calcite and silica from quartz (Rao *et al*., 2011). The fact that lime is not related to alumina either, along with the relatively high contents of the latter (> 10 wt.%), may be explained by the origin of those clays being related to the weathering of limestones (Walton & Tite, 2010).

The light colour range observed in the majority of the tiles is consistent with their calcareous nature, although the calcium content is not enough to explain the final shade of a ceramic object. Calcareous clays form calcium silicates that are able to incorporate the iron ions present in the mixture, resulting in fewer iron oxides that would otherwise contribute to reddish hues. These calcium silicates start to form at *ca.* 800 °C and, therefore, the firing temperature plays a fundamental role in the final colour (Fabbri *et al*., 2014; Molera *et al*., 1998; Padeletti & Fermo, 2010). Differences from pink to a yellow shade in ceramic shards with a similar composition may be explained by the firing temperature (lighter yellow shades for higher temperatures).

In general, the chemical composition of the calcareous bodies is similar among all the collections. The similarity between calcareous pastes from Valencian and Sevillian production centres has been noted before in analysis of lustre-decorated tin-opacified ceramics (Plovorinos del Rio & Castaing, 2010). Nevertheless, in *Figures 4.3* and *4.4* one can see small compositional differences among the collections, where the majority of SCV samples stands before the 20 wt.% CaO line, whereas the opposite happens with the MCV set. *Figure 4.2* also illustrates how the average lime content is lower in IVDJ-T and SCV assemblages. However, the variability of the CaO values is very high within each collection – for instance, the five CPS tiles can be divided into two groups with very different lime contents, one with CaO < 19 wt.% and the other with CaO > 25 wt.%. Considering this is a well-documented collection with a secure Sevillian

provenance – the tiles from Casa de Pilatos were ordered to the workshop of the Pulido brothers in Seville –, these compositional differences may then be considered as normal and do not allow for a distinction between collections. They can represent the use of different clays or clay mixtures in the several batches of tiles that were manufactured for each order.

MCV collection contains an average of 22.5 ±5.3 wt.% CaO, with only four samples whose CaO contents are below 20 wt.%. Such high CaO averages were also identified in SCV, PNS, IVDJ-S and CPS sets, although MCV is the highest. The MCV collection also displays the highest K_2O contents among the calcareous group (3 wt.%), although such values for this oxide have been frequently identified in Islamic and Hispano-Moresque tin-glazed ceramics from Spain (Molera *et al*., 1997a, 2001b; Pérez-Arantegui *et al*., 2005, 2009a).

When looking at the CaO contents observed in other studies on Islamic and Hispano-Moresque tin-glazed ceramics (Garofano *et al*., 2015; Molera *et al*, 1997, 2001b; Pérez-Arantegui *et al*., 2005, 2009a; among others), one can see that it is not very common to find values above 20 wt.% except for lustre-decorated ceramics from Manises (Polvorinos *et al*., 2011) or a group of calcareous 11th-15th-century ceramics found in the Alcazar Palace in Seville (Garofano *et al*., 2015). Data from later Sevillian productions have identified lower CaO contents (*ca.* 14 wt.%) in the ceramic shards (Iñañez 2007), except for lustre-decorated objects, where the average CaO content was *ca.* 22 wt.% (Polvorinos del Rio & Castaing, 2010). The chemical compositions of Hispano-Moresque ceramics found in the literature were gathered in Table I.1 (Appendix I).

Despite the relative homogeneity of the results for the calcareous bodies, there are samples that stand out in each collection:

Flat tiles MCV 10.1 (blue), MCV 10.2 (brown) and MCV 10.3 (white) exhibit homogeneous bodies with coarser clays. Results have shown that the brown and the blue-decorated tiles have identical bodies, but the white-glazed tile seems to have been produced with a different clay or mixture of clays. It has a lower SiO_2 and much lower Al_2O_3 content, and higher K_2O, Fe_2O_3 and much higher CaO contents. It is the MCV sample that appears further from the group in *Figures 4.3* and *4.4*. The glaze is also different (see Chapter 5 – *Glaze analysis*).

In PNS collection, besides the two non-calcareous shards, another sample stands out from the group – the relief tile PNS 30. This sample shows the highest Al_2O_3 value (20 wt.%) in this set and the lowest SiO_2 content (43 wt.%). Despite the fact that this is only one tile, other differences were identified regarding the glaze, supporting the possibility that it belongs in fact to a different production from the other relief tiles (see Chapter 5.3).

Finally, in SCV collection, shards SCV SPM8434 (*Figure 4.1f*) and SCV SPF8435 are placed very close together in *Figure 4.4*, with the lowest iron contents in SCV collection (< 3 wt.%). The ceramic body of these two tiles is very homogenous. These are unfinished arista tiles. SCV SPF8435 is the only glazed one and the glaze was applied on the back of the tile. These two samples seem different from the others, perhaps a later local production for the new Santa Clara monastery that was built in the

17th century. There is another SCV sample that stands out, but in this case with the highest CaO content (32 wt.%).

PbO was identified in the ceramic bodies of the tiles in small amounts (<1 wt.%). A possible explanation for the presence of PbO in the ceramic body arises from the reaction with the lead-rich glaze (Vendrel-Saz *et al*., 2006). SEM analyses have shown how lead diffuses from the glaze into the ceramic body (*Figure 4.5*); as a consequence, PbO content is related to the location from where the sample was taken – the nearer to the glaze, the higher is the PbO content. On the other hand, the possibility that lead was added to the ceramic paste cannot be discarded, as unglazed sample SCV SPM8434 contains 0.54 wt.% PbO.

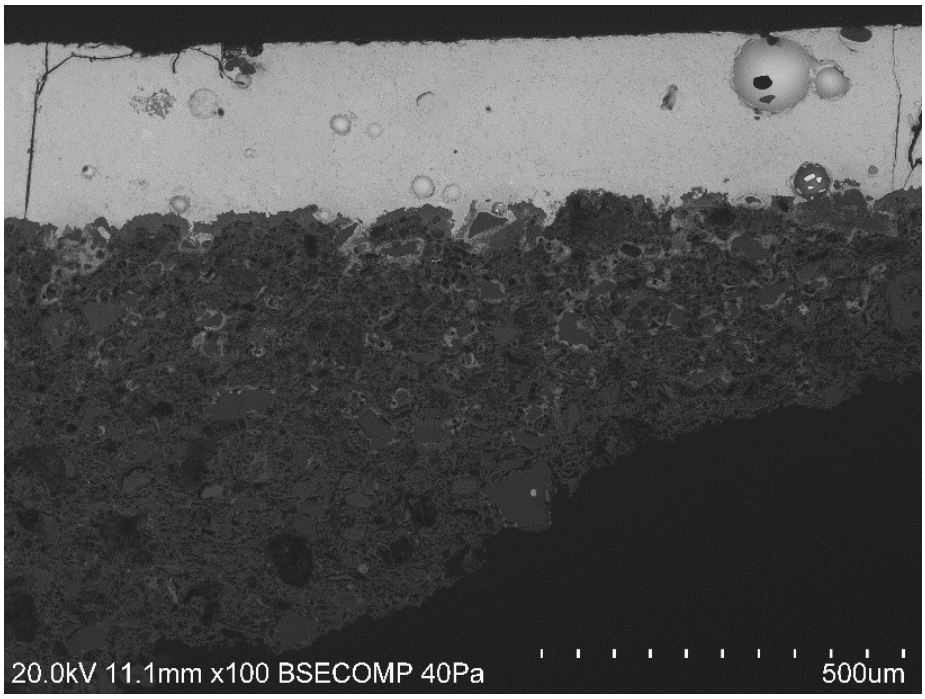

Figure 4.5. SEM (BSE) image of sample SCV 24Ci3386 (green glaze), where the diffusion of lead from the glaze into the ceramic body is well visible. The lighter areas in the body correspond to the presence of lead and become scarcer the further the distance from the interface.

The results of the chemical analysis of the ceramic bodies must be interpreted carefully, however, due to several factors that may affect them: the methodology and analytical techniques differ in each study reported in the literature; the archaeological context is known to influence the calcium content with the formation of secondary calcite (see *Chapter 4.2*); and finally, the literature does not mention architectural tiles, which may have been produced with Ca-rich clay mixtures and have other specific characteristics. Different treatments of the same clay can also lead to different chemical results (Tite, 2008). Furthermore, archaeological ceramics are subjected to other chemical alterations during burial, which must be considered when comparing groups of ceramic shards from different contexts. One frequent alteration process is the formation of analcime ($NaAlSi_2O_6 \cdot H_2O$), a common weathering compound of highly vitrified ceramic materials (*ca.* 1000 °C) in a wet environment (Pradell *et al*., 2010; Schwedt *et al*., 2006). The

formation of analcime results in higher Na_2O contents and lower K_2O and Rb because the latter two are leached from the ceramic object (Buxeda i Garrigós *et al*., 2002; Guirao *et al*., 2014; Schwedt *et al*., 2006). In this study, analcime has only been rarely identified in SCV tiles (Coentro *et al*., 2014) and their Na_2O contents fit within the values for the other collections, suggesting only small negligible alterations. Finally, the analysis of the chemical composition of the ceramic body of architectural tiles must take into account another issue, which is the lime mortar used to fix the tiles onto the walls. The mortar is always (at least partially) absorbed into the ceramic body of the tile and might influence the results of the chemical analyses (especially the calcium content), even when the samples are carefully washed. This is most important when comparing architectural tiles with other ceramic typologies. Unfortunately, there are no published data on this subject as far as we know, so this may be an interesting question to study in a near future. On the other hand, sample MCV M62 – an unglazed *arista* tile – contains one of the highest CaO contents (26 wt.%) measured in this group of tiles, which could not have come from the mortar, since this tile was not placed on a wall. The lime content in sample SCV SPM8434 (unglazed) is also perfectly consistent with the rest of the SCV group. To solve this question, it would be important to compare the CaO contents in more "unused" tiles found at kiln sites with the contents in other tiles in architectural contexts.

4.2. Mineralogical characterisation by μ-XRD and μ-Raman

The μ-XRD analysis identified quartz (SiO_2), calcite ($CaCO_3$), gehlenite ($Ca_2Al(AlSi)O_7$), diopside ($MgCaSi_2O_6$), hematite (Fe_2O_3) and plagioclase in PNS, SCV, IVDJ-S, CPS and MCV collections. It was not possible to precisely identify the plagioclase, although it is expected to be mostly anorthite $CaAl_2Si_2O_8$, considering that these are calcareous clays, or albite ($NaAlSi_3O_8$). Representative diffractrograms for each collection, as well as the semi-quantification results obtained from the diffractograms, are presented in Appendix VI.

The semi-quantitative analysis of the results (Appendix V) revealed that the most important mineral phases are quartz, gehlenite and calcite, followed by diopside, since they occur in practically all samples, whereas the hematite and plagioclase were not identified as frequently. These mineral phases are typical for calcareous clay, which is also consistent with the results from chemical analysis by μ-PIXE (Padeletti & Fermo, 2010).

The semi-quantification of calcite presents very different results, although its identification in archaeological ceramics must be considered carefully when comparing collections. Calcite may exist in the raw material (primary calcite) or it can be formed through chemical reactions that occur after firing (secondary calcite). During firing, the calcite grains in the ceramic object gradually decompose, releasing CO_2 and forming free lime (CaO). This reaction – the de-carbonation of calcite – usually takes place at 600-800 °C and it is expected that the complete decomposition of calcite occurs at 800-900 °C, depending on the size of the calcite grains, the duration of the firing and the atmosphere inside the kiln (Fabbri *et al*., 2014; Molera *et al*., 1997, 1998). Above 800 °C, Ca-silicates start to form, such as gehlenite ($Ca_2Al(AlSi)O_7$), diopside ($MgCaSi_2O_6$), and wollastonite ($CaSiO_3$), incorporating the calcium from the free lime (Fabbri *et*

al., 2014; Padeletti & Fermo, 2010, Molera *et al*., 1996, 1998; Trindade *et al*., 2009). The chemical reactions that normally occur in calcareous clays during firing are summarised in *Table 4.1*.

The identification of gehlenite and diopside in the studied samples allows estimating the firing temperature above 900 °C (Fabbri *et al*., 2014; Padeletti & Fermo, 2010, Molera *et al*., 1996, 1998; Trindade *et al*., 2009). However, the reported temperature range at which these mineral phases are formed varies among the literature on the subject, since it depends on the chemical composition of the raw clays and the firing cycle as well (Padeletti & Fermo, 2010).

Table 4.1. Chemical reactions in calcareous clays during firing (Fabbri *et al*., 2014; Padeletti & Fermo, 2010, Molera *et al*., 1996, 1998; Trindade *et al*., 2009).

	Reaction	Temperature
Decomposition of calcite	$CaCO_3 \rightarrow CaO + CO_2$	600-900 °C
Formation of gehlenite (Ge)	$SiO_2 + 2CaO + Al_2O_3 \rightarrow Ca_2Al_2SiO_7$ (Ge)	> 800 °C
Formation of wollastonite (Wo) and plagioclase (anorthite, An)	$2SiO_2$ (Qz) + $Ca_2Al_2SiO_7$ (Ge) $\rightarrow$ $\rightarrow$ $CaSiO_3$ (Wo) + $CaAl_2Si_2O_8$ (An)	> 800 °C

Considering the above-mentioned data, the calcite identified in the samples is most likely secondary. Secondary calcite may be reformed (re-carbonated calcite formed during cooling), precipitated (when it precipitates from solutions that enter the ceramic matrix during burial) or from alteration (when it forms from the alteration of Ca-minerals during burial, in particular from gehlenite) (Fabbri *et al*., 2014). Re-carbonation is promoted during cooling when enough free-lime is available because it did not react with the newly-formed silicates, which is frequent in very calcareous pastes (> 15 wt.% CaO) (Fabbri *et al*., 2014; Molera *et al*., 1997). Whereas reformed calcite or even the type obtained from alteration of gehlenite do not necessarily affect the calcium content of the ceramic object, precipitated calcite raises it and, therefore, it invalidates the comparison among ceramic groups in provenance studies based on the calcium content. Nevertheless, analytical data obtained from secondary calcite must always be used carefully.

When comparing the μ-XRD results obtained for each analysed collection, MCV samples show higher gehlenite contents, while plagioclase is scarcely detected. Since the formation of plagioclase from the reaction of gehlenite is promoted by high firing temperatures and longer firing times – and considering that the chemical composition of all collections is very similar – it is likely that MCV samples were fired at a lower temperature and/or with a shorter firing cycle than the ones used for the other collections (Padeletti & Fermo, 2010). Inversely, the highest plagioclase and diopside contents were reported for SCV samples, which suggest higher firing temperatures and longer firing times.

Ceramic bodies of IVDJ-T samples were analysed by Synchrotron Radiation μ-XRD and show similar results. Quartz, calcite, gehlenite, wollastonite, anorthite, diopside and hematite were identified. The

highest sensitivity of this technique allowed for identifying other phases that were not detected by μ-XRD, such as muscovite ($K_3Al_3Si_3O_{11}$), augite ($Ca(Mg,Fe,Al)(Si,Al)_2O_6$) and a Fe-rich diopside. Sanidine was identified only in the glaze-ceramic interface of the tiles, whereas orthoclase was identified throughout the body. The diffractograms from the Synchrotron μ-XRD analysis can be found in Appendix VI.

4.3. SUMMARY OF THE RESULTS

Three types of ceramic bodies were identified among the studied collections: calcareous (CaO > 10 wt.%), less calcareous (2 wt.% < CaO < 10 wt.%) and non-calcareous (CaO < 2 wt.%). The calcareous group represents the vast majority of the tiles, as *Figure 4.6* illustrates.

Calcareous pastes show high lime contents (20±4 wt.% CaO), even when compared with other calcareous tin-glazed ceramics from the literature. Four samples (PNS03, PNS04, SAC01 and SAC02) are non-calcareous, all of them with very high SiO_2 and Al_2O_3 contents. The non-calcareous group contains two red paste samples (PNS) and two light-buff samples (SAC), differing on the Fe_2O_3 content which is very low in the light coloured tiles. Another four samples were considered as less calcareous because of the lime content below 10 wt.%. These are one IVDJ-T and three IVDJ-S tiles with red-coloured ceramic bodies.

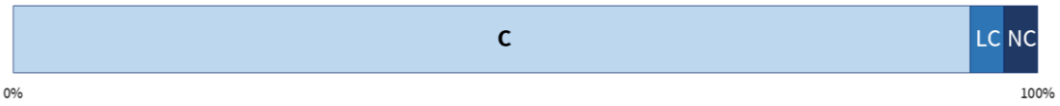

Figure 4.6. Clay types represented as percentages: C (calcareous – 122 samples), LC (less calcareous – 4 samples), NC (non-calcareous – 4 samples).

The most important mineral phases identified in the ceramic bodies were quartz, calcite, gehlenite, diopside, hematite and plagioclase (likely anorthite). The firing temperature was estimated between 900 °C and 1000 °C although the almost total absence of wollastonite in the body suggests a temperature closer to 900 °C.

The chemical composition of the calcareous clays is very similar among all the studied collections and no major differences were identified. However, the set of tiles with a Valencian provenance (MCV) are the ones that stand out the most for their higher CaO contents, as well as the stronger presence of gehlenite when compared to the other collections.

CHAPTER 5

GLAZES AND COLOURS

The main results of the chemical, mineralogical and morphological characterisation of the glazes are discussed in this chapter. Several common characteristics were observed in all the tiles, thus a first approach to the results is taken considering the aspects that will be transversal to all the techniques and colours. A more in-depth discussion follows, with the results presented according to the type of tile and decoration: *arista* and *cuerda seca* are discussed together, followed by flat monochrome tiles; reliefs and tiles with underglaze and/or lustre decoration are discussed separately. Finally, the LA-ICP-MS results are discussed with all analysed samples, regardless of their typology, since the aim is to compare all the minor and trace elements in glaze composition.

The large majority of the studied samples comprises *arista* and *cuerda seca* tiles, whose correspondent results are presented together due to the similarities between the glaze recipes used in both techniques, as identified during the course of this work. The glazes used in *cuerda seca* and in *arista* tiles were applied in specific areas delimited by a physical barrier, either a groove filled with a greasy substance and manganese oxide (in *cuerda seca*) or a protruding "wall" (in *arista*). Therefore, the discussion of the results is separated by glaze colour in order to study and compare the glaze formulations used in each collection. In the same way, the results obtained from the analysis of flat monochrome tiles are discussed together with *cuerda seca* and *arista* ones, according to their colour.

Relief polychrome tiles are the most original set in the Hispano-Moresque tile context and, therefore, they are analysed separately. Underglaze-decorated tiles refer to blue-and-white glazes in which the blue decoration has been applied under the white glaze. Some samples also present manganese-brown or lustre along with the blue decoration. This type of decoration is characteristic of Valencian *rajolas*, but it was identified in Sevillian-attributed IVDJ samples and in the SCV collection as well. The number of samples studied and their typology is indicated in *Table 5.1*.

Table 5.1. Number of tiles by typology in each collection.

	Arista	*Cuerda seca*	Relief	Underglaze	Flat	*Total*
SCV	30	9	2	4	2	47
PNS	6	9	19	-	5	39
SAC	2	-	-	-	-	2
IVDJ-T	4	1	-	-	-	5
IVDJ-S	5	8	1	2	-	16
CPS	5	-	-	-	-	5
MCV	3	-	-	8	6	17

5.1. GENERAL RESULTS: CHEMICAL COMPOSITION, MORPHOLOGY AND COLOUR PALETTE

Hispano-Moresque tiles were produced with high-lead glazes, following the Islamic technology that was implemented in the Iberian Peninsula and used for all types of ceramic objects. Lead glazes were used in all the samples studied, regardless of the colour or decoration technique.

The use of lead glazes is believed to have started in the Roman Empire or in China, between the 1st century BC and the 1st century AD, and then spread to Europe and the Middle East. They were used profusely in the Islamic Empire, which included the Iberian Peninsula, and throughout Medieval Europe (Carvalho *et al*., 2016; Gradmann *et al*., 2015; Holakooei *et al*., 2013; Molera *et al*., 1997a, 1997b; Tite *et al*., 1998; Walton & Tite, 2010). Lead works in the glassy matrix as a flux, a stabiliser and a network former. This happens because lead is present both as Pb^{2+} and Pb^{4+}, the latter being able to form $[PbO_4]$ coordinations (Navarro, 2003). Lead also presents the advantages of less susceptibility to glaze defects, such as crazing or crawling, and a higher glaze brilliance (Tite *et al*., 1998). Nevertheless, alkaline glazes were usually used alongside with lead glazes, except in the Iberian Peninsula, where archaeological excavations of Islamic and Hispano-Moresque workshops have only identified the lead type (Molera *et al*., 1997a, 1997b, 2009; Paynter *et al*., 2004; Pérez-Arantegui *et al*., 2005, 2009a). The large availability of galena (PbS) in the Iberian region is appointed as one of the major factors for this (Trindade, 2007).

Silica (SiO_2) and lead oxide (PbO) are the major constituents of the glazes making up to 90 wt.% of the total composition. They show an inverse correlation (*Figure 5.1*), with higher SiO_2/PbO ratios for tin-opacified glazes (mostly white and blue ones). The decrease in PbO is compensated by a higher Na_2O content as a fluxing agent in tin-opacified glazes (*see Chapter 5.2.1*). Potassium, unlike sodium, is present in variable amounts both in transparent and in tin-opacified glazes, with no definite correlation with the major components.

Some compounds such as Na_2O, MgO, Al_2O_3, CaO, K_2O, TiO_2 and Fe_2O_3 are present in all colours, probably related to the raw materials, e.g. sand used as a source of silica, but they can also enter the glaze composition during firing through the reaction with the ceramic body (Molera *et al*., 1997a, 1997b). The

content of such compounds in the glaze can, therefore, be influenced by the production technique (e.g. number of firings, firing temperature and type of raw materials used). Sodium, magnesium, aluminium, calcium and potassium oxides – whether intentionally added or not – act as fluxes, lowering the melting temperature of the glaze (Molera *et al*., 1999).

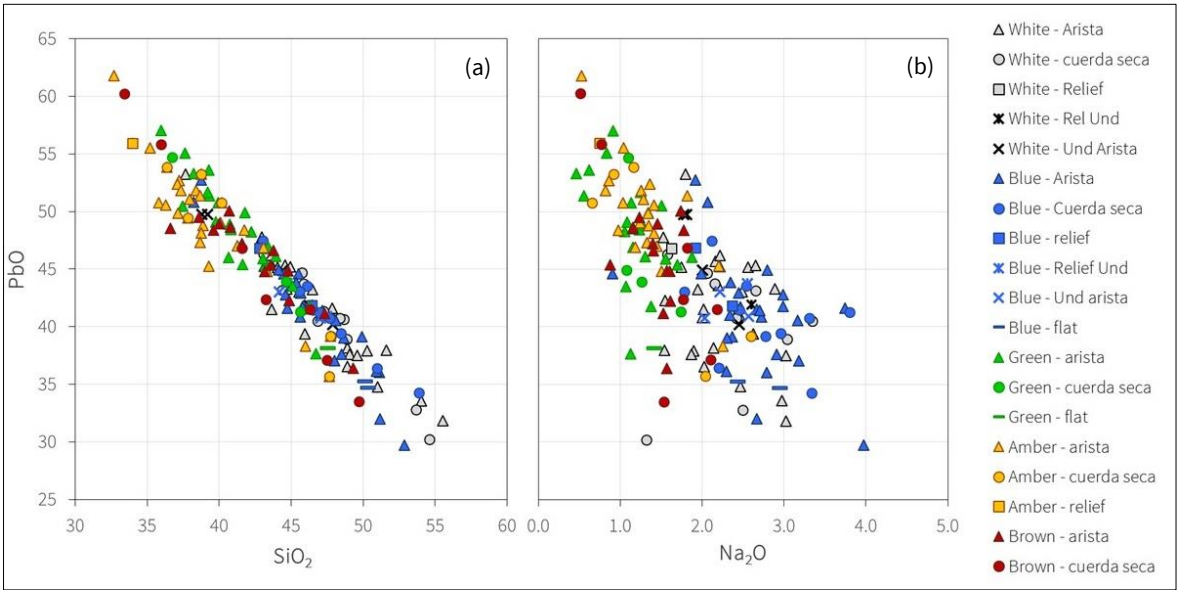

Figure 5.1. Scatter plots SiO_2 *vs*. PbO **(a)** and Na_2O *vs*. PbO **(b)** for SCV collection, where white and blue glazes (tin-opacified colours) show higher SiO_2, higher Na_2O and lower PbO contents.

All samples in this study were decorated with glazes of the same five colours – white, blue, green, amber and brown – which look similar by visual inspection amongst all groups. However, different shades were identified and will be discussed separately for each colour.

Microprobe PIXE X-ray mapping and point analysis showed the occurrence of elemental distributions of Sn, Co, Cu, Fe and Mn in tight correlation with the glaze colours: white (SnO_2), blue (SnO_2 and CoO), green (CuO), amber (Fe_2O_3) and brown (MnO). The chromophores in Hispano-Moresque glazes are usually dissolved in the glaze matrix – the exception is cassiterite (SnO_2) – and thus colour-related mineral inclusions are hard to find. Even rarer are traces of raw materials related to the colours. However, due to insufficient grinding or to reactions occurred during firing, some colour-related mineral inclusions were identified by μ-Raman and SEM-EDS.

The chemical composition of the majority of glazes (namely in *arista* and *cuerda seca* tiles) can be divided into two groups according to their SnO_2 content (*Figure 5.2*), with blue and white glazes having higher SnO_2 contents on one side (*ca.* > 5 wt.%), and most green, amber and brown glazes with lower values (< 2 wt.% SnO_2). However, there are exceptions in the IVDJ and, in particular, the PNS collection, namely with some green and brown glazes having higher SnO_2 content.

The presence of SnO_2 in yellow, green and black glazes was somewhat unexpected since these are mostly transparent. However, small amounts of tin oxide have been identified in such glazes in 10^{th}-12^{th} century Islamic *cuerda-seca* ceramics from Spain and Portugal by Chapoulie *et al*., (2005). It is possible that the

small amounts of tin could be intentionally added to increase the compatibility between the different glazes and preventing the transparent ones from spreading (Chapoulie *et al*., 2005; Padeletti & Fermo, 2010).

Considering their morphology, Hispano-Moresque glazes are generally homogenous. Gas bubbles and mineral inclusions usually formed in the glaze-ceramic interface are scarce throughout the glaze thickness. *Figure 5.3* illustrates two typical glazes. In *cuerda seca* sample PNS19 (*Figure 5.3a*), the glaze is very homogenous like most of the analysed glazes in this collection, with K-rich crystals formed in the interface. The glaze-ceramic interface is not regular, showing the glaze entering the ceramic body in several areas. *Arista* sample CPS01 (*Figure 5.3b*) shows a blue glaze with bubbles and mineral inclusions, which is less common but still visible in several studied samples. However, in the same tile and even in the same glaze, both homogeneous and less homogeneous areas (e.g. with bubbles and/or small inclusions) can be observed.

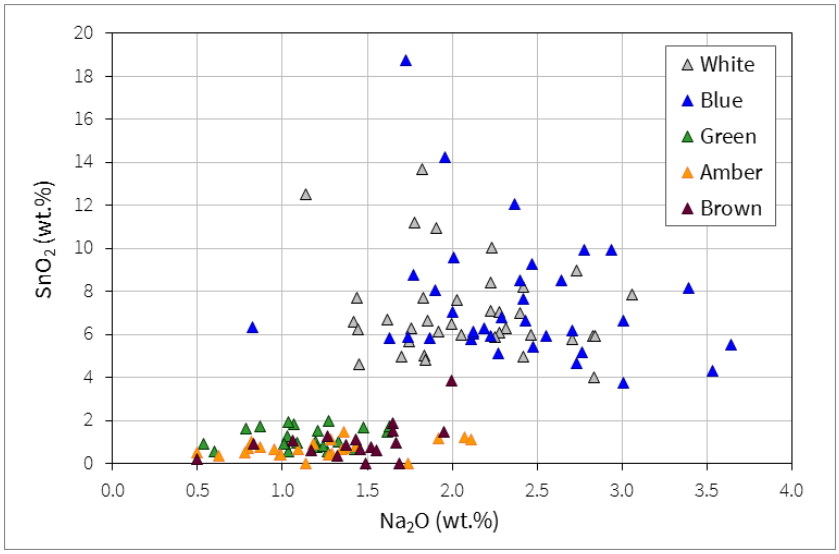

Figure 5.2. Scatter plot of Na_2O *vs.* SnO_2 obtained from μ-PIXE analysis of SCV *arista* and *cuerda seca* glazes, showing higher Na_2O and SnO_2 contents in tin-opacified glazes (blue and white).

Bubbles appear in glazes when trapped gas that was formed during firing (or already existed in the raw material) cannot reach the surface. This gas can have several different sources – it could be present in the glaze raw material, as well as in the ceramic body; or it could result from reactions occurred during firing, such as organic matter decomposing or volatiles being released (e.g. water molecules, sulphates or carbonates). A gas bubble in the glaze tends to travel to the surface and this is more likely to happen when bubbles are larger and the glaze melt is less viscous. Glazes without bubbles may indicate high temperatures and/or long firing times, or that frits were used (Pradell *et al*, 2010).

A frit is ground glaze or glass. It can be used for part or for the total recipe. Frits show several advantages over raw glaze mixtures: they eliminate water-soluble compounds (e.g. chlorides) that could crystallise on the glaze surface, as well as interfere with the fluidity of the suspension when applying the glaze on the object; they avoid the release of gas bubbles (that could be trapped in the glaze) from carbonates and

sulphates, since these have been previously calcined; finally, they increase the control over temperature and final result of the glaze, by reducing the necessary firing time (Molera *et al*, 1997a). Frits, therefore, provide superior compositional and structural homogeneity of the glazes by being closer to the final composition sought and less prone to production defects. To make a frit, the molten glaze is poured into cold water, which shatters it into millions of fragments that are ground afterwards. Abu l'Qasim describes the noise that results from pouring the glaze melt in cold water: *"When water and fire meet there is a great noise and roaring like thunder, which for all the world could be real thunder and lightning, such that everyone who has not seen it and hears the noise falls on his knees shuddering and trembling"* (Allan, 1973).

The mineral inclusions observed in the glaze (excluding the interface) are essentially K-feldspars (general formula $KAlSi_3O_8$) or quartz (SiO_2). They are scarce and small, but there are exceptions where mineral inclusions with large dimensions were consistently observed (see e.g. Toledo-attributed tiles in *Chapter 5.2*).

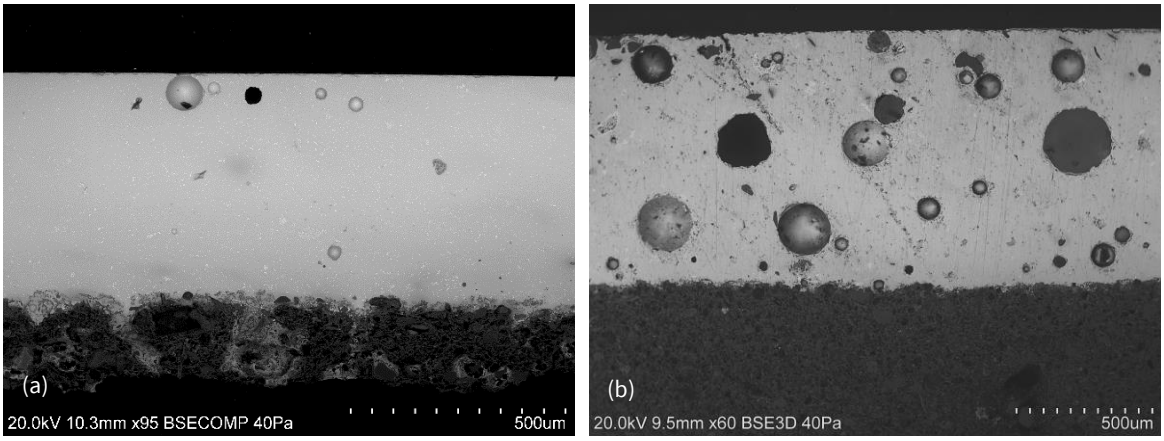

Figure 5.3. SEM images illustrating different glaze morphologies: **(a)** homogeneous glaze (PNS 19 white); **(b)** glaze with some small inclusions and gas bubbles (CPS blue).

The thickness and composition of the interface between the glaze and the ceramic body have been shown to give information on the production technology: the number of firings influences the interface thickness between lead glazes and calcareous bodies, as single fired ceramics present much thicker interfaces. According to Molera *et al*. (2001a), a single fired object will present thicker interfaces (>30 μm) than a double fired one (*ca.* 10 μm), due to the reaction between glaze and ceramic body, which is stronger when the latter is unfired. Studies on Islamic and Hispano-Moresque lead-glazed ceramics have indicated that a double-firing process was used in Islamic workshops, but it was progressively abandoned in Hispano-Moresque ones, as suggested by the study of 14th-15th-century ceramic fragments from workshops in Paterna (Molera *et al*., 1997). However, Hispano-Moresque tin-glazed ceramics from Teruel, Spain, and also every coeval lustre-decorated ceramics from several Iberian production centres exhibit thinner interfaces (<10 μm), consistent with a continuity of a double-firing process (Molera 1997, 2001a; Pérez-Arantegui *et al*., 2005, 2009b).

Figure 5.4 illustrates the typical glaze-ceramic interfaces found in tin-opacified and in transparent glazes. The interface thickness is considered here as that of the layer with mineral inclusions that results from

the reaction between the glaze and the ceramic body of the tile. In the particular case of analysed tiles, thicker interfaces (up to 100 μm) are visible in non-opacified glazes in all collections – especially brown and amber glazes –, with a larger number of crystals that become more dispersed the further the distance from the ceramic body. When there is a stronger reaction between the glaze and the ceramic body, it originates a large number of small mineral inclusions that are spread through the glaze until reaching the surface. However, the results do not allow for determining whether one or two firings took place, as more data is needed for tin-glazed ceramics. It is also possible that the ceramic body was previously fired at a low temperature or that a slip was used to increase the adherence of the glaze onto the ceramic substrate, although no indication of the latter was observed by SEM.

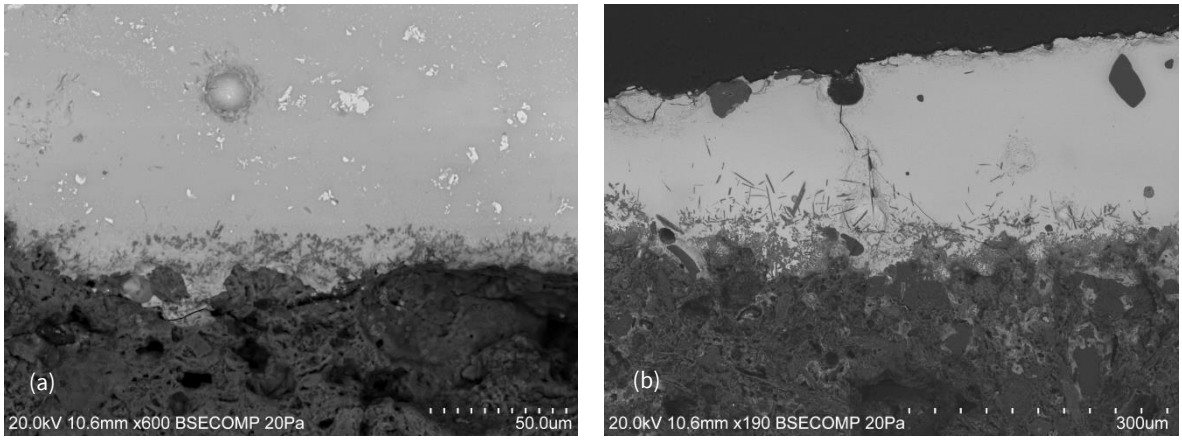

Figure 5.4. BSE cross-section images illustrating typical glaze-ceramic interfaces: (a) tin-opacified turquoise (IVDJ-S 3561); (b) transparent brown (IVDJ-S 4127).

Both regular (*Figure 5.3b*) and irregular (*Figure 5.4b*) interfaces were observed unrelated to a specific type of glaze or decoration technique. The morphology and thickness of the glaze-ceramic interface depend largely on the formation of crystalline phases – the quantity and size of the crystals, as well as their spread throughout the glaze into the surface – and the formation of gas bubbles, which may leave "imprints" or depressions in the ceramic body. The formation of these crystalline phases in the glaze-ceramic interface aids the opacification and contributes to the adhesion between the glaze and the ceramic body, which is exceptional in these samples when compared, e.g., to majolica tiles. The latter show a clear separation between the glaze and the ceramic body in SEM images (Coentro *et al*., 2012), while glaze detachment is their main conservation problem.

In fact, the conservation state of most Hispano-Moresque tiles is very good, especially considering that SCV tiles were submerged for centuries. A recent study by Costa *et al.* (2014) has suggested that glaze detachment is more related to the volume and pore size of the ceramic body than to the thickness of the glaze/ceramic interface. On the other hand, it is likely that a combination of factors contribute to the good adhesion of the glaze to the ceramic body of Hispano-Moresque tiles besides the thick interface, such as the division of the glaze in small areas, which facilitates the compatibility between the materials and their expansion/contraction indexes, avoiding crazing and detachment, as well as the porous physical barrier in *cuerda seca* and *arista* tiles, which allows water circulation and thus avoids salt crystallization between

the glaze and ceramic body. However, these are just hypothesis and, therefore, a proper scientific study is needed to access the degradation process of such tiles.

Chemical and phase analysis of the mineral inclusions in the interface by SEM-EDS and μ-Raman revealed that it is mostly constituted of K-feldspars (orthoclase and microcline, $KAlSi_3O_8$) and, in some cases, of diopside ($CaMgSi_2O_6$) and wollastonite ($CaSiO_3$) crystals as well. Through μ-Raman analysis, quartz (SiO_2), anatase (TiO_2), rutile (TiO_2) and sodium feldspars (albite $NaAlSi_3O_8$) were also identified, although they are much less common. These spectra can be found in *Appendix VI*.

The presence of diopside in the glaze-ceramic interface indicates firing temperatures above 900 ºC when it is formed, most likely as a reaction product from magnesium-rich minerals, such as dolomite ($CaMg(CO_3)_2$) and silicates. The identification of rutile could be an indicator of still higher firing temperature (>1000 ºC), but it is known that it could also be related to the raw clay material. Therefore, it should not be used here as a temperature marker (Ricciardi 2008).

Feldspars undergo transformations when heated, resulting in new phases such as sanidine $K(AlSi_3O_8)$ and leucite $K(AlSi_2O_6)$ (Tarvornpanich *et al.,* 2008a). The formation of new phases of K-feldspars in the glaze-ceramic contact zone has been documented in Hispano-Moresque ceramics as a consequence of the reaction between already-existent potassium feldspars in the ceramic body and the lead glaze. Two types of K-feldspars were identified by Molera *et al*. (1993) – small euhedral crystals formed near the glaze-ceramic interface and large K-feldspar particles surrounded by developing crystals, both observed in Hispano-Moresque tiles as well (*Figure 5.5*). Sanidine crystals can incorporate Pb ions in their structure in substitution of potassium, in a reaction between lead-rich glazes and potassium-rich ceramic bodies promoted by high temperatures (800 °C – 1000 °C) (Molera *et al*., 1993; Pradell *et al*., 2010). The euhedral morphology observed in *Figure 5.5b* indicates that these crystals are formed during the melting of the glaze and their growth is also promoted by a slow cooling process. K-feldspars were extensively identified by μ-Raman in the glaze-ceramic interface of the tiles, but the specific spectrum of sanidine was much rarer (*Figure 5.6*). Sanidine forms at higher temperatures than orthoclase and with faster cooling rates, resulting in a less ordered crystal structure, although almost identical and thus very hard to differentiate by μ-Raman (Freeman *et al*., 2008).

The identification of K-feldspars in the glaze-ceramic interface is by far the most common result obtained by μ-Raman in all the analysed tiles (*Figure 5.6*). The spectra often show variations in the bands that do not allow for determining the specific K-feldspar. On the other hand, the transformations that occur during the firing and cooling of the tiles, as previously explained, result in intermediate phases and ion substitutions that are very difficult to differentiate by μ-Raman. Spectra consistent with microcline is mostly obtained in larger K-feldspar crystals, such as the one in *Figure 5.5a*, when it is possible to point the laser at the centre of the crystal where it did not react with the glaze around it. The spectrum of the orthoclase is the most frequent one, whereas sanidine is rarer, probably because the crystals are very small and spectra are harder to obtain. From microcline to sanidine, *Figure 5.6* illustrates how the number of bands becomes lower because of the less ordered structure of the crystal (Freeman *et al*., 2008).

Synchrotron μ-XRD analysis allowed for the identification of K-Pb-sanidine in the glaze-ceramic interface of samples IVDJ 3944, IVDJ-S 3561, IVDJ-S XV and PNS 16. Lead was also identified in a lead-aluminium

silicate ($PbAl_2Si_2O_8$). It is expected that lead reacts with silicates in the glaze and the ceramic body of the tiles, due to the high contents of this element in the glaze composition. The diffractograms from the Synchrotron μ-XRD analysis can be found in *Appendix IX*.

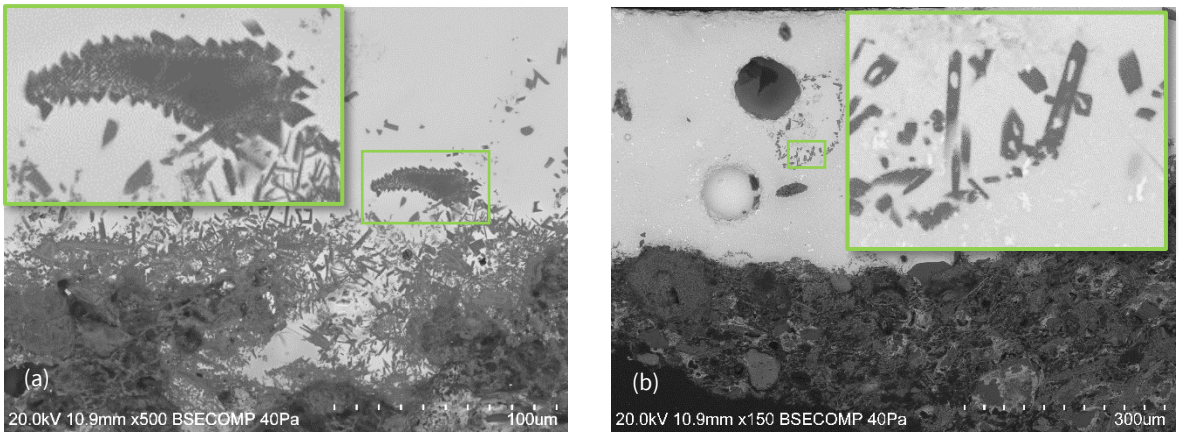

Figure 5.5. SEM images of sanidine: **(a)** developing crystals growing around a large K-feldspar grain (PNS26 – green); **(b)** euhedral crystals formed in the glaze melt (PNS26 - white).

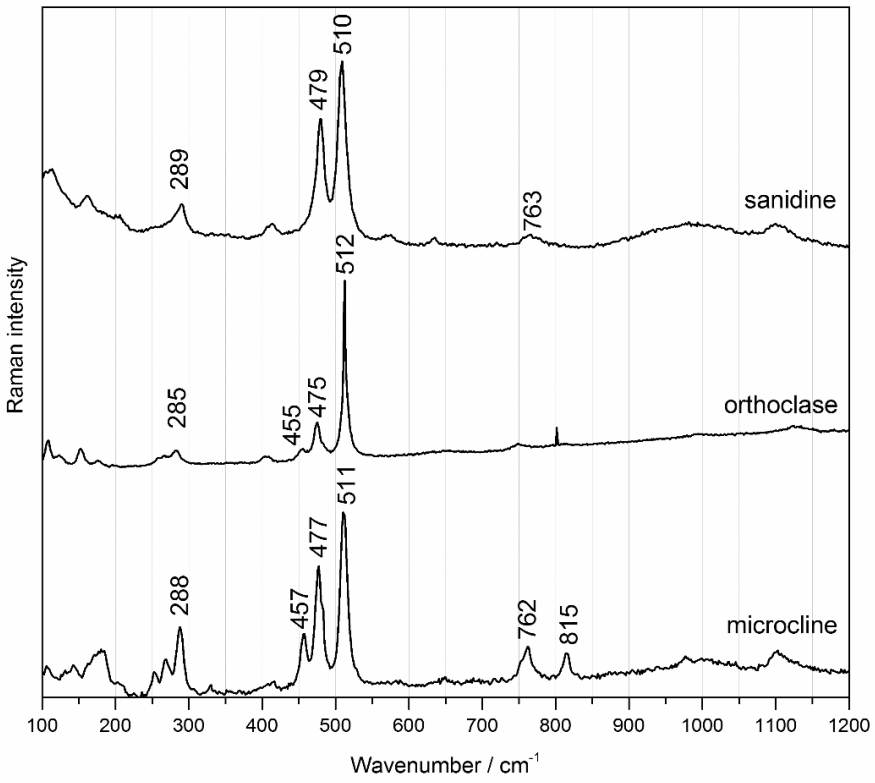

Figure 5.6. μ-Raman spectra of K-feldspars identified in the glaze-ceramic interface of three analysed Hispano-Moresque tiles, according to the distinction made by Freeman *et al*. (2008): microcline (PNS 26 – white glaze), orthoclase (PNS 02 – green glaze) and sanidine (PNS 03 – green glaze).

5.2. *CUERDA SECA* AND *ARISTA* TILES

Cuerda seca and *arista* tiles were massively produced in the Iberian Peninsula during the 15th and the first half of the 16th centuries. The *cuerda seca* technique was well known in Islamic ceramics as a method for separating different coloured glazes. The resulting dark line served as a contour and provided its own aesthetical importance, resembling the cloisonné technique used on metals or the lead came in stained glass. *Cuerda seca* tiles eventually evolved to mould production with the grooves being marked with moulds instead of manually drawn. The protuberances used as walls for the *cuerda seca* grooves eventually rendered the *cuerda seca* line unnecessary for separating the colours. Finally, only one protuberant line was impressed on the tiles, in a similar process to the one used in medieval monochromatic floor tiles in Northern Europe, although only in this case used for separating different coloured glazes.

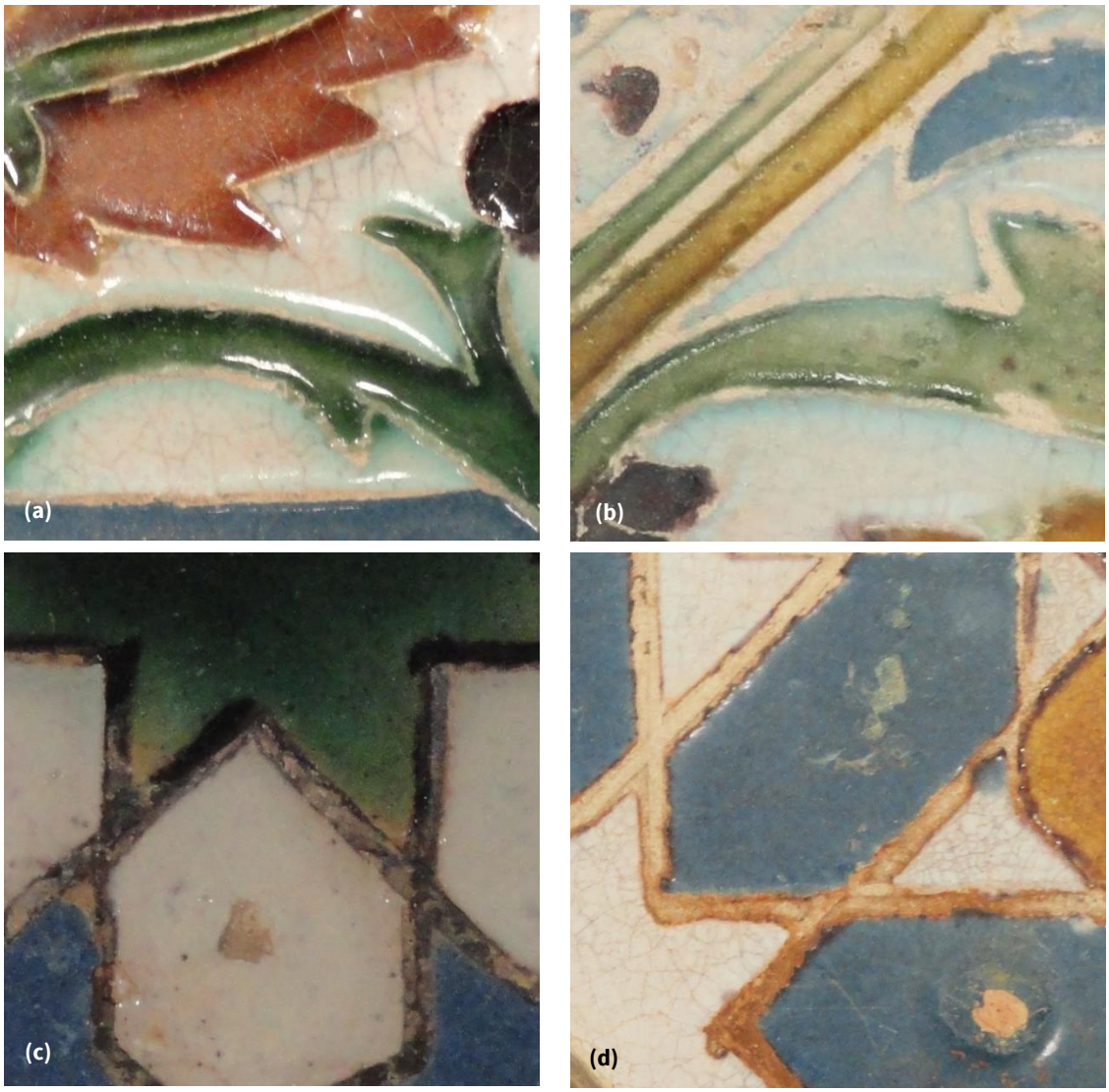

Figure 5.7. Details of *arista* and cuerda tile: (a) *arista* in a good conservation state (SCV 10Bi1673) and (b) *arista* worn out (SCV 9i1469); (c) *cuerda seca* in a good conservation state (PNS 23) and (d) *cuerda seca* worn out (SCV 27Ai7744).

In worn out tiles, the distinction between *arista* and *cuerda seca* tiles can be challenging, because the *cuerda seca* brown line sometimes disappears, as does the *arista* relief, both resulting in a line of similar colour as the ceramic body's (*Figure 5.7*). However, the *cuerda seca* can often be identified by the spreading of manganese brown onto the other colours (*Figure 5.7d*).

The evolution from *cuerda seca* to *arista* is also visible in BSE images. *Figure 5.8a* shows an example where the *cuerda seca* groove is visible in cross section, although the white glaze has spread onto the manganese line. *Figure 5.8b*, on the other hand, shows very well separated glazes in an *arista* tile. Despite *cuerda seca* having been progressively replaced by *arista*, these two techniques coexisted during the first decades of the 16th century and the glaze colours are the same. Therefore, the results concerning these tiles are presented together.

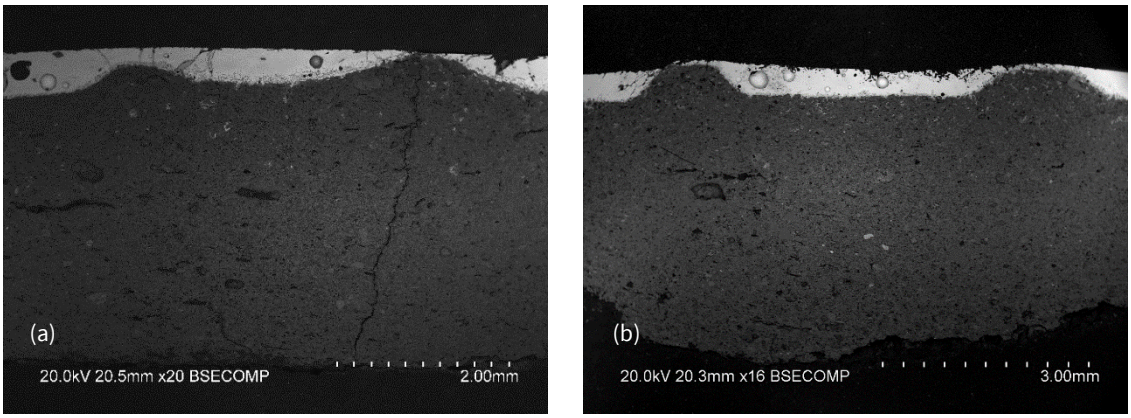

Figure 5.8. BSE cross-section images of (a) *cuerda seca* SCV 45M4260, with the groove in the centre filled with glaze; (b) *arista* SCV 10EF175 with well-defined relief "walls" separating the different glazes.

5.2.1. WHITE GLAZES

White glazes owe their opacity to small agglomerates of tin oxide particles (cassiterite, SnO_2), which scatter the incident light. These SnO_2 particles precipitate in the glaze during firing and can form agglomerates of different sizes which can be distributed throughout the glaze in different degrees of homogeneity (Vendrell *et al*., 2000). Tin oxide crystals were consistently identified in opaque glazes by μ-Raman, with the characteristic strong band at 633 cm^{-1} (see *Appendix VI*). Through SEM analysis (Figure 5.9), SnO_2 is easily observed as very small white spots in BSE images, suggesting the use of glaze frits.

Tin oxide is the third major component of white glazes (4-14 wt.% SnO_2), following SiO_2 (35-48 wt.%) and PbO (33-50 wt.%). As *Figure 5.1a* had shown, higher SiO_2 and lower PbO contents are found in white and blue than in the other – not tin-opacified – coloured glazes.

As previously described in *Chapter 1.4*, there is no exact knowledge on the recipe used for making tin glazes. The ceramic treatises by Abu l'Qasim (Persia, 1301) and Cipriano Piccolpasso (Italy, *ca.* 1557) mention a lead-tin calx made from calcining lead and tin together prior to its addition to the glaze frit (Allan, 1973; Piccolpasso, 1980). The analysis of archaeological findings that included glaze wastes from kiln sites do not confirm nor deny this step in the recipe since only mixtures of the final glaze frit were

found but without any evidence of a previously prepared lead-tin calx (Molera *et al*., 2009; Paynter *et al.*, 2004). However – and in accordance with the findings by Molera *et al*. (2009) – our results do not suggest that lead and tin were calcined together before being incorporated into the glaze mixture either since there is no apparent correlation between PbO and SnO_2.

The PbO content in tin-opacified glazes is lower than in transparent ones, but it is compensated by a higher Na_2O content (mostly between 1.5 wt.% and 3 wt.%, whereas in transparent glazes it rarely surpasses 1.8 wt.%). *Figure 5.2*, using SCV collection as an example, illustrated how high SnO_2 contents are related to higher Na_2O values, showing a clear division between opaque and transparent glazes based on these oxides. When comparing collections (*Figure 5.10*), IVDJ-T shows the lowest Na_2O contents (0.7-1 wt.%), followed by MCV tiles (1.2-1.6 wt.%). On the opposite side, *arista* PNS white glazes show the highest values as a group (2.5-2.8 wt.% Na_2O).

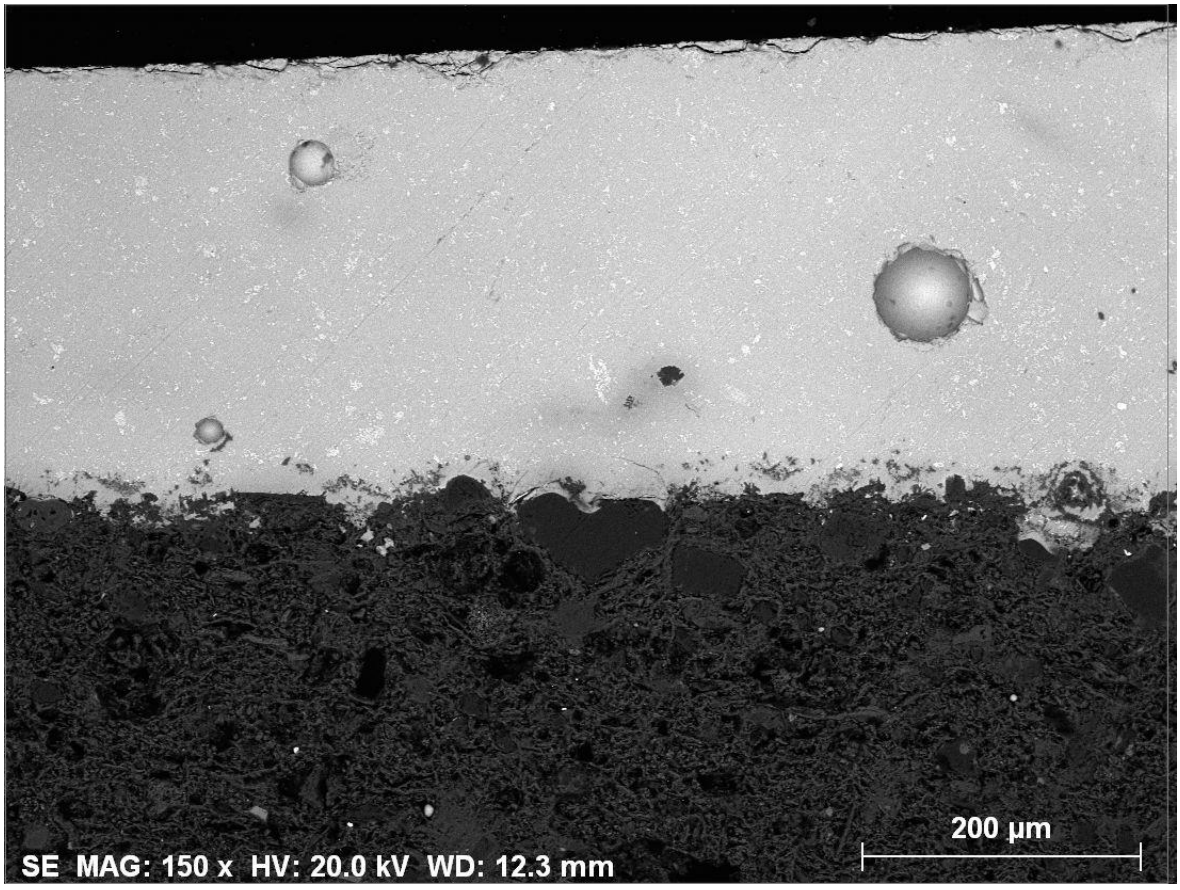

Figure 5.9. BSE image of the white glaze in sample SCV 33Bi3839, where very small and well-distributed SnO_2 crystal agglomerates can be observed.

One of the most common sources of sodium in tin-opacified glazes is sodium chloride (NaCl). The addition of common salt (NaCl) to several glaze recipes has been mentioned in the Italian treatise on majolica by Cipriano Piccolpasso (*ca.* 1557) (Piccolpasso, 1980). Molera *et al*. (1997) also point out two Valencian authors (Valls, 1894; González Martí, 1952) that describe a similar recipe where salt is added to the glaze mixture. *Figure 5.11* shows how Na_2O correlates to Cl, using SCV and PNS tiles as examples. Both

sodium and chlorine exhibit higher contents in tin-opacified glazes, with PNS samples displaying a stronger positive correlation and SCV samples showing a larger dispersion of Cl values. In PNS collection, in particular, the visible increase of Na content with the Cl one strongly agrees with common salt being the main source of sodium in tin-opacified glazes. On the other hand, another common source of sodium for glass production are coastal plant ashes, which also contain chlorine in their composition and therefore must not be discarded as a possible raw material as well (Tite *et al*., 2006). Depending on the type of plant and the treatment of the ashes, other elements in their composition are also added to the glass or glaze batch, such as Mg, Ca, K and Fe (Tite *et al*., 2006). In glazes, the presence of such elements may also arise from the interaction with the ceramic body, so the identification of alkali sources becomes problematic.

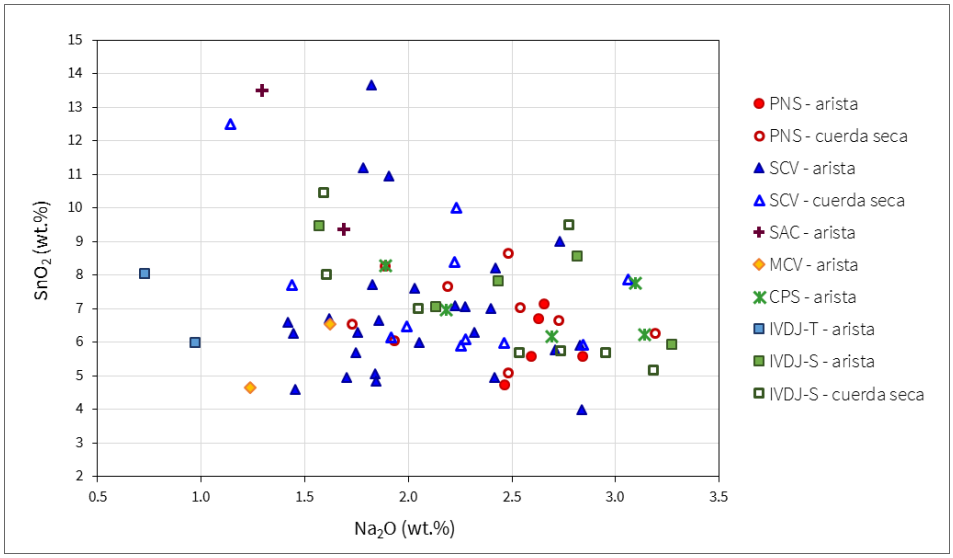

Figure 5.10. Scatter plot Na_2O *vs.* SnO_2 obtained from μ-PIXE analysis of white glazes from all the collections under study.

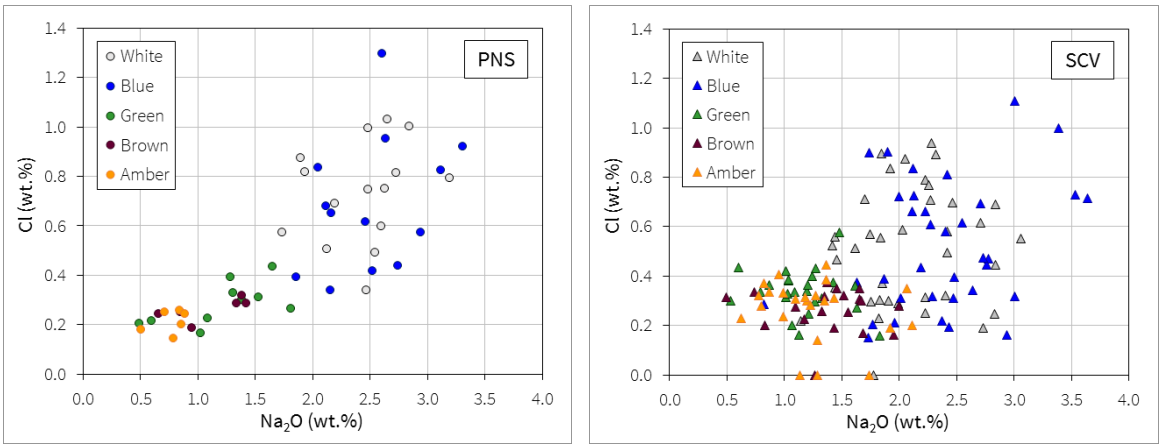

Figure 5.11. Scatter plots of Na_2O *vs.* Cl obtained from μ-PIXE analysis of the glazes from PNS and SCV collections.

SiO_2 and Al_2O_3 show a positive correlation although with different ratios for tin-opacified and transparent glazes. *Figure 5.12* illustrates how the same amount of silica corresponds to a lower amount of alumina in tin-opacified glazes, using PNS and SCV collections as examples. On the other hand, there is a positive correlation between Al_2O_3, CaO and MgO but the latter two oxides do not show such a correlation to SiO_2. Al_2O_3, CaO and MgO contents do not evidence any change regarding the type of glaze.

The positive correlation between MgO, CaO and Al_2O_3, suggest that the latter three oxides come from the same source. It is possible that they do not belong to the initial recipe and enter the glaze mixture during the firing of the tiles. This has been identified because of a *digestion* process in which the interaction between the ceramic body and the glaze results in a chemical diffusion of elements that is stronger in single fired ceramics, but also in lead glazes with higher sodium contents and in slow-cooling processes (Molera *et al*., 2001; Ben Amara & Schvoerer, 2006). The diffusion of elements between the glaze and the body modifies their final chemical composition – Al and Si diffuse from the body into the glaze and the inverse occurs with Pb, which enters the body. Once again, this is more pronounced with glazes applied on unfired bodies. The implication of this happening is a final glaze composition richer in Si and Al (and poorer in Pb) than the initial recipe (Ben Amara & Schvoerer, 2006). Leal (2014) went further in investigating these phenomena with tin-opacified lead glazes and obtained similar conclusions. Furthermore, the latter author also observed that the presence of MgO, Al_2O_3 and CaO (0.5-1 wt.% for double-fired and 0.3-3 wt% for single-fired ceramics) resulted from the reaction with the ceramic body since these oxides were not present in the prepared glaze frit.

On the other hand, the presence of Al_2O_3 correlated to SiO_2 in different ratios according to the glaze type suggests that alumina is already present in the sand used as the silica source. *Figure 5.12* shows how tin-opacified glazes, which contain more silica, are the ones with less alumina. The use of different sands according to the glaze type or different treatments of the same sand may explain this – a purer sand will result in a final glaze with fewer impurities, such as aluminium, calcium, titanium and – most importantly – iron, which is responsible for giving glazes and glasses a yellow to green tinge. Fe_2O_3 contents in white glazes are mostly inferior to 1 wt.%, which could mean that raw materials underwent a purification process, or that a high-quality sand was used, low in impurities (Pérez-Arantegui *et al*., 2005, 2009b). However, it is important to stress the contribution of the ceramic body to the final composition, which must not be discarded, and may have different consequences depending on the glaze type – glazes with a higher lead content may have stronger reactions with the ceramic body and consequently, result in stronger ionic exchanges between them.

Iron oxide contents were compared only between white and copper green glazes since iron is already present in amber, brown and blue glazes in association with the colours. There is a positive correlation between Fe_2O_3 and Al_2O_3 (*Figure 5.13*), and in the PNS group, the Fe_2O_3 contents are lower for the white-coloured glazes than for the green ones (*Figure 5.13a*). From these results, it is plausible to conclude that only one silica source (sand) was used for all the coloured glazes.

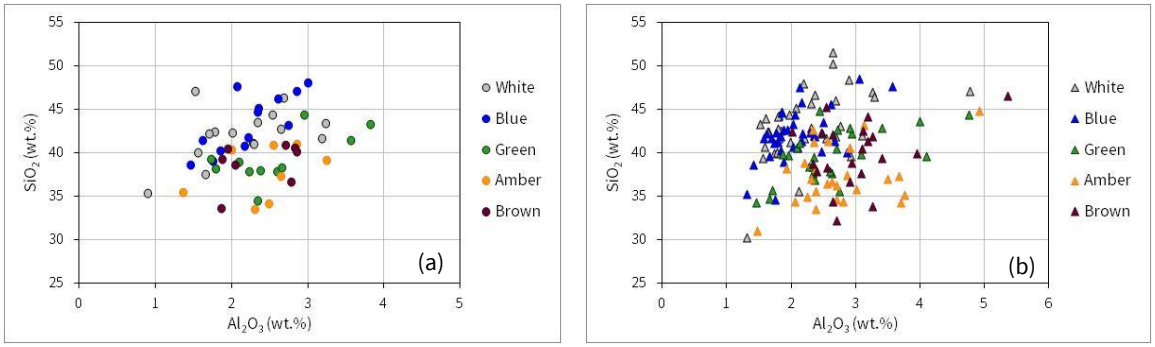

Figure 5.12. Scatter plots obtained from the μ-PIXE analysis of **(a)** PNS and **(b)** SCV *arista* and *cuerda seca* tiles, showing different Al_2O_3/SiO_2 ratios for tin-opacified and transparent glazes.

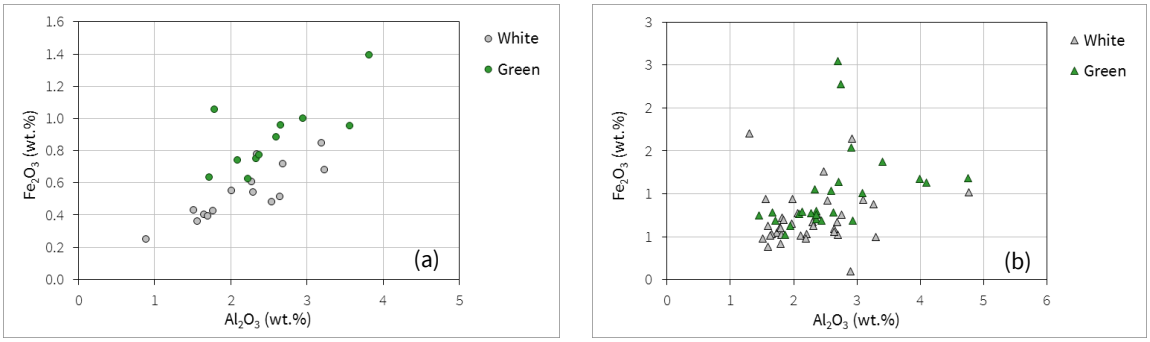

Figure 5.13. Scatter plots obtained from the μ-PIXE analysis of **(a)** PNS and **(b)** SCV *arista* and *cuerda seca* tiles, showing similar Al_2O_3/Fe_2O_3 ratios for white and green glazes.

MORPHOLOGY

Most tiles display very homogeneous white glazes, with scarce crystalline inclusions that, when existent, are more abundant at the glaze-ceramic interface. Tin oxide crystals are homogeneously dispersed throughout the glaze in small and well-distributed cassiterite agglomerates, as *Figure 5.9* illustrated.

The glaze-ceramic interface sometimes shows an intermediate layer (*ca.* 50-80 μm), very homogeneous and without cassiterite crystals, delimited by the ceramic body and a line of Ca-rich crystals, which were identified by μ-Raman as wollastonite ($CaSiO_3$). This was observed occasionally in SCV and CPS samples (*Figure 5.14*). Wollastonite also appears in some PNS samples. In IVDJ-S, MCV and PNS tiles analysed by SEM-EDS, both potassium and calcium-rich inclusions show up in EDS maps (*Figure 5.15*). In the three IVDJ-T analysed samples, a K-rich interface appears in all of them.

The samples from the SAC archaeological kiln display very different morphological features, namely in the glaze-ceramic interface. This was expected due to the distinct chemical composition of the ceramic body, which has almost no calcium content. *Figure 5.16* illustrates the glaze-ceramic interface observed for the white glaze of sample SAC 02, where a K-rich interface can be observed. There are also inclusions in the glaze, although areas with and without inclusions were both observed (see *Appendix VII*).

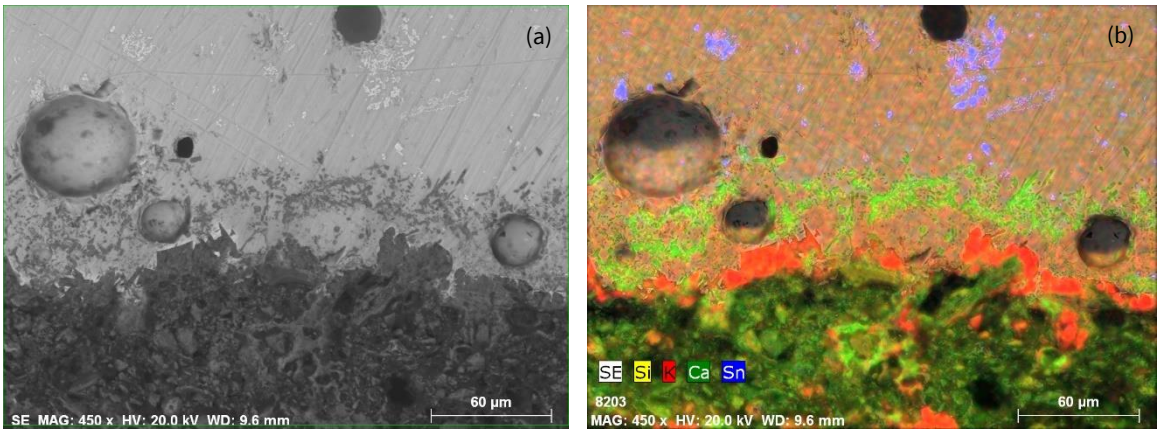

Figure 5.14. (a) BSE cross section image of white glaze CPS 02 and (b) corresponding EDS map. An intermediate area without Sn can be observed between the ceramic body and a layer of Ca-rich inclusions.

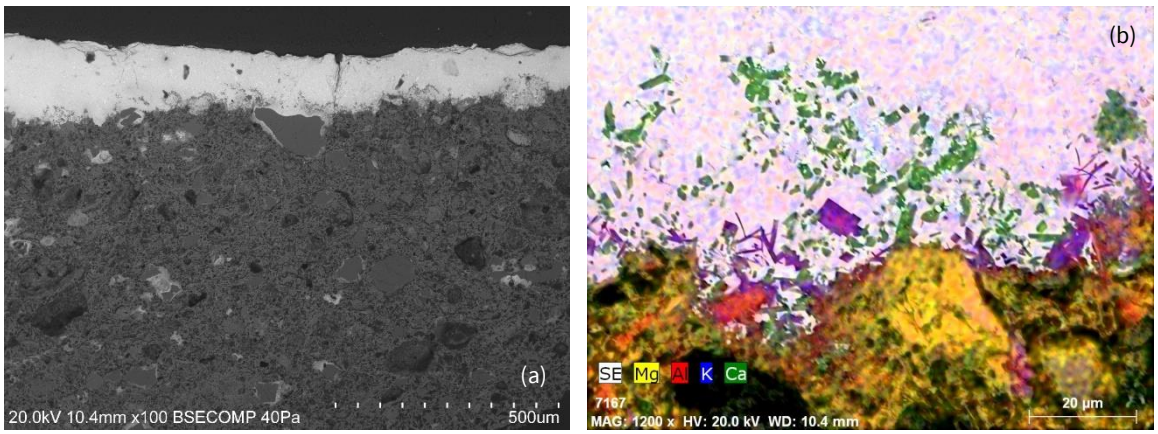

Figure 5.15. (a) BSE cross section image of white glaze MCV 4-1ML and (b) corresponding EDS map. Both K-rich and Ca-rich inclusions are observed, although there is no intermediate layer such as the one illustrated in *Figure 5.14*.

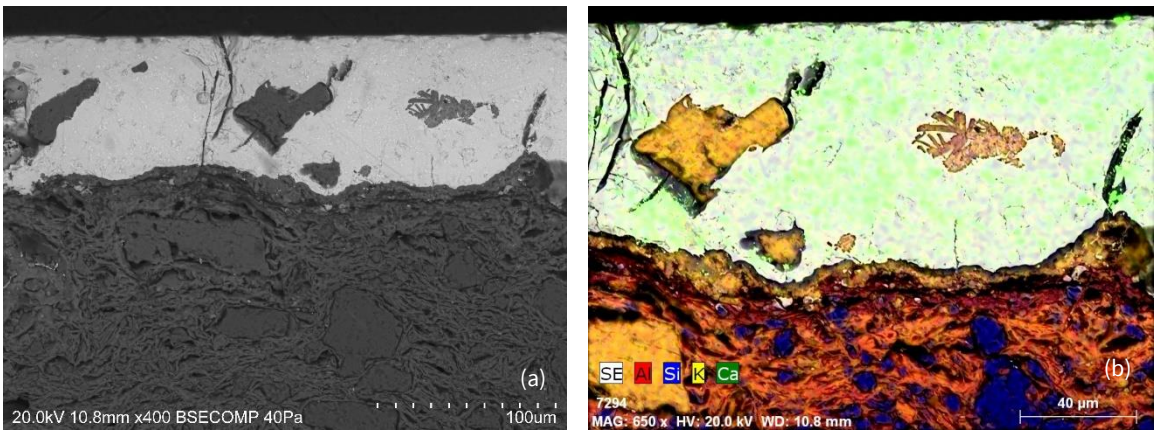

Figure 5.16. (a) BSE cross section image of white glaze SAC 02 and (b) corresponding EDS map.

5.2.2. BLUE GLAZES

The blue glaze in *cuerda seca* and *arista* tiles is very characteristic with its light cerulean shade and opacity. Results from the quantitative analysis showed that, when removing the colour-related oxides, the chemical composition of the blue glaze is identical to the white glaze's composition. This strongly

suggests that the white and blue glazes used the same recipe, with the addition of the cobalt pigment to obtain the blue colour. The discussion of the results obtained for the white glaze also applies here in what concerns the base recipe, SiO_2 and PbO contents, differences in general chemical composition and morphology among collections. Therefore, in this subchapter, the discussion will focus solely on the aspects related to the cobalt blue colour of these glazes.

The majority of the blue *cuerda seca* and *arista* glazes analysed in this work display a Fe-Co-Ni-Cu association, as determined by μ-PIXE and LA-ICP-MS. Adding to Hispano-Moresque cuerda-seca and *arista* blue glazes (Coentro *et al*., 2014; Fares *et al*., 2012), the association between copper and cobalt has been identified in coeval blue-decorated ceramics from Teruel and Manises-Paterna (Pérez-Arantegui *et al*., 2009b; Resano *et al*., 2005; Roldán *et al*, 2006), in Renaissance Della Robbia glazes dated prior to 1520 (Zucchiatti *et al*., 2006) and in an Islamic 17th century tile panel in Northern India (Gill & Rehren, 2011). Copper may be linked with the raw material used for obtaining cobalt, or it could be added intentionally. As an example, a blue enamel recipe from Antonio Neri (*L'Arte Vetraria,* 1612) includes copper (*ramina di tre cotte*) along with cobalt (*zaffera*) (Vilarigues & Machado, 2015). Another possibility – less likely although it must be mentioned – is linked with a "contamination" occurred during the preparation of the blue cobalt pigment or the blue glaze frit. The main European source for cobalt was the mining district in the Freiberg-Erzgebirge region (today's Germany), where copper ores have also been mentioned to exist alongside with cobalt ones (Gratuze *et al*., 1996; Tengrove, 1965). Some authors (Pérez-Arantegui *et al*., 2009b; Rodán *et al*., 2006) have also suggested the use of local Cu-containing cobalt ores, which are known to exist in the Iberian Peninsula (Castellón, Granada, Málaga, Almería, Zaragoza and Huesca in the Spanish territory), although no written documents have been found to prove the use of cobalt from these locations in medieval ceramics (Coll, 2009a, Roldán *et al*., 2006). On the other hand, the cobalt mines in Qamsar (Iran) are known to contain cobaltite (CoAsS) and chalcopyrite ($CuFeS_2$) along with magnetite (Fe_3O_4) veins (Mohammaddoost *et al*., 2010), so this is also a possible source. In his Persian ceramics treatise from 1301, Abu l'Qasim mentions two important sources of cobalt: Qamsar and *Farangistan*, which was the Persian word for Europe and probably refers to the Freiberg-Erzgebirge region (Kessler, 2012). An Islamic source for cobalt must not be discarded since the origin of the use of cobalt in the Iberian Peninsula comes from the Muslim occupation and dates back at least since the 13th century. Cobalt deposits were known in the Morocco and Persian (Iran) regions, from where several ceramists came to the Iberian Peninsula (Trindade, 2009).

A small group of blue glazes display arsenic contents above 1000 μg/g and bismuth contents above 500 μg/g, as measured by LA-ICP-MS. This group is composed exclusively of *arista* samples (IVDJ-T 96, IVDJ-T 133, IVDJ-S 3561, IVDJ-S 3601, SCV 80F4745, PNS 25, PNS 26, PNS 29, MCV 5-1R and SAC01). As shown in *Figure 5.17*, the group with higher As contents also shows the lower Cu contents, which is consistent with the literature (Gill & Rehren, 2011; Pérez-Arantegui *et al*., 2009b; Roldán *et al*, 2006; Zucchiatti *et al*., 2006). Arsenic has been appointed as a possible chronological marker when associated with cobalt since the cited literature identifies As only from the beginning of the 16th century onwards. Elemental associations for cobalt imported from the Freiberg-Erzgebirge region are Fe-Co-Ni and, from the early 16th century onwards, Fe-Co-Ni-As (Gratuze *et al*., 1996; Pappalardo *et al*., 2004; Zucchiatti *et al*., 2006). Since the heyday of the production of *arista* tiles is coeval with the transition in cobalt production appointed by

Pappalardo *et al*. (2004), it is likely that some *arista* tiles have been produced with As-containing cobalt ore, which was available from *ca.* 1520 onwards (Pappalardo *et al*., 2004; Zucchiati *et al*., 2006). This change is transversal to all collections and cannot be associated with a specific provenance, reflecting instead a chronological period of transition.

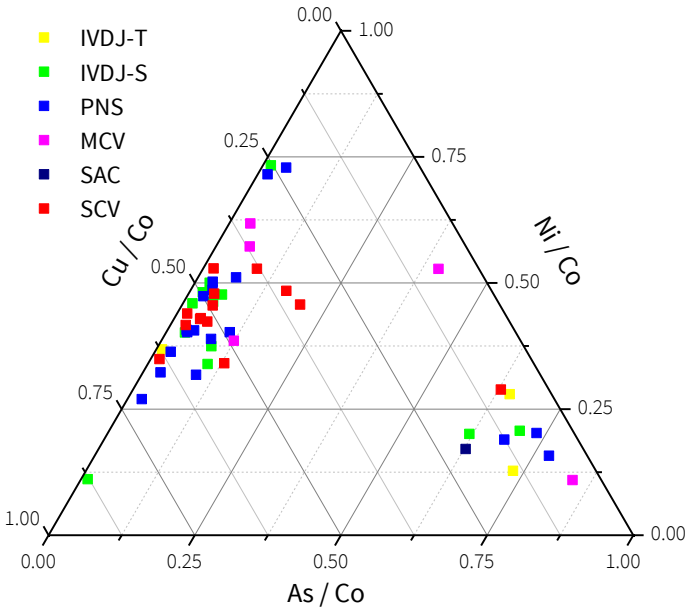

Figure 5.17. Ternary plot with Ni/Co, Cu/Co and As/Co ratios, obtained from LA-ICP-MS analysis.

The glaze morphology in blue glazes is mostly similar to that of white glazes (*Chapter 5.2.1*). This is true even in samples IVDJ-T 96 and 4095, which are an exception in the way that they both display large inclusions in the white and blue glazes (*Figure 5.18*). The mineral inclusions observed by SEM-EDS were afterwards analysed by μ-Raman, which identified a predominance of K-feldspar inclusions in sample IVDJ-T 4095, whereas the glaze in IVDJ-T 96 shows mostly quartz grains. Large quartz inclusions have also been identified in Islamic tin-glazes from Zaragoza, Almería and Granada, and Hispano-Moresque tin-glazes from Teruel. This has been interpreted as an intentional procedure for lowering the production costs by reducing the necessary amount of tin for achieving an opaque glaze (Molera *et al*., 2001b; Pérez-Arantegui *et al*., 2005, 2009a). Considering the dark orange ceramic body of Toledo tiles, it is likely that the mineral inclusions were intentionally added to help to reduce the contribution of the ceramic body to the final colour of the glaze.

Blue glazes obtain their colour from the cobalt oxide dissolved in the glaze matrix, as previously explained. Therefore, particles related to the cobalt raw material are seldom identified in *cuerda seca* and *arista* glazes.

However, a structure consistent with a ferrite spinel was occasionally identified by μ-Raman in blue glazes (*Figure 19a*). These spectra are characterised by two stronger bands at *ca.* 695-705 cm^{-1} and *ca.* 467-472 cm^{-1}. Such values are reported in the literature for both nickel ferrites ($NiFe_2O_4$) and cobalt ferrites ($CoFe_2O_4$) (Kamble *et al*., 2015; Majumdar, 2012; da Silva *et al*., 2006). Less frequent was the identification

of similar spectra, but with the band at *ca.* 467-472 cm^{-1} shifted to *ca.* 492 cm^{-1}. Nickel and iron were found associated with cobalt in these blue glazes, an association known to be common in the cobalt ores used as sources of raw material for these glazes (Coentro *et al*., 2012; 2017).

In one sample (CPS03), a large inclusion (*ca.* 110 µm) was observed (*Figure 19b*). Through EDS analysis, it was possible to distinguish areas with different chemical compositions within the inclusion – a central Co-Fe-Ni-rich agglomerate and an exterior aureole where mainly Ca, Mg, As and Pb were identified. It must be pointed out that this aureole coincides with a void in the EDS map for Si. *Figure 19b* shows how the EDS map of cobalt and nickel are almost identical, whereas iron is visible only in small specific areas.

The µ-Raman analysis allowed identifying both spinel and olivine structures in the agglomerate. Spectra concerning the spinels show the strongest bands centred around 700 cm^{-1} and 490 cm^{-1} (*Figure 19a A-C*). The olivine structure is identified by the characteristic doublet centred at 816 cm^{-1} and 840 cm^{-1} (*Figure 19a C-E*), which correspond to the Si-O asymmetric stretching band and to the Si-O symmetric stretching band, respectively (Mouri & Enami, 2008). These values are within the series for Co-Fe-Ni-olivines, whose reported bands are *ca.* 819 and 839 cm^{-1} for nickel olivines (Ni_2SiO_4), *ca.* 811 and 838 cm^{-1} for cobalt ones (Co_2SiO_4), and 814 and 837 cm^{-1} for iron ones (Fe_2SiO_4) (Mouri & Enami, 2008). A medium-intensity band at *ca.* 560 cm^{-1} has also been reported for nickel olivines, which may explain the band at 567 cm^{-1} in *Figure 19a C* (Lin, 2001). The band at *ca.* 667 cm^{-1} is consistent with magnetite and belongs to the spectrum obtained in the centre of the inclusion, where Fe is concentrated (RRUFF).

These results give important clues on the raw material used for the blue colour. The used cobalt compound for colouring these blue glazes was likely a mixture of Co-Ni-Fe-olivines and Co-Ni-ferrites (spinels). Considering that the sample in question (CPS03) is dated from the 1530s (Martínez, 1991), zaffre was the most likely source of cobalt for its production. In the early 16th century, Schneeberg (in Saxony, Germany) was the main source of cobalt for European glass and ceramics, which was exported as zaffre. Zaffre resulted from the calcination of a mineral cobalt ore, such as cobaltite (CoAsS), erythrite ($Co_3(AsO_4)_2{\cdot}8H_2O$ or skutterudite (Co,Ni,Fe)As_3, or, according to different references, it was the result of the calcination of the cobalt ore mixed with sand (Machado & Vilarigues, 2016; Gratuze *et al*., 1997; Zucchiatti *et al*., 2006). The formation of the olivine structures may result from the interaction with the silica in the sand or later with the silica in the glaze during firing.

Finally, the aureole surrounding the main inclusion shows a spectrum with one prominent intense band at 834 cm^{-1} (*Figure 19a F*) that is consistent with the spectrum of carynite (Na,Pb)(Ca,Na)$CaMn^{2+}_2(AsO_4)_3$ (RRUFF ID R060663).

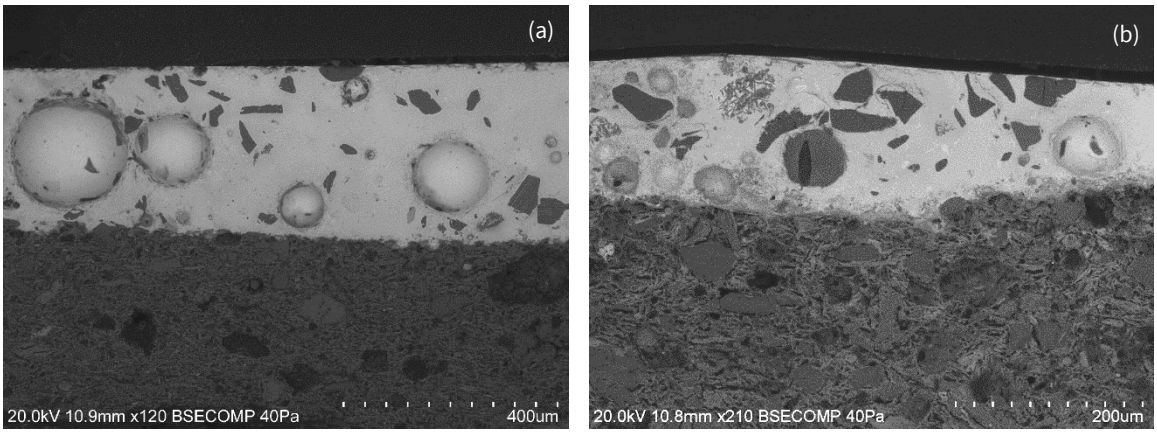

Figure 5.18. BSE images of cross-sections of the blue glazes IVDJ-T 96 (a) and IVDJ-T 4095 (b).

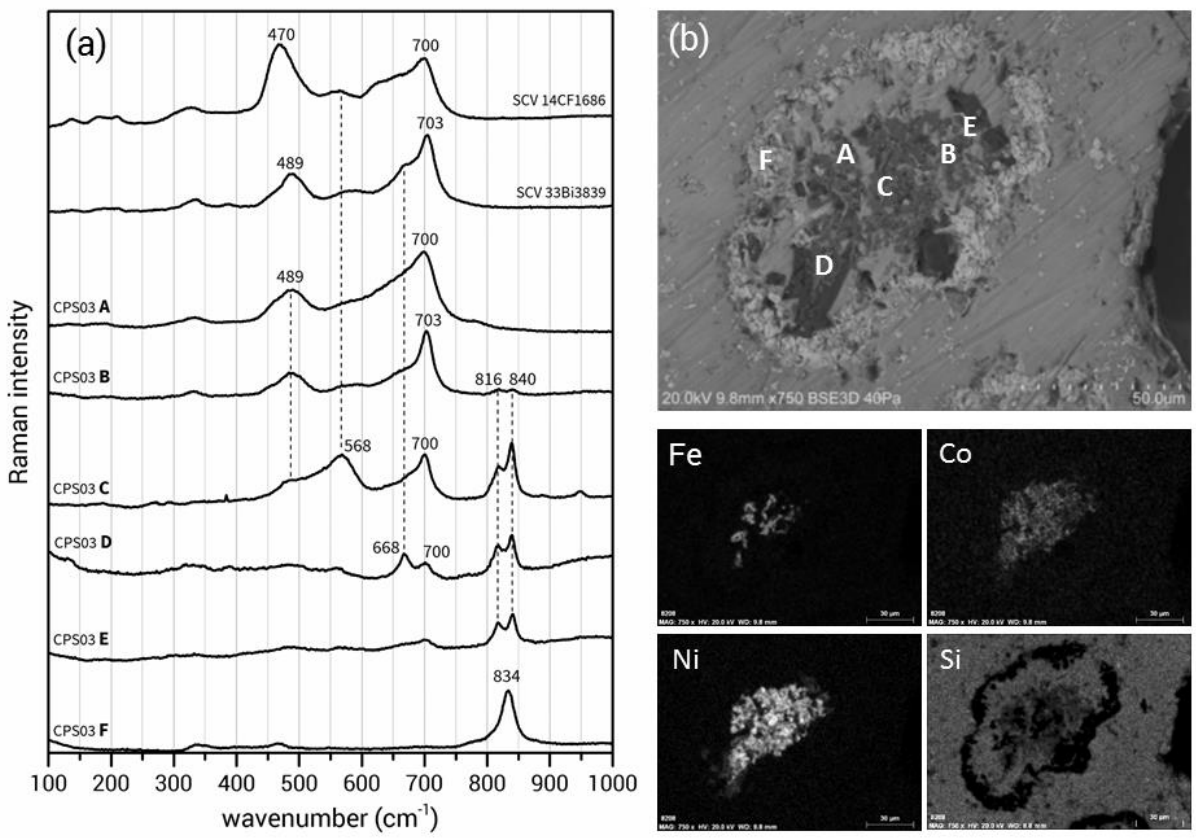

Figure 19. (a) μ-Raman spectra of Co-Ni-ferrites and Co-Ni-olivines obtained in different areas pointed out in *Figure 19b* (CPS 03), and in two other samples (SCV 14CF1686 and SCV 33Bi3839); (b) BSE image of a cobalt inclusion in sample CPS03 and corresponding EDS maps for Fe, Co, Ni and Si.

5.2.3. GREEN GLAZES

Three shades of green were identified: a transparent dark green, an opaque tin-opacified green and an opaque turquoise green (*Figure 5.20*). The compositions of the green "transparent" glazes identified in most *arista* and *cuerda seca* samples were found to comprise *ca.* 1-3 wt.% CuO and <2.5 wt.% SnO_2. This

dark transparent type is the most common in Hispano-Moresque tiles and, as *Figure 5.21* illustrates, it is also the most common in analysed samples. Such low amounts of tin are not enough to render the glaze opaque and therefore seem unnecessary in the glaze recipe. On the other hand, as previously discussed in *Chapter 5.1*, the presence of tin oxide in transparent glazes might be a question of compatibility between all the different colours during the firing cycle (e.g., melting temperatures or glaze viscosity) (Chapoulie *et al*., 2005; Padeletti & Fermo, 2010).

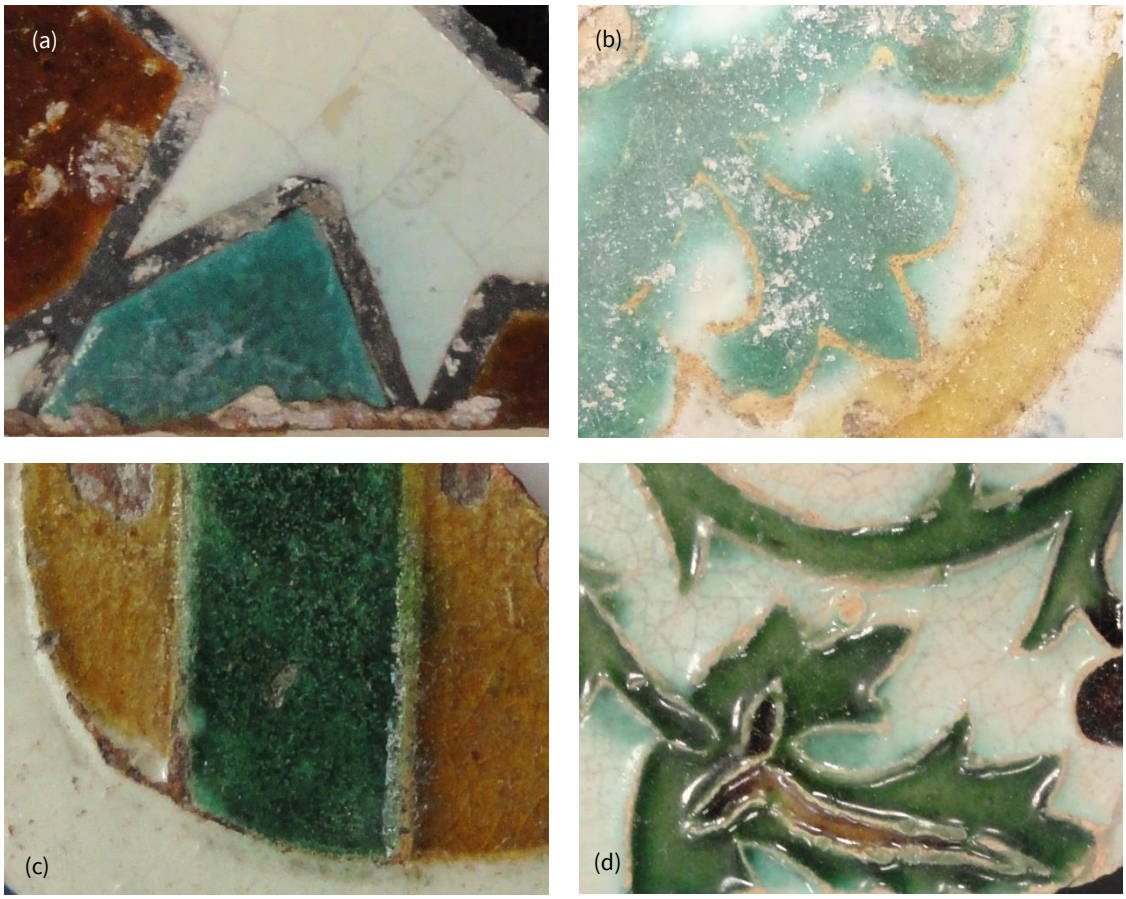

Figure 5.20. Details of the three copper-green shades identified in *arista* and *cuerda seca* tiles: **(a)** opaque turquoise green with 8 wt.% SnO_2 (IVDJ-S 3919); **(b)** opaque turquoise green with 4 wt.% SnO_2 (MCV 5-1R); **(c)** opaque green with 4 wt.% SnO_2 (IVDJ-T 96); **(d)** dark transparent green with 1 wt.% SnO_2 (SCV 10Bi1673).

In PNS, MCV and IVDJ collections, some tiles contain tin-opacified green glazes, with SnO_2 contents between 3.5-9 wt.%. Glazes with SnO_2 values above 7 wt.% also show the highest Na_2O contents (>2 wt.%), which agrees with the previously discussed results for other tin-opacified glazes (see Chapter 5.2.1). In these glazes, besides the lighter colour, a turquoise shade is achieved when the copper pigment is used with a white tin background. Turquoise glazes were characteristic of Islamic ceramics and their use has been reported in monochromatic pavement tiles in the Spanish cities of Onda and Valencia (Estall & Alfonso, 2003), in a Christian context in the Monastery of Alcobaça (Portugal) (Carvalho *et al*., 2016) and in the chapter house of the Jacobin Convent in Toulouse, France (Norton, 1984). This colour was however set aside from the usual palette of *cuerda seca* and *arista* tiles, where a transparent dark green was used

instead. Turquoise was then used only sporadically: it was identified in *cuerda seca* samples IVDJ-S 3794 and 3919, which belong to the oldest *cuerda seca* tiles produced in the Iberian Peninsula[1], and in *arista* sample IVDJ-S 3561, whose pattern was also found in Portugal in the Penha Longa Monastery, near Sintra (Silva, 1992). The turquoise in IVDJ-S 3561 is a rare colour in Hispano-Moresque tiles and was used simultaneously with other green shades. The use of an opaque green in samples IVDJ-S 3794 and 3919 could also have been a necessity to masque the dark pink-red ceramic body, as otherwise observed in flat green tile PNS03 (*Chapter 5.3*). With high calcareous pastes, whose use was later generalised for tin-glazed tiles, the light beige background allowed for obtaining the typical "bottle" green shade.

Other tin-opacified greens with 3-4 wt.% SnO_2 were found in samples PNS06, IVDJ-T 96, IVDJ-S 4127 and MCV 5-1R. The latter two also exhibit a turquoise green colour, whereas the first two tiles show an opaque green glaze without the turquoise shade. No remarkable differences were found in the compositions of these four glazes that would explain the different green hues.

Sample PNS06 (the armillary sphere) shows the highest tin oxide content (4 wt.%) in PNS collection, but PNS05, with the same pattern, fits within the general results for *cuerda seca* green glazes (< 2.5 wt.% SnO_2). A higher number of samples would be necessary to assess if the armillary sphere could represent a different production. From our results, the composition of the glazes points to the same production set.

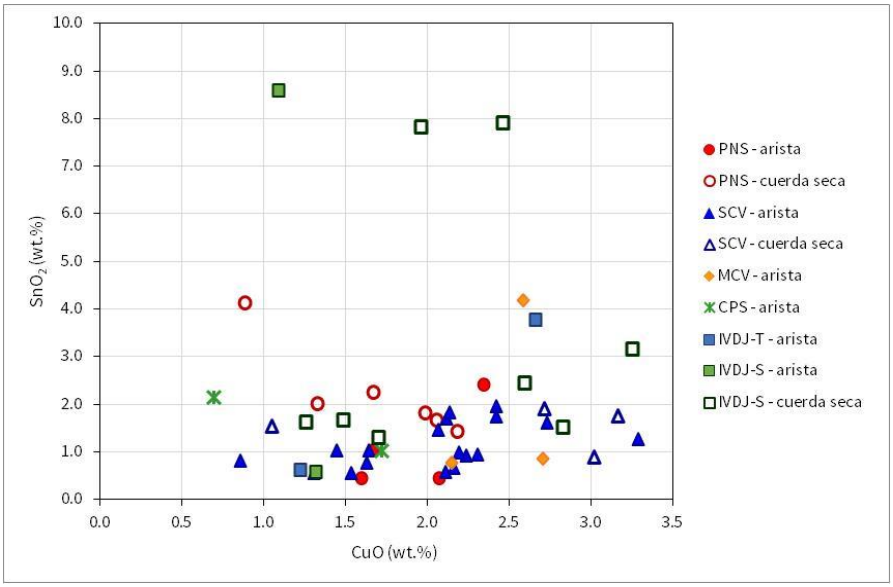

Figure 5.21. Scatter plot CuO *vs*. SnO_2 obtained from the μ-PIXE analysis.

Green glazes are homogeneous and no copper inclusions were identified that would give information on the raw material used for obtaining the colour. However, malayaite ($CaSnO(SiO_4)$) was identified by μ-Raman in two SCV green glazes (SCV 21AM3076, SCV 33Bi3839) and by Synchrotron μ-XRD in the IVDJ3561 turquoise glaze (see *Appendix VI*). This calcium-tin silicate can be synthesised from equimolar parts of CaO, SiO_2 and SnO_2 through a thermal process, but it can also be formed from a reaction between SnO_2 and wollastonite ($CaSiO_3$) in the glaze melt. The formation of these crystals may be related to the colour,

[1] IVDJ-S 3794 belongs to a set also called "Niebla tiles"

since the reaction is promoted by the presence of a transition metal ion such as cobalt or copper (Mulholland, 1984; Piña *et al*., 2005).

5.2.4. AMBER GLAZES

Amber glazes exhibit the highest lead contents of all colours – an average of *ca.* 47 wt.% PbO, while green and brown glazes both exhibit an average of *ca.* 45 wt.% PbO. Tin oxide is present mostly below 1 wt.%, making it a possible contamination or an intentional addition related to compatibility purposes, as previously suggested for green transparent glazes as well. These are usually the most transparent glazes and the ones exhibiting most crazing, despite their good conservation state (*Figure 5.22*).

In amber glazes, high Fe contents (2-5 wt.% Fe_2O_3) were measured. When compared to the other colours, the Fe_2O_3/SiO_2 ratio is considerably higher in amber glazes, which indicates the intentional addition of Fe compounds to obtain the colour.

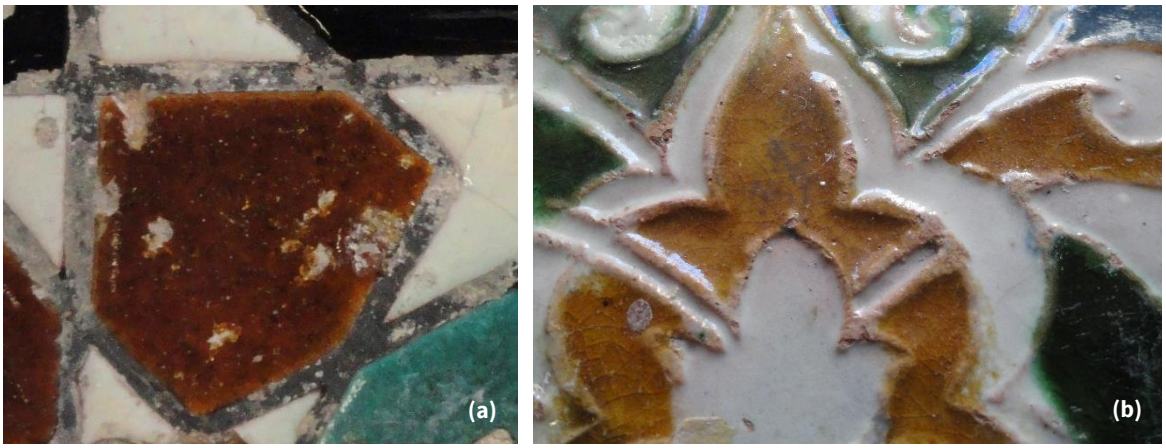

Figure 5.22. Different shades of amber glazes: (a) IVDJ-S 3919 and (b) IVDJ-T 133.

Highest iron contents are observed in SCV collection, mostly above 4 wt.% Fe_2O_3, whereas in the majority of the other collections, it is almost always below this value (*Figure 5.23*). IVDJ-T is the group with lower iron contents, perhaps because the orange ceramic body of the tiles below the transparent glaze already helps to achieve the final amber colour. Despite the contribution of the ceramic body to the final chemical composition of the glaze (Molera *et al*., 2001a), no direct correlation was found between the Fe contents in the glaze and in the body, which strengthens the hypothesis that different recipes were used with slightly different Fe_2O_3 amounts. In *Figure 5.23* it is also possible to see that PNS and IVDJ-T groups show the lowest Na_2O contents.

Although *Figure 5.23* shows some groups, namely *arista* PNS, CPS, IVDJ-S and IVDJ-T, they are very closely positioned. These results identify small variations in a similar recipe that was used probably by different workshops.

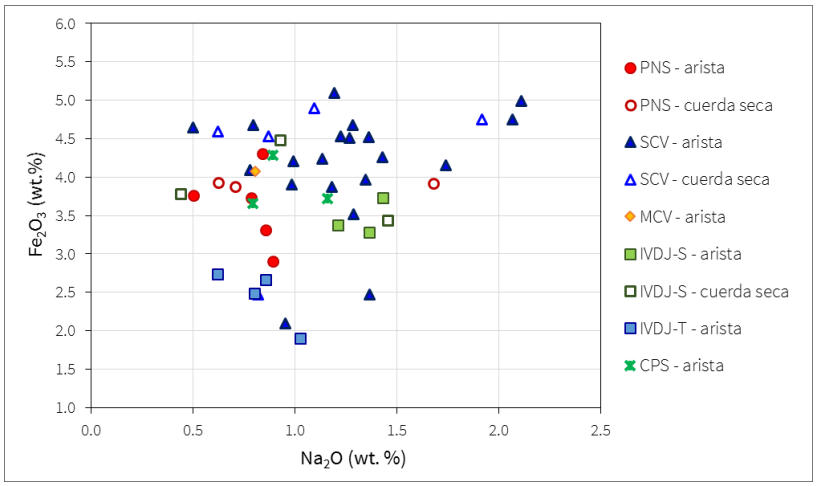

Figure 5.23. Scatter plot Na_2O *vs*. Fe_2O_3 obtained from the μ-PIXE analysis.

Amber glazes observed by SEM-EDS revealed to be very homogeneous, with scarce inclusions mostly located at the glaze-ceramic interface (*Figure 5.24*). These inclusions follow what has been identified for green glazes, generally with K-feldspar layer and in some cases – mostly in SCV samples – Ca-rich crystals immediately above the interface (wollastonite and diopside).

Through μ-Raman analysis, two compounds were identified that are only related to amber glazes. Andradite ($Ca_3Fe_2(SiO_4)_3$), a nesosilicate from the garnet group, was identified in amber glazes PNS24 and SCV 33Bi3839, by the characteristic bands at 882, 514 and 361 cm^{-1} (Figure 5.25). The shifts in the Raman bands are consistent with an andradite structure where Fe^{3+} is partially substituted by ions such as Ti^{4+} or Mg^{2+}. This neosilicate could arise from the reaction between wollastonite and iron oxides in excess such as magnetite or hematite in an oxidising atmosphere (Zhang & Saxena, 1991). Alongside andradite, μ-Raman also identified a magnesioferrite ($MgFe_2O_4$) by its strong Raman band at *ca.* 619 cm^{-1} (Figure 5.25). Again the Mg contents could lead to the formation of magnesium and iron spinels, such as magnesioferrite.

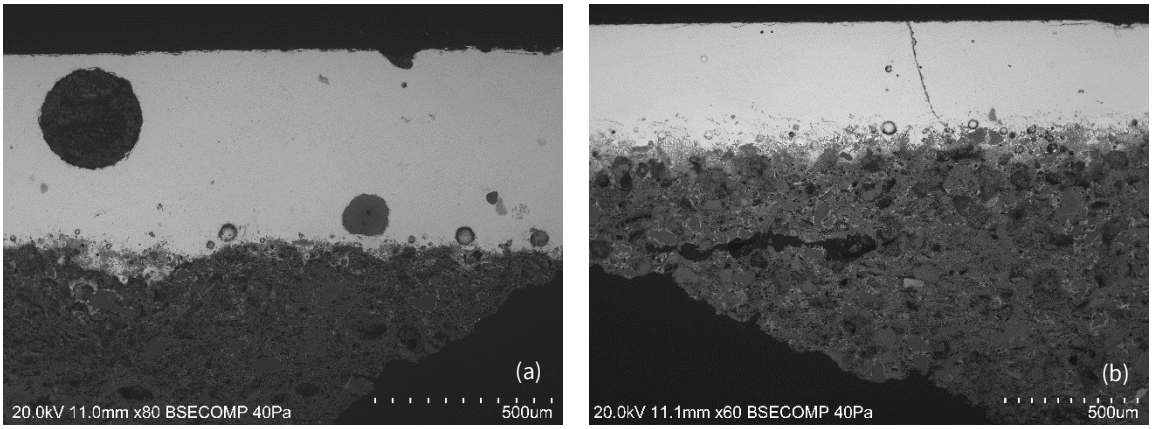

Figure 5.24. BSE cross-section images of amber glazes in tiles SCV 34 Ai4057 **(a)** and SCV 4Bi414 **(b)**.

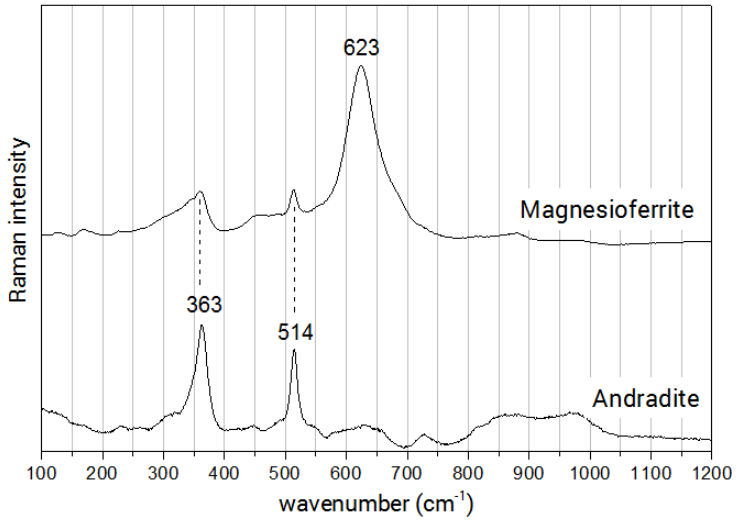

Figure 5.25. μ-Raman spectra of minerals found in the glaze-ceramic interface of amber glazes and their reference spectra: andradite and magnesioferrite.

5.2.5. BROWN GLAZES

Brown glazes appear as a dark colour with various shades, sometimes also referred to as "purple" or "black". Brown is obtained from manganese oxide and has been one of the earliest colours to characterise Iberian ceramics, namely the green-and-brown tin-glazed medieval productions of Teruel and Paterna (Pérez-Arantegui *et al*., 2009a), as well as Islamic ceramics found in Portuguese and Spanish territories (Molera *et al*., 2013; Pérez-Arantegui *et al*., 1999).

In the *arista* and *cuerda seca* tiles under study, manganese-brown glazes are often very dark. From the μ-PIXE analysis, manganese has been identified in concentrations of *ca.* 2-3 wt.% MnO in the majority of the glazes, with a few exceptions of *ca.* 5 wt.% MnO (PNS 11, SCV 45M4260 and IVDJ-S 4127). The glaze recipe is identical for all collections and there are no clear differences between *arista* and *cuerda seca* tiles. The exception is PNS collection, where the results show higher lead and manganese contents in *cuerda seca* tiles (≥ 45 wt.% PbO and ≥ 2.6 wt.% MnO), whereas the brown glazes in *arista* samples show lower PbO and MnO values, but higher silica contents (≥ 40 wt.% SiO_2).

Iron and – less frequently – barium exhibit an association with manganese in brown glazes. This association has been already detected in 11th-century Islamic *cuerda-seca* ceramics (Pérez-Arantegui *et al*., 1999) and also in 17th-century Portuguese majolica tiles (Coentro *et al*., 2012). The presence of barium could suggest the use of the mineral psilomelane ($BaMn^{2+}Mn^{4+}{}_8O_{16}(OH)_4$) as a source of manganese, and typically the absence of it hinted at the use of pyrolusite (β-MnO_2). These two manganese minerals correspond to two important and worldwide distributed manganese sources (Pérez-Arantegui *et al*., 1999; Tite *et al*., 2009). However, there is a wide range of Mn minerals in nature together with veins of barite ($BaSO_4$) and also Ba-feldspars, which would also explain the presence of barium in the manganese pigment (Tite *et al*., 2009).

Contrarily to green and amber, many colour-related compounds can be identified in manganese-brown glazes. These compounds are mostly located near the glaze-ceramic interface and are a product of the interaction between the Mn-rich glaze matrix and other compounds that arise from the ceramic body at the temperatures used for firing the tiles. These newly formed compounds can be observed spreading from the interface in direction of the glaze surface, as *Figure 5.26* exemplifies.

Figure 5.27 shows the μ-Raman spectra of all the manganese compounds identified in the analysed *cuerda seca* and *arista* brown glazes. Manganese brown glazes often show bustamite ($CaMnSi_2O_6$) crystals in the glaze-ceramic interface, observed by SEM-EDS as Ca-Mn-rich inclusions and identified by μ-Raman in samples PNS07, PNS09, PNS19, SCV 9i1469 and *cuerda seca* line of SCV 33Bi3839. The formation of bustamite is promoted by calcium diffusion from the ceramic body to the glaze melt during firing at temperatures above 950 ºC (Molera *et al*., 2013), which explains why these inclusions are concentrated near the interface and spread from there to the surface. It also allows estimating the lowest firing temperature for these glazes. Depending on several factors, such as the glaze composition and firing conditions (e.g. time and specific temperature), the development of the bustamite crystals could remain confined to the interface or developed throughout the glaze thickness until reaching the surface.

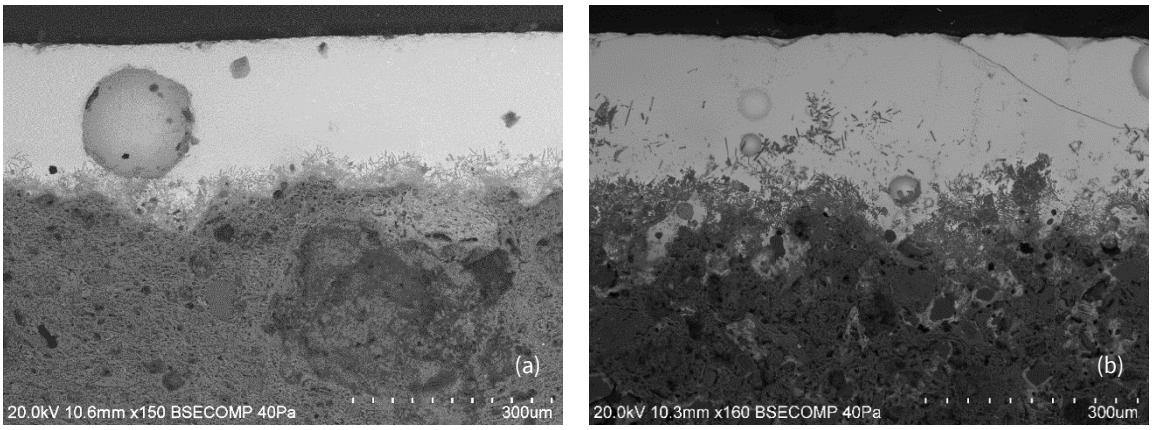

Figure 5.26. BSE cross-section images of manganese-brown interfaces: **(a)** typical interface with a layer of minerals formed from the reaction between the ceramic body and the Mn-rich glaze (IVDJ-T 3683); **(b)** irregular interface with Mn-rich mineral inclusions that spread to the surface of the glaze (PNS 19).

Braunite ($Mn^{2+}Mn^{3+}{}_6SiO_{12}$), which was identified in samples PNS23, PNS24, PNS25 and SCV 45M4260, can be formed from the reaction between pyrolusite (MnO_2), the most common manganese ore, and a silica-rich glaze matrix, at temperatures above 1000 ºC (Molera *et al*, 2013). Braunite has been identified on 17th century Portuguese tiles (Coentro *et al*., 2012), as well as in 11th century Almohad tin-glazed ceramic from Mallorca, in 10th-11th century Islamic glazes from Murcia and from Mallorca, on Hispano-Moresque glazes from Valencia (13th-14th century), on a 17th century glaze from Catalonia (Molera *et al*., 2013; Pradell *et al*., 2010) and on 19th century polychrome relief tiles from National Palace of Pena, Sintra (Coutinho *et al*., 2016a).

Hausmannite ($Mn^{2+}Mn^{3+}{}_2O_4$) (identified in samples PNS09 and PNS23), can result from firing pyrolusite at a temperature of circa 1000 °C (Molera *et al*, 2013). In sample PNS23, jacobsite ($MnFe_2O_4$) was also identified. Jacobsite is a spinel often present in manganese-bearing deposits, although it can be formed by firing together manganese and iron oxides above 600 °C (Anthony *et al*, 2003; Buzgar *et al*., 2013; Molera *et al*., 2013). The latter process requires the presence of organic matter to reduce the Fe^{3+} from goethite to Fe^{2+} in jacobsite. As the Fe^{2+} content increases, the main Raman band of jacobsite shifts to higher values (from 620 cm^{-1} to 626 cm^{-1}) and can become approximate to those of magnetite (*ca.* 670 cm^{-1}), which is isostructural with jacobsite (Buzgar *et al*., 2013).

In sample IVDJ-T 4095, kentrolite ($Pb_2Mn_2Si_2O_9$) was identified along with braunite in a *cuerda seca* residue that was trapped beneath the white glaze (*Figure 5.28*). In the *cuerda seca* line of SCV 33Bi3839, kentrolite was also identified along with bustamite. Kentrolite has been identified around braunite and hausmannite crystals that reacted with the lead glaze in Islamic ceramics (Molera *et al*., 2013) and in Hispano-Moresque tile PNS30 (see *Chapter 5.5*). The presence of kentrolite suggests lower firing temperatures since this compound is stable between approximately 650 °C and 840 °C (Molera *et al*., 2013).

The presence of braunite and/or hausmannite along with kentrolite in the same glaze can be understood considering that the manganese-bearing pigment suffered the first firing at higher temperatures (*ca.* 1000 °C), either roasted alone or prepared with the glaze frit, and then a second firing at lower temperatures, probably the final firing of the tile, allowed the formation of kentrolite. The high lead content of the glazes is also a strong contributor to the formation of kentrolite (Molera *et al*., 2013).

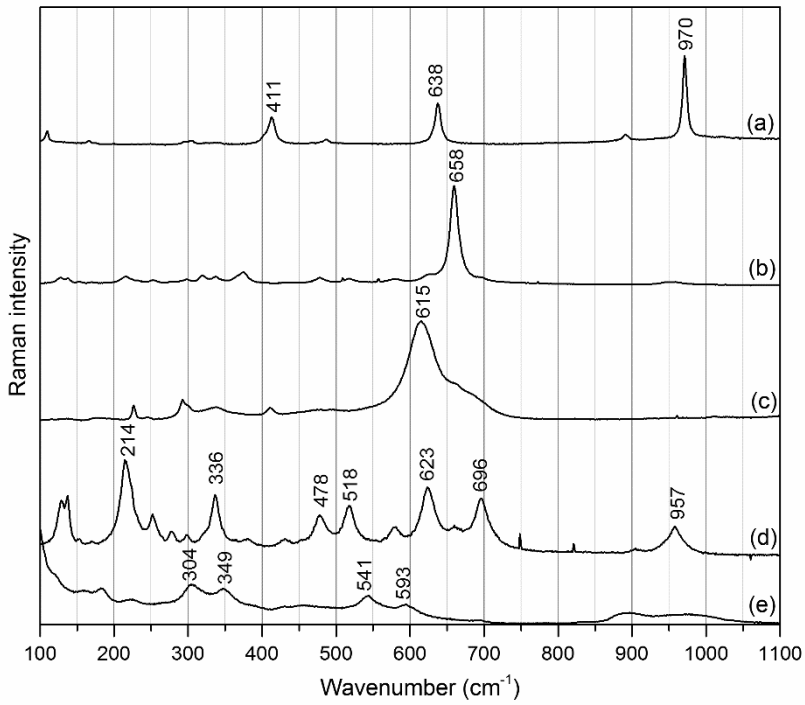

Figure 5.27. μ-Raman spectra of manganese compounds identified in brown glazes: **(a)** bustamite; **(b)** hausmannite; **(c)** jacobsite; **(d)** braunite and **(e)** kentrolite.

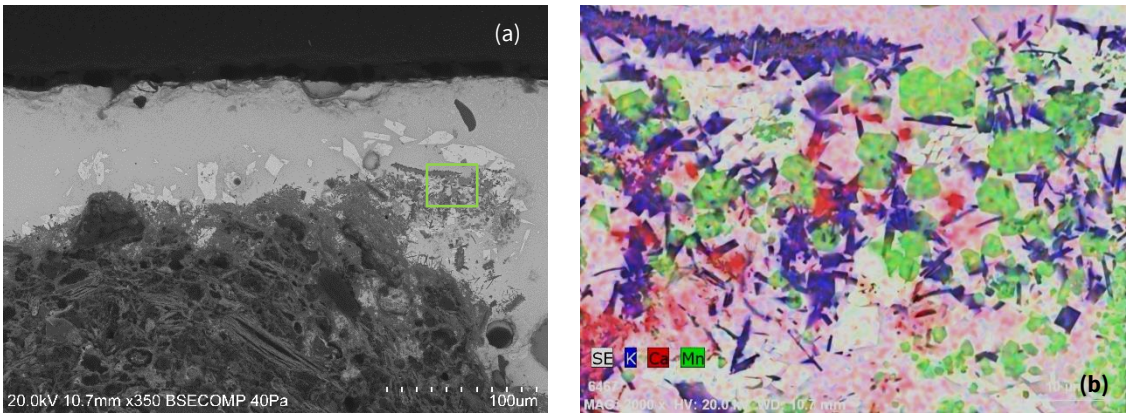

Figure 5.28. BSE image of a cross section in tile IVDJ-T 4095 where a *cuerda seca* residue was trapped below the white glaze. Kentrolite crystals are observed as the lightest inclusions in **(a)**, whereas the EDS map in **(b)** shows braunite crystals in more detail.

5.3. FLAT MONOCHROME TILES

A small group of the analysed samples is composed of flat monochromatic tiles: PNS 01, PNS 02, PNS 03, PNS 04, PNS 37, MCV 9-1Ag, MCV 9-2Ap, MCV 10-1, MCV 10-2 and MCV 10-3. These tiles were used in geometric compositions, such as the ones decorating some of the rooms in the National Palace of Sintra (see *Figure 5.29*). They were analysed separately and the results were compared to those of the other typologies.

Figure 5.29. The *Arab room* in the National Palace of Sintra, where monochrome tiles were used to make a geometric composition resembling the *alicatado* technique. © Parques de Sintra.

The chemical composition of the blue glaze in sample PNS01 suggests a slightly different recipe than that of most analysed Hispano-Moresque blue glazes, showing the lowest SiO_2/PbO ratio. The blue shade is darker than most blues in PNS collection, although both CoO and SnO_2 contents fit within the average values.

Samples PNS02 and PNS37 are covered with green glazes that show a similar composition, albeit sample PNS37 belongs to the *sgraffito* set that can be observed in *Sala das Pegas*. Results show a similar chemical composition, which indicates a similar glaze recipe (or likely the same) used for both tiles. These green glazes fit among the ones in *cuerda seca* and *arista* tiles.

The third green sample – PNS03 – shows a very different glaze composition, where tin content is considerably higher (7 wt.% SnO_2), creating a turquoise-shade glaze. Furthermore, this glaze shows the lowest values in SiO_2, MgO, Al_2O_3, K_2O, CaO and Fe_2O_3 in the green glazes group, along with one of the highest PbO contents (54 wt.%).

White sample PNS04 shows a chemical composition similar to the one of PNS03, except for the copper content, which was not detected by μ-PIXE. These two samples, as previously stated, are also distinguished by their red-coloured ceramic body. Sample PNS04 is an exception because white glazes were usually applied over calcareous ceramic bodies in order to take advantage of their light colour to achieve the white opaque final glaze. This justifies the high tin content in sample PNS04 (11 wt.% SnO_2), which is the highest in PNS collection, probably to compensate for the red colour of the ceramic body. The glaze recipe contains more lead and less sand, or perhaps the reaction with the ceramic body was minimal during firing.

MCV flat tiles show heterogeneous results. MCV 10-2 (brown), MCV 10-3 (white) and MCV 9-1Ag (blue) exhibit higher SiO_2 and K_2O contents (> 50 wt.% SiO_2 and > 6 wt.% K_2O) than most analysed corresponding coloured glazes. In sample MCV 10-3, the white glaze stands out for its excessive amount of tin (23 wt.% SnO_2) and very low PbO content (5.5 wt.%). This is very odd since the amount of SnO_2 in the other glazes is enough to achieve opacification. A parallel regarding this white glaze can be found in the 13th century Cistercian pavement of the Alcobaça's Abbey, in Portugal (Carvalho *et al.*, 2016), where very heterogeneous tin-glazes were identified with very high SnO_2 contents (15-20 wt.%). However, these were applied on non-calcareous pastes and their PbO content was still much higher than the one of the white glaze in sample MCV 10-3. In this case, it would be important to analyse other samples similar to MCV 10-3 to clarify if this was an intentional recipe used in a specific production, or if – instead – it is an exception among Valencian white plain tiles. However, it seems that these flat monochrome tiles do not fit well within the results for other MCV samples, suggesting different recipes and, therefore, a different production set.

5.4. RELIEF TILES

The relief tiles from Sintra's National Palace make this collection unique. Except for one particular pattern in which *cuerda seca* was used, these tiles do not have a physical barrier to separate the colours, resembling more the majolica technique instead of the coeval Hispano-Moresque *cuerda seca* and *arista*. The variety and characteristics of the PNS relief tiles suggest a process where the first attempts did not work so well (the tiles in King Sebastião's room – PNS30), so *cuerda seca* was used to separate the colours (samples PNS09, PNS14 and PNS 35) and, finally, the white glaze, the colours and the firing process seem to have been perfected to allow the production of colourful high-reliefs with less colour-spreading (e.g.: samples PNS32, PNS 38 or PNS39).

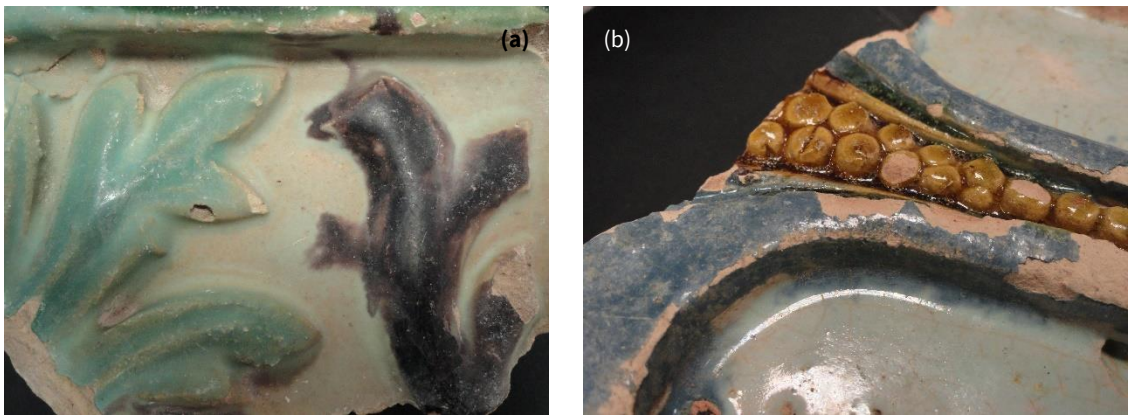

Figure 5.30. Detail of tiles PNS34 (a) and PNS 39 (b), where the spreading of the colours can be observed.

Glaze compositions do not evidence a single recipe. Also, the analyses show no evidence of a white homogenous background – like the one in majolica or the Hispano-Moresque "green and brown" ceramics – on which the colours are applied. Instead, it seems that different coloured glaze frits are used like in *arista* or *cuerda seca* tiles. The relief itself causes the glaze frit to be absorbed in different ways, becoming more concentrated in specific areas and spread in others. The result is a variety of shades of the same colour with the details of the motif accentuated by the relief.

Green and brown glazes in PNS relief tiles stand out among all samples in this study. Higher SnO_2 contents (5-9 wt.%) appear in the green glazes of relief samples PNS09, PNS17, PNS30, PNS34-L and PNS35, and in brown glazes of relief samples PNS08, PNS09, PNS10, PNS18, PNS30 and PNS38. The SnO_2 content is not necessarily the same in all the coloured glazes of the same relief tile, as *Figure 5.31* illustrates. The exceptions are PNS30 and the relief tile with *cuerda seca* PNS09, which exhibit higher SnO_2 contents both in green and brown colours.

When manganese was mixed with a white tin glaze, the brown glaze resulted in an opaque lighter colour that is unique in this collection and in this group of tiles in particular. It is a different shade from the one observed in later majolica tiles, where the manganese pigment was applied over the glaze with a brush.

In PNS relief tiles, manganese brown is a homogenous colour. The tin-opacified green, on the other hand, exhibits a turquoise shade which, as already explained, was typical of Islamic ceramics but lost importance in Hispano-Moresque tiles (see *Chapter 5.2.3*).

Samples PNS08, PNS10, PNS16 and PNS18 belong to the same pattern and show tin-opacified brown glazes, whereas the tin oxide content in the green glazes is inferior to 2.5 wt.%. This pattern also exhibits the highest PbO contents of the relief set (53-55 wt.%).

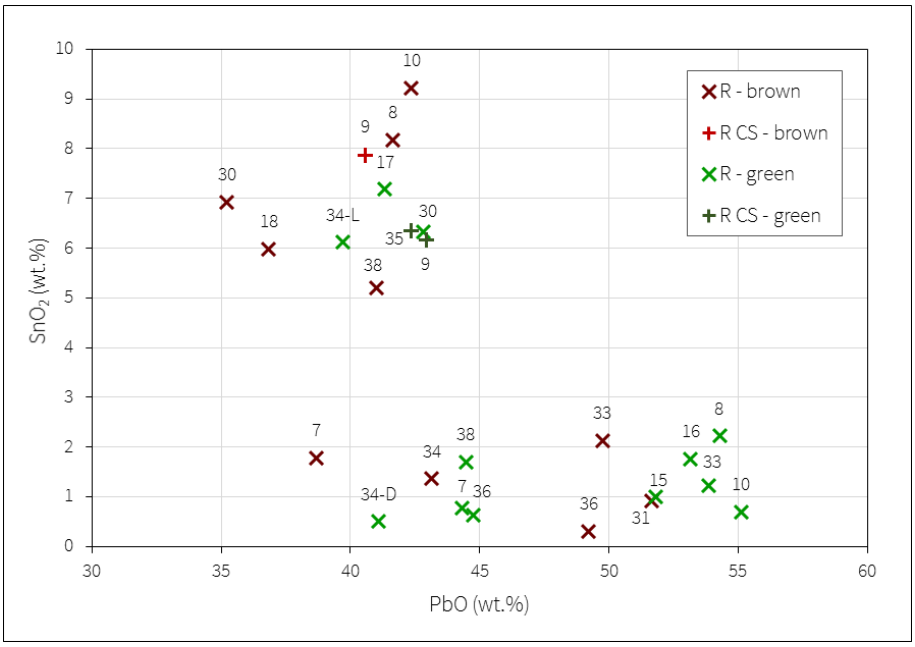

Figure 5.31. Scatter plot obtained from μ-PIXE analysis of the green and brown relief glazes in PNS tiles. Each sample is identified by its number.

Samples PNS07, PNS34-D, PNS36 and PNS38, whose green glazes are low both in tin and lead oxides, are all friezes and the green samples were taken from the frame (PNS34-D – darker green). Sample PNS34 was sampled in two green areas (one of which was the leaf) and the results show two different compositions. Comparing the two greens, the differences lie on the values of SnO_2 and Na_2O, which are higher in the light green (PNS34-L – the leaf). When observing sample PNS36, for instance, two shades of green can also be identified: a darker green on the frame and a lighter green in the interior motif. Thus, in this group of tiles, two greens were used. The darker green, however, differs from the "transparent" green that is common in most *cuerda seca* and *arista* tiles because its chemical composition resembles the tin-opacified glazes more than the transparent ones. In fact, the SiO_2/PbO ratio is identical in both greens of sample PNS34. This suggests that the same base recipe was used, to which was added more copper to obtain the darker green and more tin oxide to obtain the lighter one.

The chemical composition of white and blue glazes fits within the values obtained for the *cuerda seca* and *arista* tiles (5-9 wt.% SnO_2). Blue glazes show a Fe-Co-Ni-Cu association, consistent with Hispano-Moresque ceramics, with CoO contents between 0.23 wt.% and 0.45 wt.%. In blue glaze from relief sample PNS39, a mineral inclusion rich in Ni and Fe was observed by SEM-EDS (*Figure 5.32*). The μ-Raman

spectrum is consistent with a nickel ferrite ($NiFe_2O_4$) (Graves *et al*., 1988), which has also been identified in the blue glazes of samples SCV 14CF2686, SCV33Bi3839, CPS03, SCV 49-15F4338 and MCV 2-1T (see *Chapters 5.2.2* and *5.5*). As previously explained, nickel and iron are associated with the cobalt ore that was used for these glazes.

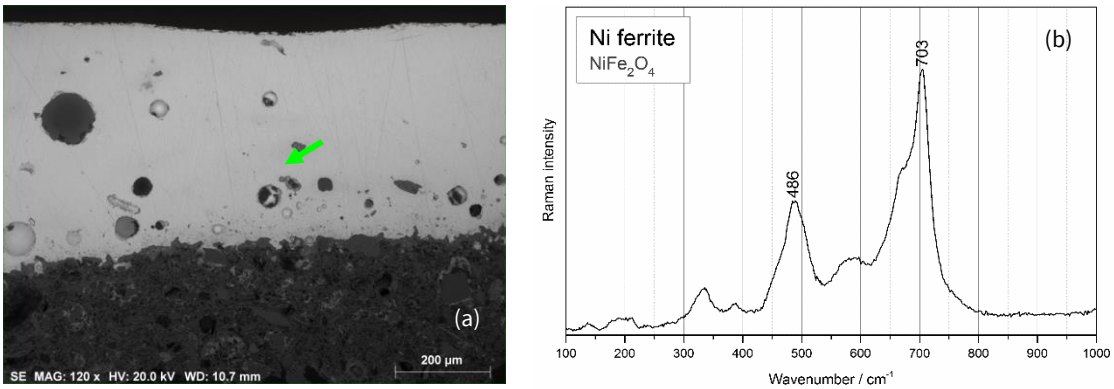

Figure 5.32. SEM image of the blue glaze in sample PNS39 **(a)** and µ-Raman spectrum **(b)** of a nickel ferrite identified in the inclusion pointed out in (a).

The reaction between the glaze and the ceramic body during the firing of the tile causes the formation of potassium feldspars in the interface. In SEM-EDS maps, a K-rich layer is observed in the large majority of the studied samples, sometimes together with small Ca-rich crystallites that form above (*Figure 5.33*). Through µ-Raman analysis, mostly K-feldspars (general formula $KAlSi_3O_8$) were identified. The Ca-rich particles were identified as wollastonite ($CaSiO_3$) and diopside ($MgCaSi_2O_6$).

In sample PNS08, malayaite ($CaSnO(SiO_4)$) was identified in the glaze-ceramic interface of the green glaze, which has also been noted in other green *arista* and *cuerda seca* glazes (see Chapter *4.2.3*). The fact that this compound has only been identified in green glazes reinforces the idea that it is somehow related to the colour since it is known that the reaction is promoted by the presence of a transition metal ion such as cobalt or copper (Mulholland, 1984; Piña *et al*., 2005).

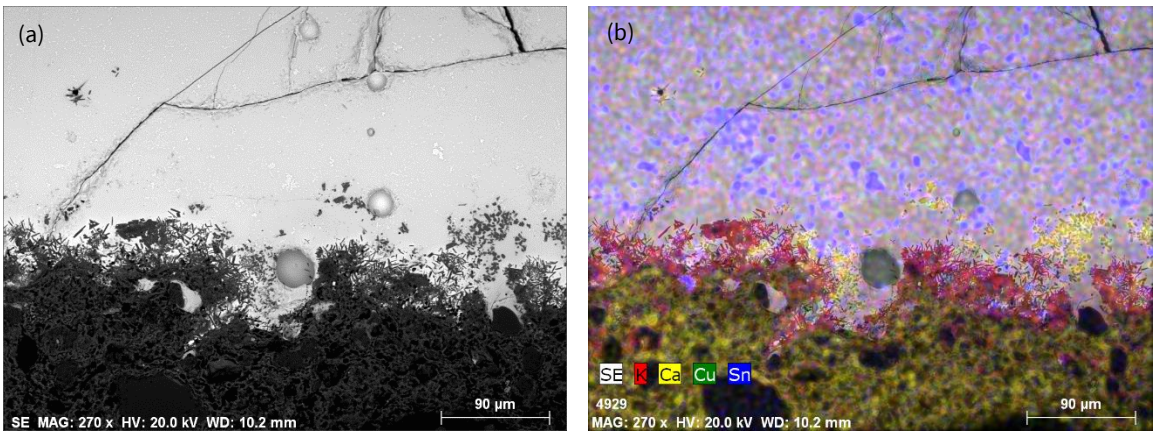

Figure 5.33. **(a)** BSE image and **(b)** EDS map of the green glaze in sample PNS09 illustrating a typical glaze-ceramic interface in PNS samples with a K-rich layer and some Ca-rich crystallites above.

The morphology of the glaze in sample PNS30 differs from the other tiles due to the many mineral inclusions it contains (*Figure 5.34*). Mostly large quartz crystals were identified by μ-Raman, whereas K-feldspars are scarce, small and mostly concentrated near the interface. Similar glazes were observed in Hispano-Moresque tiles attributed to Toledo from the IVDJ collection (see *Chapter 5.2.2*). Concerning the literature, large quartz inclusions have also been identified in Islamic tin-glazes from Zaragoza, Almería and Granada, and Hispano-Moresque tin-glazes from Teruel, Spain. This has been interpreted as an intentional procedure for lowering the production costs by reducing the necessary amount of tin for achieving a white opaque glaze (Molera *et al*., 2001b; Pérez-Arantegui *et al*., 2005, 2009a).

Sample PNS30 displays another characteristic that was not observed in the other relief tiles – a layer of Mn-rich inclusions located right above the glaze-body interface of the brown glaze, including a large particle (*ca.* 80 μm) that suggests an underglaze decoration instead of a reaction zone between the body and the Mn-containing glaze (*Figures 5.34b and 5.35*). In PNS30, the pigment is concentrated near the interface, like it was observed in Valencian tiles with underglaze decoration (see *Figure 5.41*). The Mn-rich layer is mostly constituted by braunite ($Mn^{2+}Mn^{3+}{}_6SiO_{12}$) and kentrolite ($Pb_2Mn_2Si_2O_9$) crystals, as identified by μ-Raman analysis (*Figure 5.36*). Kentrolite has been identified around braunite and hausmannite crystals that reacted with the lead glaze in Islamic ceramics (Molera *et al*., 2013) and in Hispano-Moresque tile IVDJ-T 4095. The presence of kentrolite suggests lower firing temperatures since this compound is stable between approximately 650 °C and 840 °C (Molera *et al*., 2013). Additionally, the presence of large braunite inclusions indicates that the manganese pigment was first fired at a higher temperature prior to its application on the tile, which was then fired at a temperature that might not have exceeded 900 °C.

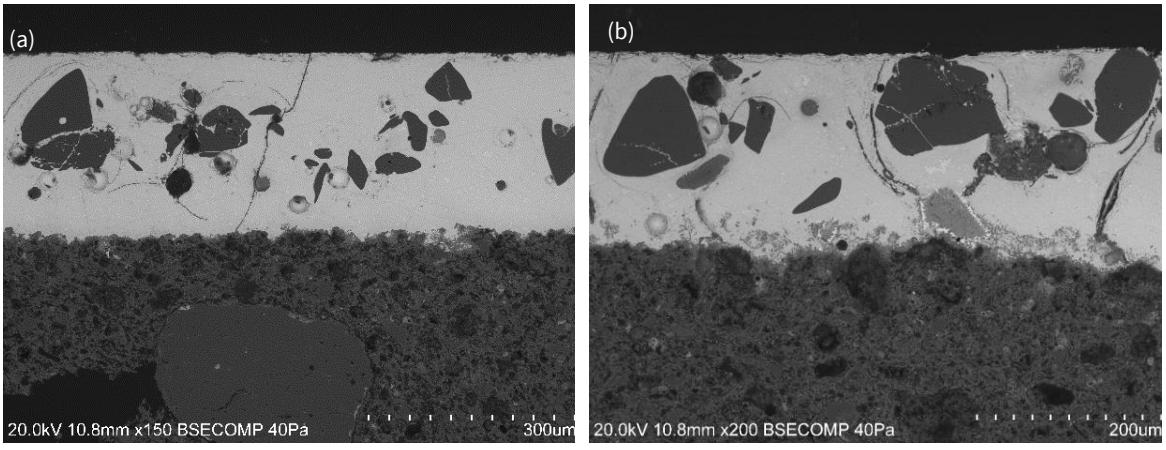

Figure 5.34. BSE images of cross section samples from PNS 30, showing many large inclusions in the glaze: (a) white; (b) brown.

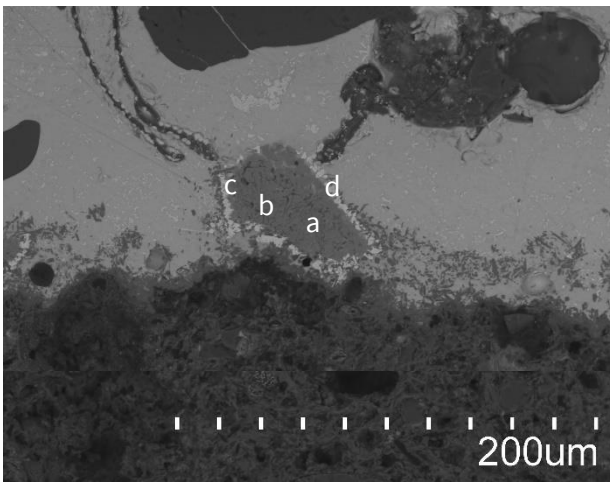

Figure 5.35. BSE image of the PNS 30 brown glaze, showing a large Mn-inclusion near the interface. The letters (a), (b), (c) and (d) refer to the location where the spectra in *Figure 5.35* were obtained from.

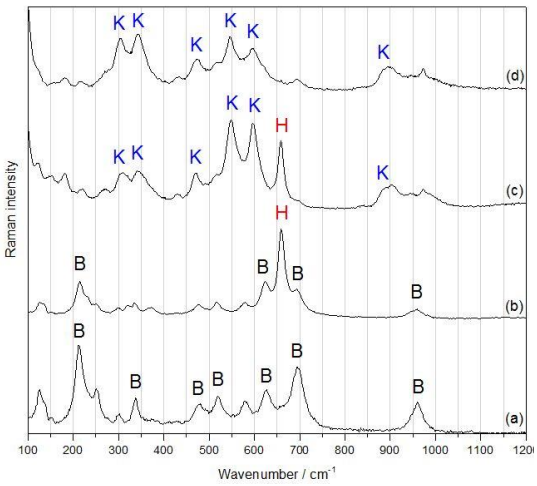

Figure 5.36. μ-Raman spectra obtained at different points of the Mn-inclusion observed in *Figure 5.34*: **B** Braunite, **H** Hausmannite, **K** Kentrolite.

5.5. UNDERGLAZE-DECORATED *RAJOLAS*, *ARISTA* AND LUSTRE-DECORATED TILES

In this chapter, three groups of tiles from three collections were studied together because of their specific characteristics that differ from the other typologies: either a blue-and-white underglaze decoration and/or a lustre layer make them stand out from the other Hispano-Moresque tiles under study. Both blue and white glaze areas were analysed, the blue being a white glaze with more or less cobalt pigment (and its associated elements) in its composition.

MCV samples (1-1 R, 2-1T, 3-1R, 4-1G, 4-2G, 8-1G, 8-2C and 8-3G) are the well-known Valencian *rajolas,* with blue-and-white underglaze decoration (*Figure 5.37*). These are flat tiles on which the cobalt blue pigment was applied on a bone-dry unfired ceramic body, followed by the first firing (biscuit-fire), after which the glaze frit was applied and a second firing took place (Coll, 2009a). Samples MCV 1-1R, 4-1G, 4-2G and 8-1G also have manganese-brown decorations, the latter three with the same motif.

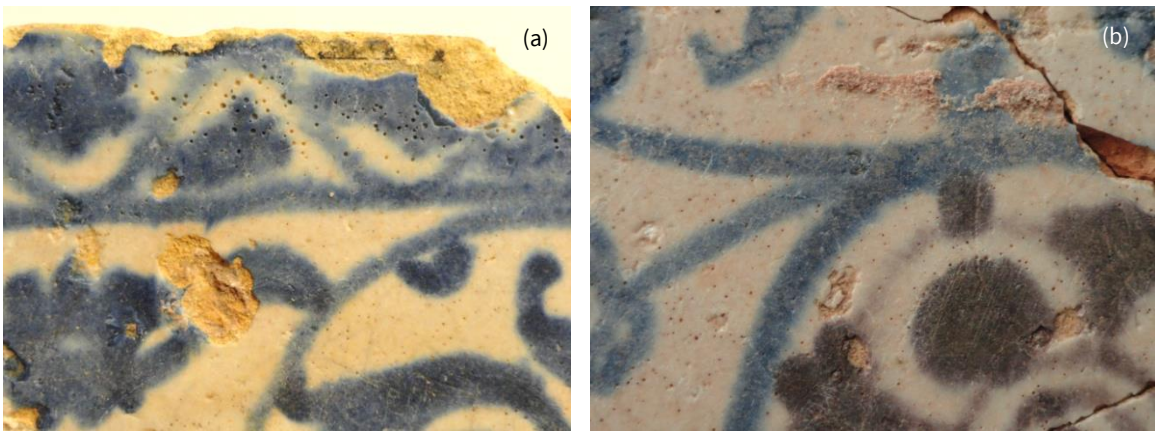

Figure 5.37. Details of the underglaze-decorated tile MCV 8-1G.

SCV group comprises three tiles (SCV 34Ei4068, SCV 494i4327 and SCV 49-15F4338) with cobalt blue underglaze decorations that were probably lustre-decorated as well – although there is no longer any residue of such lustre layer – and one blue-and-white relief tile (SCV 51-1M4467). The first three samples display slightly protruding the lines that define the contours of the decorative motifs. It seems that the decorations were marked onto the ceramic body of the tile by pressing the clay onto a mould in a similar process as the one used for *arista* tiles. In fact, the contours look like a very discrete *arista* protuberance which becomes even less visible once the glaze is applied on the totality of the surface. The hypothesis of the SCV group had been lustre-decorated comes from an identical pattern to the one of tile SCV 49-15F4338 observed in a framed panel in the Instituto Valencia de Don Juan, in Madrid. Nevertheless, this brocade pattern is the same as the one in *arista* sample IVDJ-S 4134 (*Figure 5.38*), as well as in other SCV *arista* and *cuerda seca* tiles.

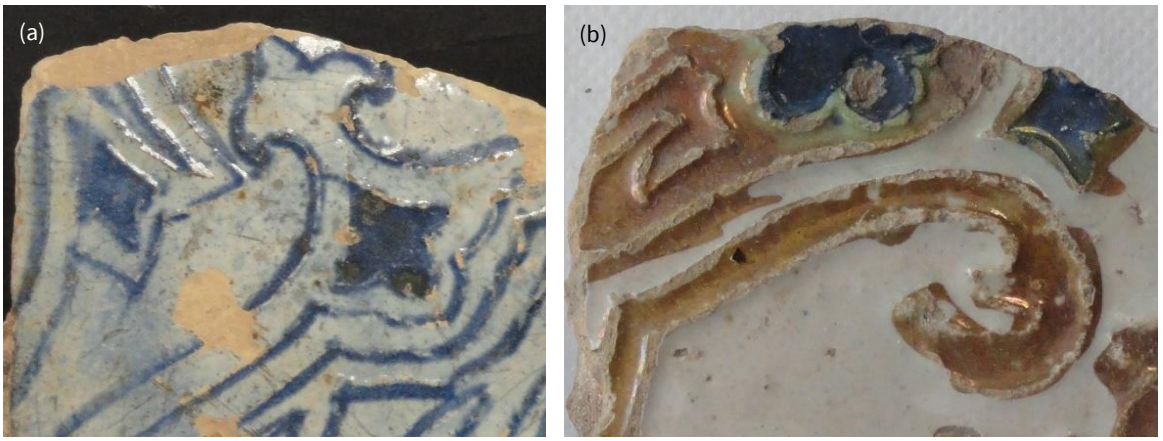

Figure 5.38. Detail of the surface of tiles: **(a)** SCV 49-15F4338, where the *arista* contours are discrete and marked in cobalt blue; **(b)** IVDJ-S 4134, where the *arista* contours are well visible and not painted in blue.

IVDJ-S group comprise two *arista* tiles with lustre-decorated blue-and-white glazes. Contrarily to the SCV samples, the *arista* contours are well visible. The glaze areas with different colours are well separated in sample IVDJ-S 4185, but in IVDJ-S 4134 both the blue and the lustre areas spread beyond the *arista* contours. Blue areas in IVDJ-S 4185 (*Figure 5.39*) are homogenous and therefore, it is not clear whether the blue pigment was applied underglaze or if a blue glaze mixture was used as for other *arista* and *cuerda seca* tiles.

The analysis of the glaze compositions by μ-PIXE identified tin contents within expected values for Hispano-Moresque tin-glazed ceramics (Coentro *et al*., 2014; Coentro *et al*., 2017; Molera *et al*, 1997, 2001b; Pérez-Arantegui, 2005, 2009a; Polvorinos del Rio & Castaing, 2010). The SnO_2 content is a distinctive factor among the three groups of samples, where the lowest values were identified for MCV tiles (3.7 – 4.7 wt.% SnO_2), followed by SCV (6.4 – 8.3 wt.% SnO_2) and IVDJ-S (7.8 – 9.7 wt.% SnO_2) samples.

Figure 5.39. Detail of the surface of sample IVDJ-S 4185.

Figure 5.40 illustrates the division between MCV samples and the other two groups, which is most visible in SnO_2 and K_2O contents, the latter being lower in SCV and IVDJ-S tiles. This difference in potassium content has been previously identified in a study comparing Sevillian and Valencian lustre-decorated ceramics (Polvorinos del Rio & Castaing, 2010). The higher potassium content in MCV glazes is more likely a consequence of several factors, such as its higher content in the sand used as a silica source for the glaze and the reaction with the also K-rich clay in the ceramic body, since the latter also presents higher potassium values in its composition (see *Chapter 4.1*). On the other hand, potassium could come from ashes obtained from forest plants or wine lees (Piccolpasso, 1980; Tite *et al*., 2006), but the source is very difficult to prove in a glaze due to the influence of the ceramic body in its final composition. Nevertheless, one can see a slight positive correlation between K_2O and SnO_2 in MCV group, which suggests that the potassium content is related to the glaze recipe in this collection.

The enrichment of the glaze in potassium is also documented for obtaining better results in lustre-decorated ceramics since there is an ionic exchange between the alkaline ions in the glaze (K^+ and Na^+) and the lustre-forming metallic elements (Cu and Ag) (Pradell *et al*., 2005). Therefore, the higher potassium contents could be not just derived from the characteristics of the available raw materials, but the result of an improved recipe as well, whose use became widespread in Valencia regardless of the lustre decoration.

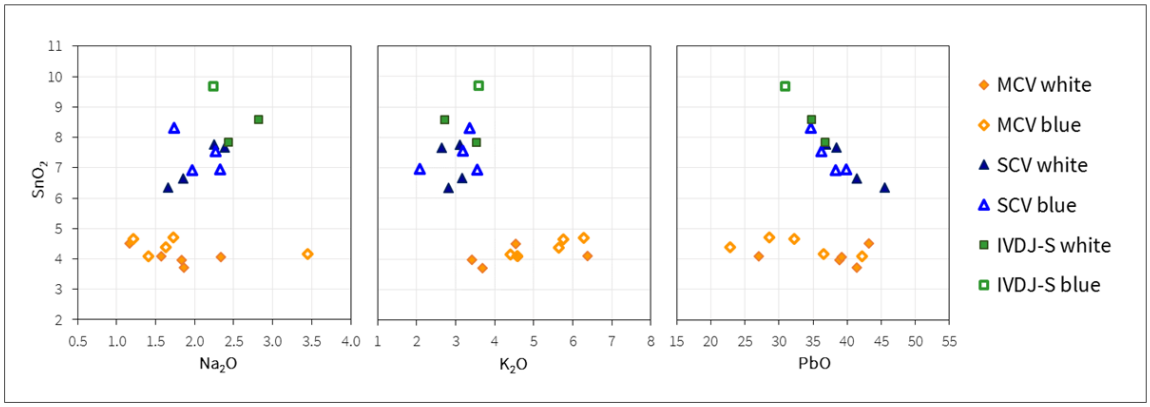

Figure 5.40. Scatter plots of SnO_2 vs. Na_2O, K_2O and PbO, obtained by μ-PIXE.

A positive correlation between sodium and tin oxides, as well as a negative correlation between lead and tin oxides, is visible in *Figure 5.40* for SCV and IVDJ-S samples. Results suggest that – in these two sets – tin was added to the glaze recipe together with a sodium-rich flux, but not with lead, contrarily to what is mentioned in the Persian treatise from 1301 by Abu l'Qasim (Allan, 1973) or in the Italian treatise on majolica by Cipriano Piccolpasso (*ca.* 1557) (Piccolpasso, 1980). They are, however, in accordance with the results obtained by Molera *et al*. (2009) from the analysis of frits found in archaeological context in a medieval kiln in Paterna, as previously discussed in *Chapter 5.2*. The white glaze in these tiles shows a similar composition to the one used for the other typologies. The differences seem to be related to production centres and not with the type of decoration.

Cobalt blue is the predominant colour in this set of tiles, being also what characterises Valencian ceramics the most. The analysis of blue-decorated glazes by μ-PIXE identified nickel in association with cobalt in most samples, as well as copper in approximately half of the analysed blue samples (see *Appendix IV – μ-PIXE results*). This result fits within the expected Fe-Co-Ni-Cu association identified in Hispano-Moresque ceramics until the beginning of the 16th century, as previously discussed in *Chapter 5.2.2* (*Blue glazes*).

Both the underglaze cobalt and manganese pigments were observed by SEM-EDS near the glaze-ceramic interface in MCV samples (*Figure 5.41*). The analysis by μ-Raman identified the inverse spinel nickel ferrite ($NiFe_2O_4$) in the blue glaze of samples SCV 49-15F4338 and MCV 2-1T, characterised by the bands at *ca.* 487 cm^{-1} *ca.* 703 cm^{-1} (Graves *et al*., 1988). Manganese-rich inclusions were identified as braunite ($Mn^{2+}Mn^{3+}{}_6SiO_{12}$) in samples MCV 1-1R and MCV 8-1G. As previously explained in *Chapter 5.2.5* (*Brown Glazes*), braunite is likely the result of the reaction between a manganese oxide used as pigment – such as pyrolusite (MnO_2), a common manganese ore – and the glaze matrix above 1000 ºC (Molera *et al*, 2013).

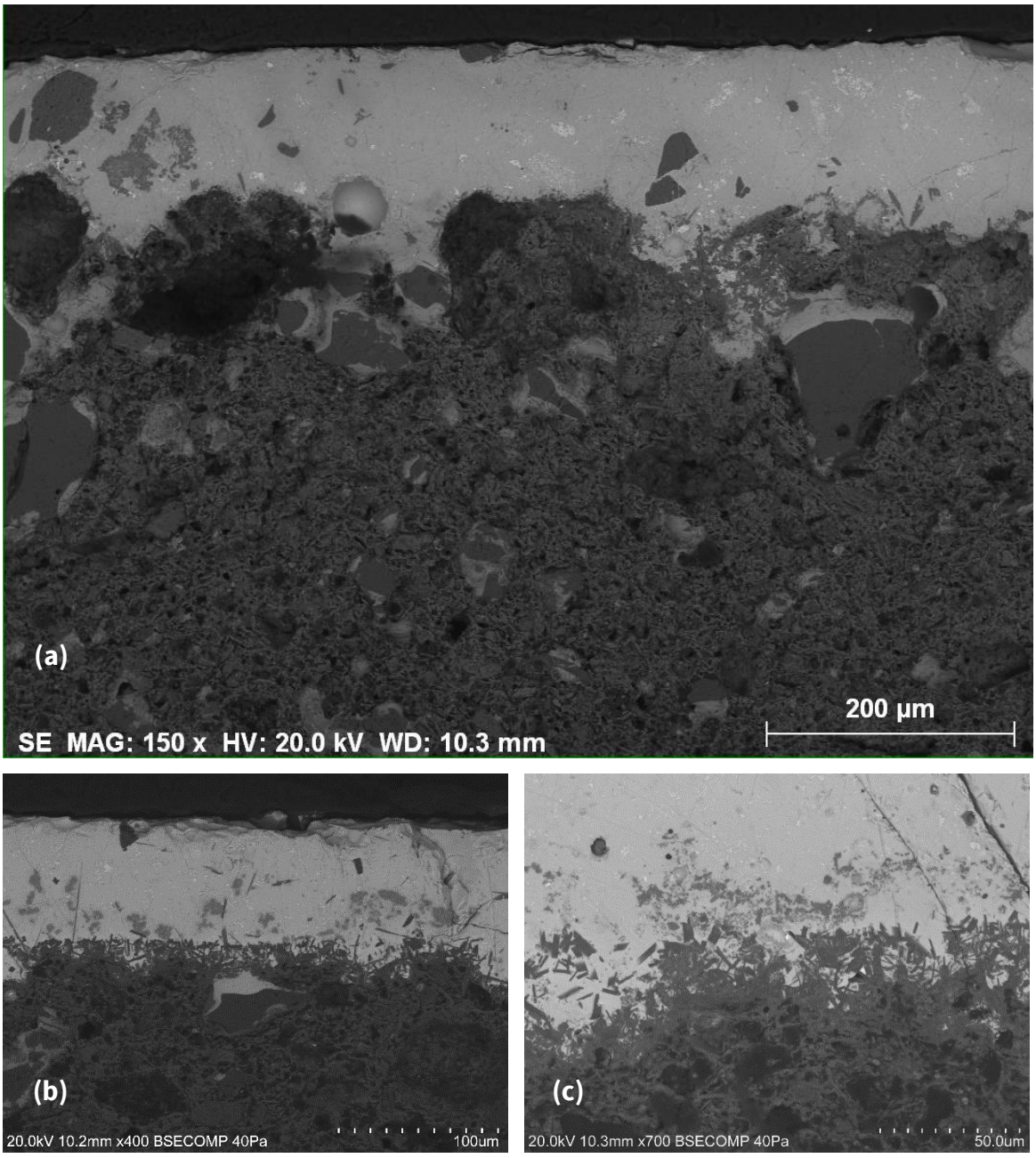

Figure 5.41. Cross-section BSE images of MCV underglaze-decorated tiles: (a) white glaze of sample MCV 3-1R, showing an irregular interface, mineral inclusions in the glaze and SnO_2 agglomerates; (b) brown glaze of sample 1.1R, with Mn-rich inclusions pointed out; (c) detail of the glaze-ceramic interface of sample 2-1T with a layer of Fe-Co-Ni inclusions pointed out in the glaze.

The interface shows a predominance of K-feldspar crystals, as identified by µ-Raman, displayed in an irregular layer. Tin oxide is homogeneously distributed throughout the glaze, although some larger agglomerates can be observed, as *Figure 5.41* illustrates.

The underglaze decoration in these tiles is their most innovative feature, as there are no known examples of tin-opacified underglaze-decorated ceramics until then. In order to better understand the behaviour of the pigments when applied under an opaque glaze, an experiment is being undertaken at the time of writing this thesis. The preliminary results were included in Appendix X.

5.6. REE AND TRACE ELEMENT ANALYSIS BY LA-ICP-MS

The analysis of the results obtained by LA-ICP-MS is here discussed concerning each collection regardless of the decoration technique. A further look into the silica-related REE and trace elements may provide some clues on the raw materials (e.g. sand) used for making the glaze. The main source of silica is generally sand, which, depending on its purity, also contains other minerals such as kaolinite, feldspars, zircon, rutile and a variety of iron oxides (Wedepohl *et al*., 2011). Minor and trace elements associated with the silica source are usually related to these minerals and not to the quartz crystals (Brems & Degryse, 2014).

Looking at the results from the LA-ICP-MS analysis, one can see that the concentrations of Zr and Ti are lower in IVDJ-T and MCV collections than in the others (*Figure 5.42a*). The scatter plot in *Figure 5.42b* shows a strong correlation between Zr and Hf – two elements related to the mineral zircon ($ZrSiO_4$), which has been identified in the glaze-ceramic interface by μ-Raman (*Appendix VI*). In *Figure 5.42b*, five samples stand out for their higher Zr and Hf contents (PNS07, PNS21, PNS32, IVDJ-S SN and IVDJ-S 4184), although they do not evidence other common characteristics that would suggest a different provenance. In opposition, IVDJ-T and MCV samples, both with secure different provenances (Toledo and Valencia, respectively), seem to have been produced with sands with low Ti, Zr and Hf contents. These three elements are usually correlated, as they often belong to the heavy mineral fraction of the sand raw materials used in glass and glazes (Brems & Degryse, 2014). The Zr/Hf ratio between 30 and 40, which has been measured for all collections, is associated with zircon derived from granites (Brems & Degryse, 2014).

Potassium and rubidium also show a correlation (*Figure 5.42c*), which suggests that Rb is related to K-feldspars (Brems & Degryse, 2014). The exception, with higher K and Rb contents, is MCV group (except in two samples), and tiles SCV SPF8435 and PNS 13. The latter two tiles also stand out in *Figures 5.42a* and *5.41b* with lower Ti, Zr and Hf contents. The two SAC tiles, as well as IVDJ-S 3794 and IVDJ-S 3919, show the lowest K and Rb values.

Barium and strontium show a correlation to calcium, although this is most visible in the PNS set (*Figure 5.42d*). Once again, SCV SPF8435 shows a different composition, with the lowest values measured for these elements. The correlation among Ba, Sr and Ca may relate to the carbonates in the raw material (Brems & Degryse, 2014).

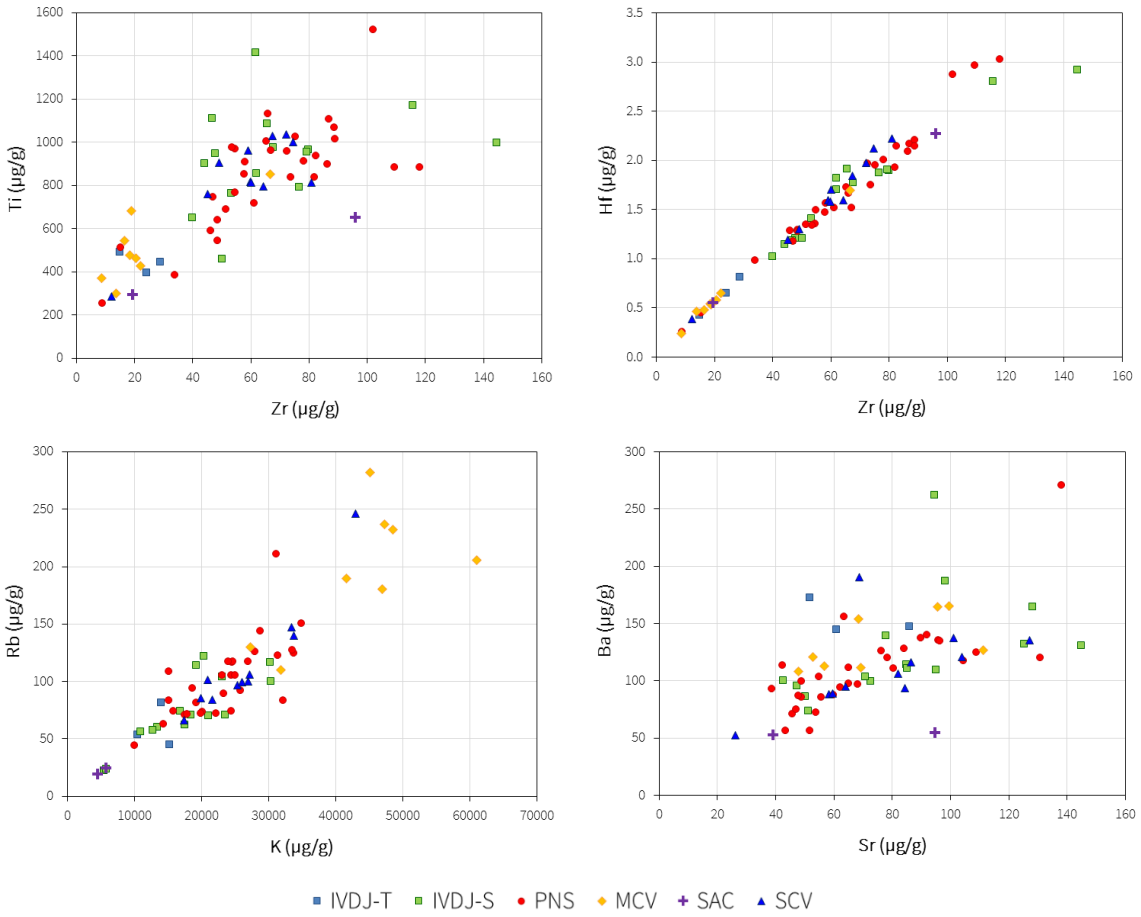

Figure 5.42. Scatter plots of white glazes obtained from the LA-ICP-MS results: **(a)** Zr *vs.* Ti; **(b)** Zr *vs.* Hf; **(c)** K *vs.* Rb; **(d)** Sr *vs.* Ba.

CONCLUSIONS
AND FUTURE WORK

This was the first archaeometric study comparing Hispano-Moresque tiles from different Portuguese and Spanish collections. Despite the increasing interest in the Iberian ceramic cultural heritage, a specific study dedicated to architectural tiles was lacking. With this in mind, this thesis offers a first approach to the technological characterisation of these impressive – although somehow undervalued – architectural tiles.

The experimental methodology was designed to be as minimally invasive as possible. Only small samples were collected from the tiles and the procedure could take place *in situ*, allowing for the study of tiles without transporting them from their original location. Non-destructive analytical techniques were preferred so that the same sample could be analysed by more than one method. This way, the studied samples are preserved for future analysis and the methodology may easily be reproduced in studies that may follow.

Hispano-Moresque ceramics in their varied manifestations represent times of great cultural and political changes. The evolution of the patterns and the simplification of the production process of architectural tiles reflect these changes, but no remarkable differences were detected in the chemical compositions of glazes and ceramic pastes that would otherwise reflect a chronological or geographical specificity.

This work shows that the glaze technology employed in Hispano-Moresque tiles followed the Islamic tradition that was introduced in the Iberian Peninsula from the 8th century onwards. High-lead glazes (ca. 30-50 wt.% PbO) were identified in all analysed samples. The quantification of the chemical composition of the final glaze is affected by the reactions that occur between the glaze and the ceramic body during firing. Therefore, the analyses must take into account the diffusion of elements from the ceramic body into the glaze, such as Mg, Ca, Al, Fe and K, as well as the loss of lead content that diffuses from the glaze into the ceramic body. Such influencing factors make it more difficult to compare the chemical

composition of different glazes among groups of samples. Nevertheless, the final compositions are still the result of the glaze recipes, together with the compositions of the bodies and firing conditions, which all make up the technological process of specific workshops / production centres.

Two types of high-lead glazes were identified: "transparent" and tin-opacified. Transparent glazes contain a very small percentage of tin as well (< 2 wt.% SnO_2), although not enough to render the glaze opaque. It is not clear whether this is a contamination or an intentional addition to increase the compatibility between the different coloured glazes on the tile. The systematic presence of tin in transparent glazes of all the studied collections, however, suggests an intentional procedure. Tin glazes exhibit similar characteristics to the ones reported in the literature for coeval ceramics – homogeneity, small well-distributed SnO_2 agglomerates and occasional gas bubbles – that suggest the use of frits. Besides the disparity in tin contents, the two glaze types also evidence differences in sodium and lead values. Early-20th-century testimonies (González Martí, 1952) mention the addition of sodium chloride to the white tin glaze, although there is no 15th-16th-century proof that confirms if it was common salt or any other Na-rich flux (e.g., coastal plant ashes) that was added to the glaze recipe. The diffusion of other elements from the ceramic body also masks the association between Na and, e.g., P, Ti or Fe, which would otherwise give clues on the flux added. Nevertheless, it is likely that some sodium compound was added to compensate for the lower PbO content in tin-opacified glazes.

The pictorial layer is composed of five colours: white, blue, green, amber and brown. These colours exhibit different shades that depend on the glaze recipe, its thickness and the influence of the underlying ceramic body. The findings of this work are that white and blue are consistently tin-opacified, whereas most green, amber and brown glazes are transparent. Blue glazes present a cerulean shade that is very characteristic of Hispano-Moresque tiles and which was found to result from the cobalt oxide (ca. 0.2-06 wt.% CoO) diluted in the white tin glaze. Green glazes owe their most common bottle-green shade to the copper oxide dissolved in the transparent lead glaze matrix, whereas a turquoise shade was associated with the addition of copper oxide to the tin-opacified glaze. Amber is found associated with iron oxide and the brown colour with manganese oxide.

The homogeneity of the glazes does not leave much information on the raw materials used for the colours. However, through μ-Raman and SEM-EDS analysis, some inclusions were detected and identified on the blue and brown glazes. Manganese brown glazes show the highest number of colour-related inclusions: braunite, hausmannite, jacobsite, kentrolite and bustamite. The finding of coexisting braunite and/or hausmannite in the same location while kentrolite is confined to a surrounding border region in inclusions, is taken as an indication that the manganese ore was previously calcined at ca. 1000 °C, whereas the final firing of these kentrolite-containing glazes did not surpass 900 °C.

Most blue glazes show a Fe-Co-Ni-Cu association, as identified by μ-PIXE and LA-ICP-MS, which is consistent with a late 15th century to early 16th-century chronology. Only a small part of the analysed blue glazes shows trace evidence of copper, as well as higher arsenic and bismuth contents, consistent with

the zaffre that was exported from the Saxony region (in actual Germany). All glazes with higher As contents belong to arista tiles, which confirms a later chronology.

This archaeometric study concluded also that calcareous clays were the standard material used for the ceramic body of the tiles. Often the lime content was found higher than 20 wt.%, which is a high value among the typical calcareous clays analysed in the literature, although within the expected results for tin-opacified ceramic bodies. Among other advantages, calcareous clay bodies offer a light-coloured background on which to apply the different glazes and this becomes especially relevant to achieve a white tin glaze.

An important overall conclusion is that the technology employed in the production of Hispano-Moresque tiles appears identical among all the studied collections. Even among the tile sets with secure provenances (MCV, CPS, IVDJ), only small differences were observed, attesting for a widespread technology throughout the Iberian Peninsula, inherited from the Muslim presence.

The chemical composition of the glazes in PNS relief glazes was found to be similar to the other Hispano-Moresque glazes, albeit introducing some novelties in brown and green tin-opacified glazes, such as the simultaneous use of two green shades – a dark green and a tin-opacified light green – in some tiles. Also, the combination of *cuerda seca* and relief techniques seems to be unique in Sintra. This set of tiles evidence a period of experimentation and evolution of both the decoration techniques and the motifs.

Sample PNS30 shows important differences from the other tiles. The ceramic body shows higher alumina and silica contents. The concentration of manganese-rich particles right above the glaze-ceramic interface suggests an under-glaze decoration, which was only known at that time for relief polychrome ceramics in the Islamic *laqabi* ware (Mason *et al*., 2001). Other tiles with the same pattern as PNS30 were placed on the walls of the Palace (in the room of king D. Sebastião) despite the major glaze runoffs, metalized copper-green glazes and other defects which attest to the inexperience in this production, suggesting that PNS30 might represent the first attempt to produce relief tiles for the National Palace of Sintra. From then on, other (more pronounced) relief tiles were made and the technology was perfected. Samples like PNS38 and PNS39 might represent the final stage of this technology, with homogeneous glazes and strong colours, resembling the Della Robbia or the Niculoso Pisano's glazed terracotta works from the beginning of the 16th century.

The tiles from the Santo António da Charnerca's archaeological kiln are chemically and morphologically very different from all the other studied samples. Their non-calcareous ceramic bodies and the heterogeneous matte glazes have no parallel in published studies on Hispano-Moresque tiles so far. These tiles look like an isolated experience and probably remained in the kiln because they did not turn out well. Despite being the only archaeological evidence in a kiln context representing a Portuguese Hispano-Moresque tile production in the early 16th century, these samples cannot attest for a large-scale production due to the above-mentioned differences in chemical composition.

The absence of other kiln sites in Portugal with tile shards – or other production markers that would serve as the basis for comparison – withholds the resolution of the provenance problem, since the results of the archaeometric study identify a widespread ceramic technology. Nevertheless, it is still visible a higher proximity between the CPS, IVDJ-S, SCV and PNS collections – although with differences among them –, whereas the MCV tiles show the strongest differences, with a predominance of cobalt blue – and occasionally manganese brown – underglaze decorations, and glazes with higher potassium contents.

FUTURE WORK

One of the aims of this work is to point out the importance of this tile heritage that represents a key transition period in the Iberian history. Important collections were studied here although there are many others still left to study. Therefore, the main intention is that this work will continue with multi-disciplinary collaborations that will allow connecting all the different aspects characterising these amazing tiles: the glaze and ceramic technology, raw materials, production centres, decorative patterns and the colour palette.

A further study of the glaze recipes would not be complete without their reproduction. This has been started within the project *Az-Med* (with the work of Leal (2014) and other unpublished data). The absence of ceramic treatises on medieval European ceramics leaves the comparisons to other two main sources: the Persian treatise from Abu l'Qasim (1301) and the Italian majolica treatise from Cipriano Piccolpasso (ca. 1557). An important parallel must be made with the sources on enamels, since the technology is similar.

The study of architectural tiles must take into account the possible influence of the mortar that was used to place them on the walls and floors. Lime mortar was commonly used and its effects on the alteration of the ceramic body composition are not well-known, namely the possible impact on the formation of secondary calcite. This would be important to access in a future study.

Finally, one of the most remarkable characteristics observed during this study was the very good state of conservation of the majority of the tiles. Even archaeological samples that were buried for centuries show minimal (or inexistent) glaze detachment. The thick glaze-ceramic interface layer is likely an important factor promoting the adhesion between the two components of the tile, but a dedicated study on this matter is still lacking. The specific nature of arista and cuerda seca tiles, with small continuous, homogeneous glazed areas that are separated by unglazed lines, probably avoid major thermal expansion incompatibilities that would result in shivering or crazing of the glaze. At the same time, water is allowed to circulate throughout the complete thickness of the tile due to the porous nature of the dividing lines between the glazed areas, which partly avoid the crystallization of salts that are often observed trapped between the glaze and the ceramic body in majolica tiles. These factors ought to be studied, as the conservation challenges of Hispano-Moresque tiles may be different than the ones of other architectural decorations.

REFERENCES

AA.VV., 2013 — AA.VV. (2013). *O Brilho das Cidades. A Rota do Azulejo*. Lisboa: Fundação Calouste Gulbenkian.

Aguado, 1977 — Aguado Villalba, J. (1977). La azulejería toledana a través de los siglos, *Toletum: boletín de la Real Academia de Bellas Artes y Ciencias Históricas de Toledo*, 8, p. 31-88.

Alho *et al*., 2015a — Alho, A.P., Trindade, R., Coentro, S., & Muralha, V.S.F. (2015a). Um olhar sobre a documentação de Setúbal e a azulejaria medieval em Portugal, in: (eds) Delgado Rodrigues, J., and Mimoso, J.M., *Proceedings of GlazeArch 2015 – International Conference on Glazed Ceramics in Architectural Heritage*. Lisboa: LNEC, Colecção: Reuniões Nacionais e Internacionais, p. 111-113.

Alho *et al*., 2015b — Alho, A.P., Trindade, R., Coentro, S., & Muralha, V.S.F. (2015b). Á luz da documentação: A azulejaria entre os séculos XIV e XVI na cidade de Lisboa, um estudo de proveniência. In: Santos, A.A., Alberto, E.M., and Coutinho, M.J.P., *Arquivo Municipal de Lisboa: Um acervo para a História II*, Arquivo Municipal de Lisboa, p. 27-38.

Allan, 1973 — Allan, J. W. (1973). Abu'l-Qasim's Treatise on Ceramics, *Iran*, 11, p. 111-20.

Anthony *et al*., 2003 — Anthony, J.W., Bideaux, R.A., Bladh, K.W., & Nichols, M.C. (2003). *Handbook of Mineralogy,* Tucson, USA: Mineral Data Publishing (Available online at: http://www.handbookofmineralogy.org/search.html?p=all)

Ben Amara & Schvoerer, 2006 — Ben Amara, A., & Schvoerer, M. (2006). Interaction between leads glazes and bodies: Research on the mode of application of the glazing mixture, In: (coord) Pérez-Arantegui, J. , *Proceedings of the 34th International Symposium on Archaeometry,* p. 399-404

Bernal, 2011 — Bernal, A.A. (2011). El origen de la Casa de Pilatos de Sevilla. 1483-1505, *Atrio*, 17, p. 133-172.

Barros *et al*., 2003 — Barros, l., Cardoso, G., & Gonçalves, A. (2003). Primeira notícia do forno de S. António da Charneca – Barreiro, *Actas das 3as Jornadas de cerâmica medieval e pós-medieval*, p. 295-307.

Brems & Degryse, 2014 — Brems, D. & Degryse, P. (2014), Trace Element Analysis in Provenancing Roman Glass-Making. *Archaeometry*, 56, p. 116-136.

Brill, 1999 — Brill, R. H. (1999). *Chemical Analysis of Early Glasses*. Corning, New York: The Corning Museum of Glass.

Buxeda i Garrigós *et al*., 2002 — Buxeda i Garrigós, J., Mommsen, H. & Tsolakidou, A. (2002), Alterations of Na, K and Rb concentrations in Mycenaean pottery and a proposed explanation using X-ray diffraction. *Archaeometry*, 44, p. 187–198.

Buzgar *et al*., 2013 — Buzgar, N., Apopei, A.I., & Buzatu, A. (2013). Characterization and source of Cucuteni black pigment (Romania): vibrational spectrometry and XRD study, *Journal of Archaeological Science*, 40 (4), p. 2128-2135.

Calligaro, 2008 — Calligaro, T. (2008). PIXE in the study of archaeological and historical glass, *X-Ray Spectrometry*, 37, p. 169-177

Campbell *et al*., 2010 — Campbell, J.L., Boyd, N.I., Grassi, N., Bonnick, P., & Maxwell, J.A. (2010). The Guelph PIXE Software Package IV. *Nuclear Instruments and Methods B*, 268, p. 3356-3363.

Carvalho *et al*., 2016 — Carvalho, F., Coentro, S., Costeira, I., Trindade, R.A.A., Alves, L.C., da Silva, R.C., & Muralha, V.S.F. (2016). The Cistercian glazed tiles of the Monastery of Alcobaça: characterisation of the colour palette. *Journal of Medieval Iberian Studies*, 8 (2), p. 196-216.

Chapoulie *et al*., 2005 — Chapoulie, R., Delery, C., Daniel, F., & Vendrell-Saz, M. (2005). Cuerda seca ceramics from Al-Andalus, Islamic Spain and Portugal (10^{th}–12^{th} centuries AD): investigation with SEM-EDX and cathodoluminescence, *Archaeometry*, 47 (3), p. 519-534.

Coentro *et al*., 2012 — Coentro, S., Lima, A.M., Silva, A.S., Pais, A.N., Mimoso, J.M., & Muralha, V.S.F. (2012), Pigments and pigment mixtures in Portuguese 17^{th} century Azulejos. *Journal of the European Ceramic Society*, 32 (1), p. 37-48.

Coentro *et al*., 2014 — Coentro, S., Trindade, R.A.A., Mirão, J., Candeias, A., Alves, L.C., da Silva, R.C., & Muralha, V.S.F. (2014). Hispano-Moresque ceramic tiles from the Monastery of Santa Clara-a-Velha (Coimbra, Portugal), *Journal of Archaeological Science*, 41, p. 21-28.

Coentro et al., 2017 — Coentro, S., Alves, L.C., Relvas, C., Ferreira, T., Mirão, J., Molera, J., Pradell, T., Trindade, R.A.A., da Silva, R.C., & Muralha, V.S.F. (2017). The Glaze Technology of Hispano-Moresque Ceramic Tiles: A Comparison Between Portuguese and Spanish Collections. *Archaeometry,* doi: *10.1111/arcm.12280*

Coll Conesa, 2009a — Coll Conesa, J. (2009a). Cobalt blue in medieval ceramic production in the Valencian workshops. Manises, Paterna and Valencia, Spain, *Medieval Ceramics,* 31, p. 11-24.

Coll Conesa, 2009b — Coll Conesa, J. (2009b). *La Cerámica Valenciana: Apuntes para una sínteses*. Asociacion Valenciana de Cerámica. Valencia: Avec-Gremio/RM Ediciones.

Coll Conesa & Pérez, 1993 — Coll Conesa, J., & Pérez Camps, J. (1993). Aspectos de la técnica de fabricación en la cerámica de Manises (siglos XIV-XVI), *IV Congreso de Arqueologia Medieval Española: Sociedades en transición*. Alicante: Associación Española de Arqueologia Medieval.

Colomban, 2013a — Colomban, Ph. (2013a), Rocks as blue, green and black pigments/dyes of glazed pottery and enamelled glass artefacts – A review, *European Journal of Mineralogy*, 25 (5), p. 863-879.

Colomban, 2013b — Colomban, Ph. (2013b). Non-Destructive Raman Analysis of Ancient Glasses and Glazes, In: Koen Janssens (Ed), *Modern Methods for Analysing Archaeological and Historical Glass*, UK: John Wiley & Sons, Inc., p. 275-300.

Côrte-Real, 2003 — Côrte-Real, A. (2003). *O Mosteiro de Santa Clara-a-Velha. Olhares Ocultos. Olhares Submersos*, Coimbra: Quarteto Editora.

Costa *et al*., 2014 — Costa, M., Cachim, P., Coroado, J., Rocha, F., & Velosa, A. (2014). Ancient Wall Tiles – The Importance of the Glaze/Ceramic Interface in Glaze Detachment, *Materials Science (Medžiagotyra)*, 20 (1), p. 108-113.

Coutinho *et al.*, 2016a — Coutinho, M.L., Veiga, J.P., Alves, L.C., Mirão, J., Dias, L., Lima, A.M., Muralha, V.S., & Macedo, M.F. (2016a). Characterization of the glaze and in-glaze pigments of the nineteenth-century relief tiles from the Pena National Palace, Sintra, Portugal, *Applied Physics A,* 122: 696.

Coutinho *et al.*, 2016b — Coutinho, I., Medici, T., Alves, L.C., Gratuze, B., & Vilarigues, M. (2016b). Provenance studies on façon-de-Venise glass excavated in Portugal, *Journal of Archaeological Science: Reports*, 7, p. 437-448.

De Clercq *et al*, 2015 — De Clercq, W., Braekevelt, J., Coll Conesa, J., Kaçar, H., Vicente Lerma, J., & Dumolyn, J. (2015). Aragonese Tiles in a Flemish Castle: A Chivalric Gift-Exchange Network in Fifteen-Century Europe, *Al-Masāq*, 27 (2), p. 153-171.

Eames, 1992 — Eames, E. (1992). *English Tilers* – Collection "Medieval Craftsmen", London: British Museum Press.

Estall & Alfonso, 2003 — Estall, V., & Alfonso, J. (2003). Pavimentos Medievales y Post-Medievales de Onda (siglos XIII-XVIII). *Arqueología del Pavimento Cerámico desde la Edad Media al Siglo XIX.* Manises: Asociación de Ceramología.

Fabbri *et al.*, 2014 — Fabbri, B., Gualtieri, S., & Shoval, S. (2014). The presence of calcite in archaeological ceramics*, Journal of the European Ceramic Society*, 34, p. 1899-1911.

Fares *et al.*, 2012 — Fares, M., Pais, A.N., Martins, I.M., Coentro, S., Pereira, S., Muralha, V., & Mimoso, J.M., (2012). *Azulejo blues – an analytic study of the blue shades in Portuguese azulejos*, Proceedings of the International Congress AZULEJAR, 10-12th October 2012, Aveiro, Portugal

Fehervari, 2012 — Fehervari, G. (2012). *Tareq Rajab Museum, Kuwait: Ceramics in the Museum* [online]. Available at: http://www.trmkt.com/ceramics.htm (accessed in 22-07-2016)

Freeman *et al.*, 2008 — Freeman, J.J., Wang, A., Kuebler, K.E., Jolliff, B.L., & Haskin. L.A. (2008). Characterization of natural feldspars by Raman spectroscopy for future planetary exploration. *Canadian Mineralogist*, 46(6), pp.1477–1500.

Garcia Iñañez, 2007 — Garcia Iñañez, J. (2007). *Caracterització arqueomètrica de la ceràmica vidriada decorada de la Baixa Edat Mitjana al Renaixement als centres productors de la Península Ibèrica*. PhD Thesis, Universitat de Barcelona.

Garofano *et al.*, 2015 — Garofano, I., Robador, M.D., Perez-Rodriguez, J.L., Castaing, J., Pacheco, C., & Duran, A. (2015). Ceramics from the Alcazar Palace in Seville (Spain) dated between the 11th and 15th centuries: Compositions, technological features and degradation processes, *Journal of the European Ceramic Society*, 35 (15), p. 4307-4319.

Gestoso y Pérez, 1903 — Gestoso y Pérez, José. *Historia de los Barros Vidriados Sevillanos desde sus orígenes hasta nuestros días*, Sevilla: Tipografia La Andalucía Moderna; 1903

Gill & Rehren, 2011 — Gill, M.S., & Rehren, T. (2011). Material characterization of ceramic tile mosaics from two 17th century Islamic monuments in northern India. *Archaeometry*, 53, p. 22-36.

Giussani *et al.*, 2009 — Giussani, B., Monticelli, D., & Rampazzi,L. (2009). Role of laser ablation-inductively coupled plasma-mass spectrometry in cultural heritage research: a review, *Analytica Chimica Acta*, 635, p. 6-21.

Góis, 1926 — Góis, Damião de (1926), *Crónica do Felicíssimo Rei D. Manuel*, Parte I, Coimbra, Imprensa da Universidade.

Gomes, 2011 — Gomes, J.R.P. (2011). *Exemplos da Azulejaria dos Séculos XVI e XVII, em Coimbra*. Master's Thesis. Faculdade de Letras da Universidade de Coimbra.

González Martí, 1952 — González Martí, M. (1952), *Cerámica del Levante Español*, I, II y III. Barcelona: Ed. Labor.

Gradmann *et al*., 2015 — Gradmann, R., Berthold, C., & Schüssler, U. (2015). Composition and colouring agents of historical Islamic glazes measured with EPMA and μ-XRD^2, *European Journal of Mineralogy*, 27, p. 325-335.

Gratuze *et al*., 1997 — Gratuze, B., Soulier, I., Blet, M., & Vallauri, L. (1997). De l'origine du cobalt : du verre à la céramique, *Revue d'Archéométrie*, 20, p. 77-94.

Gratuze, 2003 — Gratuze, B. (2013). Glass Characterisation Using Laser Ablation Inductively Coupled Plasma Mass Spectrometry Methods. In: Janssens, K. (Ed), *Modern Methods for Analysing Archaeological and Historical Glass*, UK: John Wiley & Sons, Inc., p. 201-234.

Graves *et al*., 1988 — Graves, P.R., Johnston, C., & Campaniello, J.J. (1988). Raman scattering in spinel structure ferrites, *Materials Research Bulletin*, 23 (11), p. 1651-1660.

Grime & Dawson, 1995 — Grime, G.W., & Dawson, M. (1995). Recent Developments in Data Acquisition and Processing on the Oxford Scanning Proton Microprobe, *Nuclear Instruments and Methods B*, 104, p. 107-113.

Guirao *et al*., 2014 — Guirao, D., Pla, F. & Acosta, A. (2014). The Archaeometric Characterization of Majolica Ceramics from Talavera de la Reina and El Puente del Arzobispo (Toledo, Spain). Archaeometry, 56, p. 746–763.

Hall *et al*., 1999 — Hall, M., Amraatuvshin, Ch., & Erdenbat, E. (1999). X-ray fluorescence analysis of pottery from Northern Mongolia, Journal of Radioanalytical and Nuclear Chemistry, 240 (3), p. 763-773.

Holakooei *et al*., 2013 — Holakooei, P., Petrucci, F.C., Tassinari, R., & Vaccaro, C. (2013). Application of WDXRF in the provenance studies of Persian haft rang tiles: a statistical approach. *X-Ray Spectrometry*, 42, p. 105–115.

Janssens, 2013a — Janssens, K. (2013a). X-Ray Based Methods of Analysis. In: Janssens, K. (Ed), *Modern Methods for Analysing Archaeological and Historical Glass*, UK: John Wiley & Sons, Inc., p. 79-128.

Janssens, 2013b — Janssens, K. (2013b). Electron Microscopy. In: Janssens, K. (Ed), *Modern Methods for Analysing Archaeological and Historical Glass*, UK: John Wiley & Sons, Inc., p. 129-154.

Janssens & van Grieken, 2004 — Janssens, K., & van Grieken, R. (2004). Non-Destructive Microanalysis of Cultural Heritage Materials. Wilson & Wilson's Comprehensive Analytical Chemistry - Volume XLII, Amsterdam: Elsevier B.V., p. 1-10.

O'Kane, 2011 — O'Kane, B. (2011). And Diverse are Their Hues: Color in Islamic Art and Culture. In: (Eds) Bloom, J., & Blair, S., *The Biennial Hamad bin Khalifa Symposium on Islamic Art.* New Haven: Yale University Press.

Kamble *et al*., 2015 — Kamble, R. B., Varade, V., Ramesh, K. P., & Prasad, V. (2015). Domain size correlated magnetic properties and electrical impedance of size dependent nickel ferrite nanoparticles. *AIP Advances*, 5 (1), 17119.

Kessler, 2012 — Kessler, A.T. (2012). *Song Blue and White Porcelain on the Silk Road*, Studies in Asian Art and Archaeology, Vol 27, Leiden: Brill.

Lapuente & Pérez-Arantegui, 1999 — Lapuente, P., & Pérez-Arantegui, J. (1999). Characterisation and Technology from Studies of Clay Bodies of Local Islamic Production in Zaragoza (Spain), *Journal of the European Ceramic Society*, 19, p. 1835-1846.

Leal, 2014 — Leal, A.S.P. (2014). *Estudo da Tecnologia de Produção dos Azulejos Hispano-Mouriscos da Colecção do Museu do Teatro Romano de Lisboa*, Master's Thesis. Monte de Caparica: Faculdade de Ciências e Tecnologia da Universidade Nova de Lisboa.

Lin, 2001 — Lin, C.C. (2001). Vibrational spectroscopic study of the system α-Co_2SiO_4 - α-Ni_2SiO_4. *Journal of Solid State Chemistry*, 157 (1), p. 102–109.

Lino, 1948 — Lino, R. (1948). *Os Paços Reais da Vila de Sintra*. Lisboa: Valentim de Carvalho, Lda.

Lorenzo *et al*., 1987 — Lorenzo Morilla, J., Vera Reina, M. & Escudero Cuesta, J. (1987). Intervencion Arqueologica en c/ Pureza num. 44 de Sevilla, III Actividades de Urgencia, *Anuario Arqueológico de Sevilla*, p. 574-580.

Macedo, 2006 — Macedo, F.P. (2006). *Santa Clara-a-Velha de Coimbra: Singular Mosteiro Mendicante.* PhD Thesis. Coimbra: Faculdade de Letras da Universidade de Coimbra.

Machado & Vilarigues, 2016 — Machado, A., & Vilarigues, M. (2016). Cobalt blue – reproduction and characterisation of blue enamel recipes from The Handmaid to the Arts by Robert Dossie. *Glass Technology: European Journal of Glass Science and Technology Part A*, 57 (4), p. 131–140

Majumdar, 2012 — Majumdar, M.G. (2012). Analysis of Stress-Coupled Magneto-Electric Effect in $BaTiO_3$-$CoFe_2O_4$ Composites using Raman Spectroscopy. *International Journal of Scientific & Engineering Research*, 3 (11).

Malo, 2001 — Malo Cerro, M. (2001). *Azulejería en Castilla y León. De la Edad Media al Modernismo*. PhD Thesis, Valladolid: Universidad de Valladolid.

Martínez, 1978 — Martínez Caviró, B. (1978). *Cerámica española en el Instituto Valencia de Don Juan.* Madrid: Instituto Valencia de Don Juan.

Martínez, 1991 — Martínez Caviró, B. (1991). *Cerámica Hispanomusulmana andalusí y mudéjar*, Madrid: Ediciones El Viso.

Magalotti, 1933 — Magalotti, L. (1933). *Viaje de Cosme de Médicis por España y Portugal (1668-1669)*, Edition and notes by Angel Sánchez Rivero and Angela Mariutti de Sánchez Rivero, Madrid: Sucesores de Rivadeneyra.

Mason & Tite, 1997 — Mason, R.B., & Tite, M.S. (1997). The Beginnings of Tin-Opacification of Pottery Glazes. *Archaeometry*, 39, p. 41–58.

Mason *et al*., 2001 — Mason, R.B., Tite, M.S., Paynter, S. & Salter, S. (2001). Advances in polychrome ceramics in the Islamic world of the 12th century AD, *Archaeometry*, 43 (2), p. 191-209.

McSweeney, 2011 — McSweeney, A. (2011). The Tin Trade and Medieval Ceramics: Tracing the Sources of Tin and its Influence on Mediterranean Ceramics Production, *Al-Masaq*, 23 (3), p. 155-169

Meco, 1985 — Meco, J. (1985). *Azulejaria Portuguesa*. Colecção Património Português. 3ª Edição Lisboa: Bertrand Editores.

Meco, 2003 — Meco, J. (2003). Os azulejos do forno de Santo António da Charneca (report) in: Barros, l., Cardoso, G., Gonçalves, A. (2003). Primeira notícia do forno de S. António da Charneca – Barreiro, *Actas das 3as Jornadas de cerâmica medieval e pós-medieval*, p. 306-307

Mohammaddoost *et al*., 2010 — Mohammaddoost, H., Ghaderi, M., & Rashidnejad-Omran, N. (2010). Ore Mineralization at Qamsar Cobalt Deposit: Skarn and Metasomatism Evidences, *Proceedings of The 1st International Applied Geological Congress*, Department of Geology, Islamic Azad University – Mashad Branch, Iran, 26-28 April 2010.

Molera *et al*., 1993 — Molera, J., Pradell, T., Martinez-Manent, S., & Vendrell-Saz, M. (1993). The growth of sanidine crystals in the lead of glazes of Hispano-Moresque pottery. *Applied Clay Science*, 7(6), pp.483–491.

Molera *et al*., 1996 — Molera, J., García-Vallés, M., Pradell, T., & Vendrell-Saz, M. (1996). Hispano-Moresque pottery production of the fourteenth-century workshop of Testar de Molí (Paterna, Spain), *Archaeometry*, 38 (1), p. 67-80.

Molera *et al*., 1997a — Molera J., Pradell, T., Merino, L., García-Vallés, M., García-Orellana, J., Salvadó, N. & Vendrell-Saz, M. (1997). La tecnología de la cerámica Islámica y Mudéjar, *Caesaraugusta*, 73, p. 15-41.

Molera *et al*., 1997b — Molera, J., Vendrell-Saz, M., García-Vallés, M., & Pradell, T. (1997). Technology and colour development of Hispano-Moresque lead-glazed pottery, *Archaeometry*, 39 (1), p. 23-39

Molera *et al*., 1998 — Molera, J., Pradell, T., & Vendrell-Saz, M. (1998). The colours of Ca-rich ceramic pastes: origin and characterization, *Applied Clay Science*, 13, p. 187-202.

Molera *et al*., 1999 — Molera, J., Pradell, T., Salvadó N., & Vendrell-Saz, M. (1999), Evidence of Tin Oxide Recrystallization in Opacified Lead Glazes. *Journal of the American Ceramic Society*, 82, p. 2871–2875.

Molera *et al*., 2001a — Molera, J., Pradell, T., Salvadó N., & Vendrell-Saz, M. (2001). Interactions between clay bodies and lead glazes, Journal of the American Ceramic Society, 84 (5), p. 1120–1128.

Molera *et al*., 2001b — Molera, J., Vendrell-Saz, M., & Pérez-Arantegui, J. (2001). Chemical and textural characterization of tin glazes in Islamic ceramics from Eastern Spain, *Journal of Archaeological Science*, 28, p. 331-340.

Molera *et al*., 2009 — Molera, J., Pradell, T., Salvadó, N. & Vendrell-Saz, M. (2009). Lead Frits in Islamic and Hispano-Moresque glazed productions, In: Shortland, A.J., Freestone, I. & Rehren, T. (Eds), *From Mine to Microscope: Advances in the study of Ancient Technology*, Oxford: Oxbow Books, p. 1-10.

Molera *et al*., 2013 — Molera, J., Coll, J., Labrador, A. & Pradell, T. (2013). Manganese brown decorations in 10th to 18th century Spanish tin glazed ceramics, *Applied Clay Science*, 82, p. 86-90.

Mouri & Enami, 2008 — Mouri, T, & Enami, M. (2008). Raman spectroscopic study of olivine-group minerals. *Journal of Mineralogical and Petrological Sciences*, 103, p. 100-104.

Mulholland, 1984 — Mulholland, I.R. (1984). Malayaite and tin-bearing garnet from a skarn at Gumble, NSW, Australia, *Mineralogical Magazine*, 48, p. 27-30.

Museo, 2013 — Museo Nacional de Cerámica y Artes Suntuarias "González Martí" – Ministerio de Educación, Cultura y Deporte - Gobierno de España (2013). *Historia* [Online] Available from: http://www.mecd.gob.es/mnceramica/home.html [Accessed: 21 March 2016]

Mwenesongole, 2008 — Mwenesongole, E. (2008). *A Raman- and XRD study of the crystal chemistry of cobalt blue*, Dissertation for the Degree of Master of Science (Chemistry), Faculty of Natural and Agricultural Sciences, University of Pretoria, 2008.

Navarro, 2003 — Navarro, J.M.F. (2003). *El Vidrio.* Series Textos Universitários (Consejo Superior de Investigaciones Científicas), 6. 3rd Edition. Madrid: Sociedad Española de Cerámica y Vidrio.

Norton, 1984 — Norton, E. (1984), Medieval tin-glazed painted tiles in north-west Europe, *Medieval Archaeology*, Vol 28, p. 133-172.

Ortega *et al*., 2012 — Ortega, L., Zuluaga, M.C., Alonso-Olazabal, A., & Bienes, J.J.. (2012). Production and Technological Evolution from Islamic to Christian Glazed Pottery during 11th to 16th centuries. *Macla,* 16, p. 36-37.

Padeletti & Fermo, 2010 — Padeletti, G., & Fermo, P. (2010). A scientific approach to the attribution problem of renaissance ceramic productions based on chemical and mineralogical markers, *Applied Physics A*, 100 (3), p. 771-784.

Pavón, 1973 — Pavón Maldonado, B. (1973). *Arte Toledano Islamico y Mudejar*. Madrid: Ministerio de Asuntos Exteriores, Instituto Hispano-Arabe de Cultura.

Pappalardo *et al*., 2004 — Pappalardo, G, Costa, E., Marchetta, C., Pappalardo, L., Romano, F.P., Zucchiatti, A., Prati, P., Mandò, P.A., Migliori, A., Palombo, L., & Vaccari, M.G. (2004). Non-destructive characterization of Della Robbia sculptures at the Bargello museum in Florence by the combined use of PIXE and XRF portable systems, *Journal of Cultural Heritage*, 5, p. 183–188.

Paynter *et al*., 2004 — Paynter, S., Okyar, F., Wolf, S., & Tite, M.S. (2004). The production technology of Iznik pottery – a reassessment. *Archaeometry*, 46, p. 421-437.

Pérez-Arantegui *et al*., 1999 — Pérez-Arantegui, J., Soto, M., & Ramón Castillo, J. (1999). Examination of the 'cuerda seca' decoration technique on Islamic ceramics from al-Andalus (Spain), *Journal of Archaeological Science*, 26, p. 935-941.

Pérez-Arantegui *et al*., 2005 — Pérez-Arantegui, J., Ortega, J.M., & Escriche, C. (2005). La tecnología de la cerámica Mudéjar entre los siglos XIV y XVI: las producciones esmaltadas de las zonas de Teruel y Zaragoza, *VI Congreso Ibérico de Arqueometría: Avances en Arqueometría*, p. 89-96.

Pérez-Arantegui *et al*., 2009a — Pérez-Arantegui, J., Ortega, J., & Escriche, C. (2009). The Hispano-Moresque tin glazed ceramics produced in Teruel, Spain: a technology between two historical periods, 13th to 16th c. AD. In: Shortland, A.J., Freestone, I. & Rehren, T. (Eds), *From Mine to Microscope: Advances in the study of Ancient Technology*, Oxford: Oxbow Books, p. 61-67.

Pérez-Arantegui *et al*., 2009b — Pérez-Arantegui, J., Montull, B., Resano, M., & Ortega, J.M. (2009). Materials and technological evolution of ancient cobalt-blue-decorated ceramics: Pigments and work patterns in tin-glazed objects from Aragon (Spain) from the 15th to the 18th century AD, *Journal of the European Ceramic Society*, 29 (12), p. 2499-2509.

Piccolpasso, 1980 — Piccolpasso, C. (1980). *The Tree Books of Potter's Art (Il Tre Libri Dell'Arte Del Vasaio)* – A Facsimile of the Manuscript in the Victoria and Albert Museum [*Translated by Alan Caiger-Smith*]. London: Scolar Press.

Piña *et al.*, 2005 — Piña, C., Arriola, H., & Nava, N. (2005). Study of malayaite and malayaite cobalt pigment, *Hyperfine Interactions*, 161, p. 93-97.

Pleguezuelo, 1992 — Pleguezuelo, A. (1992). Francisco Niculoso Pisano: Datos Arqueologicos. *Faenza – Bollettino del Museo Internazionale delle Ceramiche di Faenza,* 28, N.3-4, p. 171-196.

Pleguezuelo, 2011 — Pleguezuelo, A. (2011). *Lozas y azulejos de Triana – Coleccion Carranza,* Sevilla: Ayto.

Polvorinos del Rio *et al.*, 2006 — Polvorinos del Rio, A., Castaing, J., & Aucouturier M. (2006). Metallic nano-particles in lustre glazed ceramics from the 15th century in Seville studied by PIXE and RBS, *Nuclear Instruments and Methods in Physics Research Section B: Beam Interactions with Materials and Atoms*, 249 (1–2), p. 596-600.

Polvorinos del Rio & Castaing, 2010 — Polvorinos del Rio, A., & Castaing, J. (2010). Lustre-Decorated Ceramics from a 15th to 16th Century Production in Seville, *Archaeometry*, 52 (1), p. 83-98.

Polvorinos *et al.*, 2011 — Polvorinos, A., Aucouturier, M., Bouquillon, A., Castaing, J. & Camps, J. (2011), The Evolution of Lustre Ceramics from Manises (Valencia, Spain) between the 14th and 18th Centuries. *Archaeometry*, 53, p. 490-509.

Pradell *et al.*, 2005 — Pradell, T., Molera, J., Roque, J., Vendrell-Saz, M., Smith, A.D., Pantos, E., & Crespo, D. (2005). Ionic-Exchange Mechanism in the Formation of Medieval Luster Decorations, *Journal of the American Ceramic Society*, 88 (5), p. 1281-1289.

Pradell *et al.*, 2008 — Pradell, T., Molera, J., Smith, A.D., Climent-Font, A., & Tite, M.S. (2008). Technology of Islamic lustre, *Journal of Cultural Heritage*, 9 (Supplement), p. 123-128.

Pradell *et al.*, 2010 — Pradell, T., Molera, J., Salvadó, N., & Labrador, A. (2010). Synchrotron radiation micro-XRD in the study of glaze technology. *Applied Physics A*, 99, p. 407-417.

Pradell *et al.*, 2013 — Pradell, T., Molina, G., Molera, J., Pla, J., & Labrador, A. (2013). The use of micro-XRD for the study of glaze color decorations, *Applied Physics A*, 111, p. 121-127.

Rao *et al.*, 2011 — Rao, D.S., Vijayakumar, T.V., Prabhakar, S. & Bhaskar Raju, G. (2011). Geochemical assessment of a siliceous limestone sample for cement making, *Chinese Journal of Geochemistry*, 30, p. 33-39.

Rehren, 2008 — Rehren, Th. (2008). A review of factors affecting the composition of early Egyptian glasses and faience: alkali and alkali earth oxides, *Journal of Archaeological Science*, 35 (5), p. 1345-1354.

Resano *et al.*, 2005 — Resano, M., Pérez-Arantegui, J., Garcia-Ruiz, E., & Vanhaecke, F. (2005). Laser ablation-inductively coupled plasma mass spectrometry for the fast and direct characterization of antique glazed ceramics, *Journal of Analytical Atomic Spectrometry*, 20, p. 508-514

Roldán *et al.*, 2006 — Roldán, C., Coll, J., & Ferrero, J. (2006). EDXRF analysis of blue pigments used in Valencian ceramics from the 14th century to modern times, *Journal of Cultural Heritage*, 7, p. 134-138.

RRUFF — RRUFF Project Database. [http://rruff.info/] (last accessed 10-10-2016)

Sabrosa *et al.*, 2003 — Sabrosa, A., Carvalho, E., & Julião, T. (2003). Um Forno Medieval no Palácio da Vila (Sintra). *al-Madan*. II série (12), p. 196-197.

Sabugosa, 1903 — Sabugosa, C. (1903) *O Paço de Cintra, desenhos de Sua Majestade a Senhora Dona Amélia, apontamentos historicos e archeologicos do Conde de Sabugosa. (collab. artistica de E. Casanova e R. Lino*). Lisboa: Imprensa Nacional.

Sancho, 1978 — Sancho Corbacho, A. (1978). *La cerámica vidriada sevillana*, In: Jornadas científicas sobre cerámica y vidrio, Serie: Ciencias, N.º 21, Anales de Universidad Hispalense, Publicaciones de la Universidad de Sevilla.

Santos, 1957 — Santos, Reynaldo dos. (1957) *O Azulejo em Portugal*, Lisboa: Editorial Sul Limitada

Santos Simões, 1945 — Santos Simões, J.M. (1945) *Azulejos Arcaicos em Portugal*, Tomo del XVIII Congreso de la Asociacon Espanõla para el Progresso de las Ciencias (Cordoba 1944), Madrid.

Santos Simões, 1990 — Santos Simões, J.M. (1990). *Azulejaria em Portugal nos Séculos XV e XVI. Introdução Geral*, 4th Edition. Lisboa: Fundação Calouste Gulbenkian.

Schwedt *et al*., 2006 — Schwedt, A., Mommsen, H., Zacharias, N., & Buxeda I Garrigós, J. (2006). Analcime crystallization and compositional profiles – comparing approaches to detect post-depositional alterations in archaeological pottery, *Archaeometry*, 48, p. 237-251.

Sebastian, 2010 — Sebastian, L. (2010). *A Produção Oleira de Faiança em Portugal (Séculos XVI-XVIII)*, PhD Thesis in History (field of Archaeology), Lisboa: Faculdade de Ciências Sociais e Humanas da Universidade Nova de Lisboa.

Shovelton, 2016 — Shovelton, E. (2016). "Ceramic dish" in *Discover Islamic Art*, Museum With No Frontiers, 2016. [online] Available at: *http://www.discoverislamicart.org/database_item.php?id=object;ISL;uk;Mus01;14;en* (accessed 20-07-2016)

Silva, 1992 — Silva, D. (1992). Os azulejos de aresta do Jardim do Núncio. *Azulejo*, 2, p. 3-8.

Silva, 1995 — Silva, J.C.V., *Paços Medievais Portugueses*, Lisboa, IPPAR, 1995.

da Silva *et al*., 2006 — da Silva, S.W., Pedroza, R.C., Sartoratto, P.P.C., Rezende, D.R., da Silva Neto, A.V., Soler, M.A.G., & Morais, P.C. (2006). Raman spectroscopy of cobalt ferrite nanocomposite in silica matrix prepared by sol–gel method, *Journal of Non-Crystalline Solids*, 352, p. 1602-1606.

Šmit, 2013 — Šmit, Ž. (2013). Ion-Beam Analysis Methods, In: Janssens, K. (Ed), *Modern Methods for Analysing Archaeological and Historical Glass*, UK: John Wiley & Sons, Inc., p. 155-183.

Sosa, 2007 — Sosa Suaréz, E. (2007). La cerâmica de "Cuerda Seca" del antíguo convento de San Francisco de Asís de las Palmas de Gran Canaria. *Cuadernos de prehistoria y arqueología*, 33, p. 155-174.

Tarvornpanich *et al*., 2008a — Tarvornpanich, T., Souza, G.P., & Lee, W.E. (2008a), Microstructural Evolution in Clay-Based Ceramics I: Single Components and Binary Mixtures of Clay, Flux, and Quartz Filler. Journal *of the American Ceramic Society*, 91, p. 2264-2271.

Tarvornpanich *et al*., 2008b — Tarvornpanich, T., Souza, G.P., & Lee, W.E. (2008b), Microstructural Evolution in Clay-Based Ceramics II: Ternary and Quaternary Mixtures of Clay, Flux, and Quartz Filler. *Journal of the American Ceramic Society*, 91, p. 2272–2280.

Tengrove, 1965 — Trengove, L. (1965). Chemistry at the Royal Society of London in the eighteenth century—III(B)—metals, *Annals of Science*, 21 (3), p. 175-201.

Tite, 1989 — Tite, M.S. (1989). Iznik Pottery: an Investigation of the Methods of Production, *Archaeometry,* 31 (2), p. 115-132.

Tite *et al*., 1998 — Tite, M.S., Freestone, I., Mason, R., Molera, J., Vendrell-Saz, M., & Wood, N. (1998). Lead glazes in Antiquity – methods of production and reasons for use, *Archaeometry,* 40 (2), p. 241-260.

Tite *et al*., 2006 — Tite, M.S., Shortland, A., Maniatis, Y., Kavoussanaki, D., & Harris, S.A. (2006). The composition of the soda-rich and mixed alkali plant ashes used in the production of glass, *Journal of Archaeological Science*, 33, p. 1284–1292.

Tite, 2008 — Tite, M.S. (2008). Ceramic production, provenance and use – a review. *Archaeometry*, 50 (2), p. 216-231.

Tite *et al*., 2008 — Tite, M., Pradell T., & Shortland, A. (2008). Discovery, Production and Use of Tin-Based Opacifiers in Glasses, Enamels and Glazes from the Late Iron Age Onwards: a Reassessment, *Archaeometry*, 50 (1), p. 67-84.

Tite *et al*., 2009 — Tite, M.S., Maniatis, Y., Kavoussanaki, D., Panagiotaki, M., Shortland, A.J., & Kirk, S.F. (2009). Colour in Minoan faience, *Journal of Archaeological Science*, 36, p. 370-378.

Trindade, 2007 — Trindade, R.A.A. (2007). *Revestimentos Cerâmicos Portugueses. Meados do século XIV à primeira metade do século XVI*. Lisboa: Edições Colibri/Faculdade de Ciências Sociais e Humanas da Universidade Nova de Lisboa.

Trindade, 2009 — Trindade, R.A.A. (2009). Imagens de Azul. Evidências do emprego do azul cobalto na cerâmica tardo medieval portuguesa. *Revista de História da Arte*, 7, p. 236-263.

Trindade *et al*., 2009 — Trindade, M.J., Dias, M.I., Coroado, J., & Rocha, F. (2009). Mineralogical transformations of calcareous rich clays with firing: A comparative study between calcite and dolomite rich clays from Algarve, Portugal. *Applied Clay Science*, 42(3-4), p. 345-355.

Trindade & Gambini, 2009 — Trindade, S.D., & Gambini, L.I. (2009). *Mosteiro de Santa Clara de Coimbra. Do Convento à Ruína, da ruína à contemporaneidade.* (Coord.) Artur Côrte-Real. 2nd Edition. Direcção Geral de Cultura do Centro.

Valls, 1894 — Valls, D.R. (1894). *La cerámica, apuntes para la historia y su fabricación*. Tomo II. Valencia: Imprenta de Juan Guix.

Vendrell *et al*., 2000 — Vendrell, M., Molera, J., & Tite, M.S. (2000). Optical Properties of Tin-Opacified Glazes, *Archaeometry*, 42 (2), p. 325–340.

Vendrell-Saz *et al.*, 2006 — Vendrell-Saz, M., Molera, J., Roqué, J., & Pérez-Arantegui, J. (2006). Islamic and Hispano-Moresque (Múdejar) lead glazes in Spain: a technical approach, in: Maggetti, M., & Messiga, B. (Eds.), *Geomaterials in Cultural Heritage*, London: The Geological Society of London, p. 163-173.

Vieira Ferreira *et al*., 2014 — Vieira Ferreira L.F., Conceição, D.S., Ferreira, D.P., Santos, L.F., Casimiro, T.M., & Ferreira Machado, I. (2014). Portuguese 16th century tiles from Santo António da Charneca's kiln: a spectroscopic characterization of pigments, glazes and pastes, *Journal of Raman Spectroscopy*, 45, p. 838-847.

Vieira Ferreira *et al*., 2015 — Vieira Ferreira, L.F., & Ferreira Machado, I. (2015). Portuguese tiles from the Santo António da Charneca's kiln: a spectroscopic characterization of pigments, glazes and pastes. In: "GLAZE ARCH 2015 – International Conference: Glazed Ceramics in Architectural Heritage", Lisboa: LNEC.

Vieira Ferreira *et al*., 2016 — Vieira Ferreira, L.F., Varela Gomes, R., Pereira, M.F.C., Santos, L.F., & Ferreira Machado, I. (2016). Islamic ceramics in Portugal found at Silves Castle (8th to 13th c.): An archaeometric characterization, *Journal of Archaeological Science: Reports*, 8, p. 434-443.

Vilarigues *et al*., 2011 — Vilarigues, M., Redol, P., Machado, A., Rodrigues, P.A., Alves, L.C., & da Silva, R.C. (2011). Corrosion of 15th and early 16th century stained glass from the monastery of Batalha studied with external ion beam, *Materials Characterization*, 62 (2), p. 211-217.

Vilarigues & Machado, 2015 — Vilarigues, M., & Machado, A. (2015). Pintar com Luz: O esmalte azul na pintura de vitral. *Boletim da Sociedade Portuguesa de Química*, Série II, 137, p. 31-35.

Walton & Tite, 2009 — Walton, M.S., & Tite, M.S. (2010). Production technology of Roman lead-glazed pottery and its continuance into late Antiquity, *Archaeometry*, 52 (5), p. 733-759.

Wedepohl *et al*., 2011 — Wedepohl, K.H., Simon, K. & Kronz, A. (2011) Data on 61 Chemical Elements for the Characterization of Three Major Glass Compositions in Late Antiquity and the Middle Ages. *Archaeometry.* 53 (1), p. 81-102.

Zhang & Saxena, 1991 — Zhang, Z., & Saxena, S.K., (1991). Thermodynamic properties of andradite and application to skarn with coexisting andradite and hedenbergite. *Contributions to Mineralogy and Petrology,* 107 (2), p. 255-263.

Zucchiatti *et al*., 2006 — Zucchiatti, A., Bouquillon, A., Katona, I., & D'Alessandro, A. (2006). The 'Della Robbia blue': a case study for the use of cobalt pigments in ceramics during the Italian Renaissance, *Archaeometry*, 48 (1), p. 131-152.

Zuluaga *et al*., 2012 — Zuluaga, M.C., Alonso-Olazabal, A., Olivares, M., Ortega, L., Murelaga, X, Bienes, J.J., Sarmiento, A., & Etxebarria, N. (2012). Classification of glazed potteries from Christian and Muslim territories (Late Medieval Ages, IX–XIII centuries) by micro-Raman spectroscopy, *Journal of Raman Spectroscopy*, 43, p. 1811-1816.

Table I.1. Chemical compositions of Islamic and Hispano-Moresque ceramics from the Iberian Peninsula, obtained from the literature.

Provenance	N	Centuries	Technology	Technique	Chemical composition							Ref
					Na_2O	MgO	Al_2O_3	SiO_2	K_2O	CaO	Fe_2O_3	
Murcia	N=13	10^{th}	Islamic	WDS, EDS	0.36 (0.04)	3.64 (0.62)	10.89 (0.61)	40.57 (1.87)	2.52 (0.32)	18.27 (2.79)	4.05 (0.34)	[1] [2]
Cordoba	N=3	10^{th}	Islamic	WDS, EDS	n.d.	<1.00	11.57 (0.71)	54.98 (2.55)	4.23 (0.76)	18.54 (1.90)	10.21 (2.55)	[2]
Mallorca	N=6	11^{th}	Islamic	WDS, EDS	0.80 (0.11)	2.40 (0.23)	13.16 (0.58)	49.67 (1.78)	2.65 (0.29)	13.30 (1.51)	5.01 (0.19)	[1] [2]
Zaragoza	N=6	11^{th}	Islamic	WDS, EDS	0.93 (0.19)	3.68 (0.44)	15.86 (0.47)	49.73 (1.89)	2.85 (0.42)	16.55 (0.83)	5.51 (0.13)	[2]
Silves	N=2	12^{th}-13^{th}	Islamic	XRF	n.d.	3.57 – 4.12	15.09 – 15.43	43.16 – 44.45	2.93 – 3.51	19.05 – 19.06	10.92 – 12.59	[4]
Denia	N=9	13^{th}	Islamic	WDS, EDS	0.40 (0.15)	1.17 (0.07)	11.41 (1.55)	45.78 (2.03)	1.92 (0.39)	18.78 (2.63)	3.78 (0.24)	[1] [2]
Granada	N=7	14^{th}	Islamic	WDS, EDS	1.10 (0.34)	2.43 (0.22)	13.18 (0.21)	49.58 (1.28)	1.93 (0.52)	13.56 (0.57)	5.09 (0.15)	[1] [2]
Paterna	N=16	13^{th}	Hispano-Moresque	WDS, EDS	0.13 (0.15)	1.99 (0.32)	14.62 (1.05)	53.40 (1.16)	12.30 (0.72)	12.30 (0.72)	4.08 (0.38)	[1]
Paterna	N=9	14^{th}-15^{th}	Hispano-Moresque	WDS, EDS	0.40 (0.44)	1.98 (0.29)	13.08 (0.95)	50.58 (3.17)	2.72 (0.46)	18.21 (2.29)	3.87 (0.23)	[1]
Teruel	N=7		Hispano-Moresque	ICP-AES	0.47 (0.05)	1.43 (0.19)	16.1 (1.9)		2.66 (0.45)	13.5 (2.2)	4.41 (0.58)	[3] [5]
Muel	N=5		Hispano-Moresque	ICP-AES	0.94 (0.23)	3.05 (0.28)	15.5 (1.1)		2.50 (0.45)	13.2 (0.7)	5.73 (0.27)	[3]
Seville	N=13	14^{th}- 19^{th}	Lustre	XRF	0.9 (0.21)	3.5 (0.42)	11.6 (0.4)	49 (1.7)	1.8 (0.7)	22 (2.16)	3.8 (0.24)	[6]

[1] Molera *et al.,* 1997a; [2] Molera *et al*., 2001b; [3] Pérez-Arantegui *et al*., 2005; [4] Vieira Ferreira *et al*., 2016; [5] Pérez-Arantegui *et al*., 2009a;
[6] Polvorinos del Rio & Castaing, 2010

Table I.2. Chemical compositions of Islamic and Hispano-Moresque glazes from the Iberian Peninsula, obtained from the literature.

Provenance	N	Technology	Cent.	Technique	Glaze colour	Chemical composition													Ref
						Na_2O	MgO	Al_2O_3	SiO_2	K_2O	CaO	MnO	Fe_2O_3	CoO	NiO	CuO	As_2O_5	SnO_2	PbO	
Murcia, Spain	24	Islamic	10th	EPMA	Yellow	0.82	0.39	2.91	34.22	1.78	3.2	-	1.43			0.04		-	54.23	[1]
					Brown	0.52	0.38	3.31	32.54	1.63	3.5	-	1.71			0.02		-	53.01	
	13				White	1.46	0.24	0.48	33.13	1.1	1.48	-	0.31			-		7 - 10	53.82	[1] [2]
Zaragoza, Spain	16	Islamic	11th	EPMA	White - Group 1	1 - 2	0,36 - 0,87	0.61	46.05	3.74	3.73	-	0.7			-		5 - 7	38.04	[1] [2]
					White - Group 2	1 - 2	0,36 - 0,84	1.02	41.51	3.26	3.72	-	0.77			-		9 - 14	37.79	
Mallorca, Spain	5	Islamic	11th	EPMA	Brown and green	1.00	0.23	3.23	31.06	1.18	2.4	-	1.21			-		7 - 9	53.91	[1] [2]
Denia, Spain	6	Islamic	13th	EPMA	Green	0.85	0.29	2.92	33.39	1.53	3.04	-	1.15			2.7		-	52.83	[1]
	9				Green	1.80	0.22	0.99	30.94	0.55	0.46	-	0.14			-		6 - 7	56.19	[1] [2]
Granada, Spain	5	Islamic	14th	EPMA	Luster	1.26	0.3	0.88	40.85	2.69	1.67	-	0.49			-		7 - 9	43.69	[1] [2]
Cordoba, Spain	3	Islamic	10th	WDS, EDS		1.40	0.4	2.15	35.2	1.22	2.39	-	1.14			-		8 - 15	47.2	[2]
Paterna, Spain	35	Hispano-Moresque	13th	EPMA	Green	0.25	0.49	5.25	32.76	0.93	2.59	-	2.53			0		-	54.62	[1]
					Yellow	0.10	0.43	5.44	30.28	0.86	2.41	-	1.94			0		-	57.68	
					Brown	0.10	0.7	5.94	33.59	0.84	1.44	-	2.56			0		-	53.11	
	56				White	1.03	0.21	2.89	42.28	2.6	1.66	-	0.45			-		7 - 8	41.14	
					Green brown	0.53	0.38	3.51	43.85	2.32	2.15	-	0.44			-		6 - 7	38.6	
					Turquoise	0.58	0.36	3.43	39.14	2.04	1.97	-	0.43			-		6 - 7	44.04	
					Blue	0.90	0.55	2.45	38.17	2.24	2.28	-	0.3			-		8 - 9	45.5	
					Luster	0.60	0.43	2.33	45.21	4.62	1.65	-	0.22			-		8 - 10	35.74	
Paterna, Spain	38	Hispano-Moresque	14th -15th	EPMA	Honey	0.09	0.58	5.61	32.84	0.63	1.55	-	2.17			0		-	55.78	[1]
					Brown	0.17	0.66	4.88	32.83	0.87	0.89	-	2.12			0		-	57	
	34				Luster	0.91	0.29	3.63	50.39	5.06	2.49	-	2.14			-		5 - 8	32.64	
					Blue	1.17	0.29	3.01	48.41	5.26	2.62	-	3.75			-		5 - 8	32.62	
					White	0.72	0.22	2.83	44.55	3.77	1.52	-	0.84			-		5 - 8	41.47	
Catalonia, Spain	23	Hispano-Moresque	14th -15th	EPMA	Blue	0.87	0.35	2.97	39.01	2.31	2.08	-	0.94			-		5 - 8	45.63	[1]
					White	1.03	0.34	2.94	35.83	2.74	2.05	-	0.69			-		5 - 8	49.76	

Table I.2. *(Cont.)* Chemical compositions of Islamic and Hispano-Moresque glazes from the Iberian Peninsula, obtained from the literature.

Provenance	N	Technology	Cent.	Technique	Glaze colour	Chemical composition														Ref
						Na_2O	MgO	Al_2O_3	SiO_2	K_2O	CaO	MnO	Fe_2O_3	CoO	NiO	CuO	As_2O_5	SnO_2	PbO	
Mértola, Portugal	12	Islamic	12th	SEM-EDX	Green	0,9 - 4,92	0,5 - 1,01	0,37 - 7,51	38 - 50	0 - 2,42	1,46 - 8,42	-	0,42 - 3,77			0,83 - 3,76		0 - 5,27	35 - 44	[3]
					Black	1,06 - 3,46	0,38 - 0,94	2,71 - 4,29	34 - 46	1,55 - 2,52	3,43 - 5,68	0,22 - 3,96	1,55 - 4,64			0		0 - 4,71	31 - 53	
					Yellow	0,99 - 3,8	0,41 - 0,73	3,44 - 5,19	34 - 44	2,18 - 2,89	3,45 - 5,05	0 - 0,39	2,54 - 7,08			0 - 0,49		-	32 - 52	
					White	1,59 - 2,19	0,64 - 0,86	0,31 - 2,64	44 - 47	2,13 - 3,62	2,4 - 3,7	-	0,67 - 1,12			0		2,52 - 14,81	33 - 38	
Pechina, Spain	2	Islamic	10th	SEM-EDX	Green	1,99 - 3,15	0.63	1,13 - 3,32	41 - 43	0	3,08 - 3,34	-	0,96 - 2,13			2,08 - 2,88		*	44 - 47	[3]
Almeria, Spain	1	Islamic	10th	SEM-EDX	Green	0.44	0.72	0.78	35.08	0.84	2.14	-	0.57			1.94		-	55.15	[3]
Malaga, Spain	1	Islamic	12th	SEM-EDX	Green	2.79	0.82	2.81	45.05	0	3.94	-	1.26			2.64		-	40.57	[3]
					Black	1.72	0.55	2.68	38.24	1.04	4.2	1.95	2.34			0.15		*	46.92	
Seville, Spain	6	Hispano-Moresque	15th	PIXE	white	1.2	0.4	2.5	50	4.7	2.6	0.04	0.7		0.01	0.06		6.4	31	[4]
					white	1	1.4	2.8	49	4.2	3.2	0.02	0.42		0.01	0.12		6.5	25	
					blue	0.4	0.3	1.6	46	1.9	2.3	0.03	0.5	0.17	0.06	0.24	0.07	7.4	38	
					white	0.3	0.3	5.7	44	1	3.5	0.04	0.6		0.01	0.26	0.04	8.2	36	
					white	1.1	0.4	2	53	5	2.6	0.03	0.5		0.01	0.06		7.8	28	
Valencia, Spain	3	Hispano-Moresque	15th	PIXE	white	0.7	0.4	2.3	46	4	3	0.04	0.7		0.01	0.06		7.1	35	
					white	0.3	0.4	2.3	56	6.2	2	0.02	0.4		0.01	0.04		6.7	25	
					white	1.2	0.5	2.5	53	6.8	2.8	0.02	0.22		0.01	0.05		6.9	22	
					blue	1.7	0.5	2.5	53	6.5	4.2	0.04	0.6	0.6	0.1	0.08		8.8	21	

[1] Vendrell-Saz *et al.*, 2006; [2] Molera *et al*., 2001b; [3] Chapoulie *et al*., 2005; Polvorinos del Rio *et al*., 2006

APPENDIX II
SAMPLED TILES

II.1 – NATIONAL PALACE OF SINTRA (PNS)


PNS 12


PNS 13


PNS 14


PNS 15


PNS 17


PNS 16


PNS 18

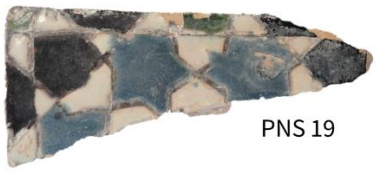
PNS 19


PNS 20


PNS 21


PNS 22


PNS 23


PNS 24


PNS 25


PNS 26


PNS 27

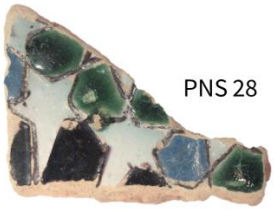
PNS 28

PNS 29


PNS 30

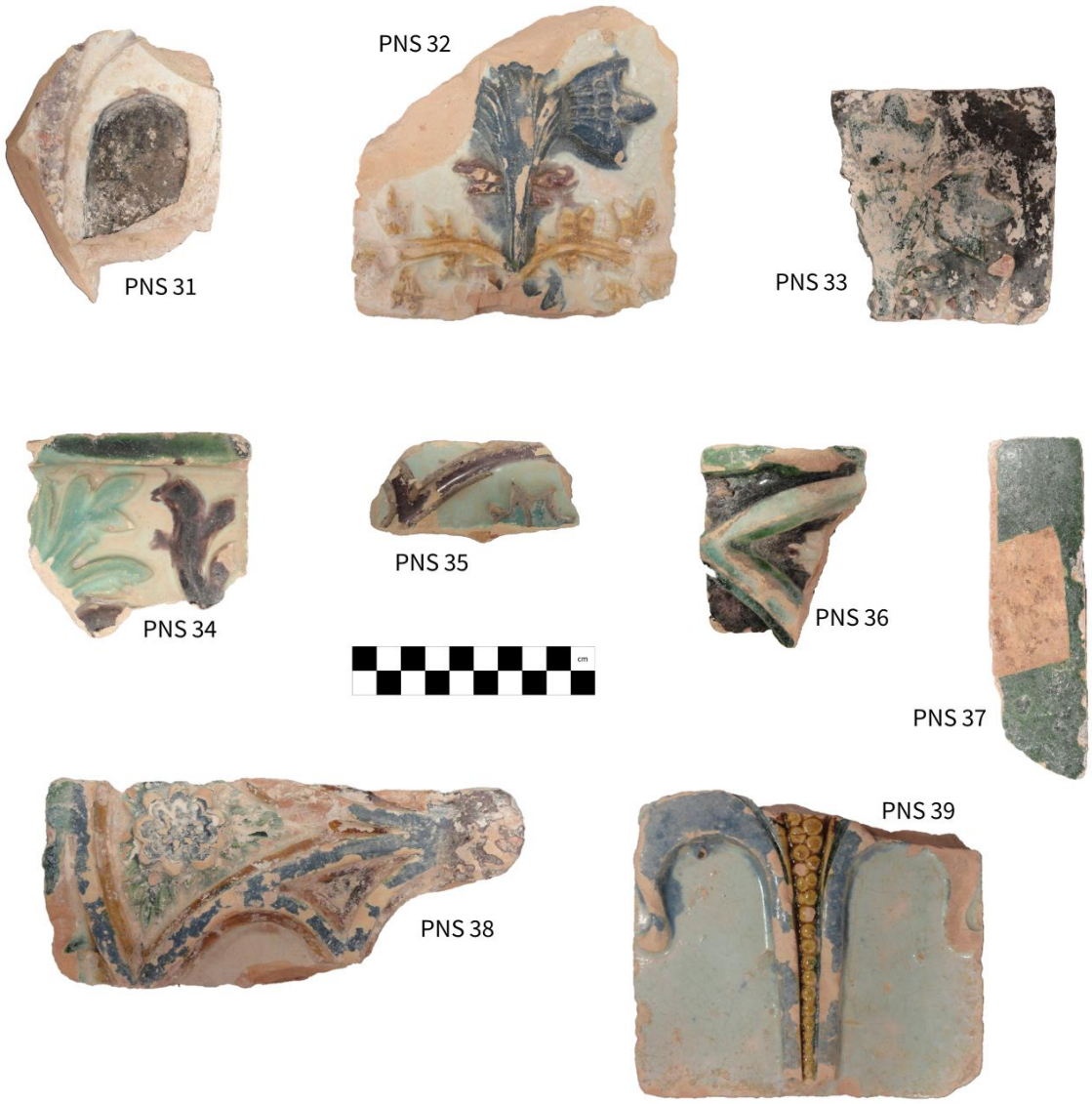

II.2 – Santo António da Charneca, Barreiro (SAC)

II.3 – Monastery of Santa Clara-a-Velha, Coimbra (SCV)

SCV 4Bi414

SCV 4i365

SCV 6Ai1152

SCV 8i7532

SCV 9i1469

SCV 10EF175

SCV 10Bi1673

SCV 10DF7637

SCV 14i2580

SCV 14CF2686

SCV 18Ai2914

SCV 20i2989

SCV 21AM3076

SCV 24Ci3386

SCV 27i3426

SCV 30F7756

SCV 32M3674

SCV 32M3680

SCV 33Bi3839

SCV 33Bi3841

SCV 33Bi3870

SCV 33Bi3872

SCV 3333BF4013

SCV 34Ai4057

SCV 34Bi4060

SCV 34Ci4065

SCV 34Ei4068

SCV 35Hi7790

SCV 37AF4179

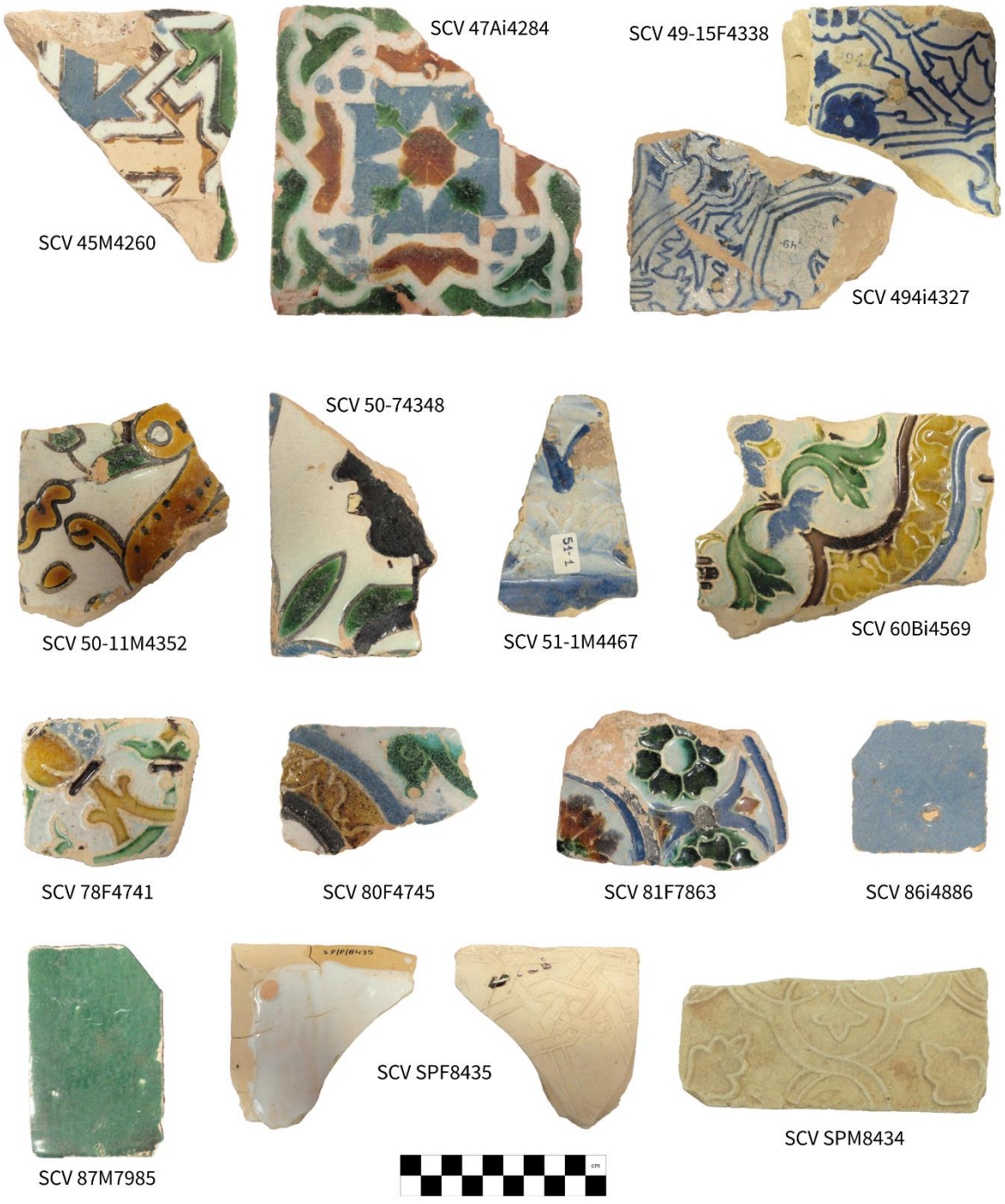
SCV 45M4260
SCV 47Ai4284
SCV 49-15F4338
SCV 494i4327
SCV 50-11M4352
SCV 50-74348
SCV 51-1M4467
SCV 60Bi4569
SCV 78F4741
SCV 80F4745
SCV 81F7863
SCV 86i4886
SCV 87M7985
SCV SPF8435
SCV SPM8434

II.4 – Instituto Valencia de Don Juan, Madrid (IVDJ)

Tiles attributed to Seville

IVDJ-S 3576

IVDJ-S 3561

IVDJ-S 3584

IVDJ-S 3591

IVDJ-S 3718

IVDJ-S 3774

IVDJ-S 4106

IVDJ-S 4107

IVDJ-S 4127

IVDJ-S 3919

IVDJ-S XV

IVDJ-S 3794

IVDJ-S SN

IVDJ-S 4185

IVDJ-S 3601

IVDJ-S 4134

TILES ATTRIBUTED TO TOLEDO

IVDJ-T 96

IVDJ-T 133

IVDJ-T 3944

IVDJ-T 3683

IVDJ-T 3684

IVDJ-T 4095

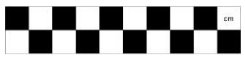

II.5 – Museo Nacional de Ceramica y Artes Suntuarias "González Martí", Valencia (MCV)

MCV 1.1R

MCV 2.1T

MCV 3.1R

MCV 4.1G

MCV 4.1ML

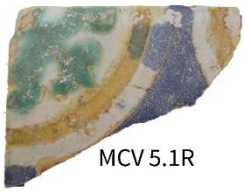

MCV 5.1R

MCV 4.2G

MCV 6.1C

MCV 8.1G

MCV 9.1Ap

MCV 9.1Ag

MCV 7.1C

MCV 8.2C

MCV 8.3G

MCV 10.3

MCV 10.1

MCV 10.2

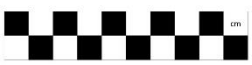

II.6 – CASA DE PILATOS, SEVILLE

APPENDIX III

ANALYSIS OF GLASS STANDARDS CMOG A, CMOG B, CMOG C AND N612

Table III.1. Chemical composition of glass standards Corning Museum of Glass (CMoG) B and C: certified (Brill, 1999) and average (n=9) measured by μ-PIXE.

	Na_2O	MgO	Al_2O_3	SiO_2	K_2O	CaO	TiO_2
CMoG B							
Certified (wt.%)	17.0	1.03	4.36	62.27	1.00	8.56	0.089
Measured by μ-PIXE (wt.%)	17.1	0.96	4.29	64.75	0.96	7.53	0.12
RSD (%)	7.3	5.7	6.9	1.6	5.4	4.9	17.9
CMoG C							
Certified (wt.%)	1.07	2.76	0.87	34.3	2.84	5.07	0.79
Measured by μ-PIXE (wt.%)	1.14	2.36	0.89	35.8	2.60	4.42	0.55
RSD (%)	7.7	5.2	4.9	3.7	2.2	1.7	19.4

	MnO	Fe_2O_3	CoO	NiO	CuO	BaO	PbO
CMoG B							
Certified (wt.%)	0.25	0.34	0.046	0.099	2.66	0.12	0.61
Measured by μ-PIXE (wt.%)	0.22	0.30	0.08	0.10	2.30	0.10	0.43
RSD (%)	18.3	10.9	36.7	21.2	7.7	40.2	29.8
CMoG C							
Certified (wt.%)	-	0.34	0.18	-	1.13	11.40	36.7
Measured by μ-PIXE (wt.%)	-	0.30	0.16	-	1.09	11.53	38.8
RSD (%)	-	6.4	18.5	-	5.8	1.6	4.6

RSD – relative standard deviation

Table III.2. Chemical composition of glass standards Corning Museum of Glass (CMoG) A and Nist 612: average (n=5) measured by LA-ICP-MS and certified composition (Wagner et al., 2012; USA Department of Commerce, 2012).

	Na_2O	MgO	Al_2O_3	SiO_2	P_2O_5	Cl	K_2O	CaO	TiO_2	MnO	Fe_2O_3	Sb_2O_3
CMoG A												
Reference (wt.%)	13.4	2.50	0.820	67.82	0.085		3.46	4.94	0.739	1.13	0.979	1.86
Measured (wt.%)	14.3	2.56	0.97	66.2	0.10	0.15	2.85	5.88	0.73	1.04	1.11	1.60
(±)	0.9	0.16	0.06	1.7	0.01	0.01	0.14	0.35	0.01	0.06	0.06	0.06
N612												
Reference (wt.%)	14		2	72			0.0064	12	0.0050	0.0037	0.0051	0.0034
Measured (wt.%)	13.6	0.013	2.11	72.3	0.0269	0.0794		11.6	0.0079	0.0048	0.0078	0.0042
(±)	0.8	0.001	0.12	1.5	0.0222	0.0133		0.7	0.0009	0.0003	0.0055	0.0003

	Li_2O	B_2O_3	V_2O5	Cr_2O_3	CoO	NiO	CuO	ZnO	GaO	As_2O_3	Rb_2O	SrO
CMoG A												
Reference (µg/g)	110	2740	70	30	1700	230	11000	480			90	1060
Measured (µg/g)	111	1972	60	22	1709	226	11722	516	1	29	90	1078
(±)	11	107	2	7	130	16	667	17	0	1	6	75
N612												
Reference (µg/g)	40			35.0	35.5	38.8	37.7			37.4	31.4	78.4
Measured (µg/g)	89	115	65	44.5	44.1	52.6	45.5	43	44	40.9	33.8	89.9
(±)	8	6	2	12.0	2.9	5.6	2.3	3	2	1.5	2.4	5.9

	Y_2O_3	ZrO_2	Nb_2O_3	MoO	Ag	Cd	In	SnO_2	Cs_2O	BaO	La_2O_3	CeO_2
CMoG A												
Reference (µg/g)		50										
Measured (µg/g)	0.85	51.9	0.64	2.66	14.7	0.48	4.79	1710	0.25	4647	0.94	0.32
(±)	0.05	1.9	0.03	0.16	2.1	0.06	0.26	71	0.02	234	0.49	0.03
N612												
Reference (µg/g)					22.0	29.9				38.6	36	39
Measured (µg/g)	45.3	50.9	42.0	37.4	20.5	37.6	35.8	46.7	42.1	41.0	43.0	46.1
(±)	1.2	2.1	1.2	1.2	2.8	2.5	2.9	2.3	3.2	2.1	3.8	4.0

	PrO_2	Nd_2O_3	Sm_2O_3	Eu_2O_3	Gd_2O_3	Tb_2O_3	Dy_2O_3	Ho_2O_3	Er_2O_3	Tm_2O_3	Yb_2O_3	Lu_2O_3
CMoG A												
Reference (µg/g)												
Measured (µg/g)	0.03	0.25	0.04	3.38	0.18	0.007	0.055	0.008	0.027	0.005	0.036	0.007
(±)	0.01	0.14	0.01	3.28	0.01	0.001	0.009	0.003	0.006	0.003	0.011	0.001
N612												
Reference (µg/g)		36	39	36	39		35		39		42	
Measured (µg/g)	43.0	40.0	42.1	40.4	39.0	40.4	38.8	40.9	39.5	38.3	43.1	39.3
(±)	2.5	1.3	1.4	2.6	9.9	1.2	1.2	1.2	1.4	1.4	3.5	1.4

	HfO_2	Ta_2O_3	WO	Pt	Au	PbO	Bi	ThO_2	UO_2
CMoG A									
Reference (µg/g)									
Measured (µg/g)	1.07	0.11	0.10	3.29	0.10	641	8.6	0.34	0.20
(±)	0.05	0.01	0.02	0.45	0.04	53	3.0	0.05	0.01
N612									
Reference (µg/g)		15.7			5	38.57		37.79	37.38
Measured (µg/g)	40.9	33.8	36.0	2.2	4.1	42.0	28.7	41.8	40.5
(±)	1.1	0.9	1.5	0.3	0.3	6.0	3.5	2.9	1.4

APPENDIX IV

CHEMICAL COMPOSITION OF THE CERAMIC BODY AND THE GLAZES OBTAINED BY μ-PIXE

Table IV.1. Chemical composition of the ceramic body obtained by μ-PIXE (wt.%).

	Na_2O	MgO	Al_2O_3	SiO_2	P_2O_5	SO_3	Cl	K_2O	CaO	TiO_2	MnO	Fe_2O_3	CuO	ZnO	BaO	SrO	PbO
PNS 01	1.12	3.58	12.25	52.9		0.21	0.04	2.10	23.24	0.45	0.05	3.87					0.16
PNS 02	0.97	3.14	11.48	58.3	0.19	0.17	0.11	1.52	18.72	0.57	0.07	4.65	0.10				
PNS 03	1.23	1.69	18.87	67.7		0.04	0.03	2.83	0.92	0.64	0.06	5.91		0.09			
PNS 04	0.96	2.58	14.99	72.2		0.06	0.06	2.52	1.21	0.80	0.05	4.52					
PNS 05	1.72	3.52	13.39	52.7	0.11	0.17	0.24	1.74	20.13	0.51	0.09	5.48		0.07		0.14	
PNS 06	0.71	7.91	11.69	56.9	0.21	0.43	0.04	2.28	14.66	0.46	0.07	4.65					
PNS 07	1.00	3.82	11.15	51.2		0.30	0.03	1.36	25.46	0.76	0.07	4.32					0.53
PNS 08	1.14	3.56	12.12	52.5		0.26	0.06	2.03	23.82	0.42	0.06	3.69					0.31
PNS 09	1.14	4.67	12.24	56.3		0.29	0.19	2.27	18.17	0.46	0.06	4.09					0.10
PNS 10	1.24	4.04	13.57	53.4		0.30	0.07	2.10	19.38	1.05	0.08	4.39					0.35
PNS 11	1.02	3.52	12.78	57.0		0.38	0.14	2.26	17.74	0.53	0.05	4.41					0.19
PNS 12	0.86	3.09	11.66	54.7	1.20	0.10	0.02	1.95	21.59	0.50	0.06	4.23					0.06
PNS 13	0.46	1.44	16.91	48.1	0.17	0.40	0.15	2.70	23.96	0.72	0.04	4.95					
PNS 14	1.45	3.37	11.41	57.6	0.13	0.13	0.06	1.22	19.56	0.65	0.07	4.31					
PNS 15	0.98	5.50	11.47	53.3	0.15	0.33	0.03	1.86	21.20	0.49	0.06	4.64					
PNS 16	1.05	3.33	12.03	57.1	0.34	0.33	0.06	1.89	18.77	0.50	0.07	4.58					
PNS 17	0.53	2.39	17.07	48.6		0.23	0.21	2.68	23.00	0.61	0.04	4.69					
PNS 18	1.14	3.78	12.35	56.3		0.16	0.06	1.63	19.28	0.52	0.08	4.12					0.56
PNS 19	1.23	3.36	11.55	52.1	0.33	0.31	0.19	1.83	24.47	0.50	0.07	4.10					
PNS 20	1.66	4.88	13.06	47.5	0.60	0.30	0.22	1.83	24.12	0.56	0.07	5.13					0.08
PNS 21	1.32	3.81	12.42	52.0		0.25	0.08	1.73	23.67	0.51	0.08	4.02					0.10
PNS 22	0.92	3.48	12.36	56.9		0.36	0.30	1.88	18.34	0.64	0.09	4.77					
PNS 23	1.12	4.26	14.52	49.1		0.20	0.11	2.04	22.18	0.65	0.10	5.27	0.19				0.24
PNS 24	1.14	5.77	13.75	48.3		0.26	0.23	2.29	22.01	0.63	0.06	5.15	0.23				0.14
PNS 25	1.10	3.72	12.68	55.9	0.22	0.14	0.16	1.89	18.63	0.59	0.08	4.64					0.20
PNS 26	1.62	4.25	12.55	49.8		0.24	0.76	2.13	22.48	0.75	0.10	5.14	0.22				
PNS 27	1.09	4.02	13.21	49.3		0.29	0.53	3.26	22.14	0.66	0.07	4.94	0.26	0.11			0.10
PNS 28	1.03	4.85	12.53	51.4		0.29	0.18	1.77	22.14	0.55	0.08	4.90	0.21				0.07
PNS 29	1.25	4.60	12.83	55.5		0.20	0.16	1.96	17.25	0.58	0.06	4.98					0.62
PNS 30	0.77	4.28	19.93	43.1		0.42	0.11	2.61	22.80	0.75	0.02	5.07			0.12		
PNS 31	1.82	5.23	15.39	46.7		0.26	0.05	1.55	23.06	0.64	0.07	5.23					
PNS 32	1.43	5.32	15.49	50.6		0.23	0.09	1.88	19.74	0.48	0.06	4.22					0.40
PNS 33	1.60	4.87	14.51	50.2		0.34	0.18	2.43	20.24	0.68	0.03	4.83			0.07		
PNS 34	1.66	4.71	14.55	51.6		0.32	0.13	1.10	20.56	0.45	0.06	4.56					0.28
PNS 35	1.59	4.49	15.17	49.4		0.34	0.17	1.79	21.68	0.58	0.07	4.66			0.06		
PNS 36	1.32	4.79	15.47	53.1		0.41	0.14	2.13	17.56	0.61	0.04	4.47					
PNS 37	1.35	6.14	13.83	49.7		0.29	0.10	1.90	21.86	0.71	0.07	4.01					
PNS 38	1.74	4.57	14.19	51.6		0.22	0.20	1.96	20.80	0.51	0.07	4.10					
PNS 39	1.05	4.59	15.17	52.4		0.38	0.02	2.44	18.27	0.65	0.07	4.93					

Table IV.1. (Cont.) Chemical composition of the ceramic body obtained by μ-PIXE (wt.%).

	Na_2O	MgO	Al_2O_3	SiO_2	P_2O_5	SO_3	Cl	K_2O	CaO	TiO_2	MnO	Fe_2O_3	CuO	ZnO	BaO	SrO	PbO
SCV 4Bi414	1.19	5.66	12.31	57.7	0.34	0.15	0.07	1.61	14.99	0.55	0.08	5.10		0.08		0.11	
SCV 4i365	1.20	4.92	12.58	51.3		0.20	0.04	1.45	19.52	0.09	4.17	4.53					
SCV 6Ai1152	0.67	6.69	10.64	57.0	0.26	0.20	0.10	1.08	16.67	0.62	0.15	5.94					
SCV 9F1501	1.14	3.73	12.59	53.3	0.62	0.43	0.08	1.78	20.22	0.76	0.07	5.27					
SCV 9i1469	1.10	3.97	11.82	55.8	0.10	0.26	0.05	1.14	19.69	0.54	0.07	4.25					1.16
SCV 10DF7637	1.11	5.51	12.25	59.5	0.23	0.15	0.04	0.98	15.41	0.39	0.06	4.20		0.08		0.09	
SCV 10EF175	0.86	4.86	11.83	54.1		0.51	0.07	1.43	17.51	0.13	4.34	4.37					
SCV 14CF2686	1.13	3.51	13.98	57.7	0.70	0.18	0.08	1.40	15.30	0.57	0.15	4.73		0.07		0.16	0.31
SCV 14i2580	0.84	4.45	12.02	58.3	0.16	0.15	0.11	1.94	16.24	0.71	0.09	4.86				0.17	
SCV 18Ai2914	1.02	6.26	13.88	55.8	0.67	0.35	0.04	1.18	13.18	0.64	0.12	6.03		0.11			0.73
SCV 20i2989	0.89	4.52	13.45	59.4	0.84	0.16	0.07	1.45	12.02	0.85	0.10	6.03					0.18
SCV 21AM3076	1.20	5.68	12.51	51.3		0.22	0.10	1.21	18.99	0.10	4.23	4.48					
SCV 24Ci3386	0.80	4.00	14.02	57.5	0.66	0.08	0.14	1.46	14.63	0.61	0.08	6.06					
SCV 27i3426	0.87	7.27	12.08	51.0	0.11	0.18	0.08	2.04	21.84	0.44	0.06	3.93					0.06
SCV 30F7756	1.14	4.57	14.45	54.6		0.24	0.09	1.68	17.28	0.63	0.08	5.12					0.16
SCV 32M3674	0.81	5.01	11.98	58.9	0.36	0.38	0.13	1.45	14.25	0.60	0.13	6.01					
SCV 32M3680	0.88	4.30	13.47	52.7	0.16	0.15	0.08	1.49	21.25	0.59		4.90					
SCV 33Bi3839	1.17	4.25	13.21	54.1		0.22	0.08	1.98	19.34	0.60	0.10	4.83					0.15
SCV 33Bi3841	1.02	3.51	14.48	56.0	0.77	0.25	0.18	0.87	14.74	0.73		7.45					
SCV 33Bi3870	1.12	3.95	14.67	57.4	0.69	0.15	0.12	1.08	14.16	0.64		6.00					
SCV 33Bi3872	0.99	4.30	12.69	52.6	0.26	0.12	0.03	1.77	21.64	0.51	0.08	4.96					
SCV 34Ai4057	0.95	5.41	12.80	49.4	0.11	0.18	0.16	2.13	22.93	0.51	0.08	5.24				0.09	
SCV 34Bi4060	0.98	6.27	11.71	57.3	0.19	0.17	0.12	1.17	16.02	0.46	0.11	5.17				0.22	
SCV 34CFM4072	0.94	5.69	12.80	50.6	0.33	0.36	0.19	1.14	19.74	0.66		7.58					
SCV 34Ci4065	0.75	6.01	12.72	50.6	0.22	0.16	0.06	1.81	22.19	0.48	0.08	4.87				0.10	
SCV 34Ei4068	1.02	4.35	12.69	59.2	0.24	0.26	0.10	1.21	14.94	0.52	0.09	5.18				0.20	
SCV 35Hi7790	0.71	4.55	12.56	52.6	0.20	0.25	0.14	1.58	20.64	0.59	0.17	5.98					
SCV 37AF479	0.87	5.39	13.55	54.7	0.23	0.24	0.07	1.54	16.35	0.51	0.09	6.07		0.06			0.36
SCV 45M4260	0.82	4.54	14.45	57.4	0.80	0.21	0.04	1.68	13.53	0.78	0.09	5.53		0.17			
SCV 47Ai4284	0.82	3.24	12.40	58.0	1.51	0.18	0.08	1.84	16.20	0.64	0.10	4.98					
SCV 49-15F4338	0.82	3.32	11.37	59.0	0.19	0.30	0.11	1.61	17.29	0.74	0.11	5.13					
SCV 49-4i4327	0.52	4.35	11.83	56.7	0.15	0.15	0.08	1.53	19.01	0.55	0.10	5.08					
SCV 50-11M4352	0.85	4.99	10.58	44.2	0.11	0.08	0.01	1.80	32.16	0.49	0.06	3.99		0.06	0.57	0.09	
SCV 50F4348	0.90	6.17	12.78	53.2	0.19	0.15	0.02	1.93	18.89	0.63	0.06	4.92				0.15	
SCV 51-1M4367	0.99	6.56	11.10	54.4	0.24	0.28	0.08	1.57	18.14	0.60		6.07					
SCV 60Bi4569	1.04	4.01	12.79	54.5	0.19	0.37	0.12	1.78	19.28	0.66	0.11	5.17					
SCV 78F4741	1.34	4.35	13.61	50.8	1.63	0.49	0.13	1.53	19.93	0.54		5.63					
SCV 80F4745	1.23	4.49	12.39	56.1	0.48	0.10	0.14	1.47	17.28	0.52	0.12	4.29					1.39
SCV 81F7863	0.82	4.28	10.86	58.2	0.33	0.61	0.07	1.94	17.29	0.49	0.08	4.99					
SCV 86i4886	1.12	5.70	12.19	53.2		0.30	0.05	1.49	20.60	0.51	0.09	4.76					
SCV SPF8435	0.48	4.58	14.46	59.8			0.07	1.69	14.33	0.80		2.84					0.94
SCV SPM8434	0.49	4.62	17.15	56.0	0.07	0.02	0.06	2.69	14.83	0.71	0.04	2.81					0.54

Table IV.1. (Cont.) Chemical composition of the ceramic body obtained by μ-PIXE (wt.%).

	Na_2O	MgO	Al_2O_3	SiO_2	P_2O_5	SO_3	Cl	K_2O	CaO	TiO_2	MnO	Fe_2O_3	CuO	ZnO	BaO	SrO	PbO
SAC 01	0.49	1.01	22.66	69.1		0.03	0.05	2.89	0.14	1.12		2.49					
SAC 02	0.64	0.80	18.95	74.3			0.04	2.29	0.09	1.11		1.80					
IVDJ-T 96	0.90	3.23	13.14	53.3	0.19	3.61	0.15	2.85	18.08	0.47	0.05	4.00					
IVDJ-T 133	1.06	3.27	15.87	62.3	0.36	0.36	0.15	3.26	7.84	0.60		4.95					
IVDJ-T 3944	0.84	2.98	14.62	58.5	0.78	0.28	0.04	3.63	13.15	0.53	0.08	4.60					
IVDJ-T 4095	1.22	5.25	16.83	51.1	0.08	0.48	0.68	2.99	15.08	0.58	0.08	5.64					
IVDJ-S 3584	0.77	3.17	11.12	51.1	0.03	0.53	1.09	2.27	23.85	0.65	0.07	5.19		0.02		0.09	
IVDJ-S 3601	0.76	5.67	18.71	56.2	0.09	0.43	0.19	2.84	8.95	0.58	0.07	5.42				0.06	
IVDJ-S 3718	0.79	3.62	13.37	59.0	0.07	0.32	0.12	2.93	14.74	0.62	0.05	4.35					
IVDJ-S 3774	1.34	4.14	13.05	48.8		0.45	0.16	1.75	25.50	0.54	0.10	4.16					
IVDJ-S 3794	1.54	2.18	15.07	62.4	0.15	0.37	0.13	2.74	9.49	0.84		5.08					
IVDJ-S 3919	1.35	2.31	17.57	60.8		0.38	0.21	3.67	6.92	0.96		5.82					
IVDJ-S 4098	1.11	4.48	12.58	48.0		0.91	0.06	1.50	25.97	0.48	0.07	4.43					0.38
IVDJ-S 4106	1.80	3.78	10.98	48.2		1.91	0.63	2.26	24.49	0.53	0.08	4.59					0.73
IVDJ-S 4106	1.50	3.33	11.38	53.8		0.84	0.35	2.36	20.51	0.79		5.11					
IVDJ-S 4107	1.63	4.43	12.93	49.4	0.04	0.53	0.19	1.50	23.40	0.50	0.06	4.83	0.02	0.03	0.03	0.10	0.38
IVDJ-S 4127	1.47	4.04	13.95	50.8		0.31	0.10	2.28	20.70	0.53	0.07	5.55					0.17
IVDJ-S 4134	1.41	4.90	14.43	53.1	0.13	0.60	0.12	2.10	17.86	0.58	0.09	4.49	0.02	0.02		0.09	0.04
IVDJ-S 4185	1.50	3.90	13.55	52.9	0.15	0.28	0.10	1.72	20.52	0.43	0.07	4.29	0.01	0.03		0.10	0.36
IVDJ-S XV	0.75	1.83	13.60	59.2	0.09	0.89	0.12	3.15	15.72	0.56	0.05	3.99			0.08		
IVDJ-S SN	1.12	4.20	14.47	50.8	0.16	0.32	0.10	2.02	21.29	0.53	0.09	4.81		0.02		0.06	
MCV 1-1R	0.64	3.19	13.46	46.6		0.34	0.25	2.49	27.15	0.44	0.07	4.66				0.09	0.60
MCV 2-1R	0.45	3.50	13.83	50.9	0.01	0.15	0.13	2.97	22.40	0.44	0.04	4.56				0.10	0.55
MCV 3-1R	0.46	4.14	13.22	51.6	0.05	0.13	0.18	3.18	21.66	0.56	0.08	4.65					
MCV 5-1R	0.58	3.97	13.06	49.7		0.40	0.33	2.78	24.11	0.59		4.51					
MCV 6-1C	0.67	3.29	12.07	51.7	0.10	0.47	0.17	2.71	23.94	0.50	0.08	4.32					
MCV 7-1C	0.48	3.24	11.48	48.2		0.21	0.23	2.37	27.33	1.11	0.09	5.26					
MCV 8-1G	0.70	6.64	12.99	55.9		0.70	0.08	2.41	14.91	0.50		5.17					
MCV 8-2C	0.43	2.67	14.57	57.6	0.19	0.20	0.05	3.59	15.81	0.39		4.45					
MCV 8-3G	0.47	3.27	13.28	51.1		0.45	0.09	3.77	22.56	0.43	0.11	4.23				0.23	
MCV 9-1AG	0.52	3.20	12.77	47.9	0.11	0.25	0.07	2.10	26.49	0.69	0.10	5.82					
MCV 9-2 AP	0.42	2.38	11.42	43.2		0.62	0.15	3.72	21.95	0.95		15.13					
MCV 10-1	0.40	1.90	12.14	53.8		0.11	0.13	3.22	14.79	0.59		6.47					6.50
MCV 10-2	0.94	2.27	12.87	54.8		0.21	0.06	2.64	15.77	0.48		5.09					4.83
MCV 10-3	0.75	1.21	3.18	45.2		0.30	0.55	5.67	32.96	1.56		8.59					
MCV M62	0.57	2.45	11.58	51.8		0.44	0.09	2.34	26.06	0.68		4.01					
CPS 01	0.968	3.24	13.698	55.6	1.173	0.24	0.11	2.31	16.32	0.66	0.07	5.0921					
CPS 02	1.329	3.34	12.194	57.5	0.169	0.15	0.33	1.85	17.95	0.54	0.08	4.2603			0.05		
CPS 03	1.183	2.91	11.262	57.6	0.152	0.16	0.17	2.19	18.98	0.57	0.07	4.2857			0.01		
CPS 04	1.273	2.9	11.173	49.6	0.207	0.55	0.04	1.75	27.22	0.6	0.09	4.1802					
CPS 05	1.274	3.48	12.713	48.1	0.063	1.2	0.14	2.00	25.12	0.57	0.09	4.7089					

The relative standard deviation was calculated as 5-10% for SiO_2, Al_2O_3 and CaO; < 20% for MgO and K_2O; and <30% for the other oxides identified in the ceramic body of the tiles.

Table IV.2. Chemical composition of the white glazes obtained by μ-PIXE (wt.%).

		Na_2O	MgO	Al_2O_3	SiO_2	Cl	K_2O	CaO	TiO_2	Fe_2O_3	CuO	SnO_2	PbO
F	PNS 04	1.49	0.29	0.42	29.2	0.98	0.21	0.28		0.21		11.65	55.3
CS	PNS 05	2.19	0.53	2.01	42.3	0.69	2.75	2.64	0.16	0.55		7.66	38.6
CS	PNS 06	2.54	0.73	1.77	42.4	0.49	2.84	2.19	0.11	0.43		7.02	39.4
R	PNS 07	2.97	0.44	1.95	39.9	0.63	3.63	1.95	0.20	0.46		7.58	40.3
R	PNS 08	1.78	0.48	1.73	38.4	0.69	3.22	2.30	0.11	0.51	0.17	7.64	43.0
R	PNS 09	2.60	0.29	1.35	35.6	0.99	2.08	1.17	0.00	0.25	0.20	7.90	47.4
R	PNS 10	1.79	0.32	1.47	37.3	1.30	2.62	1.21	0.08	0.28	0.20	7.32	46.1
CS	PNS 11	1.89	0.31	0.89	35.4	0.88	2.91	1.19	0.06	0.25	0.13	8.27	47.9
CS	PNS 12	2.48	0.45	2.64	42.7	0.75	3.23	1.84	0.10	0.51		5.07	40.3
R	PNS 13	1.74	0.24	1.13	34.9	1.26	2.80	1.47	0.07	0.42		8.58	47.4
R CS	PNS 14	2.98	0.91	2.61	49.2	0.19	2.99	4.07	0.21	0.89	0.08	6.54	29.4
R	PNS 15	2.03	0.47	1.97	41.0	0.10	2.50	2.99	0.18	0.67	0.38	6.97	40.9
R	PNS 17	3.47	0.39	1.36	40.7	0.87	1.89	1.67		0.33	0.16	7.93	41.3
R	PNS 18	2.62	0.72	2.38	39.9	0.96	3.15	2.78	0.12	0.49	0.11	7.89	38.9
CS	PNS 19	3.19	0.50	2.29	41.0	0.79	1.97	2.41	0.14	0.54		6.25	40.9
CS	PNS 20	1.93	0.36	1.65	37.6	0.82	1.43	1.77	0.12	0.40		6.03	47.8
A	PNS 21	2.13	0.61	2.28	41.1	0.51	1.49	2.89	0.15	0.61		7.80	40.5
A	PNS 22	2.47	0.45	3.19	41.6	0.34	1.39	2.62	0.17	0.85		4.73	42.2
CS	PNS 23	2.73	0.44	1.70	42.1	0.82	3.77	1.87	0.12	0.39		6.64	39.4
A	PNS 24	2.65	0.90	1.52	47.1	1.03	1.86	1.68	0.10	0.43		7.15	35.6
A	PNS 25	2.63	0.57	2.68	46.3	0.75	3.14	3.10	0.16	0.71		6.71	33.2
A	PNS 26	2.59	0.64	3.23	43.4	0.60	3.57	3.60	0.16	0.68		5.60	36.0
CS	PNS 27	2.48	0.65	1.56	40.0	0.99	1.82	1.32	0.13	0.36	0.09	8.64	42.0
CS	PNS 28	1.73	0.64	2.34	43.5	0.57	3.74	2.53	0.16	0.78	0.16	6.52	37.4
A	PNS 29	2.84	0.46	2.54	44.4	1.00	1.99	1.92	0.14	0.48		5.60	38.7
R	PNS 30	2.11	0.34	0.93	44.8	0.48	2.68	1.23		0.32	0.13	6.40	40.5
R	PNS 31	2.58	0.53	1.66	40.3	0.58	2.96	1.77	0.17	0.40	0.00	6.29	42.7
R	PNS 32	3.57	0.24	1.51	41.5	0.98	2.45	1.12	0.07	0.23	0.08	6.42	41.8
R	PNS 34	2.61	0.70	2.63	42.5	0.31	2.53	3.15	0.16	0.62	0.20	7.05	37.5
R	PNS 35	2.33	0.52	2.42	43.6	0.32	3.47	2.55	0.11	0.37	0.17	6.16	37.9
R	PNS 36	3.38	0.46	1.79	42.1	0.82	2.18	1.09	0.06	0.28	0.11	5.16	42.5
R	PNS 38	2.57	0.46	2.02	40.2	0.75	2.54	2.16	0.16	0.40	0.00	5.01	43.7
R	PNS 39	1.97	0.42	1.56	39.7	1.08	3.21	1.04		0.25	0.11	6.00	44.7
A	SCV 4Bi414	1.42	0.44	1.73	39.9	0.52	1.91	2.48	0.12	0.55		6.60	44.3
A	SCV 8i7532	2.71	0.45	2.69	41.9	0.62	2.24	2.43	0.14	0.52	0.00	5.79	40.5
A	SCV 10Bi1673	1.76	0.55	2.37	46.6	0.30	3.08	2.75	0.12	0.76	0.21	6.31	35.2
A	SCV 10EF175	2.40	0.83	3.10	42.0	0.32	2.48	4.06	0.20	0.93	0.64	7.02	36.0
A	SCV 10DF7637	1.82	1.20	2.54	41.6	0.23	1.86	3.18	0.19	0.92	0.25	13.68	32.5
R	SCV 14i2580	1.50	0.49	1.33	39.7	0.44	2.71	2.85	0.12	0.66	0.13	6.79	43.3
A	SCV 18Ai2914	2.32	0.40	1.65	42.4	0.89	2.77	2.49	0.11	0.53		6.30	40.1
A	SCV 20i2989	1.90	0.91	2.34	38.4	0.30	1.95	2.05	0.09	0.72	0.13	10.95	40.3
CS	SCV 27i3426	1.99	0.87	1.84	42.5	0.29	1.97	2.51	0.13	0.70	0.12	6.49	40.6
A	SCV 24Ci3386	1.62	0.48	1.81	41.6	0.51	2.07	2.52	0.10	0.72		6.70	41.8
CS	SCV 30F7756	2.46	0.51	1.99	41.2	0.70	3.08	2.66	0.18	0.94	0.30	5.98	40.0
CS	SCV 30F7756	2.23	0.77	2.19	47.9	0.25	4.29	2.24	0.14	0.48	0.15	10.02	29.3
A	SCV 32M3674	2.05	0.35	1.63	42.4	0.87	3.13	2.16	0.09	0.51		5.98	40.7
A	SCV 32M3680	1.85	0.48	1.97	44.3	0.37	3.26	2.46		0.65	0.25	6.64	37.7
A	SCV 32M3685	1.84	0.30	1.60	43.9	0.55	3.48	1.87	0.10	0.38	0.00	5.05	40.9
CS	SCV 33Bi3839	2.22	0.67	1.81	44.3	0.31	3.10	1.49	0.11	0.53	0.06	8.40	37.0
CS	SCV 33Bi3841	2.28	0.42	1.80	44.1	0.94	3.36	1.86		0.42		6.10	38.7

Table IV.2. (Cont.) Chemical composition of the white glazes obtained by μ-PIXE (wt.%).

		Na_2O	MgO	Al_2O_3	SiO_2	Cl	K_2O	CaO	TiO_2	Fe_2O_3	CuO	SnO_2	PbO
A	SCV 33Bi3870	2.23	0.38	1.52	43.3	0.79	2.98	1.52	0.09	0.48		7.08	37.6
A	SCV 33Bi3872	2.03	0.44	1.78	40.0	0.59	2.65	1.75	0.12	0.61	0.06	7.60	42.4
CS	SCV 3333BF4013	1.14	1.16	4.77	47.1	0.22	2.09	3.54	0.18	1.02	0.20	12.51	26.1
A	SCV 34Ai4057	1.70	0.23	2.11	35.6	0.71	1.91	1.81	0.09	0.51	0.09	4.96	50.3
A	SCV 34Bi4060	2.42	0.38	2.21	41.6	0.58	2.42	2.18		0.53		4.96	42.7
A	SCV 34CFM4072	1.45	0.61	2.48	42.2	0.47	3.56	3.40	0.16	1.26		4.61	39.8
A	SCV 34CFM4072	1.75	0.62	2.69	45.9	0.57	4.15	2.73		0.67		5.69	35.2
CS	SCV 34Ci4065	1.44	0.37	1.56	39.3	0.35	3.09	2.80	0.10	0.94		7.71	42.3
A Un	SCV 34Ei4068	1.85	0.35	1.57	41.0	0.66	3.15	2.13	0.13	0.95	0.12	6.65	41.4
A	SCV 35Hi7790	2.42	0.39	1.59	40.6	0.49	1.96	2.19	0.12	0.62		8.22	41.3
A	SCV 37af4167	2.73	0.94	2.64	50.2	0.19	1.93	2.87	0.11	0.59		9.00	28.8
A	SCV 37af4179	1.78	1.82	2.76	43.0	0.00	3.70	2.60	0.13	0.76	0.11	11.21	32.2
CS	SCV 45M4260	3.06	0.51	2.30	42.9	0.55	2.41	2.56	0.17	0.67		7.88	37.1
CS	SCV 45M4260	2.84	0.56	2.31	45.6	0.69	2.35	2.57	0.11	0.63		5.92	36.4
A	SCV 47Ai4284	1.84	0.33	1.30	30.2	0.90	1.88	2.80	0.17	1.70		4.84	54.0
A Un	SCV 494i4327	2.25	0.53	1.69	43.9	0.51	3.11	2.72	0.13	0.51		7.75	36.9
A Un	SCV 49-15F4338	1.66	0.35	1.68	35.9	0.42	2.82	2.98	0.18	2.12		6.35	45.5
A Un	SCV 49-15F4338	1.62	0.36	1.69	35.4	0.52	2.85	3.16	0.26	2.57		6.28	45.3
CS	SCV 50-11M4352	2.25	0.53	2.06	45.1	0.77	2.42	2.02	0.12	0.77		5.91	38.0
CS	SCV 50-74348	1.92	0.37	1.80	42.7	0.83	2.05	1.80	0.15	0.60		6.16	41.7
R Un	SCV 51-1M4467	2.38	0.58	2.21	42.3	0.34	2.64	2.62	0.14	0.73		7.67	38.4
A	SCV 60Bi4569	1.83	0.75	2.92	39.5	0.30	2.92	4.57	0.19	1.64		7.73	37.6
A	SCV 78F4741	2.27	0.52	3.26	46.9	0.71	3.16	3.03	0.13	0.88		7.05	32.0
A	SCV 80F4745	2.84	0.55	2.64	51.6	0.45	2.93	2.30	0.14	0.55	0.00	4.01	32.0
A	SCV 81F7863	2.83	1.02	3.29	46.4	0.25	2.13	2.45	0.12	0.50		5.92	35.1
A	SCV SPF 8435	1.44	0.08	2.90	48.3	0.56	4.38	0.39	0.04	0.10	0.00	6.26	35.5
A	SAC 01	1.69	0.18	2.53	34.9	0.60	0.52	7.33	0.12	0.26	0.00	9.35	42.6
A	SAC 02	1.29	0.14	2.56	35.3	0.56	0.70	1.72	0.00	0.32	0.00	13.51	43.9
A	IVDJ-T 133	0.97	0.42	4.27	47.9	0.22	1.66	0.96	0.08	0.41	0.05	5.99	37.0
A	IVDJ-T 3683	0.73	0.61	3.59	45.2	0.30	2.12	1.70	0.08	0.31		8.05	37.3
CS	IVDJ-S SN	3.18	0.31	2.07	45.5	1.08	3.04	2.06	0.12	0.45	0.08	5.16	37.0
A	IVDJ-S 3576	3.27	1.05	3.44	45.4	0.12	2.24	5.71	0.19	0.87		5.93	31.8
A	IVDJ-S 3584	2.13	0.70	2.21	43.3	0.25	1.40	2.89	0.11	0.48	0.08	7.06	39.4
A	IVDJ-S 3601	1.57	0.81	3.77	36.6	0.28	1.25	1.65	0.09	0.60		9.48	43.9
CS	IVDJ-S 3718	1.59	0.52	4.96	40.0	0.36	2.51	1.51	0.15	0.52		10.46	37.4
CS	IVDJ-S 3774	2.54	0.57	2.47	42.9	0.38	1.76	2.80	0.16	0.61	0.07	5.68	39.9
CS	IVDJ-S 3794	1.61	0.48	2.05	33.9	0.40	0.72	3.45	0.08	0.87	0.10	8.00	48.3
CS	IVDJ-S 3919	2.05	0.41	1.22	34.9	0.98	0.74	0.67	0.05	0.32	0.06	6.99	51.6
CS	IVDJ-S 4106	2.74	0.78	2.82	40.8	0.30	2.72	2.59	0.14	0.56	0.08	5.73	40.7
CS	IVDJ-S 4107	2.95	0.57	2.14	44.4	0.41	2.47	2.34	0.12	0.45		5.67	38.5
CS	IVDJ-S 4127	2.78	0.35	1.62	38.7	0.83	1.44	1.56	0.16	0.37		9.48	42.7
A	IVDJ-S 4134	2.43	0.51	2.51	42.7	0.30	3.53	2.65	0.14	0.53	0.04	7.84	36.8
A	IVDJ-S 4185	2.82	0.88	2.46	43.0	0.45	2.71	3.43	0.14	0.71	0.06	8.58	34.7
A	CPS01	3.14	0.48	2.32	41.0	0.97	1.93	1.71	0.14	0.56		6.22	40.8
A	CPS02	2.69	0.66	2.64	40.3	0.62	2.08	3.13	0.13	0.69	0.08	6.17	40.8
A	CPS03	2.18	0.61	2.10	42.7	0.40	1.77	2.99	0.11	0.86	0.09	6.98	39.2
A	CPS04	3.10	0.97	3.07	43.6	0.33	2.11	3.56	0.18	0.86	0.10	7.76	34.4
A	CPS05	1.89	0.38	1.82	40.5	0.72	2.85	2.11	0.10	0.56		8.28	40.8

Table IV.2. (Cont.) Chemical composition of the white glazes obtained by μ-PIXE (wt.%).

		Na_2O	MgO	Al_2O_3	SiO_2	Cl	K_2O	CaO	TiO_2	Fe_2O_3	CuO	SnO_2	PbO
F Un	MCV 2-1T	1.17	0.35	1.39	42.1	0.82	4.54	1.67	0.00	0.26	0.00	4.50	43.2
F Un	MCV 3-1R	1.58	0.66	2.32	54.2	0.33	6.37	2.83	0.08	0.52	0.00	4.10	27.0
A	MCV 4-1ML	1.62	0.52	1.84	43.6	0.35	3.23	2.73	0.12	0.61	0.16	6.55	38.7
F Un	MCV 4-2G	1.82	0.36	1.95	42.2	0.83	2.86	2.04	0.08	0.36	0.00	3.42	44.0
A	MCV 5-1R	1.23	0.40	2.87	46.8	0.45	4.61	1.99	0.04	0.23	0.18	4.65	36.6
F	MCV 7-1C	0.73	0.35	2.36	60.2	0.18	4.72	1.97	0.00	0.25	0.00	2.94	26.3
F Un	MCV 8-1G	2.34	0.42	1.51	45.0	0.87	4.60	1.76		0.17		4.07	39.2
F	MCV 10-3	0.68	0.95	7.85	51.6	0.30	6.67	1.74	0.14	0.62		23.99	5.5

Table IV.3. Chemical composition of the blue glazes obtained by μ-PIXE (wt.%).

		Na_2O	MgO	Al_2O_3	SiO_2	Cl	K_2O	CaO	TiO_2	MnO	Fe_2O_3	CoO	NiO	CuO	As_2O_5	SnO_2	PbO	Bi_2O_3
F	PNS 01	3.16	0.41	1.61	35.6	0.58	2.20	1.73	0.11	0.09	1.77	0.43	0.19	0.24		7.67	44.2	
CS	PNS 06	3.31	0.46	2.60	46.2	0.92	3.21	3.17	0.10		1.42	0.40	0.34			4.98	32.8	
R	PNS 07	2.31	0.46	1.84	38.2	0.43	3.86	2.39	0.17	0.18	1.64	0.35	0.19	0.45		7.41	40.1	
R	PNS 09	2.52	0.52	2.01	37.9	0.44	2.82	2.69	0.12	0.05	1.93	0.38	0.15	0.25		8.26	39.9	
CS	PNS 11	2.60	0.31	1.46	38.6	1.30	3.46	1.60	0.09	0.05	1.10	0.30	0.12	0.18		6.85	42.0	
R CS	PNS 14	2.98	0.73	2.55	44.1	0.43	2.45	3.75	0.18	0.04	1.94	0.42	0.20	0.29		5.85	34.1	
CS	PNS 19	3.12	0.56	2.74	43.2	0.83	3.03	3.17	0.13		1.51	0.30	0.16	0.15		5.77	35.4	
CS	PNS 20	2.16	0.45	1.85	40.2	0.65	1.66	2.37	0.13		1.76	0.38	0.17	0.43	2.77	6.27	38.8	
A	PNS 21	2.52	0.65	2.16	40.8	0.42	1.98	3.12	0.15		2.20	0.51	0.24	0.19		7.56	37.6	
A	PNS 22	2.05	0.81	1.75	39.0	0.83	1.04	1.79	0.09		0.80	0.38	0.00	0.00	3.01	7.23	41.3	
CS	PNS 23	2.46	0.51	2.35	45.1	0.61	4.46	2.61	0.14		1.51	0.42	0.15			6.81	32.9	
A	PNS 24	2.12	0.49	2.07	47.6	0.68	2.61	2.04	0.12		1.56	0.30	0.15	0.11		5.67	34.5	
A	PNS 25	2.74	0.88	2.85	47.1	0.44	2.87	3.16	0.13		1.10	0.41				5.78	32.5	
A	PNS 26	2.16	0.78	2.22	41.7	0.34	2.40	3.65	0.14		0.96	0.22				4.76	40.6	
CS	PNS 27	2.64	0.63	1.62	41.4	0.95	1.90	1.81	0.11	0.04	1.43	0.45	0.30	0.29		5.59	40.9	
CS	PNS 28	1.86	0.54	2.34	44.7	0.39	3.91	2.52	0.16	0.04	1.55	0.37	0.15	0.22		7.10	34.2	
A	PNS 29	2.94	0.71	2.99	48.0	0.57	1.93	2.45	0.13	0.00	0.92	0.19	0.09	0.00	2.31	4.52	30.7	1.54
R	PNS 32	4.41	0.28	1.88	41.3	0.82	1.57	0.86	0.13	0.14	1.51	0.45	0.23	0.27		5.90	40.3	
R	PNS 38	2.31	0.47	2.14	39.9	0.53	2.63	2.05	0.12	0.03	1.44	0.34	0.16	0.16		4.99	42.7	
R	PNS 39	2.48	0.47	1.94	37.6	0.86	1.89	1.38	0.09		1.06	0.23	0.25	0.36		7.34	44.0	
A	SCV 4Bi414	0.82	0.32	1.79	41.2	0.29	2.64	2.94	0.16	0.06	2.20	0.45	0.16	0.17		6.36	40.4	
A	SCV 4i365	2.78	0.80	2.35	42.0	0.47	3.10	3.39	0.16	0.02	1.97	0.39	0.15	0.11		9.96	32.4	
A	SCV 6Ai1152	3.64	0.68	3.05	48.5	0.71	4.08	3.66	0.15		2.04	0.35	0.29			5.53	27.3	
A	SCV 8i7532	2.76	0.51	2.68	41.3	0.45	2.32	2.79	0.14	0.00	1.61	0.35	0.22	0.12		5.20	39.6	
A	SCV 9i1469	2.43	0.62	2.37	41.9	0.19	2.45	3.19	0.15	0.00	1.42	0.40	0.24	0.20		6.63	37.9	
A	SCV 10Bi1673	1.87	0.42	1.75	34.6	0.39	2.68	2.64	0.16	0.00	2.92	0.71	0.00	0.00		5.82	46.0	
A	SCV 10ef175	2.40	0.64	2.47	40.1	0.58	2.87	2.78	0.16		2.36	0.51	0.22	0.38		8.52	36.0	
A	SCV 10DF7637	1.96	0.61	2.16	41.3	0.21	1.76	2.22	0.14		1.46	0.46	0.13	0.96		14.27	32.4	
R	SCV 14CF2686	2.01	0.78	2.19	39.4	0.23	1.97	2.65	0.15		1.51	0.30	0.21	0.45		12.56	35.6	
R	SCV 14i2580	1.76	0.42	1.27	39.3	0.58	2.58	2.77	0.12		1.65	0.21	0.16	0.24		5.95	43.0	
A	SCV 18Ai2914	2.11	0.41	1.85	44.6	0.66	3.56	2.57	0.14	0.04	1.96	0.28	0.10	0.13		5.76	35.8	
A	SCV 20i2989	2.64	0.76	2.10	40.5	0.34	2.55	2.53	0.12		1.92	0.53	0.23	0.29		8.51	37.0	
A	SCV 21AM3076	1.77	0.65	1.66	39.6	0.20	3.09	2.19	0.12	0.09	1.32	0.27	0.14	0.42		8.80	39.7	
A	SCV 24Ci3386	2.19	0.40	2.03	40.6	0.43	2.77	3.11	0.18	0.13	1.95	0.26	0.19	0.20	2.21	6.30	37.0	

Table IV.3. (Cont.) Chemical composition of the blue glazes obtained by μ-PIXE (wt.%).

		Na_2O	MgO	Al_2O_3	SiO_2	Cl	K_2O	CaO	TiO_2	MnO	Fe_2O_3	CoO	NiO	CuO	As_2O_5	SnO_2	PbO	Bi_2O_3
CS	SCV 27i3426	2.29	0.62	1.57	41.6	0.32	2.27	2.17	0.11	0.02	1.72	0.50	0.21	0.42		6.82	39.3	
CS	SCV 30F7756	2.71	0.38	2.05	44.3	0.69	2.85	2.22	0.15	0.00	1.73	0.24	0.13	0.18		6.21	36.1	
CS	SCV 30F7756	2.94	0.50	2.13	47.5	0.16	2.50	2.07	0.13	0.04	1.34	0.20		0.34		9.94	30.2	
A	SCV 32M3674	2.12	0.37	1.94	42.7	0.84	3.08	2.37	0.09	0.06	2.32	0.51	0.19	0.23		6.03	37.2	
A	SCV 32M3680	2.13	0.36	1.74	41.1	0.72	2.84	1.93	0.08		2.06	0.37	0.21	0.51		6.14	39.8	
A	SCV 32M3685	2.00	0.40	1.89	38.9	0.72	3.03	2.31	0.12		2.04	0.41	0.17	0.22		7.04	40.8	
CS	SCV 33Bi3839	2.47	0.72	1.88	42.6	0.31	3.46	2.59	0.20		0.87	0.29	0.12	0.29		9.28	34.9	
CS	SCV 33Bi3841	2.23	0.36	1.77	42.3	0.66	3.44	2.32	0.11	0.09	2.04	0.54	0.30	0.26		5.94	37.7	
A	SCV 33Bi3870	2.42	0.45	1.62	42.2	0.81	3.22	1.60	0.13		2.03	0.34	0.23	0.28		7.66	37.0	
CS	SCV 3333BF4013	1.73	0.60	2.87	40.0	0.15	2.22	2.20	0.15		1.68	0.39	0.21	0.41		18.74	28.6	
A	SCV 34Ai4057	1.74	0.23	1.31	35.2	0.90	1.52	1.90	0.09		2.24	0.57	0.18	0.42		5.89	47.8	
A	SCV 34Bi4060	2.55	0.42	1.84	40.3	0.62	2.26	2.21	0.09		2.07	0.32	0.21	0.16		5.95	41.0	
CS	SCV 34Ci4065	1.63	0.38	1.69	41.7	0.38	3.04	3.13	0.12	0.05	1.82	0.51	0.18	0.19		5.86	39.4	
AM	SCV 34Ei4068	2.27	0.39	1.67	41.9	0.58	3.19	2.04	0.16		2.57	0.98	0.22	0.32		7.55	36.2	
A	SCV 37AF4167	2.37	0.82	2.49	43.4	0.22	1.82	3.02	0.17		1.93	0.50	0.17	0.33		12.09	30.6	
A	SCV 37af4179	2.01	0.64	1.85	44.6	0.31	4.15	2.22	0.14		1.85	0.55	0.17	0.27		9.59	31.7	
CS	SCV 45M4260	3.39	0.39	1.83	41.9	1.00	2.12	1.67	0.12		1.71	0.44	0.23	0.27		8.15	36.8	
CS	SCV 45M4260	3.01	0.45	2.03	43.3	1.11	2.09	1.71	0.10		1.58	0.50	0.18	0.29		6.67	37.0	
A	SCV 47Ai4284	2.27	0.43	2.29	42.3	0.61	2.66	2.15	0.17		1.52	0.35	0.14	0.16		5.14	39.8	
AM	SCV 494i4327	1.73	0.47	1.78	40.1	0.50	3.35	2.45	0.11	0.04	4.51	1.47	0.36	0.13		8.31	34.7	
AM	SCV 49-15F4338	1.97	0.37	2.01	39.3	0.42	3.55	2.90	0.14		3.02	1.05				6.93	38.3	
CS	SCV 50-74348	1.90	0.38	1.41	38.6	0.90	2.47	1.34	0.10	0.02	1.54	0.36	0.17	0.22		8.05	42.6	
RM	SCV 51-1M4467	2.33	0.49	1.84	40.7	0.78	2.07	2.81	0.17		1.64	0.34				6.95	39.9	
A	SCV 60Bi4569	2.73	0.72	2.61	45.5	0.48	3.23	3.19	0.10	0.15	0.87	0.26		0.21		4.69	35.3	
A	SCV 78F4741	2.48	0.95	3.57	47.6	0.40	3.97	4.15	0.12		1.47	0.13				5.42	29.7	
A	SCV 80F4745	3.01	0.68	2.15	45.7	0.32	2.13	2.12	0.40	0.06	0.75	0.16	0.11	0.12		3.77	38.5	
A	SCV 81F7863	3.53	1.00	2.18	42.2	0.73	1.92	3.49			0.85	0.51				4.33	39.3	
F	SCV 86i4886	2.19	0.61	2.18	44.9	0.33	3.39	4.21	0.18		2.61	0.39				7.44	31.6	
F	SCV 86i4886	2.53	0.72	2.22	43.2	0.35	3.73	3.15	0.12	0.02	2.09	0.42	0.11	0.05		11.27	29.7	
A	SAC 01 1	1.65	0.22	2.27	34.2	0.30	0.59	5.26	0.00	0.00	0.46	0.24	0.00			9.04	45.7	
A	IVDJ-T 133	0.90	0.82	3.20	41.2	0.31	1.12	1.09	0.10	0.00	0.61	0.29	0.17	0.07		3.94	46.2	
A	IVDJ-T 3683	0.66	0.96	4.14	46.3		2.50	2.95	0.10	0.12	0.80	0.26	0.12	0.33		6.42	34.3	
A	IVDJ-T 4095	4.71	0.39	4.23	40.7	1.04	2.73	1.06	0.11		1.68	0.32		0.25		4.48	38.3	
CS	IVDJ-S SN	3.22	0.42	2.01	45.2	0.77	3.12	2.52	0.11	0.04	1.20	0.23	0.22	0.14		7.02	33.7	
A	IVDJ-S 3561	2.89	1.05	2.84	43.2	0.61	3.79	4.22	0.16	0.06	1.10	0.34	0.12			6.78	32.8	
A	IVDJ-S 3576	3.56	0.85	2.82	44.5	0.24	2.20	3.21	0.20	0.06	2.85	0.61	0.26	0.27		6.00	32.4	
A	IVDJ-S 3584	3.22	0.64	2.50	42.1	0.49	1.61	2.49	0.10		1.96	0.48	0.27	0.19		6.43	37.5	
A	IVDJ-S 3591	3.30	0.44	2.31	38.9	0.97	1.71	2.17	0.13		2.09	0.32	0.22	0.30		6.32	40.8	
A	IVDJ-S 3601	1.71	0.92	3.67	37.9	0.25	1.31	1.31	0.12	0.02	0.90	0.50	0.09	0.07		8.34	42.8	
A	IVDJ-S 4098	2.14	0.47	2.00	41.6	0.82	3.42	1.65	0.16		1.92	0.34	0.12	0.15		7.44	37.8	
CS	IVDJ-S 4106	3.06	0.42	2.62	40.8	0.83	2.27	1.70	0.10		2.12	0.53	0.18	0.32		4.96	40.1	
CS	IVDJ-S 4107	3.38	0.63	2.38	43.0	0.43	2.58	2.69	0.14	0.05	1.77	0.50	0.11	0.18		5.82	36.3	
CS	IVDJ-S 4127	2.72	0.22	1.51	38.6	0.61	1.42	1.12	0.09	0.03	1.33	0.54	0.29	0.35		6.25	44.9	
A	IVDJ-S 4134	2.24	0.51	3.14	40.6	0.19	3.59	2.68	0.16	0.06	3.58	1.22	0.48	0.94		9.69	30.9	
A	IVDJ-S 4185	3.60	1.52	4.72	45.9	0.10	2.81	6.52	0.22	0.05	4.06	1.27	0.58			5.48	23.2	
A	CPS02	1.93	0.91	2.67	44.9	0.24	2.54	4.35	0.18	0.04	0.97	0.16	0.12			4.44	36.5	
A	CPS03	2.65	0.71	2.12	43.5	0.38	1.93	2.81	0.09	0.03	0.91	0.41	0.14		1.32	7.02	36.0	
A	CPS04	2.41	0.96	2.53	41.8	0.32	1.78	3.56	0.15	0.05	1.00	0.28	0.07	0.27		7.26	37.5	
A	CPS05	2.33	0.63	1.64	41.8	0.60	3.36	1.87	0.10	0.04	0.85	0.45	0.08			7.73	38.5	

Table IV.3. (Cont.) Chemical composition of the blue glazes obtained by μ-PIXE (wt.%).

		Na_2O	MgO	Al_2O_3	SiO_2	Cl	K_2O	CaO	TiO_2	MnO	Fe_2O_3	CoO	NiO	CuO	As_2O_5	SnO_2	PbO	Bi_2O_3
F Un	MCV 2-1T	1.41	0.33	1.52	42.6	1.14	4.58	1.46			0.46	0.16	0.00			4.10	42.2	
F Un	MCV 3-1R	1.72	1.05	2.10	50.3	0.30	6.27	3.02	0.08	0.34	0.88	0.39	0.18			4.71	28.6	
F Un	MCV 4-1G	1.83	0.36	2.07	46.4	0.52	3.42	2.15	0.06		0.35					3.97	38.9	
F Un	MCV 4-2G	1.87	0.28	2.25	43.5	0.98	3.69	1.85			0.46					3.71	41.4	
A	MCV 5-1R	1.60	0.66	1.97	43.8	0.58	3.43	1.94		0.47	0.60	0.47	0.33			4.11	40.1	
F Un	MCV 8-1G	3.45	0.39	1.62	45.6	1.00	4.40	1.85	0.06		0.63	0.16	0.12			4.16	36.6	
F Un	MCV 8-2C	1.63	0.68	2.73	52.5	0.17	5.64	3.75	0.39	0.18	3.52	1.20	0.32	0.08		4.38	22.8	
F Un	MCV 8-3G	1.22	0.37	2.03	45.7	0.47	5.76	2.21		0.09	3.68	1.00	0.31	0.28		4.66	32.2	
F	MCV 9-1Ag	0.33	0.53	2.20	53.6	0.16	6.68	2.09			0.62	0.37				1.23	31.8	
F	MCV 9-2Ap	1.16	1.04	4.40	36.1	0.40	3.82	5.79	0.13		1.27	0.40				10.18	35.3	
F	MCV 10-1	1.20	0.28	2.51	43.5	0.36	3.82	2.06	0.11		1.67	0.45	0.24			5.26	38.5	

Table IV.4. Chemical composition of the green glazes obtained by μ-PIXE (wt.%).

		Na_2O	MgO	Al_2O_3	SiO_2	Cl	K_2O	CaO	TiO_2	Fe_2O_3	CuO	SnO_2	PbO
F	PNS 02	1.17	0.69	3.03	38.6	0.21	2.01	3.38	0.18	0.80	1.94	1.26	46.8
F	PNS 03	1.00	0.12	0.57	32.9	0.36	0.30	0.37		0.27	2.98	7.17	54.0
CS	PNS 05	1.81	0.65	3.56	41.4	0.27	2.44	3.74	0.38	0.95	1.32	2.03	41.3
CS	PNS 06	1.65	0.65	2.22	37.8	0.43	2.05	2.46	0.13	0.63	0.88	4.13	47.0
R	PNS 07	1.15	0.61	2.52	40.0	0.24	3.08	3.42	0.23	0.84	2.85	0.78	44.3
R	PNS 08	1.05	0.31	1.77	34.2		1.51	2.09	0.10	1.83		2.22	54.3
R	PNS 09	2.31	0.48	1.98	37.3	0.47	2.54	2.49	0.10	0.84	2.37	6.16	42.9
R	PNS 10	0.80	0.39	2.10	33.8		1.31	2.68	0.11	0.88	2.08	0.70	55.1
CS	PNS 11	1.39	0.29	1.72	39.2	0.30	2.88	1.82	0.13	0.63	1.66	2.26	47.7
CS	PNS 12	1.30	0.29	2.38	38.0	0.33	1.18	1.80	0.17	0.77	2.05	1.68	49.8
R	PNS 15	0.86	0.42	1.99	36.4		1.89	2.59	0.15	0.67	2.22	0.99	51.8
R	PNS 16	1.22	0.53	1.98	34.4	0.66	1.34	2.00	0.12	0.61	2.17	1.76	53.2
R	PNS 17	3.06	0.34	1.04	36.0	0.55	1.29	2.22	0.03	0.77	6.23	7.18	41.3
CS	PNS 19	1.48	0.62	3.82	43.2		2.76	3.11	0.26	1.39	1.98	1.82	39.2
A	PNS 21	1.03	0.48	2.59	37.8	0.16	1.21	2.89	0.19	0.88	1.51		51.5
A	PNS 22	0.49	0.38	2.34	34.5	0.20	0.81	2.22	0.15	0.75	1.59	0.45	56.4
A	PNS 24	1.29	0.34	1.79	38.1	0.39	1.43	1.98	0.13	1.05	2.34	2.41	48.7
A	PNS 26	1.09	0.50	2.66	38.3	0.23	2.15	3.36	0.17	0.96	1.67	1.02	48.0
CS	PNS 28	1.53	0.39	2.95	44.4	0.31	3.21	1.72	0.22	1.00	2.17	1.45	40.7
A	PNS 29	0.60	0.50	2.09	39.0	0.22	1.41	2.57	0.12	0.74	2.07	0.45	50.3
R	PNS 30	2.41	0.34	1.07	41.5	0.53	2.31	1.50	0.00	0.36	0.81	6.32	42.8
R	PNS 33	0.92	0.35	1.64	36.9	0.00	0.60	1.20	0.00	0.44	2.72	1.22	53.9
R	PNS 34-L	3.29	0.58	2.14	40.8	0.64	1.84	2.77	0.14	0.63	1.36	6.12	39.7
R	PNS 34-D	2.20	0.83	3.10	42.5	0.32	2.68	3.57	0.22	1.21	2.23		41.1
R	PNS 35	2.42	0.50	1.88	38.5	0.52	2.27	2.32	0.13	0.51	2.24	6.35	42.4
R	PNS 36	1.20	0.41	3.01	44.3	0.26	1.95	1.07	0.17	0.75	1.50	0.64	44.8
P	PNS 37	1.27	0.74	3.31	39.3	0.19	1.46	3.41	0.21	0.95	2.33	1.34	45.4
R	PNS 38	1.29	0.58	2.88	42.0	0.41	1.41	2.31		0.91	2.01	1.70	44.5

Table IV.4. (Cont.) Chemical composition of the green glazes obtained by μ-PIXE (wt.%).

		Na_2O	MgO	Al_2O_3	SiO_2	Cl	K_2O	CaO	TiO_2	Fe_2O_3	CuO	SnO_2	PbO
A	SCV 4Bi414	0.53	0.48	2.34	37.6	0.30	1.69	3.41	0.16	1.05	2.30	0.94	49.1
A	SCV 6Ai1152	1.43	0.60	2.75	35.5	0.38	2.07	3.99	0.23	2.28	2.16	0.66	47.9
A	SCV 9i1469	1.83	0.80	4.10	39.6	0.16	2.13	3.78	0.16	1.13	1.35	0.00	44.8
A	SCV 10Bi1673	1.01	0.48	2.09	40.6	0.31	1.94	3.14	0.16	0.77	2.24	0.93	46.4
A	SCV 10ef175	1.62	0.87	3.09	39.7	0.36	2.12	4.15	0.20	1.01	2.06	1.46	43.3
A	SCV 21AM3076	1.03	0.91	2.62	37.6	0.33	1.85	3.62	0.19	0.79	3.29	1.27	46.5
A	SCV 24Ci3386	1.27	0.46	2.71	42.6	0.30	2.21	2.56	0.14	1.14	1.30	0.55	44.7
CS	SCV 27i3426	1.04	0.74	1.66	34.7	0.39	1.55	2.61	0.11	0.78	2.71	1.92	51.6
CS	SCV 30F7756	1.01	0.58	2.70	40.4	0.42	2.79	3.62		2.55	3.01	0.91	42.0
A	SCV 32M3674	1.48	0.46	2.13	41.0	0.58	2.86	2.86	0.18	0.79	2.12	1.71	43.8
A	SCV 32M3680	1.28	0.41	1.95	39.7	0.43	1.54	2.30		0.63	2.41	1.97	47.4
A	SCV 33Bi3870	1.21	0.51	2.59	37.8	0.36	1.61	2.34	0.19	1.03	1.63	0.76	49.9
A	SCV 34Ai4057	0.79	0.35	1.71	35.7	0.34	1.20	2.46	0.12	0.68	2.73	1.62	52.3
A	SCV 34Bi4060	1.09	0.48	2.28	38.4	0.34	1.63	2.94	0.17	0.78	2.19	0.99	48.8
A	SCV 34CFM4072	1.24	0.45	1.86	39.8	0.40	3.39	2.64	0.15	0.52	0.86	0.82	47.8
CS	SCV 34Ci4065	1.21	0.38	2.91	42.8	0.25	3.64	2.36	0.19	1.54	1.04	1.54	42.1
A	SCV 35Hi7790	0.60	0.41	2.36	38.0	0.43	0.90	2.14		0.70	2.11	0.57	51.8
A	SCV 37af4167	1.07	1.80	4.75	44.3	0.20	1.73	5.03	0.24	1.18	2.13	1.83	35.7
A	SCV 37af4179	1.33	0.66	2.44	44.7	0.31	3.82	2.80	0.16	0.69	1.64	1.03	40.4
A	SCV 47Ai4284	1.03	0.42	3.99	43.6	0.38	2.92	2.08	0.18	1.17	1.53	0.55	42.1
A	SCV 80F4745	1.12	0.53	2.94	42.2	0.16	1.75	2.77	0.15	0.69	2.12	0.00	45.6
A	SCV 81F7863	0.44	0.66	2.36	36.8		1.26	3.42		0.76	2.95		51.3
F	SCV 87M7985	1.32	2.14	3.47	44.2	0.37	1.66	4.37		0.68	2.85	2.83	35.4
A	IVDJ-T 96	1.01	0.91	3.76	35.6		1.62	2.90	0.24	0.68	2.66	3.77	44.9
A	IVDJ-T 133	0.59	0.66	3.75	42.9	0.17	1.07	1.38	0.10	0.55	1.22	0.62	46.9
R	IVDJ-S XV	1.13	0.53	3.32	37.8	0.22	1.23	2.83	0.15	1.06	1.51	3.20	47.0
CS	IVDJ-S SN	1.73	0.35	2.61	42.7	0.31	2.53	1.40	0.19	0.56	1.48	1.69	44.4
A	IVDJ-S 3561	3.58	0.71	3.18	46.4	0.46	3.25	2.83	0.13	0.83	1.09	8.59	28.9
A	IVDJ-S 3584	1.49	0.88	3.60	40.9		1.39	3.69	0.22	1.42	1.73		44.7
CS	IVDJ-S 3718	1.21	0.56	2.56	39.0	0.21	1.93	1.92	0.21	0.53	2.59	2.45	46.9
CS	IVDJ-S 3774	1.16	0.50	2.71	42.9	0.20	1.98	2.56	0.14	0.79	1.69	1.30	43.9
CS	IVDJ-S 3794	2.72	0.36	2.05	36.0	0.87	0.76	2.46	0.11	0.71	1.96	7.84	44.1
CS	IVDJ-S 3919	2.08	0.43	1.21	31.9	0.60	0.57	0.69	0.04	0.33	2.45	7.92	51.8
A	IVDJ-S 4098	1.63	0.48	2.40	39.5	0.35	3.05	2.32	0.12	0.67	1.32	0.58	47.5
CS	IVDJ-S 4106	1.31	0.40	2.23	37.9	0.24	1.42	1.86	0.16	0.54	2.82	1.53	49.5
CS	IVDJ-S 4107	1.57	0.59	2.12	42.9	0.20	2.29	2.41	0.17	0.52	1.26	1.63	44.3
CS	IVDJ-S 4127	1.76	0.46	1.84	38.2	0.24	1.89	2.21	0.14	0.62	3.25	3.18	46.2
A	CPS02	1.90	0.73	2.80	39.0	0.37	2.05	3.94	0.15	0.87	0.69	2.15	45.3
A	CPS04	1.32	0.87	3.57	36.3	0.29	1.46	3.39	0.28	1.37	1.72	1.03	48.4
A	MCV 4-1ML	0.37	0.66	2.91	38.5	0.29	1.55	3.77	0.17	1.09	2.70	0.85	47.1
A	MCV 5-1R	0.95	0.41	1.85	38.7	0.30	2.60	2.34		0.46	2.58	4.18	45.7
F	MCV 6-1C		0.24	2.87	49.7	0.25	2.64	1.72		0.23	2.15	0.77	39.5
F	MCV 7-1C	0.23	0.43	3.49	49.6	0.20	3.23	2.84	0.11	0.50	1.98	0.85	36.5
F	MCV 10-3	1.47	0.31	2.68	40.0	0.81	1.84	1.14		0.29	5.10	5.14	41.2

Table IV.5. Chemical composition of the amber glazes obtained by μ-PIXE (wt.%).

		Na_2O	MgO	Al_2O_3	SiO_2	Cl	K_2O	CaO	TiO_2	MnO	Fe_2O_3	CuO	SnO_2	PbO
CS	PNS 05	1.68	1.25	3.24	39.1		2.32	3.61	0.18	0.20	3.92		1.01	43.5
CS	PNS 11	0.63	0.12	1.36	35.4		2.14	0.71			3.92		0.55	55.1
R CS	PNS 14	2.32	0.72	4.28	47.7	0.18	3.39	3.78	0.24	1.76	1.55	0.09	2.47	31.5
R	PNS 15	1.56	0.52	2.70	40.8		2.80	3.48	0.16		3.92	0.27	0.94	42.9
A	PNS 21	0.79	0.55	2.64	37.3	0.14	1.39	3.44	0.17		3.73		0.52	49.4
A	PNS 22	0.50	0.54	2.48	34.2	0.18	1.26	2.68	0.17	0.50	3.77	0.13	0.49	53.2
A	PNS 24	0.84	0.34	2.30	33.5	0.26	1.61	2.08	0.16		4.30	0.14	0.46	54.0
A	PNS 25	0.89	0.88	2.85	41.0	0.24	2.01	4.16			2.91		0.57	44.5
CS	PNS 27	0.71	0.31	1.99	40.3	0.25	3.11	1.41	0.13	0.07	3.87		0.69	47.1
A	PNS 29	0.86	0.58	2.54	40.8	0.20	1.88	3.07	0.16		3.31		0.41	46.2
R	PNS 38	1.28	0.48	2.54	37.3	0.21	1.88	2.26	0.16		2.72		0.47	50.7
R	PNS 39	0.79	0.41	2.00	35.4	0.22	1.81	2.00	0.16		3.07	0.20		54.0
A	SCV 4Bi414	0.80	0.40	2.81	34.4	0.28	1.87	2.95	0.25		4.68	0.53	0.73	48.7
A	SCV 4i365	2.07	0.95	3.49	36.9	0.35	2.71	4.74	0.19		4.75	0.11	1.22	42.5
A	SCV 6Ai1152	1.19	0.49	2.56	36.4	0.30	1.62	3.15			5.09			49.2
A	SCV 9i1469	1.29	0.79	3.67	37.2	0.14	1.92	3.82	0.19	0.03	3.51	0.17	0.48	46.7
A	SCV 10Bi1673	0.99	0.85	3.69	34.2	0.24	1.34	5.44	0.25		3.91	0.14	0.44	48.5
A	SCV 10DF7637	1.27	0.76	3.76	35.2	0.32	1.98	3.96	0.28		4.51	0.35	0.42	47.2
R	SCV 14i2580	0.72	0.46	2.25	32.6	0.29	2.46	3.31	0.14		4.22			53.6
A	SCV 18Ai2914	2.11	0.78	3.13	43.1	0.20	3.73	4.56	0.19		4.99	0.18	1.11	35.9
A	SCV 20i2989	1.28	0.72	2.25	34.9	0.00	2.42	3.10	0.11		4.67	0.00	1.14	49.4
A	SCV 21AM3076	0.78	0.76	2.38	35.6	0.32	2.26	3.61	0.21	0.02	4.09	0.12	0.53	49.4
A	SCV 24Ci3386	1.18	0.50	2.38	38.2	0.31	2.35	3.46	0.16		3.87		0.94	46.7
CS	SCV 27i3426	1.10	0.54	2.06	34.3	0.31	2.01	3.00	0.19		4.89	0.07	0.65	50.8
A	SCV 32M3674	1.37	0.59	2.87	37.4	0.39	2.87	4.39	0.21		2.48	0.21	0.70	46.5
A	SCV 32M3680	1.35	0.84	2.70	34.6	0.30	2.13	5.01	0.18		3.96		0.67	48.2
CS	SCV 33Bi3839	0.00	1.05	3.01	35.8	0.40	3.09	4.31	0.19		5.22	0.06		46.9
A	SCV 33Bi3870	1.23	0.52	2.71	36.2	0.28	2.16	3.40	0.16		4.53	0.16		48.7
A	SCV 33Bi3870	1.28	0.72	2.81	37.4	0.32	3.05	5.18	0.19		2.50		0.88	45.7
A	SCV 33Bi3872	1.74	0.46	2.30	36.9	0.00	2.85	2.01	0.16	0.32	4.16			49.1
CS	SCV 3333BF4013	1.92	0.90	4.92	44.8	0.19	3.28	4.13	0.29	0.05	4.75	0.00	1.16	33.6
A	SCV 34Ai4057	0.50	0.22	1.47	31.0		1.09	1.79	0.13		4.65	0.18	0.50	58.5
A	SCV 34CFM4072	1.36	0.46	2.20	38.8	0.45	3.84	2.70			4.52		1.48	44.2
A	SCV 34CFM4072	1.43	0.48	2.35	41.1	0.31	3.85	2.82			4.26		0.81	42.5
CS	SCV 34Ci4065	0.62	0.29	1.92	38.2	0.23	2.72	2.54	0.29		4.59		0.36	48.3
CS	SCV 45m4260	2.32	0.60	2.34	42.7	0.37	3.25	2.62	0.18	0.05	2.47	0.11	8.03	35.0
A	SCV 47Ai4284	0.99	0.44	2.38	33.5	0.33	1.41	3.13	0.15	0.04	4.21	0.11	0.43	52.9
CS	SCV 50-11M4352	0.87	0.27	2.63	36.6	0.34	1.51	1.80	0.13	0.08	4.53		0.75	50.3
A	SCV 60Bi4569	0.95	0.50	2.91	40.6	0.41	1.83	3.01			2.10		0.69	47.0
A	SCV 80F4745	1.14	0.53	2.58	41.3		2.10	3.11	0.15		4.24			44.9
A	IVDJ-T 96	1.03	1.04	5.48	33.8	0.25	1.63	5.14	0.17	0.08	1.90		0.55	48.2
A	IVDJ-T 133	0.86	0.68	5.78	39.0	0.13	1.50	4.35	0.16	0.06	2.67	0.08	0.29	43.9
A	IVDJ-T 3683	0.62	0.96	4.40	51.5		2.93	3.46	0.13		2.73		1.06	32.2
A	IVDJ-T 4095	0.80	0.57	3.13	35.6		1.76	1.24	0.10	0.13	2.49		0.93	53.2
CS	IVDJ-S SN	1.46	0.39	1.80	42.1	0.19	3.35	2.32	0.15		3.43	0.07	0.74	44.0
A	IVDJ-S 3584	1.37	0.87	3.23	41.5		1.38	3.71	0.21		3.28			44.4
A	IVDJ-S 3591	1.43	0.77	3.10	39.2	0.21	1.46	3.23		0.14	3.73	0.19		46.6
CS	IVDJ-S 3919	0.44	0.59	1.75	35.0	0.29	0.59	1.21	0.12		3.77		0.43	55.9
A	IVDJ-S 4098	1.21	0.52	3.05	43.9	0.22	3.81	2.72	0.17		3.38			41.0
CS	IVDJ-S 4106	0.93	0.44	2.54	38.5	0.20	1.73	2.26	0.16		4.47			48.7
A	CPS02	1.16	0.57	2.87	37.8	0.30	1.90	3.21	0.17		3.73		0.40	47.9
A	CPS04	0.79	0.71	3.36	34.1	0.27	1.41	4.81	0.22	0.09	3.66		0.60	50.0
A	CPS05	0.89	0.32	1.94	34.4	0.35	1.76	1.65	0.10		4.28		0.34	54.0
A	MCV 4-1ML	0.81	0.55	2.49	36.2	0.26	2.44	3.33	0.14		4.07		0.45	49.2

Table IV.6. Chemical composition of the brown glazes obtained by μ-PIXE (wt.%).

		Na_2O	MgO	Al_2O_3	SiO_2	Cl	K_2O	CaO	TiO_2	MnO	Fe_2O_3	CuO	SnO_2	BaO	PbO
R	PNS 07	1.95	0.75	3.13	40.8		4.73	4.11	0.11	2.26	1.10	0.25	1.78	0.29	38.7
R	PNS 08	1.88	0.48	1.85	38.1		2.64	2.29	0.15	1.66	0.88	0.24	8.18		41.6
R	PNS 09	2.26	0.54	2.09	37.9	0.40	3.11	2.49	0.11	1.46	0.78	0.24	7.87	0.15	40.6
R	PNS 10	1.93	0.46	1.86	36.8	0.72	2.22	1.52		1.81	0.68	0.37	9.22		42.4
CS	PNS 11	0.76	0.24	1.86	33.6		1.97	1.55	0.11	5.28	0.74	0.23	0.45	0.12	53.1
R	PNS 18	2.04	0.68	2.80	41.2	0.49	4.02	2.82	0.17	1.61	1.15	0.15	5.98		36.9
CS	PNS 19	0.79	0.56	2.77	36.6		1.61	4.06	0.20	2.79	1.44	0.11	0.90	0.11	48.0
CS	PNS 23	1.42	0.38	1.95	40.4	0.29	2.90	1.68	0.16	3.26	1.19		0.48	0.18	45.7
A	PNS 24	0.66	0.52	2.83	40.6	0.24	2.10	2.62	0.20	2.50	1.78		0.53		45.4
A	PNS 25	1.38	0.67	2.85	40.2	0.32	1.80	3.79	0.20	1.90	0.87		0.81		45.3
CS	PNS 27	0.85	0.26	1.88	39.3	0.25	2.65	1.40	0.16	2.56	0.93	0.11	0.52	0.14	49.0
CS	PNS 28	1.34	0.41	2.05	38.6	0.29	2.68	1.69	0.16	3.37	1.37			0.19	47.9
A	PNS 29	0.95	0.94	2.70	40.9	0.19	1.86	3.96	0.18	2.37	0.82		0.63		44.5
R	PNS 30	1.27	0.27	2.84	39.8	0.35	2.36	1.61		2.80	0.27	0.09	5.02	0.85	41.5
R	PNS 31	1.01	0.53	1.89	36.4	0.23	1.83	1.42	0.14	2.01	1.86	0.13	0.92		51.7
R	PNS 33	1.49	0.49	2.19	37.1	0.17	1.19	1.79	0.16	1.83	1.21	0.48	2.13		49.7
R	PNS 34	2.10	0.81	2.96	39.8	0.17	2.48	3.12	0.21	2.14	1.05	0.63	1.36		43.1
R	PNS 36	0.83	0.53	2.48	38.9		1.44	1.76	0.19	3.15	1.14	0.10	0.31		49.2
R	PNS 38	3.06	0.53	2.23	40.1	0.73	2.63	2.12	0.25	1.39	0.75		5.19		41.0
A	SCV 4i365	1.06	1.20	3.26	33.8		2.68	5.30	0.19	2.92	3.51		1.07	0.29	44.8
A	SCV 4Bi414	1.10	0.45	2.94	38.8	0.28	2.33	2.78	0.22	2.64	2.06			0.18	46.3
A	SCV 10Bi1673	1.33	0.50	3.40	39.4	0.26	1.94	2.99	0.17	2.84	1.94		0.38	0.20	44.7
A	SCV 10DF7637	1.49	0.59	3.12	42.5		2.16	2.29	0.20	3.07	1.53	0.15	0.00	0.26	42.6
A	SCV 24Ci3386	1.35	0.49	2.65	42.0	0.32	2.18	2.08	0.17	2.54	1.23			0.23	44.8
CS	SCV 30F7756	1.95	0.85	3.19	44.1	0.16	4.80	3.12	0.23	2.67	2.68	0.28	1.50		34.5
A	SCV 32M3685	1.37	0.48	2.39	37.8	0.37	2.78	2.89	0.17	2.60	1.58	0.19	0.89	0.20	46.3
CS	SCV 33Bi3839	1.65	0.84	3.10	40.4	0.31	3.46	3.91	0.20	2.94	1.68	0.09	1.54	0.19	39.7
CS	SCV 33Bi3841	1.99	0.50	2.02	42.4	0.28	3.81	2.45	0.09	2.34	1.88		3.86	0.20	38.0
A	SCV 33Bi3870	1.17	0.60	2.90	36.6	0.23	2.31	3.91	0.19	2.74	1.70		0.62		47.0
A	SCV 33Bi3872	1.69	0.75	3.09	37.6	0.17	2.37	3.20	0.16	2.99	1.68	0.07		0.25	46.0
CS	SCV 3333BF4013	1.43	1.21	5.36	46.5	0.19	2.78	4.47	0.24	2.60	2.44	0.00	1.12	0.32	31.3
A	SCV 35Hi7790	1.65	0.46	2.33	38.7	0.35	1.72	2.11	0.16	1.90	1.19		1.88		47.6
A	SCV 37af4167	0.83	1.04	3.19	41.3	0.20	1.53	3.52	0.15	1.47	1.51	1.36	0.93		43.0
A	SCV 37af4179	1.52	0.68	2.47	42.3	0.32	4.13	2.86	0.17	3.28	1.38	0.15	0.78	0.18	39.8
CS	SCV 45M4260	1.67	0.63	2.55	38.2	0.30	2.45	2.86	0.17	4.85	1.87	0.07	0.97	0.35	43.0
CS	SCV 50-11M4352	0.74	0.41	2.64	34.4	0.34	1.54	2.07	0.13	2.47	1.55	0.12		0.22	53.4
CS	SCV 50-74348	0.49	0.33	2.70	32.2	0.31	0.83	1.33	0.11	2.17	1.20		0.22		58.1
A	SCV 60Bi4569	1.55	0.68	3.26	41.8	0.25	2.42	3.31	0.15	1.35	1.02	0.24	0.60		43.4
A	SCV 78F4741	1.46	0.51	2.53	45.2	0.35	2.91	3.12	0.14	2.41	0.97	0.47	0.69		39.3
A	SCV 80F4745	1.27	0.87	3.95	39.9	0.00	2.04	3.26	0.19	14.0	2.82	0.40	1.26	0.55	29.5
A	SAC 01	0.77	0.22	3.77	40.1	0.32	1.10	0.93	0.11	1.47	0.65	0.18	1.36		49.0
A	SAC 02	0.85	0.28	3.03	37.3	0.28	0.73	1.19	0.11	1.56	1.08	0.36	2.27		51.0
CS	IVDJ-S SN	0.67	0.40	2.07	36.9		1.23	1.51	0.20	3.39	0.86	0.08	0.37		52.3
A	IVDJ-S 3584	1.33	1.22	4.22	43.2		1.51	5.00	0.24	2.76	1.73	0.12			38.7
CS	IVDJ-S 3774	0.78	0.65	2.74	38.6		1.38	2.85	0.11	3.18	1.03			0.18	48.5
CS	IVDJ-S 3794	0.76	0.46	1.88	40.5	0.19	0.85	2.17	0.16	2.11	0.94		1.30		48.6
CS	IVDJ-S 3919	0.63	0.49	1.52	35.0	0.35	0.77	1.34	0.13	2.48	1.09		1.00		55.2
CS	IVDJ-S 4127	1.86	0.26	1.82	41.5	0.23	1.11	1.03	0.15	5.14	0.48		0.60	0.16	45.7
A	CPS01	2.41	0.47	2.37	39.8	0.50	1.79	1.85	0.11	1.99	0.97		3.34	0.13	44.3
A	CPS04	1.25	0.91	3.79	36.6	0.27	1.65	3.72	0.20	1.62	1.36	0.13	0.82		47.7
A	CPS05	1.72	0.51	2.56	39.4	0.32	2.92	2.74	0.16	1.91	0.94		1.19		45.6
F Un	MCV 1-1R	1.47	0.36	2.37	40.5	0.75	4.39	2.05	0.13	3.74	0.68		4.73		38.8
A	MCV 4-1ML	1.22	0.59	2.32	39.9	0.24	2.85	2.80	0.11	2.35	2.17	0.33	1.07		44.0
F Un	MCV 8.1G	2.42	0.43	1.57	42.1	0.88	4.43	1.99	0.06	2.73	0.51		4.58		38.3
F	MCV 10-2	1.06	0.48	3.56	51.1	0.21	6.30	2.31		2.04	0.49		8.44		24.0

Table V.1. REE and trace elements in white glazes measured by LA-ICP-MS. Results presented in µg/g.

	Li	B	P	Ti	V	Cr	Mn	Co	Ni	Cu	Zn	Ga	As	Rb	Sr	Y	Zr	Nb	Mo	Ag	Cd	In	Sb
IVDJ-T 133	81.5	25.2	191	491	7.3	4.0	77.8	7.8	23.7	552	64.6	5.0	168	81.2	51.8	2.7	14.9	1.7	0.4	10.6	0.7	214	1004
IVDJ-T 3683	99.5	20.5	188	444	7.5		55.4	3.9	17.9	119	80.6	4.4	627	44.8	85.9	3.5	28.8	1.7	2.3	16.2	0.4	149	50.4
IVDJ-T 4095	44.0	10.6	35.0	397	4.2		56.6	4.2	13.3	1944	36.9	2.2	56.1	53.9	60.8	1.6	24.0	1.1	0.9	33.2	0.6	189	241
IVDJ-S 3576	79.1	31.2	324	1414	67.3	10.6	181	6.3	23.8	196	58.7	3.1	16.6	104	145	4.2	61.8	3.0	10.3	3.1	0.5	136	318
IVDJ-S 3584	65.2	29.1	205	903	12.8	2.9	194	4.8	25.0	1343	62.7	2.5	27.5	60.3	95.2	6.4	44.1	2.3	0.3	9.8	0.6	132	113
IVDJ-S 3591	54.4	25.5	274	765	12.5	3.1	256	15.1	33.3	830	33.8	2.6	37.9	74.4	84.8	4.8	53.3	2.2	3.3	9.0	0.5	162	438
IVDJ-S 3718	93.4	20.5	79.4	947	9.4		239	10.8	24.3	575	65.3	5.9	54.9	114	94.4	4.3	47.7	3.0	0.1	13.0	0.7	216	246
IVDJ-S 3774	58.4	36.1	575	967	12.0	6.1	1918	10.6	30.1	555	89.7	2.9	42.7	71.1	98.1	5.7	79.9	2.7	2.4	8.9	0.5	162	245
IVDJ-S 3794	46.1	35.3	680	652	12.4	5.5	322	7.3	27.5	1288	122	2.2	13.5	22.2	72.6	4.3	39.9	1.8	0.4	110.5	0.3	223	321
IVDJ-S 3919	39.8	18.5	153	458	8.8	2.4	74.0	3.6	19.6	668	48.0	1.3	18.5	24.0	51.1	2.5	50.0	1.5	0.3	33.7	0.5	159	78.3
IVDJ-S 3601	90.8	23.3	331	1087	18.0	6.3	124	66.9	46.2	978	80.1	4.7	813	56.3	77.9	8.7	65.6	3.4	1.5	18.3	1.2	208	347
IVDJ-S 4106	25.4	27.0	311	791	12.2	9.3	90.2	7.7	18.2	778	63.7	3.0	21.4	57.9	50.3	4.7	76.5	2.4	0.9	31.9	0.4	111	192
IVDJ-S 4106	47.3	25.2	195	857	13.7	3.4	190	18.8	22.3	736	61.4	3.0	21.6	122	70.8	4.3	62.0	2.6	0.8	13.6	0.5	134	184
IVDJ-S 4107	49.7	35.8	240	976	11.1	1.8	116	13.6	36.5	833	76.9	2.3	11.4	70.2	85.2	4.5	67.6	2.4	0.9	16.3	0.3	138	213
IVDJ-S 4127	34.1	49.6	668	1110	10.1	7.0	66.1	13.6	22.7	721	157	2.4	29.3	62.0	42.5	5.5	46.6	2.7	1.3	46.6	0.6	207	125
IVDJ-S 4134	89.1	36.6	389	956	13.4	10.1	153	17.1	35.8	448	43.1	2.5	28.5	117	128	4.3	79.4	2.7	0.7	3.3	0.7	219	171
IVDJ-S 4185	151	39.3	552	998	16.6	11.0	170	12.1	82.8	551	78.1	3.1	50.8	70.9	125	5.9	145	2.8	0.5	3.2	1.6	209	211
IVDJ-S SN	38.2	41.7	871	1173	11.1	7.4	105	6.4	20.0	997	61.8	3.2	8.8	99.9	47.3	5.9	116	3.3	0.5	53.3	0.5	162	141
PNS04	45.7	38.7	290	854	9.3	6.8	112	7.9	27.5	551	42.0	2.2	23.3	117	54.9	6.3	57.9	2.4	1.0	34.6	0.7	207	193
PNS05	62.1	29.3	252	910	11.2	4.4	165	5.4	25.2	720	38.2	2.7	21.9	106	89.7	4.8	58.1	2.5	0.9	9.9	0.9	168	192
PNS06	46.2	39.7	458	959	9.4	9.6	107	7.6	26.8	627	42.8	2.3	23.6	118	49.0	4.2	72.5	2.6	1.0	29.9	0.6	186	206
PNS07	56.2	19.9	25.3	884	9.7	6.5	123	4.4	23.6	1098	26.9	2.1	17.6	117	68.2	5.2	110	2.4	0.3	12.8	0.5	174	215
PNS08	51.6	18.4	263	639	67.9	5.1	101	5.2	20.6	1652	21.2	1.9	63.2	144	62.1	3.4	48.6	1.6	0.2	32.2	0.6	198	480
PNS09	33.5	14.6	13.2	544	5.2	2.3	760	18.6	25.2	1810	13.4	2.7	8.2	73.9	42.2	3.7	48.7	1.5	0.4	90.8	0.6	168	150
PNS10	46.3	18.7	252	592	73.1	4.9	112	3.7	21.3	1408	22.7	2.0	61.5	105	48.8	3.1	46.1	1.6	0.1	44.8	0.8	225	471
PNS11	32.9	44.8	210	385	4.3	3.2	65.4	3.3	17.7	1057	54.7	1.0	8.4	74.1	51.8	1.6	33.9	1.0	2.0	115	0.6	272	266
PNS12	53.5	24.5	183	768	8.5	5.7	90.5	8.7	21.7	475	73.2	1.9	39.4	105	55.6	3.8	54.7	2.1	0.6	23.1	0.6	169	308

Table V.1. (cont.) REE and trace elements in white glazes measured by LA-ICP-MS. Results presented in µg/g.

	Li	B	P	Ti	V	Cr	Mn	Co	Ni	Cu	Zn	Ga	As	Rb	Sr	Y	Zr	Nb	Mo	Ag	Cd	In	Sb
PNS13	43.1	42.7	92.8	514	4.6	0.3	197	2.0	12.1	163	33.4	1.7	4.9	211	43.4	2.5	15.3	2.7	0.2	19.8	0.6	150	33.5
PNS15	70.1	41.9	574	1106	17.1	7.7	165	18.8	32.5	2551	66.9	3.1	18.1	73.5	109	5.4	86.8	3.3	0.8	6.6	1.0	176	191
PNS17	41.0	24.2	341	254	4.0	1.5	282	8.6	16.8	1136	92.0	1.0	6.5	109	63.4	1.6	8.9	1.9	0.6	21.5	0.7	210	1189
PNS19	39.9	37.0	342	936	12.5	7.2	103	4.5	19.8	435	25.5	2.8	15.2	70.6	65.1	4.8	82.5	2.7	1.6	9.0	0.4	150	84.4
PNS20	37.8	21.0	108	747	9.9		125	8.6	27.3	2202	23.1	2.4	27.4	63.0	59.7	4.0	47.0	2.1	2.1	16.3	0.4	142	156
PNS21	56.4	29.8	299	1522	18.3	9.1	163	5.7	24.9	436	44.8	3.6	89.9	83.5	104	5.1	102.0	3.8	0.6	6.9	0.6	218	598
PNS22	38.6	26.6	320	1132	19.3	8.7	257	35.3	39.1	593	52.7	4.3	130	44.2	78.5	6.6	66.0	3.3	1.4	4.3	0.4	110	316
PNS23	53.2	79.6	647	911	11.1	9.4	260	8.2	25.3	451	164	2.5	25.4	124	76.4	7.3	78.1	2.7	1.1	6.1	0.5	178	130
PNS24	30.7	28.0	176	968	10.2	6.3	116	7.9	21.4	120	21.3	2.1	8.3	94.2	53.9	4.4	54.5	2.6	0.6	6.2	0.4	197	185
PNS25	57.6	31.0	405	962	16.1	6.3	217	5.3	15.3	183	45.5	3.5	24.7	92.1	91.8	5.3	67.0	2.8	0.7	3.4	0.9	135	50.1
PNS26	60.7	48.4	354	1006	16.3	6.8	161	9.9	18.2	258	99.4	3.8	78.7	83.3	95.7	5.3	65.4	2.9	1.0	2.0	0.5	136	105
PNS27	24.6	80.4	824	838	9.1	3.4	116	12.3	39.0	884	24.2	2.4	34.4	81.3	45.7	4.5	73.7	2.2	0.4	61.1	0.7	221	483
PNS28	70.3	42.5	382	1025	14.8	11.8	248	17.4	27.9	1421	44.5	3.0	28.1	151	96.4	5.1	75.2	2.9	3.9	6.6	0.9	156	132
PNS29	37.0	21.7	177	977	12.8	8.0	122	5.5	13.9	203	32.8	3.0	67.0	71.4	65.0	4.9	53.6	2.8	0.1	4.4	0.6	130	123
PNS31	72.0	17.2	118	898	10.6	3.6	142	3.9	28.1	498	19.1	2.0	362	126	84.1	4.4	86.4	2.5	0.1	21.7	0.6	175	668
PNS32	37.5	19.7	126	885	7.1	3.3	66	4.1	21.1	476	21.0	1.8	15.3	117	47.0	4.3	118	2.4	1.3	60.0	0.4	192	305
PNS34	65.4	37.4	217	1014	14.1	10.4	143	6.7	32.0	1660	55.7	3.0	33.0	72.5	131	5.7	88.9	3.0	0.9	35.1	0.3	252	808
PNS35	88.6	40.1	352	838	13.9	3.6	146	6.5	29.1	1801	36.7	2.6	14.3	127	138	4.0	82.0	2.3	0.6	12.1	0.7	178	205
PNS36	37.5	18.0	192	720	7.1	3.1	82.3	3.2	22.2	557	21.0	1.9	41.7	72.2	38.6	3.6	61.2	2.0	0.2	13.9	0.4	146	456
PNS38	48.6	26.6	343	1067	11.3	2.1	87.7	4.4	18.1	439	27.7	2.4	17.8	89.8	80.3	4.9	88.8	4.3	0.4	17.9	0.3	155	215
PNS39	47.2	19.3	328	690	59.0		72.8	6.3	23.6	1128	23.2	1.7	71.7	123	48.0	3.6	51.5	1.9	0.3	34.9	0.6	169	494
MCV 2-1T	86.0	25.4	74.8	476	6.9	4.0	72.9	73.7	39.5	577	25.5	2.1	177	282	56.7	3.3	18.5	1.4	4.9	4.2	0.8	107	126
MCV 3-1R	146	33.4	105	464	7.4	3.9	120	28.8	29.1	168	338	3.1	59.3	205	99.5	3.0	20.6	1.5	0.6	1.4	0.6	100	99.5
MCV 4-1ML	100	27.8	283	853	12.8	9.1	319	12.3	24.9	1273	70.1	2.9	9.9	110	111	4.2	66.5	2.5	0.3	4.3	0.9	176	122
MCV 4-2G	77.4	15.6	92.5	546	6.9	2.5	80.3	32.5	23.4	393	118	2.3	13.6	130	47.8	3.2	16.5	1.7	3.7	8.9	0.5	84.1	153
MCV 5-1R	59.1	26.7	245	299	6.1	5.5	141	50.5	30.2	1223	56.4	2.4	139	190	69.3	2.4	13.7	1.0	2.6	32.9	0.6	117	98.6
MCV 6-1C	94.0	22.0	315	372	4.6	6.6	63.8	3.9	17.4	194	64.1	2.3	74.4	232	68.4	2.2	8.6	1.5	0.1	10.7	0.4	240	197
MCV 7-1C	76.3	35.9	364	429	5.6	6.4	65.9	4.6	16.5	549	70.5	3.0	171	180	95.6	4.6	22.1	1.4	0.3	7.8	0.2	114	99.5
MCV 8-1G	137	25.0	84.3	681	7.7	4.6	67.0	11.2	19.5	223	64.0	2.3	33.9	237	52.8	2.8	18.8	1.8	0.6	15.0	0.7	106	542

Table V.1. (cont.) REE and trace elements in white glazes measured by LA-ICP-MS. Results presented in µg/g.

	Li	B	P	Ti	V	Cr	Mn	Co	Ni	Cu	Zn	Ga	As	Rb	Sr	Y	Zr	Nb	Mo	Ag	Cd	In	Sb
SAC 01	35.3	23.9	152	651	6.9	4.1	88.1	8.0	14.2	471	51.9	3.6	96.9	19.5	94.6	4.0	96.0	1.6	0.5	15.1	0.3	139	102
SAC 02	62.0	25.6	228	295	5.9	1.5	124	4.2	16.8	1200	79.3	2.6	46.7	24.9	39.2	1.9	19.3	1.1	0.2	29.6	0.7	233	119
SCV 8I7532	53.9	28.7	300	1031	13.0	9.7	130	5.9	30.5	586	44.6	3.9	13.9	85.3	64.1	5.9	67.4	2.9	0.9	8.0	0.5	123	295
SCV 10IF175	68.4	31.8	272	1035	16.3	9.7	415	54.6	49.6	4306	45.5	3.3	28.5	84.3	104	5.6	72.2	3.7	3.3	6.0	0.5	155	337
SCV 10BI1673	96.6	29.2	165	1002	16.0	10.6	163	28.4	31.0	1405	50.0	3.3	22.9	106	127	5.1	74.6	2.8	2.0	5.7	0.7	167	114
SCV 20I2989	44.7	28.8	203	761	10.1	4.4	114	5.8	31.8	415	31.8	2.8	19.2	66.5	58.2	3.9	45.2	2.1	0.7	5.2	0.4	167	126
SCV 21AM3076	63.6	30.9	313	962	12.8	10.5	113	5.9	22.8	1298	41.7	4.7	10.5	96.7	59.5	5.9	59.1	2.8	0.9	6.7	0.4	108	265
SCV 30F7756	72.5	32.7	360	816	14.1	9.8	248	7.9	23.6	527	41.8	2.9	10.8	140	101	3.9	59.8	2.3	0.4	5.5	0.9	172	152
SCV 32M3685	75.0	21.7	113	813	8.9	5.1	125	10.2	30.3	896	22.6	2.3	7.6	147	86.4	4.2	80.9	2.3	0.9	4.9	0.6	175	375
SCV 33BI3839	56.4	19.7	162	795	9.2	6.1	1741	106	69.9	277	23.9	2.6	806	99.1	68.8	3.7	64.2	2.1	5.8	3.4	0.4	174	219
SCV 45M4260	50.9	26.0	99.2	813	11.8	9.9	114	7.9	29.2	537	26.2	2.9	13.2	101	84.4	4.4	60.0	2.3	1.4	6.9	0.5	194	66.6
SCV 80F4745	68.1	31.7	577	904	13.8	11.2	287	5.8	19.5	289	61.1	3.1	84.8	100	82.1	4.9	49.1	2.6	1.2	6.9	0.5	124	303
SCV SPF8435	116	25.8	151	286	2.8	1.5	36.4	9.0	12.8	213	74.2	2.9	57.3	246	26.2	3.9	12.1	1.6	0.0	2.6	0.9	188	152

Table V.1. (cont.) REE and trace elements in white glazes measured by LA-ICP-MS. Results presented in µg/g.

	Cs	Ba	La	Ce	Pr	Nd	Sm	Eu	Gd	Tb	Dy	Ho	Er	Tm	Yb	Lu	Hf	Ta	W	Bi	Th	U
IVDJ-T 133	4.4	172	11.4	25.6	2.8	10.9	1.8	0.3	1.1	0.2	0.7	0.1	0.3	0.0	0.3	0.0	0.4	0.2	54.7	61.2	4.1	0.6
IVDJ-T 3683	1.2	148	9.7	19.1	1.8	6.8	1.1	0.3	1.5	0.2	0.8	0.1	0.5	0.1	0.4	0.1	0.8	0.1	0.8	222	3.4	0.6
IVDJ-T 4095	2.5	145	4.7	9.2	1.0	4.0	0.7	0.2	0.8	0.1	0.4	0.1	0.2	0.0	0.2	0.0	0.6	0.1	3.2	108	1.9	0.4
IVDJ-S 3576	5.6	131	6.8	12.1	1.4	5.4	1.1	0.2	1.1	0.2	0.9	0.2	0.5	0.1	0.5	0.1	1.8	0.3	2.3	11.3	2.2	0.6
IVDJ-S 3584	3.3	109	6.5	11.7	1.3	5.1	1.0	0.2	1.0	0.2	1.2	0.3	0.7	0.1	0.6	0.1	1.1	0.1	0.4	9.3	1.7	0.5
IVDJ-S 3591	3.6	114	6.7	12.5	1.4	5.7	1.0	0.3	1.0	0.2	0.9	0.2	0.6	0.1	0.5	0.1	1.4	0.1	1.4	11.8	1.9	0.4
IVDJ-S 3718	5.3	262	11.1	24.9	2.9	11.0	1.7	0.4	2.0	0.3	0.9	0.2	0.6	0.1	0.4	0.1	1.2	0.3	3.6	11.7	3.6	0.9
IVDJ-S 3774	4.3	187	8.1	14.5	1.6	6.2	1.2	0.2	0.8	0.2	1.0	0.2	0.6	0.1	0.5	0.1	1.9	0.2	2.6	5.5	2.2	0.6
IVDJ-S 3794	0.9	100	6.0	9.3	1.3	5.4	1.0	0.3	0.9	0.2	0.7	0.2	0.5	0.1	0.4	0.1	1.0	0.1	7.0	26.1	1.5	0.5
IVDJ-S 3919	0.8	73.6	4.3	8.2	0.9	3.5	0.6	0.2	0.5	0.1	0.5	0.1	0.3	0.0	0.3	0.1	1.2	0.1	9.9	6.4	1.2	0.4

Table V.1. (cont.) REE and trace elements in white glazes measured by LA-ICP-MS. Results presented in µg/g.

	Cs	Ba	La	Ce	Pr	Nd	Sm	Eu	Gd	Tb	Dy	Ho	Er	Tm	Yb	Lu	Hf	Ta	W	Bi	Th	U
IVDJ-S 3601	2.5	139	10.9	21.9	2.4	9.4	1.7	0.3	1.7	0.4	1.8	0.3	1.0	0.1	0.8	0.1	1.9	0.2	3.9	376	4.3	0.8
IVDJ-S 4106	3.1	86.1	6.7	12.4	1.3	5.3	1.0	0.2	0.7	0.2	0.9	0.2	0.5	0.1	0.6	0.1	1.9	0.2	0.6	46.6	2.3	0.6
IVDJ-S 4106	6.9	104	6.6	12.2	1.4	5.4	1.0	0.2	1.1	0.2	0.8	0.2	0.6	0.1	0.5	0.1	1.7	0.2	0.8	55.4	1.9	0.5
IVDJ-S 4107	3.3	111	6.8	12.6	1.4	5.6	1.0	0.2	1.1	0.2	0.8	0.1	0.6	0.1	0.6	0.1	1.8	0.2	0.8	6.9	2.0	0.5
IVDJ-S 4127	2.9	100	7.5	13.9	1.5	5.9	1.1	0.2	0.9	0.2	1.0	0.2	0.6	0.1	0.5	0.1	1.2	0.2	1.0	46.3	2.4	0.5
IVDJ-S 4134	5.4	165	7.9	13.6	1.6	5.9	1.1	0.2	1.0	0.2	0.7	0.2	0.5	0.1	0.5	0.1	1.9	0.2	0.4	5.2	2.1	0.6
IVDJ-S 4185	3.4	132	9.4	16.5	1.9	7.2	1.3	0.3	1.2	0.2	1.1	0.2	0.7	0.1	0.7	0.1	2.9	0.2	0.6	21.4	2.6	0.7
IVDJ-S SN	4.7	95.7	9.5	18.5	2.0	7.5	1.4	0.2	1.0	0.2	1.1	0.2	0.6	0.1	0.7	0.1	2.8	0.2	0.7	4.9	2.9	0.7
PNS04	4.3	104	6.1	12.2	1.3	5.0	1.0	0.3	1.3	0.3	1.2	0.2	0.8	0.1	0.6	0.1	1.5	0.2	35.5	39.0	2.3	0.5
PNS05	6.0	138	7.4	13.8	1.5	6.0	1.1	0.4	1.4	0.3	0.9	0.2	0.7	0.1	0.6	0.1	1.6	0.2	83.1	36.0	2.0	0.5
PNS06	4.3	100	6.0	11.6	1.2	5.0	0.9	0.3	1.2	0.2	0.8	0.2	0.6	0.1	0.5	0.1	2.0	0.2	38.5	36.6	1.7	0.5
PNS07	5.2	97.1	7.1	13.4	1.5	6.0	1.2	0.3	1.6	0.3	1.0	0.2	0.8	0.1	0.7	0.1	3.0	0.2	0.4	43.9	2.3	0.6
PNS08	4.7	93.9	4.8	8.7	1.0	4.1	0.8	0.2	1.1	0.2	0.7	0.1	0.5	0.0	0.4	0.1	1.3	0.1	4.4	64.9	1.3	0.4
PNS09	3.4	114	18.3	35.3	4.0	15.6	2.9	0.3	4.3	0.6	0.9	0.1	0.9	0.1	0.4	0.1	1.3	0.1	0.7	9.4	5.9	1.5
PNS10	4.4	85.3	4.0	7.5	0.9	3.5	0.7	0.2	0.9	0.2	0.6	0.1	0.4	0.0	0.4	0.1	1.3	0.1	4.3	64.7	1.3	0.3
PNS11	3.2	56.4	2.6	4.6	0.5	2.1	0.4	0.1	0.5	0.1	0.3	0.1	0.3	0.0	0.2	0.0	1.0	0.1	5.5	20.0	0.7	0.2
PNS12	4.3	85.4	5.5	10.3	1.1	4.4	0.8	0.2	1.0	0.2	0.7	0.1	0.5	0.1	0.5	0.1	1.5	0.1	1.9	19.8	1.5	0.4
PNS13	15.7	56.7	3.3	5.5	0.7	2.9	0.6	0.1	0.8	0.1	0.5	0.1	0.3	0.0	0.3	0.0	0.4	0.2	0.4	10.1	1.1	0.3
PNS15	3.9	125	9.1	16.7	1.8	7.1	1.4	0.4	1.8	0.3	1.1	0.2	0.8	0.1	0.6	0.1	2.2	0.2	1.3	64.9	2.2	0.6
PNS17	15.6	156	2.8	4.1	0.6	2.3	0.5	0.2	0.6	0.1	0.3	0.1	0.2	0.0	0.2	0.0	0.3	0.2	0.2	15.3	0.7	0.2
PNS19	3.1	97.6	7.4	13.9	1.5	5.9	1.1	0.3	1.3	0.3	0.9	0.2	0.6	0.1	0.6	0.1	2.1	0.2	0.9	11.7	2.1	0.6
PNS20	3.1	87.6	5.8	10.5	1.2	4.6	0.9	0.2	0.8	0.2	0.7	0.1	0.5	0.0	0.4	0.1	1.2	0.1	6.4	63.7	1.8	0.4
PNS21	4.9	118	9.6	17.7	2.0	7.8	1.3	0.3	1.4	0.3	1.0	0.2	0.7	0.1	0.6	0.1	2.9	0.3	2.4	8.4	2.7	0.6
PNS22	2.5	120	13.8	24.5	2.6	9.4	1.7	0.4	1.9	0.3	1.2	0.2	0.9	0.1	0.7	0.1	1.7	0.2	60.2	2473	3.3	0.7
PNS23	5.1	126	7.2	13.2	1.4	5.7	1.2	0.3	1.2	0.3	1.3	0.3	0.9	0.1	0.7	0.1	2.0	0.2	1.0	11.3	2.1	0.5
PNS24	3.3	72.2	6.6	11.8	1.3	5.3	1.0	0.2	0.9	0.2	0.7	0.2	0.5	0.1	0.4	0.1	1.4	0.2	1.0	5.2	1.9	0.5
PNS25	3.3	140	8.2	14.7	1.6	6.3	1.2	0.3	1.1	0.2	0.9	0.2	0.6	0.1	0.5	0.1	1.5	0.2	1.1	40.7	2.5	0.7
PNS26	3.8	136	8.6	15.6	1.7	7.1	1.2	0.3	1.3	0.3	1.0	0.2	0.7	0.1	0.6	0.1	1.7	0.2	2.1	57.8	2.5	0.6

Table V.1. (cont.) REE and trace elements in white glazes measured by LA-ICP-MS. Results presented in µg/g.

	Cs	Ba	La	Ce	Pr	Nd	Sm	Eu	Gd	Tb	Dy	Ho	Er	Tm	Yb	Lu	Hf	Ta	W	Bi	Th	U
PNS27	4.2	71.3	6.8	12.7	1.3	5.3	1.0	0.2	0.9	0.2	0.8	0.2	0.5	0.1	0.5	0.1	1.8	0.2	0.4	57.2	3.0	0.5
PNS28	6.7	135	7.6	14.2	1.6	6.2	1.2	0.3	1.1	0.2	0.9	0.2	0.7	0.1	0.6	0.1	1.9	0.2	1.0	9.4	2.3	0.6
PNS29	2.7	112	7.3	14.2	1.6	6.1	1.2	0.3	1.1	0.2	0.9	0.2	0.6	0.1	0.5	0.1	1.3	0.2	2.2	27.1	2.5	0.6
PNS31	6.3	128	7.3	13.2	1.5	5.7	1.0	0.2	0.9	0.2	0.8	0.2	0.5	0.1	0.5	0.1	2.1	0.2	7.8	20.0	2.1	0.5
PNS32	4.1	75.3	6.9	13.0	1.3	5.4	1.0	0.2	0.9	0.2	0.7	0.2	0.6	0.1	0.5	0.1	3.0	0.2	3.5	60.5	2.2	0.5
PNS34	3.3	120	8.7	16.3	1.7	6.8	1.2	0.3	1.2	0.2	0.9	0.2	0.7	0.1	0.6	0.1	2.2	0.2	4.2	24.8	2.4	0.6
PNS35	6.1	271	6.9	12.5	1.3	5.3	1.0	0.3	0.8	0.2	0.7	0.1	0.5	0.1	0.5	0.1	1.9	0.1	1.2	30.3	1.9	0.5
PNS36	2.2	92.7	5.4	10.3	1.1	4.3	0.8	0.2	0.6	0.1	0.7	0.1	0.4	0.1	0.4	0.1	1.5	0.1	12.0	12.6	1.7	0.4
PNS38	3.5	111	7.4	13.9	1.5	5.6	0.9	0.2	0.9	0.2	0.9	0.2	0.5	0.1	0.6	0.1	2.1	0.2	0.8	45.0	2.2	0.5
PNS39	4.0	87.2	5.1	9.3	1.0	4.0	0.8	0.2	0.6	0.1	0.6	0.1	0.4	0.0	0.4	0.0	1.3	0.1	4.9	60.3	1.5	0.6
MCV 2-1T	30.3	113	6.0	10.4	1.2	4.6	0.9	0.2	0.7	0.1	0.6	0.1	0.3	0.0	0.3	0.0	0.5	0.1	3.5	17.6	1.6	0.5
MCV 3-1R	15.4	165	7.1	13.3	1.4	5.2	1.0	0.2	0.8	0.1	0.6	0.1	0.3	0.0	0.3	0.0	0.6	0.1	9.0	39.0	1.7	0.6
MCV 4-1ML	5.8	127	8.1	17.3	1.5	6.3	1.1	0.2	0.9	0.2	0.8	0.2	0.5	0.1	0.5	0.1	1.7	0.2	0.6	4.3	2.0	0.5
MCV 4-2G	11.3	108	7.2	12.5	1.5	5.9	1.1	0.2	0.8	0.2	0.7	0.1	0.4	0.0	0.3	0.0	0.5	0.1	2.4	4.7	1.6	0.5
MCV 5-1R	16.2	112	5.3	9.5	1.1	4.6	0.9	0.2	0.8	0.1	0.5	0.1	0.3	0.0	0.3	0.0	0.5	0.1	0.9	107	1.3	0.5
MCV 6-1C	19.3	154	5.5	8.5	1.0	3.8	0.7	0.2	0.7	0.1	0.4	0.1	0.3	0.0	0.2	0.0	0.2	0.3	0.6	9.3	1.0	0.5
MCV 7-1C	17.2	165	7.5	13.5	1.6	6.1	1.3	0.3	1.1	0.2	0.9	0.2	0.5	0.1	0.5	0.1	0.6	0.2	0.5	30.9	1.8	0.8
MCV 8-1G	19.3	121	6.3	11.3	1.3	5.2	0.9	0.2	0.8	0.1	0.6	0.1	0.4	0.0	0.3	0.0	0.5	0.2	0.5	4.8	1.8	0.6
SAC 01	0.7	55.0	9.9	18.2	2.0	7.3	1.2	0.3	1.3	0.2	0.8	0.2	0.5	0.1	0.5	0.1	2.3	0.2	25.8	30.0	2.0	0.5
SAC 02	0.9	52.7	5.7	10.7	1.1	3.9	0.7	0.2	0.7	0.1	0.4	0.1	0.3	0.0	0.2	0.0	0.6	0.1	121	23.3	1.4	0.4
SCV 8I7532	3.2	95.1	11.6	21.4	2.5	10.1	1.8	0.3	1.9	0.3	1.3	0.2	0.7	0.1	0.7	0.1	1.8	0.2	0.4	25.3	2.5	0.7
SCV 10IF175	3.6	121	7.6	13.7	1.6	6.5	1.4	0.3	1.3	0.2	1.1	0.2	0.7	0.1	0.7	0.1	2.0	0.3	1.4	15.6	2.4	0.6
SCV 10BI1673	5.1	135	7.5	13.7	1.5	6.0	1.1	0.2	1.1	0.2	0.9	0.2	0.6	0.1	0.6	0.1	2.1	0.2	18.4	31.3	2.4	0.7
SCV 20I2989	2.0	88.5	5.5	9.9	1.2	4.8	1.0	0.5	1.0	0.2	0.7	0.1	0.5	0.1	0.4	0.1	1.2	0.1	1.7	7.3	1.8	0.5
SCV 21AM3076	3.7	89.1	16.2	36.2	4.0	16.2	2.9	1.4	2.1	0.3	1.2	0.2	0.7	0.1	0.7	0.1	1.6	0.2	0.6	8.8	3.1	0.7
SCV 30F7756	7.2	138	6.7	12.5	1.4	5.3	1.0	0.2	0.8	0.1	0.7	0.1	0.5	0.1	0.4	0.1	1.6	0.2	8.3	6.6	2.0	0.4
SCV 32M3685	6.7	116	6.6	12.3	1.4	5.5	1.0	0.2	0.9	0.2	0.8	0.2	0.5	0.1	0.5	0.1	2.2	0.1	0.4	15.9	2.2	0.5
SCV 33BI3839	4.7	191	5. 6	10.0	1.1	4.4	0.8	0.9	0.5	0.1	0.7	0.1	0.4	0.1	0.4	0.1	1.6	0.1	3.8	19.2	1.8	0.4

Table V.1. (cont.) REE and trace elements in white glazes measured by LA-ICP-MS. Results presented in µg/g.

	Cs	Ba	La	Ce	Pr	Nd	Sm	Eu	Gd	Tb	Dy	Ho	Er	Tm	Yb	Lu	Hf	Ta	W	Bi	Th	U
SCV 45M4260	*4.3*	*93.9*	*6.2*	*11.6*	*1.3*	*5.5*	*1.1*	*0.3*	*1.2*	*0.2*	*0.8*	*0.2*	*0.5*	*0.1*	*0.5*	*0.1*	*1.7*	*0.2*	*0.8*	*39.9*	*1.9*	*0.5*
SCV 80F4745	*4.1*	*106*	*7.0*	*12.7*	*1.4*	*5.7*	*1.1*	*0.3*	*1.0*	*0.2*	*0.9*	*0.2*	*0.6*	*0.1*	*0.5*	*0.1*	*1.3*	*0.2*	*20.1*	*52.4*	*2.3*	*0.5*
SCV SPF8435	*47.2*	*52.6*	*3.7*	*7.5*	*0.8*	*3.7*	*1.0*	*0.3*	*0.8*	*0.2*	*0.9*	*0.2*	*0.4*	*0.0*	*0.3*	*0.0*	*0.4*	*0.2*	*0.5*	*34.2*	*1.9*	*0.7*

Table V.2. REE and trace elements in blue glazes measured by LA-ICP-MS. Results presented in µg/g.

	Li	B	P	Ti	V	Cr	Mn	Fe	Co	Ni	Cu	Zn	Ga	As	Rb	Sr	Y	Zr	Nb	Mo	Ag	Cd	In	Sb
IVDJ-T 96	*90.2*	*32.5*	*453*	*558*	*12.5*		*163*	*8051*	*4861*	*721*	*801*	*62.5*	*5.1*	*4125*	*140*	*151*	*3.8*	*18.6*	*1.7*	*85.4*	*40.4*	*0.7*	*141*	*291*
IVDJ-T 133	*54.0*	*21.2*	*252*	*670*	*11.5*	*6.4*	*90.9*	*6514*	*2680*	*1652*	*423*	*74.6*	*4.4*	*3835*	*54.3*	*63.4*	*6.4*	*97.1*	*2.2*	*14.2*	*16.4*	*0.5*	*87.1*	*615*
IVDJ-T 3683	*124*	*43.0*	*62.2*	*749*	*16.8*		*1357*	*10345*	*2424*	*991*	*4032*	*994*	*6.5*	*1917*	*62.5*	*150*	*4.1*	*38.8*	*2.7*	*31.8*	*19.6*	*0.4*	*111*	*91.2*
IVDJ-T 4095	*58.5*	*50.2*	*581*	*659*	*12.9*		*147*	*12218*	*2695*	*1568*	*2647*	*33.8*	*6.0*	*42.8*	*65.9*	*83.8*	*4.1*	*34.7*	*1.9*	*383*	*20.5*	*0.5*	*69.7*	*207*
IVDJ-S SN	*43.9*	*32.8*	*603*	*988*	*12.2*	*7.3*	*281*	*10236*	*1871*	*914*	*1305*	*94.7*	*3.4*	*223*	*94.9*	*56.3*	*4.5*	*90.2*	*2.7*	*73.8*	*39.4*	*0.6*	*204*	*522*
IVDJ-S 3561	*84.4*	*25.5*	*321*	*819*	*10.7*	*5.3*	*136*	*6462*	*4382*	*933*	*408*	*33.2*	*2.8*	*3165*	*118*	*61.3*	*4.7*	*75.7*	*2.3*	*48.1*	*3.0*	*0.7*	*183*	*50.9*
IVDJ-S 3576	*70.3*	*27.6*	*380*	*874*	*17.4*	*3.8*	*265*	*26256*	*4876*	*2158*	*2045*	*52.9*	*9.4*	*110*	*99.3*	*97.2*	*4.8*	*58.5*	*2.6*	*409*	*4.2*	*0.8*	*154*	*340*
IVDJ-S 3584	*59.0*	*29.6*	*413*	*1011*	*15.2*	*5.4*	*238*	*18028*	*4463*	*1786*	*1881*	*64.6*	*5.0*	*194*	*61.2*	*82.3*	*4.7*	*60.2*	*2.8*	*211*	*11.0*	*0.8*	*174*	*149*
IVDJ-S 3591	*41.6*	*24.2*	*305*	*928*	*15.0*	*52.8*	*287*	*19534*	*3027*	*1759*	*2477*	*32.8*	*5.4*	*142*	*72.3*	*73.2*	*3.9*	*51.8*	*2.8*	*269*	*12.3*	*0.6*	*191*	*949*
IVDJ-S 3601	*85.4*	*25.8*	*394*	*1042*	*17.1*	*2.5*	*147*	*9453*	*4716*	*1105*	*989*	*161*	*4.3*	*3408*	*59.9*	*65.9*	*10.9*	*43.4*	*3.5*	*36.0*	*18.0*	*1.5*	*200*	*347*
IVDJ-S 4098	*50.1*	*34.4*	*348*	*920*	*15.8*	*7.4*	*197*	*16292*	*2481*	*1214*	*1384*	*65.9*	*7.8*	*42.9*	*145*	*46.2*	*4.7*	*70.4*	*2.9*	*593*	*2.8*	*0.8*	*146*	*192*
IVDJ-S 4106	*34.8*	*16.6*	*180*	*747*	*14.6*	*1.1*	*236*	*14180*	*4726*	*1644*	*3173*	*42.2*	*4.7*	*154*	*102*	*60.1*	*3.8*	*66.7*	*2.2*	*177*	*27.2*	*0.5*	*134*	*197*
IVDJ-S 4107	*52.5*	*45.8*	*471*	*963*	*15.5*	*1.2*	*194*	*17545*	*4474*	*1161*	*1911*	*173*	*4.2*	*350*	*69.4*	*101*	*4.9*	*82.6*	*2.8*	*84.3*	*6.2*	*0.7*	*147*	*215*
IVDJ-S 4127	*26.8*	*24.8*	*412*	*737*	*8.6*	*0.4*	*126*	*12695*	*4903*	*2574*	*2508*	*66.2*	*3.1*	*314*	*49.2*	*36.8*	*4.0*	*77.7*	*2.2*	*127*	*114*	*0.5*	*182*	*478*
IVDJ-S 4134	*90.5*	*43.6*	*2621*	*986*	*20.4*	*5.1*	*318*	*17409*	*6831*	*1058*	*8353*	*87.8*	*5.7*	*108*	*148*	*122*	*5.8*	*91.1*	*3.0*	*272*	*3.4*	*0.8*	*131*	*132*
IVDJ-S 4185	*90.7*	*35.3*	*316*	*1024*	*15.4*	*17.8*	*250*	*14920*	*6342*	*3075*	*1063*	*100*	*3.5*	*57.4*	*65.9*	*199*	*4.6*	*76.3*	*3.1*	*55.0*	*2.0*	*0.7*	*297*	*242*
PNS01	*40.6*	*22.4*	*149*	*713*	*10.3*	*5.8*	*1073*	*14384*	*4314*	*2018*	*2736*	*30.3*	*4.9*	*432*	*77.4*	*68.7*	*3.9*	*76.3*	*2.1*	*212*	*43.6*	*0.8*	*172*	*582*
PNS06	*53.5*	*49.3*	*592*	*998*	*18.2*	*14.6*	*182*	*11457*	*2296*	*1192*	*2208*	*70.5*	*5.3*	*350*	*131*	*86.6*	*7.9*	*57.6*	*3.1*	*91.3*	*25.4*	*0.8*	*105*	*157*
PNS07	*83.0*	*24.9*	*246*	*914*	*13.1*	*8.7*	*2107*	*12850*	*3108*	*1869*	*3132*	*34.0*	*4.4*	*141*	*120*	*83.2*	*5.1*	*87.4*	*2.5*	*130*	*11.3*	*0.9*	*159*	*173*
PNS09	*62.4*	*27.8*	*131*	*643*	*11.9*	*6.2*	*486*	*13092*	*3885*	*1732*	*2383*	*36.1*	*4.8*	*139*	*94.4*	*98.4*	*3.2*	*45.7*	*1.9*	*192*	*33.3*	*1.1*	*182*	*227*
PNS11	*34.1*	*26.2*	*614*	*676*	*23.2*	*3.3*	*340*	*7595*	*2454*	*1357*	*1426*	*45.0*	*3.0*	*80.3*	*98.6*	*68.1*	*3.8*	*64.8*	*1.9*	*92.4*	*160*	*0.9*	*182*	*257*

Table V.2. (cont.) REE and trace elements in blue glazes measured by LA-ICP-MS. Results presented in µg/g.

	Li	B	P	Ti	V	Cr	Mn	Fe	Co	Ni	Cu	Zn	Ga	As	Rb	Sr	Y	Zr	Nb	Mo	Ag	Cd	In	Sb
PNS14	72.0	38.4	424	1071	19.7	12.2	298	19549	3625	1874	2616	182	6.5	168	67.5	139	5.3	69.6	2.9	205	6.7	0.6	167	173
PNS19	51.7	48.0	645	1015	16.9	11.1	326	11803	2412	1449	1349	41.9	5.6	84.9	98.5	78.5	6.1	84.7	3.1	90.2	7.1	0.5	159	69.8
PNS20	52.0	22.7	206	1679	15.7		224	14439	3165	1808	3623	42.0	4.5	169	70.1	78.2	5.0	95.9	5.0	135	13.6	0.7	186	116
PNS21	66.8	30.3	398	928	21.6	4.1	255	28773	4141	1702	2069	49.2	10.7	460	81.0	108	5.2	106	3.0	368	7.0	1.0	189	828
PNS22	32.5	19.5	57.3	896	11.1	3.9	206	7054	2742	695	584	60.1	2.8	3133	53.5	53.4	5.2	50.7	2.4	44.6	8.0	0.4	123	156
PNS23	58.9	39.0	297	935	15.7	8.7	223	16346	3418	1878	591	109	9.5	109	163	97.3	4.8	68.7	2.8	196	5.3	0.5	167	144
PNS24	32.5	30.5	407	880	17.1	4.8	133	22443	4587	1804	1496	31.2	9.7	230	115	55.8	4.2	47.4	2.8	303	5.6	0.6	144	183
PNS25	60.2	26.5	245	912	17.2	6.9	391	7446	2858	679	282	44.1	3.5	3352	86.1	86.9	4.8	33.9	2.6	39.3	2.8	1.2	85.7	44.8
PNS26	58.1	42.5	283	982	16.2	5.6	456	6599	1655	668	444	59.6	3.4	2415	85.5	84.9	5.2	83.2	3.1	44.8	2.2	0.5	215	129
PNS27	22.7	31.6	886	719	9.7	3.2	298	7956	3053	1808	2442	31.4	3.6	205	76.7	42.4	3.7	61.3	2.0	112	50.1	0.6	130	343
PNS29	36.7	30.4	164	1246	27.5	16.0	250	9287	3279	801	253	52.3	4.4	2900	70.3	105	6.9	47.8	4.4	43.7	3.4	1.2	184	138
PNS32	21.4	17.6	239	862	11.6	4.1	1148	15923	4525	2652	2599	31.1	5.0	205	53.8	34.1	4.8	117	2.4	225	64.8	0.3	179	338
PNS38	52.1	32.8	625	948	15.7	2.6	169	15584	3630	3404	1274	47.2	5.4	81.5	88.9	64.4	4.8	78.3	2.8	173	12.5	0.5	133	189
PNS39	31.4	17.2	179	785	14.4	2.1	118	9248	2321	1321	3454	23.5	3.5	120	58.5	48.2	3.3	56.8	2.3	130	28.9	0.6	221	241
MCV 2-1T	68.5	14.6	76	1169	4.1	3.6	891	2007	1473	485	618	31.1	2.1	156	306	48.7	2.6	17.4	2.0	43.9	4.7	0.7	148	117
MCV 3-1R	129	26.3	117	452	8.2	0.3	3320	2879	2976	1105	145	283	2.9	844	225	80.4	3.1	24.5	1.5	12.0	1.1	0.6	112	88.5
MCV 4-2G	85.8	19.0	145	451	10.4	2.6	989	12516	2356	950	614	65.6	4.4	96.1	166	57.0	2.9	16.3	1.7	176	8.5	0.6	84.0	158
MCV 5-1R	50.5	21.6	422	266	6.0	4.1	4501	3451	3972	1967	888	83.3	2.1	15168	132	157	2.0	14.7	1.3	663	51.9	1.2	83.2	78.7
MCV 8-1G	147	23.9	80	368	5.6	4.9	225	2079	1343	842	471	115	2.0	49.2	209	56.9	2.5	19.2	1.1	27.7	34.1	0.8	114	499
SAC 01	39.2	26.3	128	329	5.6	3.3	133	4026	1899	492	579	92.2	3.2	1808	24.6	44.3	2.3	15.8	1.1	14.7	18.8	0.4	224	128
SCV 4i365	97.9	36.1	325	888	16.2	10.4	302	17467	3101	1671	1212	45.5	6.8	568	102	111	4.5	77.6	2.5	135	3.2	0.5	179	249
SCV 8i7532	58.6	23.6	182	930	16.8	7.0	170	13803	2018	1153	1406	48.8	5.4	121	103	87.3	4.2	66.4	2.7	117	8.1	0.4	109	165
SCV 9i1469	94.6	39.7	213	933	15.2	8.7	208	14260	2623	1937	1660	96.9	5.3	65.5	74.4	115	4.4	65.5	2.6	143	4.1	0.7	178	89.3
SCV 10Bi1673	81.3	28.6	241	865	15.8	8.0	185	27493	3983	1689	1823	39.5	10.3	196	99.0	105	6.3	72.7	2.7	246	3.6	0.6	153	105
SCV 10EF175	74.8	27.0	186	792	13.4	6.9	202	19607	4350	2046	3727	35.7	8.1	89.7	103	84.3	4.5	57.7	2.5	228	6.7	0.6	142	373
SCV 20i2989	52.3	25.9	337	776	13.1	5.5	164	17104	4180	1800	2212	37.6	5.0	189	67.4	72.5	4.1	55.0	2.2	246	6.1	0.7	206	380
SCV 21AM3076	72.9	27.5	357	841	12.5	9.7	935	10875	2044	1594	1589	35.7	4.5	147	110	96.1	4.7	64.9	2.5	111	5.5	0.4	157	336
SCV 30F7756	68.0	24.6	312	908	19.6	12.6	451	22267	1887	801	1244	68.7	3.5	306	121	78.2	4.3	78.3	2.6	64.5	6.1	0.6	154	751

Table V.2. (cont.) REE and trace elements in blue glazes measured by LA-ICP-MS. Results presented in µg/g.

	Li	B	P	Ti	V	Cr	Mn	Fe	Co	Ni	Cu	Zn	Ga	As	Rb	Sr	Y	Zr	Nb	Mo	Ag	Cd	In	Sb
SCV 32M3685	*65.4*	*24.8*	*167*	*820*	*12.5*	*3.2*	*355*	*17778*	*2863*	*1498*	*2002*	*54.7*	*6.1*	*94.8*	*124*	*75.9*	*4.4*	*58.9*	*2.4*	*173*	*5.9*	*1.0*	*136*	*374*
SCV 33Bi3839	*75.4*	*29.7*	*242*	*921*	*13.7*	*7.8*	*396*	*19531*	*3465*	*1789*	*1335*	*29.1*	*7.6*	*789*	*122*	*82.6*	*4.7*	*61.0*	*2.8*	*185*	*4.2*	*0.4*	*137*	*224*
SCV 33Bi3872	*68.1*	*25.0*	*242*	*820*	*11.8*	*10.4*	*146*	*16986*	*3408*	*1614*	*1160*	*41.1*	*6.4*	*282*	*146*	*51.6*	*3.6*	*68.0*	*2.4*	*193*	*2.6*	*0.7*	*171*	*196*
SCV 45M4260	*37.7*	*22.2*	*132*	*810*	*10.2*	*6.5*	*129*	*14415*	*3875*	*1958*	*2420*	*23.4*	*5.3*	*78.1*	*98.8*	*52.3*	*3.7*	*57.4*	*2.4*	*184*	*9.3*	*0.7*	*156*	*62.8*
SCV 80F4745	*57.9*	*26.6*	*304*	*822*	*10.4*	*7.4*	*151*	*5445*	*1327*	*1366*	*388*	*95.6*	*2.6*	*2979*	*70.2*	*70.0*	*4.4*	*40.0*	*2.7*	*15.9*	*10.5*	*0.7*	*113*	*261*
SCV 86i4886	*103*	*35.0*	*211*	*803*	*15.1*	*9.5*	*184*	*16648*	*3129*	*893*	*1090*	*56.6*	*5.9*	*126*	*134*	*112*	*3.9*	*43.8*	*2.3*	*276*	*2.5*	*0.7*	*202*	*193*

Table V.2. (cont.) REE and trace elements in blue glazes measured by LA-ICP-MS. Results presented in µg/g.

	Cs	Ba	La	Ce	Pr	Nd	Sm	Eu	Gd	Tb	Dy	Ho	Er	Tm	Yb	Lu	Hf	Ta	W	Pt	Au	Bi	Th	U
IVDJ-T 96	*7.3*	*305*	*7.5*	*14.5*	*1.7*	*6.4*	*1.4*	*0.4*	*1.3*	*0.3*	*1.0*	*0.2*	*0.5*	*0.1*	*0.3*	*0.1*	*0.5*	*0.2*	*27.0*	*0.0*		*757*	*2.5*	*40.2*
IVDJ-T 133	*2.9*	*316*	*8.5*	*16.5*	*1.8*	*7.7*	*1.5*	*0.3*	*1.0*	*0.2*	*1.2*	*0.2*	*0.7*	*0.1*	*0.7*	*0.1*	*2.7*	*0.2*	*7.6*	*0.0*	*0.0*	*3003*	*3.2*	*2.5*
IVDJ-T 3683	*2.0*	*213*	*11.0*	*21.6*	*2.2*	*8.3*	*1.4*	*0.4*	*1.8*	*0.3*	*0.8*	*0.2*	*0.6*	*0.1*	*0.5*	*0.1*	*1.2*	*0.2*	*1.8*	*0.0*		*481*	*4.5*	*2.0*
IVDJ-T 4095	*3.1*	*168*	*6.9*	*12.5*	*1.5*	*6.2*	*1.2*	*0.3*	*1.3*	*0.2*	*0.7*	*0.2*	*0.6*	*0.1*	*0.5*	*0.1*	*0.9*	*0.2*	*1.1*	*0.0*		*67.2*	*2.9*	*0.7*
IVDJ-S SN	*5.0*	*95.3*	*7.6*	*14.0*	*1.5*	*5.7*	*1.1*	*0.2*	*0.8*	*0.2*	*0.9*	*0.2*	*0.5*	*0.1*	*0.5*	*0.1*	*2.2*	*0.2*	*0.8*	*0.0*	*0.1*	*15.3*	*2.6*	*0.7*
IVDJ-S 3561	*5.3*	*105*	*5.9*	*11.6*	*1.3*	*5.0*	*1.0*	*0.2*	*1.1*	*0.2*	*0.9*	*0.2*	*0.6*	*0.1*	*0.5*	*0.1*	*2.0*	*0.2*	*2.1*	*0.0*	*0.0*	*2824*	*2.1*	*3.3*
IVDJ-S 3576	*5.0*	*127*	*8.0*	*15.2*	*1.7*	*6.7*	*1.2*	*0.3*	*1.2*	*0.2*	*0.9*	*0.2*	*0.6*	*0.1*	*0.5*	*0.1*	*1.6*	*0.2*	*2.4*		*0.0*	*11.3*	*2.4*	*0.6*
IVDJ-S 3584	*2.6*	*120*	*7.9*	*14.4*	*1.6*	*6.6*	*1.3*	*0.3*	*1.1*	*0.2*	*0.9*	*0.2*	*0.6*	*0.1*	*0.5*	*0.1*	*1.6*	*0.2*	*1.0*	*0.0*	*0.0*	*10.9*	*2.5*	*0.6*
IVDJ-S 3591	*2.6*	*143*	*5.4*	*10.2*	*1.1*	*4.3*	*0.8*	*0.2*	*0.8*	*0.2*	*0.7*	*0.2*	*0.5*	*0.1*	*0.4*	*0.1*	*1.3*	*0.3*	*2.0*	*0.0*	*0.1*	*8.5*	*2.0*	*0.5*
IVDJ-S 3601	*2.9*	*170*	*11.5*	*22.4*	*2.4*	*9.8*	*2.1*	*0.4*	*1.9*	*0.5*	*2.3*	*0.4*	*1.1*	*0.1*	*0.9*	*0.1*	*1.2*	*0.3*	*5.2*	*0.0*	*0.0*	*2292*	*4.0*	*10.0*
IVDJ-S 4098	*5.6*	*86.3*	*8.1*	*15.3*	*1.6*	*6.3*	*1.2*	*0.2*	*0.7*	*0.2*	*0.8*	*0.2*	*0.5*	*0.1*	*0.5*	*0.1*	*1.8*	*0.2*	*2.6*	*0.0*	*0.0*	*24.0*	*2.7*	*0.6*
IVDJ-S 4106	*4.8*	*100*	*5.6*	*10.1*	*1.1*	*4.5*	*0.9*	*0.2*	*0.9*	*0.2*	*0.7*	*0.1*	*0.5*	*0.1*	*0.5*	*0.1*	*1.7*	*0.2*	*1.9*	*0.0*	*0.0*	*63.2*	*2.0*	*0.5*
IVDJ-S 4107	*3.5*	*121*	*8.2*	*15.3*	*1.6*	*6.3*	*1.1*	*0.3*	*1.2*	*0.2*	*1.0*	*0.2*	*0.7*	*0.1*	*0.6*	*0.1*	*2.2*	*0.2*	*4.5*	*0.0*	*0.2*	*9.5*	*2.4*	*0.6*
IVDJ-S 4127	*2.4*	*79.4*	*5.8*	*10.8*	*1.2*	*4.6*	*0.9*	*0.2*	*0.6*	*0.1*	*0.7*	*0.1*	*0.5*	*0.1*	*0.4*	*0.1*	*2.1*	*0.2*	*0.7*	*0.0*	*0.1*	*29.6*	*2.1*	*0.5*
IVDJ-S 4134	*7.2*	*221*	*11.4*	*22.2*	*2.3*	*9.0*	*1.5*	*0.3*	*1.3*	*0.3*	*1.0*	*0.2*	*0.7*	*0.1*	*0.6*	*0.1*	*2.4*	*0.2*	*0.7*	*0.0*	*0.0*	*4.4*	*3.5*	*0.7*
IVDJ-S 4185	*3.2*	*157*	*7.5*	*13.3*	*1.5*	*5.4*	*1.2*	*0.3*	*1.0*	*0.2*	*0.8*	*0.2*	*0.6*	*0.1*	*0.5*	*0.1*	*2.0*	*0.2*	*0.5*	*0.0*	*0.0*	*11.9*	*2.4*	*0.7*
PNS01	*3.7*	*129*	*5.5*	*10.5*	*1.2*	*4.8*	*1.0*	*0.3*	*1.4*	*0.3*	*0.8*	*0.2*	*0.6*	*0.1*	*0.5*	*0.1*	*2.1*	*0.2*	*7.2*	*0.0*	*0.0*	*24.7*	*1.9*	*0.5*
PNS06	*5.9*	*138*	*9.1*	*17.2*	*2.1*	*8.8*	*1.8*	*0.5*	*2.1*	*0.4*	*1.6*	*0.3*	*1.0*	*0.1*	*0.8*	*0.1*	*1.5*	*0.2*	*4.3*	*0.0*	*0.0*	*31.7*	*3.0*	*0.6*
PNS07	*5.6*	*197*	*6.7*	*12.2*	*1.4*	*5.8*	*1.2*	*0.5*	*1.7*	*0.3*	*1.0*	*0.2*	*0.8*	*0.1*	*0.6*	*0.1*	*2.3*	*0.2*	*3.3*	*0.0*	*0.0*	*68.1*	*2.1*	*0.6*

Table V.2. (cont.) REE and trace elements in blue glazes measured by LA-ICP-MS. Results presented in µg/g.

	Cs	Ba	La	Ce	Pr	Nd	Sm	Eu	Gd	Tb	Dy	Ho	Er	Tm	Yb	Lu	Hf	Ta	W	Pt	Au	Bi	Th	U
PNS09	*5.2*	*137*	*4.9*	*8.8*	*1.0*	*4.1*	*0.8*	*0.3*	*1.2*	*0.2*	*0.6*	*0.1*	*0.5*	*0.0*	*0.4*	*0.1*	*1.3*	*0.1*	*6.8*	*0.0*	*0.0*	*47.0*	*1.4*	*0.5*
PNS11	*3.6*	*109*	*5.1*	*8.8*	*1.0*	*4.3*	*0.8*	*0.2*	*1.0*	*0.2*	*0.7*	*0.2*	*0.5*	*0.1*	*0.4*	*0.1*	*1.5*	*0.2*	*1.6*	*0.0*	*0.0*	*23.6*	*1.5*	*0.5*
PNS14	*2.9*	*157*	*8.5*	*15.7*	*1.7*	*7.3*	*1.3*	*0.4*	*1.9*	*0.3*	*1.0*	*0.2*	*0.8*	*0.1*	*0.7*	*0.1*	*1.8*	*0.2*	*6.4*	*0.0*		*11.6*	*2.3*	*0.6*
PNS19	*4.2*	*122*	*8.2*	*16.0*	*1.8*	*7.1*	*1.4*	*0.4*	*1.6*	*0.3*	*1.2*	*0.2*	*0.8*	*0.1*	*0.6*	*0.1*	*2.2*	*0.2*	*1.7*	*0.0*	*0.0*	*9.1*	*2.7*	*0.7*
PNS20	*3.7*	*114*	*7.8*	*14.6*	*1.6*	*6.3*	*1.2*	*0.3*	*1.1*	*0.2*	*0.9*	*0.2*	*0.6*	*0.1*	*0.5*	*0.1*	*2.3*	*0.2*	*2.6*	*0.0*	*0.1*	*70.4*	*2.3*	*0.7*
PNS21	*4.0*	*144*	*7.4*	*13.7*	*1.5*	*5.6*	*1.0*	*0.3*	*1.1*	*0.2*	*0.9*	*0.2*	*0.7*	*0.1*	*0.6*	*0.1*	*2.7*	*0.2*	*1.1*	*0.0*	*0.0*	*5.5*	*2.6*	*0.9*
PNS22	*2.3*	*106*	*6.9*	*13.2*	*1.4*	*6.0*	*1.2*	*0.3*	*1.1*	*0.2*	*1.0*	*0.2*	*0.7*	*0.1*	*0.6*	*0.1*	*1.4*	*0.2*	*15.4*	*0.0*	*0.0*	*2839*	*2.3*	*3.5*
PNS23	*8.1*	*154*	*7.7*	*14.3*	*1.6*	*6.1*	*1.1*	*0.3*	*1.1*	*0.2*	*0.9*	*0.2*	*0.6*	*0.1*	*0.5*	*0.1*	*1.8*	*0.2*	*0.6*	*0.0*	*0.0*	*11.2*	*2.9*	*0.7*
PNS24	*3.7*	*76.1*	*6.6*	*11.7*	*1.3*	*5.2*	*1.0*	*0.2*	*0.9*	*0.2*	*0.7*	*0.1*	*0.5*	*0.1*	*0.4*	*0.1*	*1.2*	*0.2*	*1.4*	*0.0*	*0.0*	*7.4*	*2.2*	*0.6*
PNS25	*3.0*	*116*	*7.3*	*13.7*	*1.5*	*5.8*	*1.1*	*0.3*	*1.0*	*0.2*	*0.9*	*0.2*	*0.5*	*0.1*	*0.4*	*0.1*	*0.9*	*0.2*	*0.9*	*0.0*	*0.0*	*1106*	*2.0*	*2.9*
PNS26	*3.9*	*147*	*8.2*	*15.4*	*1.6*	*6.6*	*1.2*	*0.3*	*1.3*	*0.2*	*1.0*	*0.2*	*0.6*	*0.1*	*0.6*	*0.1*	*2.0*	*0.2*	*2.1*	*0.0*	*0.0*	*1831*	*2.4*	*0.9*
PNS27	*4.2*	*100*	*6.0*	*10.7*	*1.2*	*4.7*	*0.8*	*0.2*	*0.8*	*0.2*	*0.6*	*0.1*	*0.4*	*0.1*	*0.4*	*0.1*	*1.6*	*0.1*	*0.8*	*0.0*	*0.0*	*28.4*	*1.7*	*0.5*
PNS29	*3.1*	*134*	*9.6*	*16.9*	*1.9*	*7.5*	*1.5*	*0.4*	*1.3*	*0.3*	*1.4*	*0.2*	*0.7*	*0.1*	*0.7*	*0.1*	*1.3*	*0.2*	*2.9*		*0.0*	*2752*	*2.5*	*4.6*
PNS32	*1.8*	*123*	*7.1*	*13.2*	*1.4*	*5.7*	*0.9*	*0.2*	*1.0*	*0.2*	*0.9*	*0.2*	*0.6*	*0.1*	*0.5*	*0.1*	*2.8*	*0.2*	*4.9*	*0.0*	*0.1*	*62.4*	*2.4*	*0.6*
PNS38	*3.6*	*116*	*7.3*	*13.4*	*1.4*	*5.6*	*0.9*	*0.2*	*0.8*	*0.2*	*0.8*	*0.2*	*0.5*	*0.1*	*0.5*	*0.1*	*2.0*	*0.2*	*0.9*		*0.0*	*36.7*	*2.3*	*0.6*
PNS39	*2.3*	*73.9*	*5.9*	*11.0*	*1.1*	*4.5*	*0.7*	*0.2*	*0.7*	*0.2*	*0.5*	*0.1*	*0.4*	*0.1*	*0.4*	*0.1*	*1.6*	*0.2*	*1.3*	*0.0*	*0.1*	*62.3*	*1.7*	*0.5*
MCV 2-1T	*31.9*	*115*	*5.0*	*9.1*	*1.0*	*4.0*	*0.7*	*0.1*	*0.6*	*0.1*	*0.5*	*0.1*	*0.3*	*0.0*	*0.3*	*0.0*	*0.5*	*0.2*	*3.1*	*0.0*	*0.0*	*16.8*	*1.6*	*0.4*
MCV 3-1R	*19.7*	*297*	*5.1*	*8.9*	*1.0*	*4.2*	*0.8*	*0.2*	*0.7*	*0.1*	*0.5*	*0.1*	*0.3*	*0.0*	*0.3*	*0.0*	*0.6*	*0.1*	*8.5*	*0.0*	*0.0*	*2789*	*1.4*	*1.0*
MCV 4-2G	*12.0*	*149*	*6.6*	*11.3*	*1.3*	*5.0*	*0.9*	*0.2*	*0.7*	*0.1*	*0.6*	*0.1*	*0.3*	*0.0*	*0.3*	*0.0*	*0.5*	*0.2*	*2.1*	*0.0*	*0.0*	*4.6*	*1.7*	*0.7*
MCV 5-1R	*8.9*	*341*	*5.2*	*9.1*	*1.0*	*4.3*	*0.8*	*0.2*	*0.8*	*0.1*	*0.4*	*0.1*	*0.3*	*0.0*	*0.2*	*0.0*	*0.4*	*0.2*	*2.3*	*0.0*	*0.1*	*4999*	*1.1*	*3.0*
MCV 8-1G	*20.4*	*139*	*5.6*	*10.0*	*1.1*	*4.5*	*0.8*	*0.2*	*0.7*	*0.1*	*0.5*	*0.1*	*0.3*	*0.0*	*0.2*	*0.0*	*0.6*	*0.1*	*0.4*	*0.0*	*0.0*	*5.0*	*1.7*	*0.5*
SAC 01	*0.8*	*61.7*	*7.5*	*13.9*	*1.4*	*5.2*	*1.0*	*0.2*	*0.9*	*0.1*	*0.5*	*0.1*	*0.3*	*0.0*	*0.2*	*0.0*	*0.5*	*0.1*	*80.0*		*0.0*	*603*	*1.5*	*1.2*
SCV 4i365	*5.0*	*149*	*6.9*	*12.8*	*1.5*	*6.0*	*1.1*	*0.3*	*1.3*	*0.2*	*0.8*	*0.2*	*0.6*	*0.1*	*0.6*	*0.1*	*2.1*	*0.2*	*1.4*	*0.0*	*0.0*	*19.4*	*2.2*	*0.6*
SCV 8i7532	*4.0*	*181*	*7.8*	*14.0*	*1.5*	*6.1*	*1.1*	*0.3*	*1.1*	*0.2*	*0.8*	*0.2*	*0.5*	*0.1*	*0.5*	*0.1*	*1.7*	*0.2*	*1.4*	*0.0*	*0.1*	*17.6*	*2.2*	*0.6*
SCV 9i1469	*4.3*	*145*	*7.3*	*13.4*	*1.5*	*6.1*	*1.1*	*0.3*	*1.2*	*0.2*	*0.9*	*0.2*	*0.6*	*0.1*	*0.5*	*0.1*	*1.7*	*0.2*	*9.5*	*0.0*	*0.1*	*5.4*	*2.2*	*0.6*
SCV 10Bi1673	*6.0*	*107*	*10.8*	*20.5*	*2.2*	*8.9*	*1.6*	*0.3*	*1.4*	*0.2*	*1.2*	*0.2*	*0.8*	*0.1*	*0.8*	*0.1*	*1.8*	*0.2*	*16.2*	*0.0*	*0.0*	*29.2*	*2.5*	*0.8*
SCV 10EF175	*4.6*	*96*	*6.1*	*11.1*	*1.3*	*5.3*	*1.1*	*0.2*	*1.1*	*0.2*	*0.9*	*0.2*	*0.6*	*0.1*	*0.5*	*0.1*	*1.7*	*0.2*	*0.7*	*0.0*	*0.1*	*16.2*	*2.6*	*0.6*
SCV 20i2989	*2.8*	*102*	*5.8*	*10.4*	*1.2*	*5.0*	*0.9*	*0.4*	*1.1*	*0.2*	*0.8*	*0.2*	*0.5*	*0.1*	*0.5*	*0.1*	*1.5*	*0.2*	*52.3*	*0.0*	*0.0*	*23.2*	*2.0*	*0.5*

Table V.2. (cont.) REE and trace elements in blue glazes measured by LA-ICP-MS. Results presented in µg/g.

	Cs	Ba	La	Ce	Pr	Nd	Sm	Eu	Gd	Tb	Dy	Ho	Er	Tm	Yb	Lu	Hf	Ta	W	Pt	Au	Bi	Th	U
SCV 21AM3076	4.8	170	7.9	14.2	1.6	6.2	1.2	1.4	0.9	0.2	0.8	0.2	0.6	0.1	0.6	0.1	1.8	0.2	1.7	0.0	0.0	10.7	2.5	0.6
SCV 30F7756	5.6	128	6.6	12.8	1.3	5.5	1.0	0.2	0.9	0.2	0.8	0.2	0.5	0.1	0.5	0.1	2.0	0.2	3.3	0.0	0.0	8.9	2.3	0.5
SCV 32M3685	5.6	104	6.1	11.3	1.2	5.1	0.9	0.2	0.8	0.2	0.8	0.2	0.5	0.1	0.5	0.1	1.6	0.2	1.9	0.0	0.0	16.9	2.4	0.6
SCV 33Bi3839	6.2	137	8.2	15.8	1.6	6.2	1.1	2.3	0.9	0.2	0.8	0.2	0.5	0.1	0.6	0.1	1.6	0.2	2.4	0.0	0.0	19.8	2.9	0.7
SCV 33Bi3872	6.6	93.4	5.2	9.7	1.1	4.6	0.9	0.2	0.9	0.1	0.7	0.1	0.5	0.1	0.5	0.1	2.3	0.3	0.6	0.0	0.0	23.4	1.9	0.5
SCV 45M4260	4.7	78.1	5.1	9.4	1.1	4.4	0.9	0.2	1.0	0.2	0.7	0.1	0.4	0.1	0.5	0.1	1.6	0.2	0.9	0.0	0.0	43.5	1.9	0.5
SCV 80F4745	2.8	826	6.5	12.0	1.3	5.4	1.0	0.5	1.1	0.2	0.9	0.2	0.6	0.1	0.5	0.1	1.1	0.2	43.5	0.0	0.1	2048	1.8	45.1
SCV 86i4886	6.6	158	6.3	11.9	1.3	5.6	1.0	0.3	1.1	0.2	0.8	0.2	0.5	0.1	0.4	0.1	1.2	0.2	3.0	0.0	0.0	8.6	1.9	0.5

Table V.3. REE and trace elements in green glazes measured by LA-ICP-MS. Results presented in µg/g.

	Li	B	P	Ti	V	Cr	Mn	Co	Ni	Zn	Ga	As	Rb	Sr	Y	Zr	Nb	Mo	Ag	Cd	In	Sb
IVDJ-T 96	63.2	31.3	333	1435	12.3		190	12.7	36.1	199	5.2	377	67.1	137	6.0	33.6	3.7	4.2	59.3	0.9	42.7	566
IVDJ-T 133	61.0	18.4	407	621	9.7	4.0	121	22.0	34.4	86.8	5.3	375	65.8	68.1	4.8	29.1	2.1	0.7	10.5	1.0	16.8	489
IVDJ-S 3561	76.0	24.4	199	1044	14.3	1.8	135	800	205	39.7	3.3	678	98.6	74.9	4.7	59.8	2.8	10.0	5.8	0.4	203	42
IVDJ-S 3589	53.9	31.8	322	1676	26.8	11.7	386	21.0	60.7	2293	4.9	194	56.2	119	13.7	128	4.6	1.5	10.8	0.9	15.3	288
IVDJ-S 3774	39.1	27.0	437	1160	15.8	11.7	217	17.3	46.5	1706	3.7	134	90.5	63.3	8.3	97.2	3.1	0.6	10.8	0.7	37.3	465
IVDJ-S 3794	29.9	25.2	559	822	14.4	9.3	280	4.4	54.3	80.5	2.4	79.0	23.5	73.0	5.6	39.6	2.4	0.3	232	0.4	152	269
IVDJ-S 3919	28.7	16.2	142	415	7.5		94.7	4.0	25.8	76.9	1.2	118	16.2	49.2	2.3	39.8	1.2	0.4	35.6	0.6	130	105
IVDJ-S 4098	52.3	35.2	320	929	13.9	8.5	299	22.5	50.4	106	3.4	98.1	120	60.4	5.0	46.7	2.6	3.2	3.3	0.6	18.9	326
IVDJ-S 4106	32.4	19.5	255	869	10.8	7.9	345	66.6	68.1	69.8	2.7	83.0	77.3	51.2	4.8	79.6	2.4	3.8	17.5	0.9	37.5	398
IVDJ-S 4107	33.7	38.3	351	1057	12.6	1.2	180	19.9	48.7	1576	2.5	67.5	59.6	81.9	4.8	52.6	2.7	0.5	24.9	0.4	32.8	552
IVDJ-S SN	29.2	25.3	262	1204	10.0	5.9	179	11.3	40.8	144	2.5	57.4	67.3	32.1	4.8	63.7	2.9	0.7	27.0	0.3	38.9	264
IVDJ-S XV	41.7	33.0	320	743	12.6	1.8	169	3.5	24.5	172	3.5	26.4	42.2	91.2	5.3	52.7	2.2	0.1	17.8	10.7	62.8	565
PNS02	44.5	27.2	343	1112	16.3	12.5	255	7.9	33.4	40.9	3.4	27.6	54.2	89.0	5.2	71.6	2.8	0.4	5.4	1.0	10.6	235
PNS03	73.0	16.4		110	2.5		60.7	7.4	31.7	77.5	0.4	379	14.3	13.9	0.7	3.1	0.4	0.1	248.4	0.8	215	754
PNS05	51.3	31.7	380	1372	20.8	11.8	210	16.9	46.6	1070	4.4	195	82.8	117	6.7	302	3.7	1.2	11.7	0.7	56.0	347
PNS06	25.9	34.1	342	942	15.4	7.0	5817	66.6	76.7	2457	2.9	172	55.7	100	6.5	73.6	2.6	2.6	36.6	0.7	29.0	311
PNS07	37.5	46.2	1409	1117	15.7	12.3	305	5.0	50.2	37.8	3.4	86.6	78.4	69.1	6.1	119	2.9	0.4	10.7	0.8	9.9	314

Table V.3. (cont.) REE and trace elements in green glazes measured by LA-ICP-MS. Results presented in µg/g.

	Li	B	P	Ti	V	Cr	Mn	Co	Ni	Zn	Ga	As	Rb	Sr	Y	Zr	Nb	Mo	Ag	Cd	In	Sb
PNS08	28.6	30.4	511	864	15.7	8.5	234	6.6	32.5	31.3	2.6	51.0	48.1	57.3	5.3	95.5	2.3	0.5	26.1	0.6	23.7	452
PNS09	49.8	26.1	197	740	10.7	7.4	346	31.9	67.2	62.4	2.2	77.3	82.9	79.3	3.6	52.4	2.0	1.6	49.9	0.9	189	550
PNS10	29.3	30.0	480	895	14.7	9.8	395	5.8	31.1	30.6	2.9	47.3	45.5	70.3	5.2	107.1	2.4	0.4	32.6	0.5	18.4	390
PNS11	30.4	44.7	888	681	26.5	8.1	419	5.0	45.3	105	2.2	81.7	73.1	51.2	4.7	89.7	2.0	1.1	51.2	0.6	44.3	511
PNS12	22.0	25.4	396	977	14.0	7.6	270	12.2	65.5	3077	2.8	64.4	43.3	41.8	4.8	58.8	2.6	0.9	38.8	0.5	39.7	422
PNS15	36.8	50.0	259	993	15.5	8.5	147	39.6	62.3	76.0	3.3	55.5	60.3	74.7	6.0	87.4	2.7	1.9	8.9	0.7	14.2	588
PNS16	31.5	27.4	367	1010	15.0	3.5	178	2.9	38.0	35.5	3.0	86.6	72.0	69.6	5.7	102	3.0	0.2	22.1	0.7	20.0	316
PNS17	41.9	21.6	229	384	7.0		246	28.6	64.9	503	1.4	163	69.7	71.8	2.1	13.3	2.1	0.6	43.6	1.0	163	1339
PNS19	60.9	43.3	495	1714	30.6	11.2	2234	26.4	55.6	460	5.6	79.6	128	101	21.5	90.1	6.2	1.4	5.9	0.8	24.5	406
PNS21	33.6	23.6	256	959	17.1	3.8	193	5.4	27.7	80.6	3.6	110	55.2	77.2	5.7	53.6	2.8	4.0	10.1	0.5	25.2	761
PNS22	24.8	20.0	154	913	13.7	2.8	296	32.1	39.6	39.2	2.9	112	30.6	56.6	4.9	70.7	2.6	0.5	10.4	0.4	13.0	450
PNS24	19.8	25.3	445	916	11.7	5.8	389	41.0	53.5	44.5	2.3	92.0	57.6	55.1	5.1	42.8	2.5	3.7	12.4	0.8	58.7	520
PNS26	43.3	45.5	722	1088	19.3	5.9	756	31.9	34.0	68.6	3.7	147	61.7	95.7	5.9	76.2	3.4	1.8	2.3	0.7	16.8	197
PNS28	35.5	26.0	401	1465	25.0	13.8	492	25.7	59.0	318	4.7	103	115	52.8	8.5	69.4	3.8	1.6	7.2	0.4	30.1	441
PNS29	23.3	30.0	448	899	14.1	8.6	249	53.5	34.9	62.3	3.0	97.3	37.5	69.0	5.2	54.5	2.8	1.0	5.0	0.7	6.4	207
PNS30	56.5	10.0	211	163	4.4	0.5	1105	8.5	29.5	31.8	1.0	55.5	87.6	36.6	2.5	9.2	1.3	0.4	29.4	0.3	182	551
PNS33	11.9	15.2	219	652	7.9	2.9	1396	37.6	61.3	18.8	2.0	68.3	20.6	39.2	4.8	113	1.8	2.4	36.6	0.2	27.1	529
PNS34	49.9	65.6	1236	1303	22.3	7.5	328	26.2	59.2	94.0	4.1	105	65.1	92.3	8.3	141	3.8	1.4	71.3	0.6	17.5	243
PNS35	50.2	21.1	269	841	10.5	4.3	283	34.0	66.4	28.1	2.3	83.0	82.7	94.4	3.8	54.4	2.3	1.8	17.5	0.5	157.2	462
PNS36	29.7	16.5	179	1386	18.3	9.8	261	3.5	41.7	407	3.1	44.5	60.9	33.8	5.6	46.3	4.0	0.3	13.7	0.3	16.5	498
PNS37	41.8	34.3	596	1227	21.0	23.4	810	5.5	37.9	37.9	4.1	65.8	51.7	111	9.3	87.2	5.3	0.5	19.0	0.5	29.2	499
PNS38	19.4	29.6	507	979	16.4	4.4	265	18.4	55.3	55.9	3.1	86.5	31.7	55.6	5.6	91.6	2.8	1.1	30.7	0.6	38.7	576
MCV 4-1ML	41.4	36.2	390	1405	20.5	14.5	301	8.1	35.5	71.6	4.6	160	58.0	106	7.7	148	4.3	0.5	9.5	0.5	16.4	485
MCV 5-1R	49.3	29.4	256	556	11.6	10.7	92.0	30.7	53.0	53.6	3.6	183	133	74.3	5.3	17.1	1.9	1.6	37.4	1.0	98.5	201
MCV 6-1C	41.8	26.7	358	327	5.2	6.4	66.2	3.8	63.8	46.8	2.3	427	61.0	54.9	2.8	16.7	1.1	0.1	39.0	0.6	21.4	368
MCV 7-1C	83.1	57.0	321	564	11.2	9.1	131	3.8	34.0	133	4.2	44.9	108	91.7	4.1	77.9	2.1	0.3	51.2	0.6	23.0	107
SAC 02	108.5	78.8	248	794	14.9	7.4	427	17.8	120.2	434	5.0	26.2	56.5	43.2	6.2	28.4	2.8	0.6	18.8	0.2	150	318
SCV 9i1469	71.3	47.0	313	1178	23.8	17.1	925	106	75.4	70.3	5.9	35.1	77.2	127	7.1	78.6	3.4	7.9	5.9	0.5	22.9	222

Table V.3. (cont.) REE and trace elements in green glazes measured by LA-ICP-MS. Results presented in µg/g.

	Li	B	P	Ti	V	Cr	Mn	Co	Ni	Zn	Ga	As	Rb	Sr	Y	Zr	Nb	Mo	Ag	Cd	In	Sb
SCV 10Bi1673	*58.9*	*28.0*	*263*	*914*	*13.2*	*9.5*	*314*	*168*	*126*	*51.6*	*3.4*	*57.8*	*78.4*	*94.1*	*4.8*	*67.8*	*2.7*	*7.0*	*6.2*	*0.7*	*60.8*	*238*
SCV 10EF175	*49.0*	*36.3*	*460*	*1257*	*16.9*	*10.1*	*488*	*38.5*	*71.2*	*38.1*	*4.8*	*55.6*	*75.8*	*83.8*	*7.1*	*105*	*3.3*	*3.6*	*7.7*	*0.5*	*18.1*	*680*
SCV 21AM3076	*59.2*	*31.7*	*374*	*1186*	*16.7*	*12.4*	*449*	*6.9*	*61.5*	*43.3*	*4.0*	*55.4*	*75.8*	*96.5*	*6.8*	*130*	*3.4*	*0.6*	*6.5*	*0.5*	*19.8*	*329*
SCV 30F7756	*42.5*	*37.5*	*593*	*1185*	*19.5*	*11.4*	*520*	*8.0*	*44.9*	*71.1*	*4.1*	*146*	*68.8*	*78.4*	*6.1*	*88.8*	*3.2*	*0.7*	*6.9*	*0.6*	*16.2*	*432*
SCV 80F4745	*45.4*	*24.3*	*284*	*947*	*14.4*	*8.1*	*422*	*11.5*	*39.2*	*52.6*	*3.1*	*110*	*61.6*	*71.3*	*5.3*	*36.9*	*2.6*	*0.4*	*7.8*	*0.6*	*10.7*	*250*
SCV 87M7985	*86.2*	*82.6*	*1066*	*872*	*11.8*	*6.5*	*731*	*5.0*	*91.1*	*9489*	*4.4*	*77.9*	*69.8*	*105*	*4.7*	*32.5*	*3.1*	*0.2*	*55.6*	*0.3*	*81.9*	*200*

Table V.3. (cont.) REE and trace elements in green glazes measured by LA-ICP-MS. Results presented in µg/g.

	Cs	Ba	La	Ce	Pr	Nd	Sm	Eu	Gd	Tb	Dy	Ho	Er	Tm	Yb	Lu	Hf	Ta	W	Bi	Th	U
IVDJ-T 96	*3.0*	*372*	*10.6*	*21.6*	*2.5*	*10.3*	*1.8*	*0.5*	*1.8*	*0.3*	*1.2*	*0.2*	*0.8*	*0.1*	*0.6*	*0.1*	*0.9*	*0.2*	*14.0*	*93.5*	*5.9*	*1.0*
IVDJ-T 133	*4.2*	*238*	*11.4*	*23.9*	*2.5*	*10.0*	*1.9*	*0.4*	*1.2*	*0.2*	*1.0*	*0.2*	*0.5*	*0.1*	*0.4*	*0.1*	*0.8*	*0.2*	*7.5*	*210*	*3.2*	*1.0*
IVDJ-S 3561	*4.1*	*112*	*6.6*	*12.3*	*1.4*	*5.5*	*1.0*	*0.2*	*1.1*	*0.2*	*0.9*	*0.2*	*0.6*	*0.1*	*0.5*	*0.1*	*1.6*	*0.2*	*1.0*	*670*	*2.1*	*1.0*
IVDJ-S 3589	*3.1*	*145*	*13.4*	*25.0*	*2.8*	*11.0*	*2.2*	*0.4*	*2.0*	*0.4*	*2.3*	*0.5*	*1.6*	*0.2*	*1.5*	*0.2*	*3.7*	*0.3*	*1.2*	*12.2*	*4.3*	*1.0*
IVDJ-S 3774	*6.0*	*91.5*	*9.3*	*17.4*	*1.9*	*7.6*	*1.4*	*0.3*	*1.1*	*0.3*	*1.4*	*0.3*	*1.0*	*0.1*	*0.9*	*0.1*	*2.3*	*0.2*	*0.4*	*7.1*	*2.7*	*0.7*
IVDJ-S 3794	*1.0*	*101*	*7.7*	*11.3*	*1.7*	*7.0*	*1.3*	*0.3*	*1.1*	*0.2*	*1.1*	*0.2*	*0.6*	*0.1*	*0.6*	*0.1*	*1.0*	*0.1*	*3.0*	*67.6*	*1.7*	*0.6*
IVDJ-S 3919	*0.5*	*79.1*	*4.0*	*7.6*	*0.8*	*3.2*	*0.6*	*0.1*	*0.5*	*0.1*	*0.4*	*0.1*	*0.3*	*0.0*	*0.3*	*0.0*	*1.1*	*0.1*	*6.5*	*7.7*	*1.4*	*0.4*
IVDJ-S 4098	*5.4*	*93.3*	*9.5*	*17.0*	*1.9*	*7.7*	*1.5*	*0.3*	*0.9*	*0.2*	*0.9*	*0.2*	*0.6*	*0.1*	*0.5*	*0.1*	*1.2*	*0.2*	*0.5*	*21.9*	*2.7*	*0.5*
IVDJ-S 4106	*6.0*	*85.5*	*7.4*	*13.7*	*1.4*	*5.8*	*1.1*	*0.2*	*0.7*	*0.2*	*0.8*	*0.2*	*0.6*	*0.1*	*0.6*	*0.1*	*1.8*	*0.2*	*0.7*	*28.6*	*2.0*	*0.5*
IVDJ-S 4107	*2.6*	*94.9*	*7.0*	*12.7*	*1.4*	*5.7*	*1.0*	*0.2*	*1.0*	*0.2*	*0.8*	*0.2*	*0.6*	*0.1*	*0.5*	*0.1*	*1.5*	*0.2*	*1.8*	*11.2*	*2.2*	*0.5*
IVDJ-S SN	*3.2*	*66.4*	*7.2*	*15.5*	*1.5*	*5.7*	*1.0*	*0.2*	*0.8*	*0.2*	*0.9*	*0.2*	*0.5*	*0.1*	*0.5*	*0.1*	*1.6*	*0.2*	*0.8*	*7.9*	*2.2*	*0.5*
IVDJ-S XV	*2.0*	*149*	*8.2*	*16.0*	*1.8*	*7.1*	*1.4*	*0.3*	*1.3*	*0.2*	*1.0*	*0.2*	*0.7*	*0.1*	*0.7*	*0.1*	*1.5*	*0.2*	*1.0*	*27.6*	*2.7*	*1.3*
PNS02	*2.8*	*142*	*7.6*	*14.2*	*1.6*	*6.8*	*1.4*	*0.5*	*1.9*	*0.3*	*1.1*	*0.2*	*0.8*	*0.1*	*0.7*	*0.1*	*2.0*	*0.2*	*0.7*	*111*	*2.1*	*0.6*
PNS03	*0.5*	*25.9*	*1.1*	*2.0*	*0.2*	*1.0*	*0.3*		*0.3*	*0.1*	*0.1*	*0.0*	*0.1*	*0.0*	*0.1*	*0.0*	*0.1*	*0.0*	*0.2*	*10.6*	*0.3*	*0.1*
PNS05	*4.9*	*139*	*11.1*	*19.7*	*2.2*	*8.7*	*1.7*	*0.4*	*2.0*	*0.4*	*1.2*	*0.3*	*0.9*	*0.1*	*0.9*	*0.1*	*7.4*	*0.3*	*61.8*	*16.4*	*2.8*	*1.0*
PNS06	*3.4*	*367*	*7.4*	*13.1*	*1.5*	*6.4*	*1.3*	*0.6*	*1.5*	*0.3*	*1.1*	*0.2*	*0.8*	*0.1*	*0.7*	*0.1*	*2.0*	*0.2*	*121*	*8.9*	*1.9*	*0.6*
PNS07	*4.2*	*106*	*8.4*	*15.7*	*1.9*	*7.8*	*1.4*	*0.4*	*2.1*	*0.4*	*1.2*	*0.2*	*1.0*	*0.1*	*0.8*	*0.1*	*3.1*	*0.2*	*0.5*	*13.8*	*2.7*	*0.6*
PNS08	*2.7*	*85.6*	*7.8*	*14.7*	*1.7*	*6.8*	*1.3*	*0.3*	*1.8*	*0.3*	*1.0*	*0.2*	*0.8*	*0.1*	*0.7*	*0.1*	*2.5*	*0.2*	*0.8*	*28.0*	*2.4*	*0.5*

Table V.3. (cont.) REE and trace elements in green glazes measured by LA-ICP-MS. Results presented in µg/g.

	Cs	Ba	La	Ce	Pr	Nd	Sm	Eu	Gd	Tb	Dy	Ho	Er	Tm	Yb	Lu	Hf	Ta	W	Bi	Th	U
PNS09	4.2	116	5.3	9.8	1.1	4.5	0.9	0.3	1.3	0.2	0.7	0.1	0.6	0.1	0.4	0.1	1.4	0.1	0.7	32.1	1.5	0.4
PNS10	2.8	91.8	7.4	13.7	1.6	6.3	1.3	0.3	1.7	0.3	1.0	0.2	0.8	0.1	0.6	0.1	2.8	0.2	0.8	19.2	2.3	0.6
PNS11	3.1	108	6.1	10.9	1.3	5.5	1.1	0.3	1.3	0.3	0.9	0.2	0.7	0.1	0.5	0.1	2.3	0.1	0.7	18.4	1.7	0.6
PNS12	3.1	92.6	6.8	12.1	1.4	5.5	1.1	0.3	1.2	0.2	0.9	0.2	0.6	0.1	0.6	0.1	1.5	0.2	1.3	15.4	1.9	0.5
PNS15	3.3	91.4	9.6	18.1	2.1	8.4	1.7	0.4	2.0	0.3	1.1	0.2	0.8	0.1	0.7	0.1	2.3	0.2	0.6	18.6	2.9	0.6
PNS16	4.2	83.6	9.8	17.8	1.9	7.4	1.4	0.3	1.0	0.2	1.1	0.2	0.7	0.1	0.6	0.1	2.6	0.2	0.5	46.7	2.9	0.6
PNS17	10.3	126	3.6	5.4	0.8	2.9	0.5	0.2	0.8	0.1	0.4	0.1	0.3	0.0	0.2	0.0	0.4	0.2	0.2	50.5	0.9	0.3
PNS19	8.9	223	12.9	24.3	2.8	11.1	2.2	0.7	2.6	0.7	3.6	0.8	2.5	0.3	2.4	0.3	2.4	0.5	3.8	10.0	3.7	1.1
PNS21	3.0	108	9.4	17.5	1.9	7.6	1.4	0.3	1.3	0.3	1.0	0.2	0.7	0.1	0.6	0.1	1.4	0.2	0.9	13.3	2.7	0.7
PNS22	1.6	104	7.9	14.6	1.6	6.2	1.1	0.3	1.1	0.2	0.9	0.2	0.6	0.1	0.5	0.1	1.8	0.2	1.2	7018	2.2	0.6
PNS24	3.9	87.7	6.9	12.2	1.4	5.5	1.0	0.3	1.0	0.2	0.8	0.2	0.5	0.1	0.5	0.1	1.2	0.2	2.8	40.7	1.9	0.4
PNS26	3.1	146	9.3	17.2	1.9	7.7	1.4	0.4	1.4	0.3	1.1	0.2	0.8	0.1	0.7	0.1	2.1	0.2	1.3	194.1	2.6	0.7
PNS28	4.4	120	13.7	25.9	2.8	11.0	2.0	0.4	1.9	0.4	1.5	0.3	1.2	0.2	1.2	0.2	1.8	0.3	1.0	11.5	10.7	0.8
PNS29	2.3	107	7.2	13.2	1.5	5.6	1.1	0.3	1.0	0.2	1.0	0.2	0.7	0.1	0.5	0.1	1.4	0.2	0.5	63.8	2.1	0.6
PNS30	7.4	45.2	2.9	4.1	0.6	2.3	0.4	0.1	0.4	0.1	0.4	0.1	0.3	0.0	0.2	0.0	0.3	0.1	0.1	12.8	0.7	0.2
PNS33	1.0	125	6.3	11.2	1.3	5.3	0.9	0.2	0.8	0.2	0.8	0.2	0.6	0.1	0.5	0.1	4.2	0.1	3.1	22.5	2.1	0.5
PNS34	2.5	125	12.5	22.6	2.5	9.6	1.8	0.4	1.6	0.3	1.4	0.3	1.0	0.1	0.9	0.1	3.4	0.2	3.9	11.6	3.7	0.9
PNS35	3.8	110	5.9	10.7	1.2	4.4	0.8	0.2	0.7	0.2	0.7	0.1	0.4	0.1	0.4	0.1	1.5	0.2	0.8	34.2	1.7	0.4
PNS36	2.5	100	7.4	14.0	1.5	6.1	1.1	0.3	0.9	0.2	1.1	0.2	0.7	0.1	0.6	0.1	1.2	0.3	3.8	13.7	2.2	0.6
PNS37	2.9	122	9.7	17.9	1.9	7.7	1.4	0.4	1.3	0.3	1.6	0.3	1.1	0.1	1.0	0.2	2.1	0.3	2.8	19.0	3.0	1.0
PNS38	1.7	93.2	8.9	16.4	1.8	7.1	1.4	0.3	1.1	0.2	1.0	0.2	0.7	0.1	0.6	0.1	2.2	0.2	1.4	27.1	2.6	0.6
MCV 4-1ML	3.9	104	12.4	23.0	2.5	10.2	1.8	0.4	1.5	0.3	1.5	0.3	0.9	0.1	0.9	0.1	3.5	0.3	0.7	8.0	3.9	0.9
MCV 5-1R	10.6	130	6.2	10.8	1.3	5.1	1.0	0.3	1.1	0.2	1.0	0.2	0.6	0.1	0.5	0.1	0.5	0.2	2.8	228	1.8	0.6
MCV 6-1C	3.6	107	5.1	9.1	1.1	4.3	0.8	0.2	0.8	0.1	0.6	0.1	0.4	0.0	0.3	0.0	0.5	0.1	1.2	21.3	1.7	0.5
MCV 7-1C	8.0	137	9.3	17.5	1.9	7.5	1.4	0.4	1.4	0.2	0.8	0.2	0.5	0.1	0.4	0.1	1.8	0.2	0.5	22.3	1.9	0.8
SAC 02	1.7	74.1	11.5	22.0	2.3	9.0	1.8	0.4	1.5	0.3	1.3	0.2	0.7	0.1	0.6	0.1	0.8	0.5	204	7.5	2.3	0.8
SCV 9i1469	5.2	168	11.2	20.6	2.4	10.2	1.9	0.5	1.9	0.3	1.4	0.3	0.8	0.1	0.8	0.1	2.0	0.2	1.9	4.6	3.5	0.8
SCV 10Bi1673	5.4	102	8.4	15.6	1.7	7.0	1.4	0.3	1.2	0.2	0.9	0.2	0.6	0.1	0.5	0.1	1.8	0.2	1.5	21.1	2.5	0.6

Table V.3. (cont.) REE and trace elements in green glazes measured by LA-ICP-MS. Results presented in µg/g.

	Cs	Ba	La	Ce	Pr	Nd	Sm	Eu	Gd	Tb	Dy	Ho	Er	Tm	Yb	Lu	Hf	Ta	W	Bi	Th	U
SCV 10EF175	4.5	117	14.1	27.1	3.0	12.4	2.4	0.3	2.4	0.4	1.5	0.3	0.9	0.1	0.8	0.1	2.8	0.2	1.2	12.7	6.2	0.8
SCV 21AM3076	4.3	122	12.0	23.1	2.5	9.9	1.8	1.4	1.5	0.3	1.3	0.2	0.8	0.1	0.8	0.1	3.4	0.2	0.9	9.0	3.6	0.8
SCV 30F7756	3.6	128	9.6	17.6	2.0	8.3	1.7	0.3	1.3	0.2	1.2	0.2	0.7	0.1	0.7	0.1	2.3	0.2	1.5	7.7	2.8	0.6
SCV 80F4745	3.6	119	6.2	11.5	1.3	5.3	1.1	0.3	1.0	0.2	1.0	0.2	0.6	0.1	0.6	0.1	1.0	0.2	58.8	124	1.8	0.7
SCV 87M7985	7.1	171	7.6	14.4	1.7	6.7	1.3	0.3	1.1	0.2	0.9	0.2	0.5	0.1	0.5	0.1	0.9	0.4	3.7	20.1	2.4	1.1

Table V.4. REE and trace elements in amber glazes measured by LA-ICP-MS. Results presented in µg/g.

	Li	B	P	Cl	Ti	V	Cr	Mn	Co	Ni	Cu	Zn	Ga	As	Rb	Sr	Y	Zr	Nb	Mo	Ag	Cd	In
IVDJ-T 96	87.7	32.7	820	836	1006	31.4		546	14.5	15.8	752	229	8.5	326	62.0	382	12.54	66.23	3.3	11.6	42.0	0.9	4.3
IVDJ-T 133	65.1	19.5	1179	909	967	27.5	8.7	609	50.4	38.2	650	284	9.1	443	58.7	331	14.30	70.97	3.3	5.5	12.3	2.1	4.7
IVDJ-T 3683	82.6	34.6	446	990	655	15.8		97.8	10.0	13.3	115	926	5.6	1974	59.5	111	3.84	47.37	2.6	4.5	16.2	0.4	14.5
IVDJ-T 4095	29.5	18.2	251	2440	489	6.7		1428	60.7	45.6	1114	40.4	2.8	58.3	45.7	97.5	3.36	24.29	1.5	18.3	12.6	0.4	15.3
IVDJ-S SN	42.2	34.8	912	1496	1047	12.2	7.4	168	8.7	20.3	637	160	2.9	114	77.0	59.2	5.12	78.73	2.9	0.9	12.2	0.6	7.2
IVDJ-S 3589	44.2	41.4	762	1079	1309	20.7	8.2	397	22.5	26.6	763	217	4.2	234	51.0	114	7.45	89.61	3.5	4.9	10.5	0.9	9.2
IVDJ-S 3591	41.4	29.0	270	1121	1109	21.3	8.6	632	11.5	17.1	954	162	3.8	333	60.6	89.5	6.09	98.94	3.2	2.8	8.3	0.7	7.4
IVDJ-S 3919	17.6	20.4	240	1597	594	24.0	6.4	98	8.3	10.0	243	216	2.2	118	20.0	91.4	3.51	57.83	1.7	24.9	26.9	0.9	10.5
IVDJ-S 4078	56.0	42.8	681	2207	1098	18.9	11.1	186	7.2	16.3	758	191	4.3	266	130	71.2	6.58	86.79	3.2	3.2	3.5	0.7	2.1
IVDJ-S 4106	30.7	35.3	526	1186	1001	16.3	10.5	924	9.5	15.9	868	214	3.6	282	96.2	61.6	6.59	77.09	2.7	2.2	14.9	0.8	6.7
PNS05	39.7	29.4	188	1206	887	16.1	8.8	1519	7.9	21.9	1083	69.5	3.5	24.1	97.2	92.5	4.84	40.76	2.7	1.5	9.4	0.6	16.0
PNS11	15.7	27.3	234	2545	621	6.0	3.4	130	3.4	16.9	341	36.1	1.6	6.7	65.5	18.5	3.27	45.13	1.6	0.4	53.9	0.6	6.8
PNS21	40.3	29.4	259	998	1123	25.4	5.4	298	9.7	20.1	791	184	4.2	220	65.3	99.2	6.50	51.68	3.7	4.0	7.6	0.6	5.8
PNS25	35.0	41.9	794	1744	1109	19.3	8.3	365	18.2	12.6	214	182	4.3	338	53.4	101	6.65	78.11	3.3	2.1	3.3	1.3	4.0
PNS27	23.2	40.3	1670	1943	842	11.4	5.7	234	4.5	15.1	366	28.5	2.3	9.5	94.8	32.9	4.46	73.01	2.2	0.6	13.7	0.4	3.9
PNS29	27.1	33.9	507	1237	1019	17.0	8.5	280	126.7	35.2	288	229	3.8	684	52.5	80.6	5.55	63.85	3.0	3.9	3.1	1.0	5.1
PNS38	32.8	26.0	292	1226	1003	15.3	4.2	184	16.6	27.8	333	28.1	3.1	9.4	68.5	64.1	5.37	90.38	3.0	1.8	12.5	0.3	11.7
MCV 4-1ML	60.8	47.9	377	858	1049	21.6	10.8	202	7.5	16.7	480	231	4.4	192	87.8	107	6.34	81.00	3.2	1.2	3.6	0.6	8.8
SCV 4i365	87.1	51.9	361	1078	1106	29.2	14.4	255	81.4	53.4	740	188	5.1	253	87.8	124	6.91	82.82	3.2	9.4	3.3	0.8	7.3

Table V.4. (cont.) REE and trace elements in amber glazes measured by LA-ICP-MS. Results presented in µg/g.

	Li	B	P	Cl	Ti	V	Cr	Mn	Co	Ni	Cu	Zn	Ga	As	Rb	Sr	Y	Zr	Nb	Mo	Ag	Cd	In
SCV 9i1469	*60.2*	*46.7*	*339*	*963*	*1103*	*22.3*	*13.5*	*267*	*19.0*	*36.0*	*915*	*207*	*5.1*	*178*	*69.7*	*112*	*7.38*	*88.76*	*3.3*	*2.4*	*4.2*	*0.8*	*10.3*
SCV 10Bi1673	*47.3*	*43.4*	*468*	*1093*	*1587*	*31.2*	*17.1*	*335*	*10.8*	*27.8*	*739*	*160*	*5.9*	*236*	*56.4*	*130*	*7.95*	*94.98*	*4.3*	*2.4*	*5.2*	*1.0*	*6.0*
SCV 20i2989	*45.9*	*34.1*	*327*	*1559*	*1169*	*15.8*	*10.0*	*564*	*5.5*	*23.8*	*571*	*153*	*3.5*	*250*	*62.6*	*72.8*	*5.75*	*72.50*	*3.1*	*2.9*	*4.5*	*0.7*	*13.8*
SCV 21AM3076	*56.5*	*40.0*	*433*	*802*	*1209*	*22.7*	*16.3*	*511*	*14.2*	*19.0*	*537*	*166*	*4.8*	*147*	*81.2*	*105*	*7.84*	*107.11*	*3.6*	*2.1*	*8.5*	*0.8*	*8.3*
SCV 33Bi3839	*62.6*	*39.3*	*402*	*876*	*1198*	*24.0*	*13.8*	*298*	*9.1*	*12.7*	*569*	*213*	*4.9*	*251*	*64.7*	*114*	*8.31*	*99.69*	*3.6*	*2.8*	*14.3*	*0.8*	*5.0*
SCV 33Bi3872	*51.9*	*30.2*	*259*	*1929*	*789*	*15.8*	*10.7*	*3408*	*20.3*	*34.0*	*922*	*151*	*3.5*	*184*	*104*	*78.5*	*6.42*	*70.78*	*2.3*	*2.9*	*3.1*	*0.9*	*8.2*
SCV 80F4745	*51.6*	*38.9*	*510*	*956*	*1075*	*18.2*	*7.4*	*351*	*14.2*	*23.5*	*498*	*329*	*5.1*	*757*	*65.7*	*86.0*	*6.19*	*61.78*	*3.2*	*3.5*	*8.9*	*1.1*	*9.2*

Table V.4. (cont.) REE and trace elements in amber glazes measured by LA-ICP-MS. Results presented in µg/g.

	Sb	Cs	Ba	La	Ce	Pr	Nd	Sm	Eu	Gd	Tb	Dy	Ho	Er	Tm	Yb	Lu	Hf	Ta	W	Bi	Th	U
IVDJ-T 96	*870*	*3.1*	*6821*	*20.1*	*36.5*	*4.7*	*19.8*	*4.3*	*3.8*	*4.0*	*0.7*	*2.6*	*0.5*	*1.5*	*0.1*	*1.2*	*0.2*	*1.9*	*0.2*	*65.9*	*143*	*5.9*	*5.6*
IVDJ-T 133	*744*	*3.3*	*5910*	*22.4*	*42.1*	*5.2*	*21.7*	*4.6*	*1.7*	*3.1*	*0.6*	*2.9*	*0.5*	*1.4*	*0.2*	*1.2*	*0.2*	*1.9*	*0.2*	*35.8*	*519*	*5.8*	*5.4*
IVDJ-T 3683	*121*	*1.5*	*145*	*11.8*	*22.4*	*2.1*	*7.1*	*1.2*	*0.3*	*1.5*	*0.2*	*0.8*	*0.1*	*0.5*	*0.1*	*0.4*	*0.1*	*1.5*	*0.2*	*0.4*	*249*	*3.3*	*1.4*
IVDJ-T 4095	*350*	*2.9*	*261*	*5.9*	*11.1*	*1.3*	*5.5*	*1.0*	*0.3*	*1.0*	*0.2*	*0.7*	*0.1*	*0.4*	*0.0*	*0.3*	*0.1*	*0.7*	*0.1*	*2.0*	*10.4*	*2.4*	*0.5*
IVDJ-S SN	*243*	*3.8*	*84.5*	*8.2*	*15.1*	*1.7*	*6.8*	*1.2*	*0.2*	*0.8*	*0.2*	*1.0*	*0.2*	*0.6*	*0.1*	*0.6*	*0.1*	*2.0*	*0.2*	*0.8*	*6.0*	*2.2*	*0.7*
IVDJ-S 3589	*272*	*3.0*	*146*	*13.5*	*25.1*	*2.9*	*11.3*	*2.1*	*0.4*	*1.9*	*0.3*	*1.4*	*0.3*	*1.0*	*0.1*	*0.8*	*0.1*	*2.3*	*0.2*	*1.6*	*16.1*	*4.0*	*1.3*
IVDJ-S 3591	*1303*	*3.4*	*154*	*10.1*	*18.7*	*2.2*	*8.6*	*1.7*	*0.4*	*1.6*	*0.3*	*1.1*	*0.2*	*0.8*	*0.1*	*0.7*	*0.1*	*2.5*	*0.2*	*1.7*	*22.3*	*3.2*	*1.1*
IVDJ-S 3919	*45.9*	*0.8*	*213*	*5.8*	*10.5*	*1.1*	*4.7*	*0.8*	*0.2*	*0.7*	*0.1*	*0.6*	*0.1*	*0.4*	*0.0*	*0.4*	*0.1*	*1.5*	*0.1*	*4.1*	*5.5*	*1.8*	*1.1*
IVDJ-S 4078	*471*	*6.2*	*107*	*10.9*	*19.7*	*2.2*	*8.5*	*1.7*	*0.3*	*1.1*	*0.2*	*1.2*	*0.2*	*0.8*	*0.1*	*0.7*	*0.1*	*2.2*	*0.2*	*1.1*	*11.4*	*3.3*	*1.0*
IVDJ-S 4106	*358*	*8.4*	*125*	*9.4*	*15.8*	*1.8*	*7.3*	*1.4*	*0.3*	*1.0*	*0.2*	*1.1*	*0.2*	*0.7*	*0.1*	*0.6*	*0.1*	*2.0*	*0.2*	*2.2*	*17.9*	*2.5*	*0.9*
PNS05	*277*	*6.0*	*198*	*6.8*	*12.1*	*1.3*	*5.7*	*1.1*	*0.4*	*1.3*	*0.3*	*0.9*	*0.2*	*0.6*	*0.1*	*0.5*	*0.1*	*1.1*	*0.2*	*12.3*	*8.5*	*1.9*	*0.5*
PNS11	*433*	*2.9*	*60.7*	*4.8*	*8.8*	*0.9*	*3.9*	*0.8*	*0.2*	*1.0*	*0.2*	*0.6*	*0.1*	*0.5*	*0.1*	*0.4*	*0.1*	*1.2*	*0.1*	*0.9*	*11.2*	*1.5*	*0.3*
PNS21	*644*	*3.9*	*116*	*10.5*	*19.2*	*2.1*	*8.4*	*1.5*	*0.4*	*1.5*	*0.3*	*1.2*	*0.2*	*0.8*	*0.1*	*0.7*	*0.1*	*1.3*	*0.3*	*1.6*	*17.1*	*2.7*	*0.9*
PNS25	*264*	*2.5*	*151*	*10.2*	*18.8*	*2.1*	*8.1*	*1.5*	*0.4*	*1.4*	*0.3*	*1.2*	*0.2*	*0.8*	*0.1*	*0.7*	*0.1*	*2.0*	*0.3*	*1.0*	*36.5*	*2.8*	*1.0*
PNS27	*218*	*5.4*	*93.8*	*7.1*	*13.4*	*1.4*	*5.7*	*1.1*	*0.2*	*1.0*	*0.2*	*0.8*	*0.2*	*0.5*	*0.1*	*0.5*	*0.1*	*1.8*	*0.2*	*1.5*	*5.8*	*2.3*	*0.5*
PNS29	*366*	*3.0*	*124*	*7.8*	*14.3*	*1.6*	*6.5*	*1.2*	*0.3*	*1.1*	*0.2*	*1.0*	*0.2*	*0.7*	*0.1*	*0.6*	*0.1*	*1.7*	*0.2*	*1.1*	*140*	*2.3*	*1.1*
PNS38	*675*	*3.8*	*98.7*	*9.1*	*16.6*	*1.8*	*7.2*	*1.2*	*0.3*	*1.1*	*0.2*	*0.9*	*0.2*	*0.6*	*0.1*	*0.5*	*0.1*	*2.2*	*0.2*	*0.5*	*15.4*	*2.8*	*0.7*
MCV 4-1ML	*480*	*4.6*	*108*	*10.1*	*18.0*	*2.0*	*8.2*	*1.6*	*0.3*	*1.2*	*0.2*	*1.1*	*0.2*	*0.7*	*0.1*	*0.6*	*0.1*	*2.1*	*0.2*	*1.2*	*8.7*	*2.9*	*1.0*

Table V.4. (cont.) REE and trace elements in amber glazes measured by LA-ICP-MS. Results presented in µg/g.

	Sb	Cs	Ba	La	Ce	Pr	Nd	Sm	Eu	Gd	Tb	Dy	Ho	Er	Tm	Yb	Lu	Hf	Ta	W	Bi	Th	U
SCV 4I365	707	5.2	142	10.8	20.3	2.3	9.6	1.9	0.5	2.0	0.3	1.4	0.3	0.9	0.1	0.8	0.1	2.2	0.2	1.7	10.7	3.1	1.1
SCV 9I1469	373	4.2	148	10.6	19.6	2.4	9.6	1.8	0.4	1.9	0.3	1.3	0.3	0.9	0.1	0.9	0.1	2.3	0.2	1.9	9.1	3.2	1.0
SCV 10BI1673	714	3.7	122	11.6	21.5	2.4	10.0	1.9	0.4	1.7	0.3	1.5	0.3	1.0	0.1	0.9	0.1	2.4	0.3	1.8	18.2	3.5	1.2
SCV 20I2989	593	2.7	126	8.9	16.2	1.9	8.1	1.5	0.8	1.6	0.3	1.2	0.2	0.7	0.1	0.7	0.1	1.9	0.2	5.3	28.4	2.8	1.1
SCV 21AM3076	520	5.4	127	11.3	20.8	2.3	9.3	1.7	3.5	1.3	0.3	1.4	0.3	0.9	0.1	0.8	0.1	2.7	0.2	1.8	9.6	3.5	1.1
SCV 33BI3839	814	3.8	131	12.8	24.2	2.6	10.8	2.1	17.1	1.4	0.3	1.5	0.3	0.9	0.1	0.9	0.1	2.5	0.2	2.0	9.2	3.7	1.2
SCV 33BI3872	483	5.3	362	8.5	14.5	1.8	7.8	1.6	0.5	1.6	0.3	1.3	0.3	0.8	0.1	0.7	0.1	1.9	0.2	7.8	16.3	2.3	0.9
SCV 80F4745	624	3.5	121	9.2	18.3	1.8	7.3	1.3	0.3	1.3	0.2	1.2	0.2	0.7	0.1	0.7	0.1	1.7	0.2	7.9	227	2.3	1.4

Table V.5. REE and trace elements in brown glazes measured by LA-ICP-MS. Results are presented in µg/g.

	Li	B	P	Ti	V	Cr	Mn	Fe	Co	Ni	Cu	Zn	Ga	As	Rb	Sr	Y	Zr	Nb	Mo	Ag	Cd
IVDJ-T 3683	85.6	35.7	335	630	20.0		47773	13401	135	65.3	1369	318	9.5	1285	44.8	482	9.4	33.0	2.4	27.4	19.6	0.9
IVDJ-S SN	21.4	23.1	229	864	11.5	5.6	32828	5727	55.4	30.0	591	76.0	3.4	11.1	38.8	445	6.9	60.4	2.3	11.6	17.8	0.6
IVDJ-S 3576	36.0	31.2	315	953	21.7	1.9	25345	8579	179	85.9	847	65.7	5.2	41.8	49.4	244	18.5	82.5	2.6	17.8	4.7	0.4
IVDJ-S 3589	49.5	53.6	575	1328	31.2	5.0	25246	13846	34.6	28.8	660	94.6	6.0	136	59.4	274	22.6	121	3.7	5.3	9.9	0.7
IVDJ-S 3718	102	18.0	299	878	22.9		31577	12051	472	110	4461	431	7.9	22.6	67.8	124	9.9	49.3	3.0	2.0	13.9	2.2
IVDJ-S 3774	36.6	28.1	371	960	18.5	8.0	29766	8037	38.8	27.1	457	104	5.5	92.2	57.8	335	12.8	61.5	2.9	6.6	9.8	0.3
IVDJ-S 3919	18.4	26.1	316	499	23.3	3.4	20806	8572	989	715	1477	307	2.7	57.7	20.5	123	3.1	35.3	1.4	57.0	24.6	0.8
IVDJ-S 4127	26.1	22.7	301	1041	20.5	2.3	44169	3546	280	89.5	521	69.6	3.7	364	35.7	140	10.3	67.9	3.0	8.5	23.1	0.6
PNS07	96.6	65.8	3380	1288	23.7	11.6	20401	9258	121	79.0	2522	56.4	5.9	53.7	135	227	14.4	120	3.4	8.7	8.7	1.0
PNS08	68.9	35.7	119	727	14.3	7.5	19841	6402	72.2	73.8	2294	54.6	3.8	52.7	101	153	9.8	42.8	1.9	4.5	20.3	0.7
PNS09	68.9	25.9	44.2	726	13.2	6.4	14966	13741	73.1	57.0	1917	26.4	3.3	45.5	110	165	8.7	55.8	2.0	4.2	47.2	1.0
PNS10	45.6	18.1	96	683	13.3	6.3	16545	5125	90.0	71.3	2931	21.3	3.2	52.5	72.9	127	9.6	44.4	1.9	5.9	36.6	0.7
PNS11	25.8	33.3	338	1016	15.2	10.0	26944	6140	58.6	27.2	1411	85.8	3.5	16.4	71.7	614	6.6	67.0	2.4	9.3	47.3	1.5
PNS13	32.1	42.6	112	569	5.4	1.2	150	3315	2.6	15.5	257	21.5	1.4	5.3	122	38.6	2.8	19.9	2.9	0.2	40.0	0.5
PNS19	40.5	51.1	932	1342	26.7	10.0	25255	11445	97.1	59.7	1074	144	5.8	24.1	63.4	438	9.9	93.1	3.8	9.0	6.2	0.5
PNS21	49.0	29.1	325	1115	32.5	3.7	24755	12602	21.2	23.2	697	46.8	6.1	129	67.6	256	19.6	85.3	3.6	3.1	6.7	0.6

Table V.5. (cont.) REE and trace elements in brown glazes measured by LA-ICP-MS. Results are presented in µg/g.

	Li	B	P	Ti	V	Cr	Mn	Fe	Co	Ni	Cu	Zn	Ga	As	Rb	Sr	Y	Zr	Nb	Mo	Ag	Cd
PNS22	31.8	33.7	140	1271	19.5	3.1	24021	7468	864	266	1295	55.2	4.4	972	37.2	215	8.0	61.3	3.3	12.6	4.9	0.5
PNS23	27.1	29.2	305	1175	21.4	6.2	30873	9067	35.1	30.8	709	99.8	4.7	39.3	76.6	359	11.9	92.9	3.1	6.3	5.7	0.4
PNS24	21.7	35.4	736	1174	27.1	10.2	18293	11522	804	572	1491	45.5	6.0	94.3	50.3	152	18.2	85.0	3.5	64.7	10.5	0.6
PNS25	37.2	39.5	1044	1143	34.7	6.8	18027	6588	293	28.3	351	96.6	4.5	46.7	46.7	149	6.8	76.2	3.8	2.1	3.5	1.6
PNS28	42.3	44.0	198	998	22.6	8.2	32166	9811	44.8	36.3	883	103	4.3	39.7	66.8	372	13.0	99.6	2.6	6.9	5.2	0.6
PNS29	34.4	45.2	1168	1123	36.6	9.8	18172	6350	334	30.0	646	114	4.4	113	55.9	165	7.3	79.9	3.5	3.0	3.0	1.7
PNS30	61.6	20.0	2370	306	81.1	9.8	15402	3159	18.3	22.7	1704	68.8	2.3	96.0	165	68.0	2.4	10.0	2.4	2.7	17.0	0.6
PNS31	32.0	17.3	157	903	13.6	5.5	20224	15469	43.7	34.9	1722	35.2	3.2	35.0	65.4	98.6	12.8	89.7	2.4	3.0	14.8	0.6
PNS33	22.5	32.8	736	963	18.5	4.5	15491	10378	317	140	5114	57.0	4.2	75.4	44.4	146	11.6	74.2	3.0	24.5	30.0	0.3
PNS34	54.5	56.2	1080	1199	23.4	6.4	20525	9191	64.7	71.6	4610	64.3	4.9	61.0	62.5	193	16.0	138	3.4	4.3	48.2	0.4
PNS36	24.9	21.1	239	990	21.3	0.3	30592	9248	40.8	28.5	734	88.1	4.2	36.7	45.7	377	12.0	66.6	2.9	7.1	9.8	0.3
PNS38	42.4	23.8	230	946	15.0	2.4	12783	5598	45.1	55.0	660	22.9	3.3	45.6	79.2	133	10.3	81.4	2.8	3.3	14.1	0.3
MCV 1-1R	60.7	29.2	241	579	20.1	6.3	47034	7941	426	468	805	151	7.0	68.1	281	264	12.4	28.4	2.0	14.5	6.6	1.1
MCV 4-1ML	60.2	51.2	542	1031	20.6	7.3	21174	16627	34.2	37.0	2144	68.9	4.9	80.7	101	175	13.6	99.3	3.1	1.9	4.3	0.9
MCV 8-1G	144	26.1	154	490	12.9	4.3	28496	4400	214	107	711	84.9	3.7	48.7	203	306	6.1	23.2	1.6	11.8	15.1	0.8
SAC 01	57.7	60.9	224	950	50.8	10.0	21005	6004	111	35.8	1952	2843	7.2	142	32.4	528	12.7	24.2	2.9	8.3	41.0	1.3
SAC 02	47.6	53.8	473	691	33.2	7.3	17331	7388	116	37.9	2025	2794	5.7	83.7	35.0	385	9.2	24.8	2.3	6.8	30.6	2.0
SCV 10Bi1673	57.6	29.1	269	1186	31.2	11.9	25037	14215	33.2	38.5	1515	40.7	6.3	35.5	81.7	215	24.3	129	3.6	3.8	5.9	0.5
SCV 32M3685	67.9	30.7	258	1017	26.4	5.6	25978	11730	34.4	53.7	1920	38.5	5.1	55.9	107	232	21.1	76.5	3.0	7.3	5.7	1.0
SCV 33Bi3839	73.6	39.9	356	1044	30.0	9.7	25778	13716	25.7	23.4	530	54.1	5.8	138	83.4	226	22.0	92.5	3.2	3.6	3.4	0.4
SCV 33Bi3872	70.8	46.2	479	990	30.1	8.0	26877	13160	24.2	31.9	608	53.8	6.1	102	89.6	245	21.1	101	2.8	7.4	2.4	0.9
SCV 45M4260	68.1	40.7	545	1032	43.1	11.9	40619	17973	118	119	886	60.8	7.2	86.5	80.0	397	30.2	61.1	3.1	10.1	6.5	1.1
SCV 80F4745	59.2	71.2	518	1042	62.5		74563	12188	62.7	43.2	2171	299	9.1	398	68.5	248	10.9	42.1	3.5	15.6	5.9	1.8

Table V.5. (cont.) REE and trace elements in brown glazes measured by LA-ICP-MS. Results are presented in µg/g.

	In	Sb	Cs	Ba	La	Ce	Pr	Nd	Sm	Eu	Gd	Tb	Dy	Ho	Er	Tm	Yb	Lu	Hf	Ta	W	Bi	Th	U
IVDJ-T 3683	138	48.3	1.4	1764	11.7	24.0	2.4	10.4	2.1	1.7	2.6	0.5	1.9	0.4	1.0	0.1	0.9	0.1	1.1	0.2	1.3	482	3.3	5.3
IVDJ-S SN	14.4	162	2.3	1118	7.6	12.3	1.6	6.7	1.3	0.4	1.0	0.2	1.3	0.2	0.6	0.1	0.6	0.1	1.6	0.2	1.0	5.7	1.9	3.5

Table V.5. (cont.) REE and trace elements in brown glazes measured by LA-ICP-MS. Results are presented in μg/g.

	In	Sb	Cs	Ba	La	Ce	Pr	Nd	Sm	Eu	Gd	Tb	Dy	Ho	Er	Tm	Yb	Lu	Hf	Ta	W	Bi	Th	U
IVDJ-S 3576	15.6	409	2.9	1275	15.7	20.5	3.1	13.3	2.7	1.2	2.7	0.6	2.8	0.6	1.7	0.2	1.4	0.2	2.3	0.2	28.9	8.1	3.1	1.2
IVDJ-S 3589	16.2	170	3.5	2140	18.6	24.9	3.8	16.0	3.1	1.4	2.8	0.7	3.4	0.7	2.0	0.2	1.6	0.2	3.2	0.3	91.7	8.8	4.0	1.1
IVDJ-S 3718	27.1	447	3.9	1148	15.4	35.2	3.8	16.0	3.2	1.2	2.9	0.6	2.2	0.4	1.3	0.1	0.8	0.1	1.3	0.2	4.8	7.5	3.8	2.0
IVDJ-S 3774	4.0	373	3.8	1530	17.8	29.2	3.6	14.3	2.8	0.7	2.1	0.4	2.1	0.4	1.2	0.1	0.9	0.1	1.6	0.2	20.5	4.9	4.0	2.6
IVDJ-S 3919	18.8	37	0.8	703	4.6	8.3	0.9	3.7	0.7	0.3	0.6	0.1	0.6	0.1	0.4	0.0	0.4	0.1	0.9	0.1	4.2	5.7	1.4	0.6
IVDJ-S 4127	13.0	147	2.0	1243	8.3	17.1	1.6	6.5	1.3	0.5	1.0	0.3	1.3	0.3	0.9	0.1	0.7	0.1	1.8	0.2	99.4	6.4	2.3	1.0
PNS07	15.1	133	6.3	1196	14.3	23.8	3.1	13.3	2.7	2.2	3.7	0.7	2.6	0.5	1.8	0.2	1.3	0.2	3.1	0.2	21.3	17.3	3.0	0.9
PNS08	175	192	4.3	1055	8.0	11.7	1.6	7.3	1.6	1.7	2.1	0.5	1.7	0.3	1.1	0.1	0.8	0.1	1.2	0.1	17.6	71.3	1.6	0.6
PNS09	160	158	5.7	906	7.4	14.6	1.5	6.6	1.5	1.4	1.9	0.4	1.6	0.3	1.0	0.1	0.7	0.1	1.4	0.1	27.3	35.2	1.5	0.5
PNS10	197	197	3.6	860	7.0	11.6	1.5	6.5	1.5	1.4	1.8	0.4	1.6	0.3	1.0	0.1	0.8	0.1	1.2	0.1	18.3	66.2	1.5	0.5
PNS11	2.9	439	3.6	1392	7.2	12.1	1.6	6.4	1.4	1.6	1.7	0.3	1.3	0.2	0.8	0.1	0.6	0.1	1.7	0.2	0.7	11.5	1.8	2.8
PNS13	258	33.6	8.5	41.0	3.5	5.9	0.7	3.1	0.6	0.1	0.8	0.2	0.5	0.1	0.4	0.0	0.3	0.0	0.5	0.2	0.4	10.4	1.1	0.3
PNS19	14.9	470	4.0	1400	12.7	20.6	2.7	10.8	2.2	1.5	2.4	0.5	1.8	0.4	1.2	0.1	1.0	0.1	2.4	0.3	19.7	25.7	3.2	2.3
PNS21	10.8	637	3.7	1989	16.0	20.7	3.3	14.5	3.0	1.9	2.7	0.7	3.4	0.7	1.9	0.2	1.4	0.2	2.1	0.3	74.3	9.5	3.2	1.0
PNS22	38.3	359	2.0	1160	10.0	16.8	2.1	8.2	1.6	1.0	1.6	0.3	1.5	0.3	0.9	0.1	0.8	0.1	1.7	0.2	11.2	5748	2.4	1.4
PNS23	6.6	664	2.9	1861	14.0	20.0	2.9	12.2	2.7	1.7	2.4	0.5	2.1	0.4	1.3	0.2	1.0	0.1	2.2	0.2	41.7	70.1	3.1	2.0
PNS24	5.8	361	2.9	1356	17.4	22.4	3.5	15.0	3.1	1.4	2.7	0.7	3.1	0.6	1.8	0.2	1.4	0.2	2.2	0.2	58.9	9.1	3.2	0.9
PNS25	13.2	97	2.2	221	10.5	18.2	2.0	8.1	1.6	0.4	1.4	0.3	1.3	0.2	0.8	0.1	0.6	0.1	1.8	0.2	0.6	33.4	2.8	0.7
PNS28	5.1	707	2.7	1863	14.7	21.8	3.0	12.7	2.5	1.5	2.3	0.5	2.4	0.5	1.4	0.2	1.1	0.2	2.4	0.2	43.4	62.8	3.1	2.9
PNS29	5.9	102	3.6	232	9.8	17.3	1.9	7.6	1.4	0.4	1.4	0.3	1.3	0.3	0.8	0.1	0.8	0.1	2.0	0.2	0.6	87.0	2.4	0.8
PNS30	177	450	20.4	290	4.4	6.0	0.9	3.4	0.6	0.3	0.6	0.1	0.4	0.1	0.3	0.0	0.2	0.0	0.3	0.1	2.6	8.9	0.8	0.5
PNS31	26.7	495	3.4	609	10.7	16.0	2.2	9.2	1.9	0.7	1.6	0.4	2.1	0.4	1.3	0.2	1.1	0.2	2.1	0.2	14.9	24.6	2.3	0.7
PNS33	62.7	355	2.4	913	11.3	15.7	2.3	9.1	1.9	0.8	1.7	0.4	2.0	0.4	1.1	0.1	0.9	0.1	1.9	0.2	27.3	27.4	2.2	0.7
PNS34	31.2	167	3.0	1159	15.4	22.8	3.1	13.4	2.5	1.1	2.2	0.5	2.5	0.5	1.5	0.2	1.3	0.2	3.3	0.2	28.4	13.4	3.4	1.0
PNS36	4.5	291	2.5	1733	11.5	17.3	2.4	9.8	2.1	1.1	1.6	0.4	2.1	0.4	1.1	0.1	0.9	0.1	1.6	0.2	33.4	6.7	2.5	2.4
PNS38	141	206	3.4	721	10.5	16.7	2.2	8.4	1.6	0.6	1.3	0.3	1.6	0.3	0.9	0.1	0.8	0.1	2.0	0.2	15.8	39.2	2.3	0.7
MCV 1-1R	87.7	78.1	30.6	485	9.0	17.5	1.9	8.1	1.9	0.7	1.6	0.4	1.8	0.3	0.9	0.1	0.8	0.1	0.8	0.2	18.1	8.4	2.8	9.6
MCV 4-1ML	21.0	441	6.3	914	15.0	22.8	3.1	12.9	2.5	0.7	2.1	0.4	2.2	0.5	1.3	0.2	1.1	0.2	2.3	0.2	14.9	8.0	3.1	1.0

Table V.5. (cont.) REE and trace elements in brown glazes measured by LA-ICP-MS. Results are presented in µg/g.

	In	Sb	Cs	Ba	La	Ce	Pr	Nd	Sm	Eu	Gd	Tb	Dy	Ho	Er	Tm	Yb	Lu	Hf	Ta	W	Bi	Th	U
MCV 8-1G	*114*	*580*	*15.5*	*1100*	*7.8*	*11.6*	*1.6*	*7.1*	*1.5*	*0.6*	*1.4*	*0.3*	*1.2*	*0.2*	*0.6*	*0.1*	*0.5*	*0.0*	*0.7*	*0.1*	*0.5*	*4.9*	*1.9*	*3.8*
SAC 01	*31.0*	*517*	*1.4*	*643*	*19.3*	*35.7*	*4.5*	*19.4*	*4.2*	*1.2*	*3.6*	*0.6*	*2.9*	*0.5*	*1.5*	*0.2*	*1.2*	*0.1*	*0.7*	*0.3*	*34.5*	*72.3*	*3.4*	*7.6*
SAC 02	*52.5*	*431*	*1.4*	*600*	*14.3*	*25.6*	*3.1*	*13.3*	*3.0*	*0.8*	*2.4*	*0.5*	*2.2*	*0.4*	*1.1*	*0.1*	*0.9*	*0.1*	*0.7*	*0.3*	*46.9*	*22.2*	*2.1*	*7.7*
SCV 10Bi1673	*4.7*	*812*	*4.9*	*1722*	*18.4*	*22.0*	*3.7*	*16.1*	*3.5*	*1.2*	*3.0*	*0.7*	*3.6*	*0.8*	*2.1*	*0.3*	*1.7*	*0.2*	*2.7*	*0.3*	*76.5*	*12.1*	*2.6*	*1.0*
SCV 32M3685	*8.3*	*390*	*6.0*	*2016*	*14.3*	*16.5*	*2.9*	*12.8*	*2.8*	*1.1*	*2.5*	*0.6*	*3.5*	*0.7*	*1.9*	*0.2*	*1.6*	*0.2*	*1.9*	*0.2*	*78.2*	*17.6*	*2.5*	*0.9*
SCV 33Bi3839	*19.4*	*561*	*4.2*	*1882*	*17.2*	*23.7*	*3.4*	*14.3*	*3.0*	*4.6*	*2.3*	*0.6*	*3.6*	*0.7*	*1.9*	*0.2*	*1.6*	*0.2*	*2.1*	*0.2*	*66.8*	*6.0*	*3.4*	*1.0*
SCV 33Bi3872	*6.6*	*212*	*4.7*	*2014*	*16.4*	*19.9*	*3.3*	*14.7*	*3.3*	*1.5*	*3.2*	*0.7*	*3.9*	*0.8*	*2.3*	*0.3*	*1.7*	*0.2*	*2.4*	*0.2*	*65.1*	*16.6*	*3.1*	*0.9*
SCV 45M4260	*11.4*	*622*	*4.4*	*3805*	*18.6*	*14.3*	*3.6*	*16.0*	*3.4*	*2.4*	*4.1*	*0.8*	*4.4*	*0.9*	*2.6*	*0.3*	*2.1*	*0.3*	*1.6*	*0.2*	*126*	*28.3*	*2.0*	*1.1*
SCV 80F4745	*39.7*	*190*	*4.6*	*5122*	*13.7*	*11.4*	*2.6*	*11.1*	*2.1*	*1.7*	*2.2*	*0.3*	*1.4*	*0.3*	*0.9*	*0.1*	*0.8*	*0.1*	*1.2*	*0.2*	*1182*	*561*	*2.4*	*102*

APPENDIX VI

μ-RAMAN SPECTRA

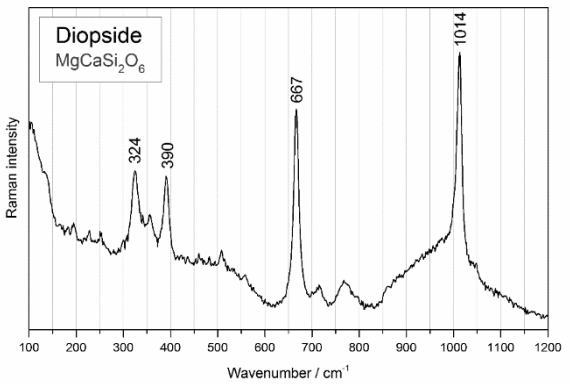

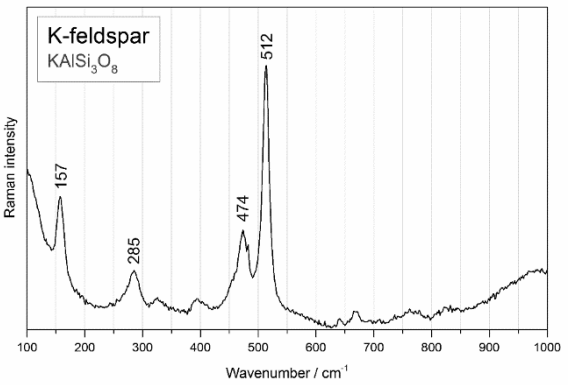

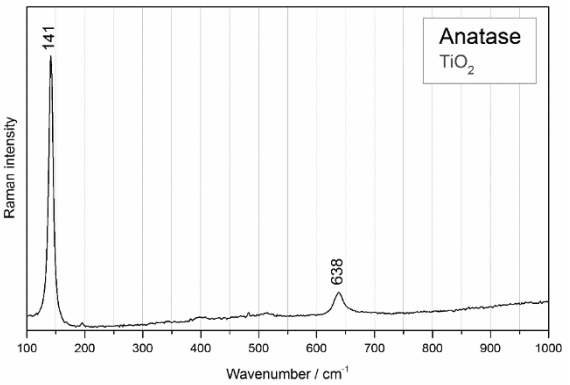

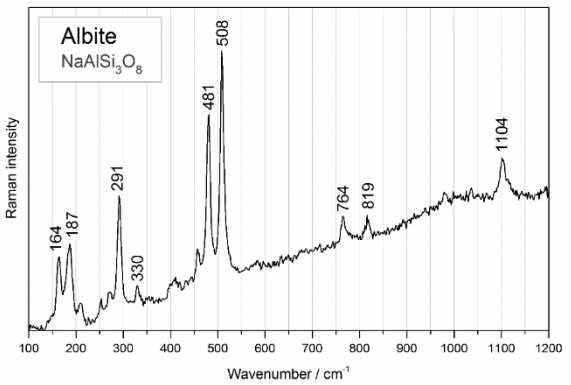

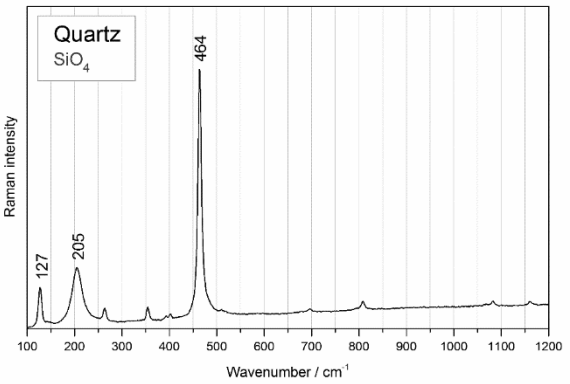

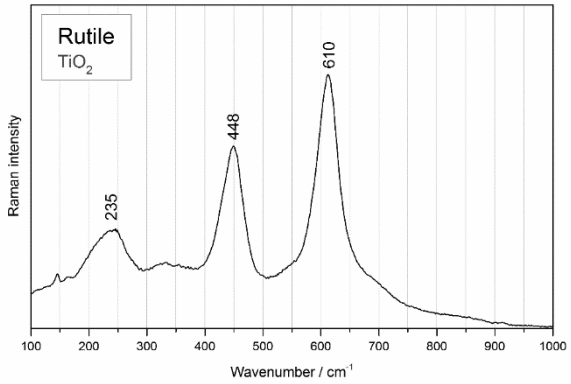

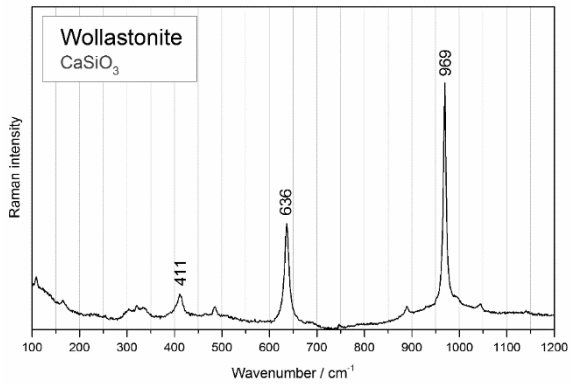

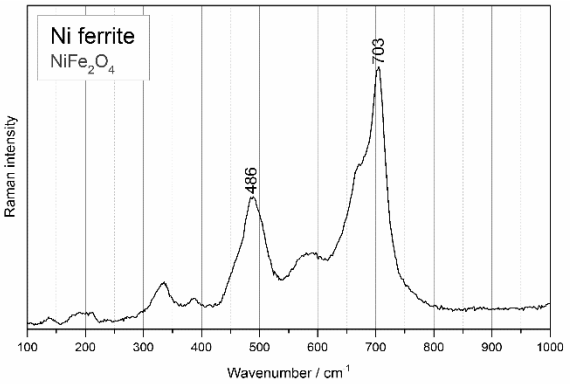

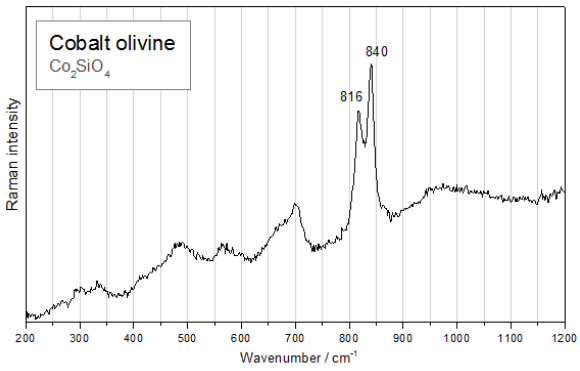
Cobalt olivine
Co_2SiO_4
840
816
Raman intensity
200 300 400 500 600 700 800 900 1000 1100 1200
Wavenumber / cm^{-1}

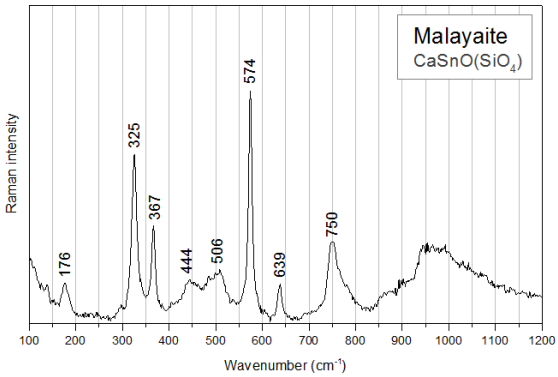
Malayaite
$CaSnO(SiO_4)$
176
325
367
444
506
574
639
750
Raman intensity
100 200 300 400 500 600 700 800 900 1000 1100 1200
Wavenumber (cm^{-1})

APPENDIX VII
SEM-EDS ANALYSES

VII.1. MONASTERY OF SANTA CLARA-A-VELHA, COIMBRA, PORTUGAL (SCV)

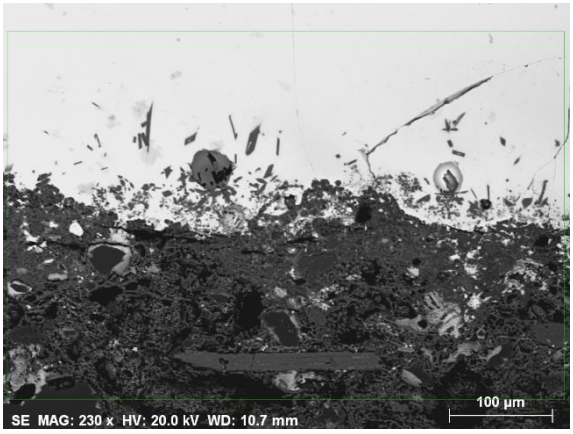

SCV 4i365 amber

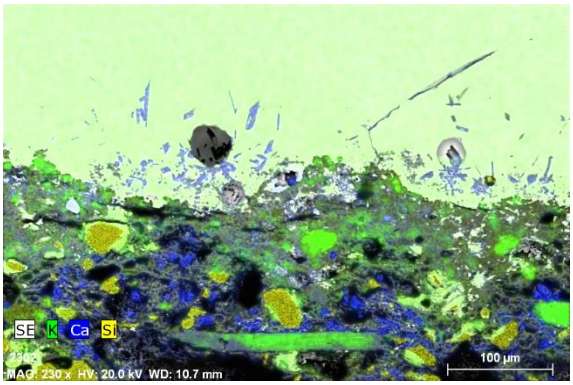

SCV 4i365 amber – EDS map

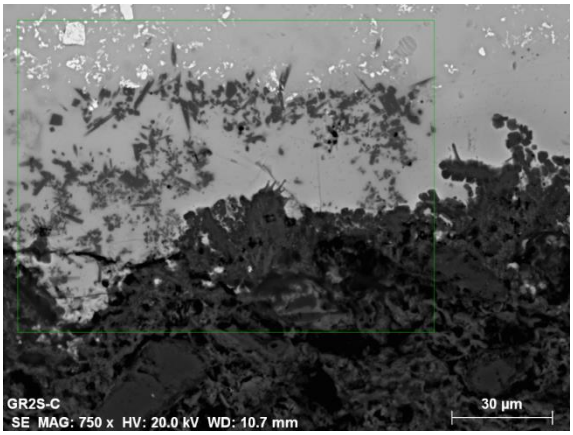

SCV 4i365 blue

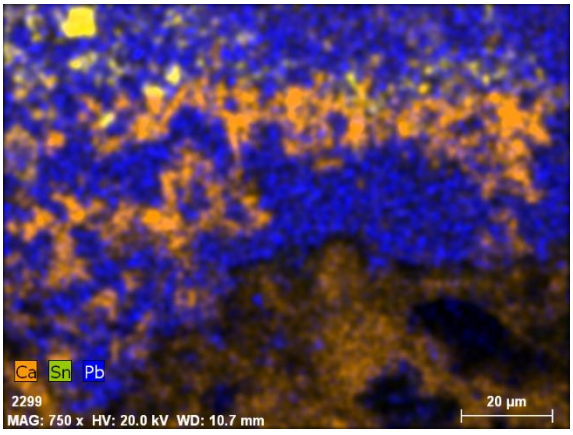

SCV 4i365 blue – EDS map

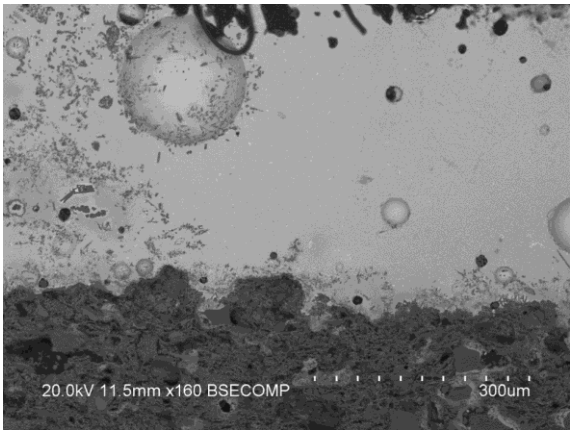

SCV 10EF175 white

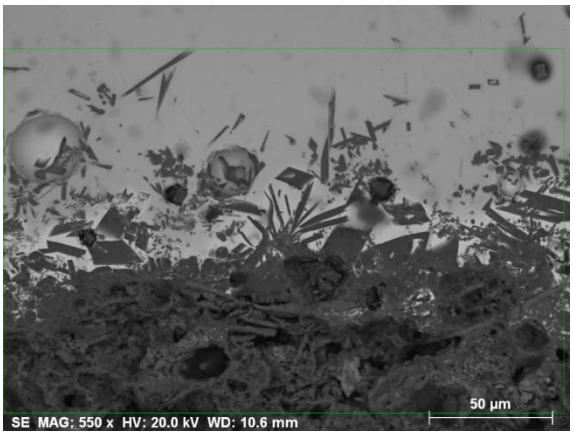

SCV 10EF175 green

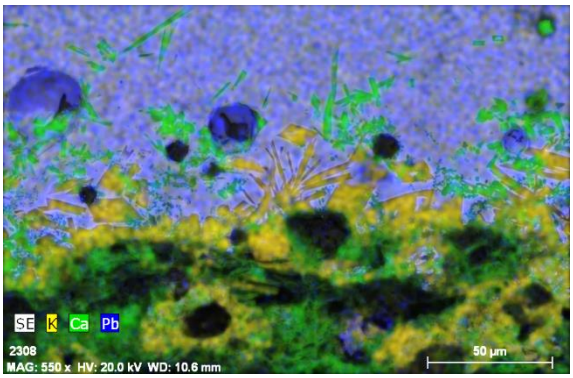

SCV 10EF175 green – EDS map

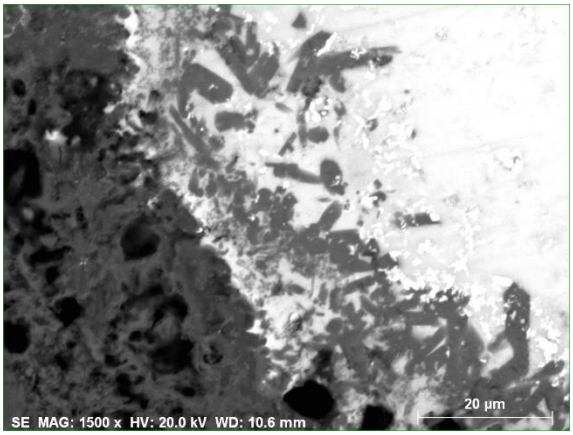

SCV 14i2580 blue

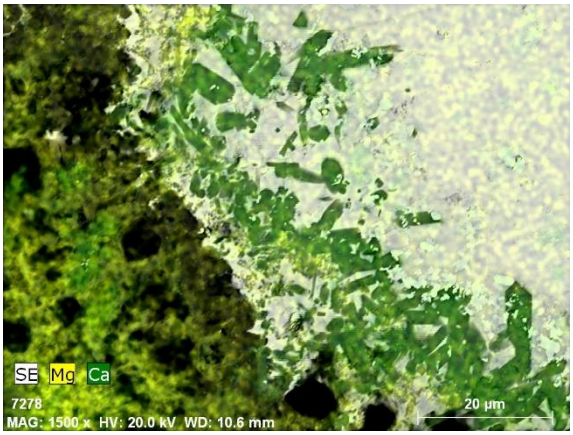

SCV 14i2580 blue – EDS map

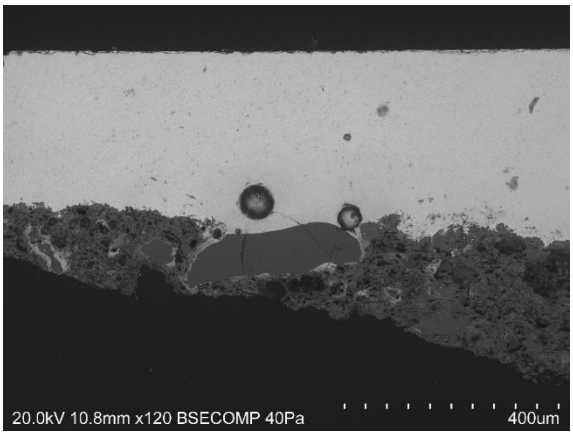

SCV 14i2580 amber

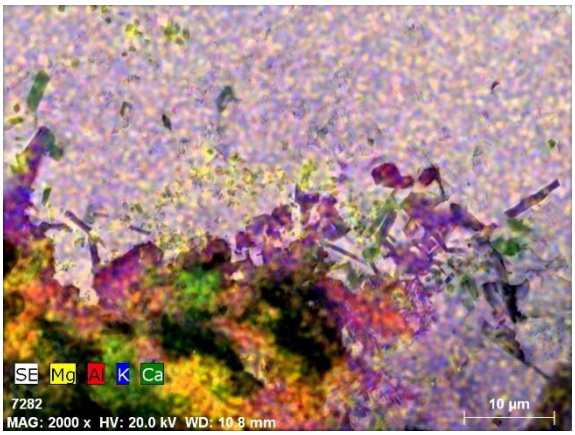

SCV 14i2580 amber – EDS map

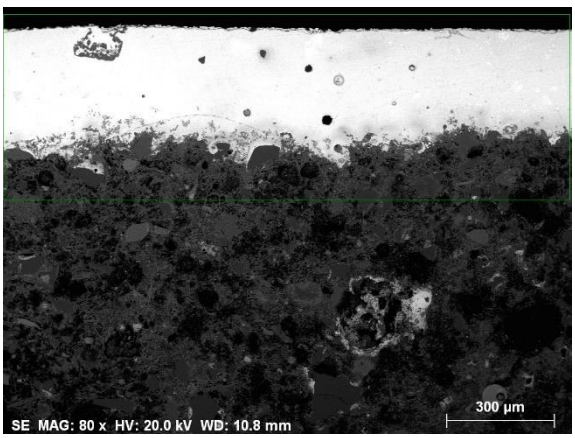

SCV 14i2580 white

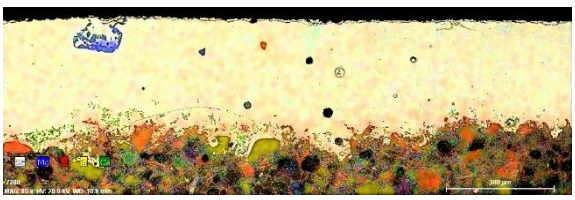

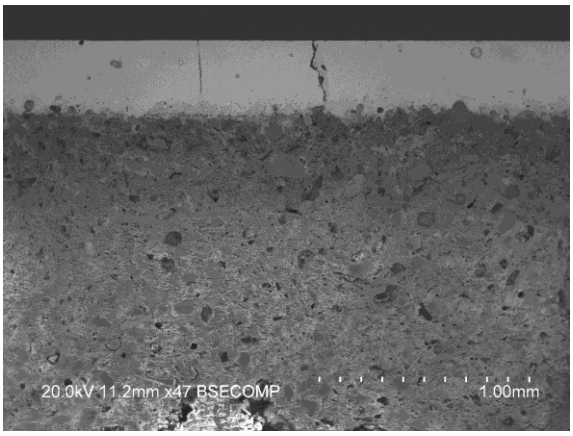

SCV 20i2989 - white

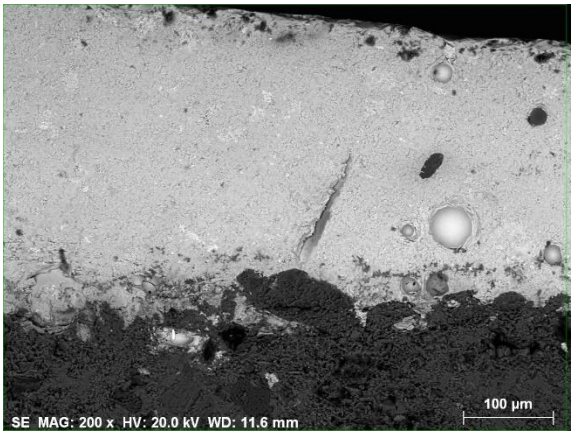

SCV 21AM3076 blue

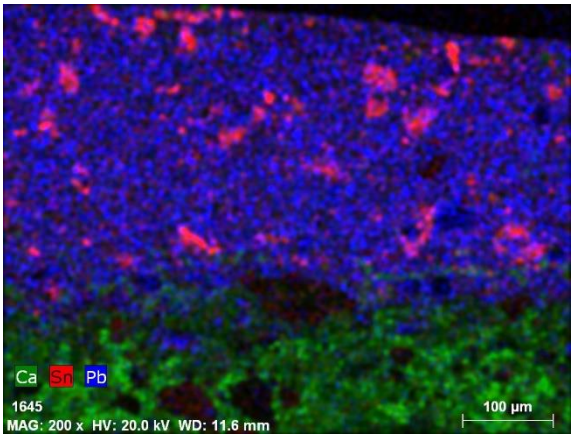

SCV 21AM3076 blue – EDS map

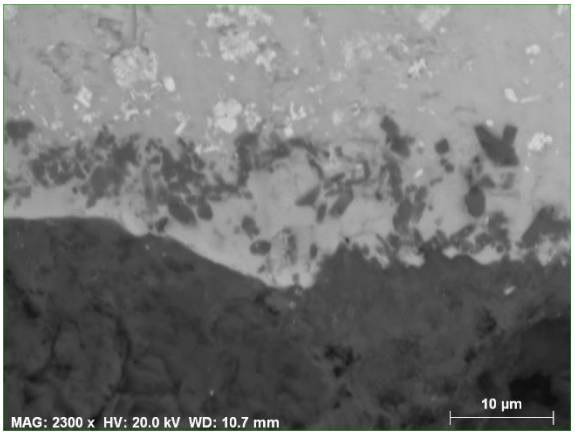

SCV 24Ci3386 white

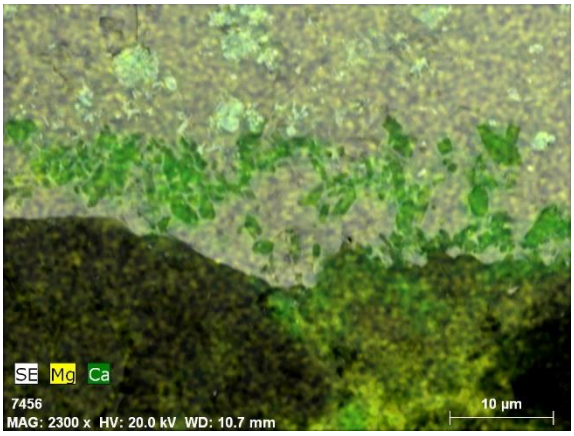

SCV 24Ci3386 white – EDS map

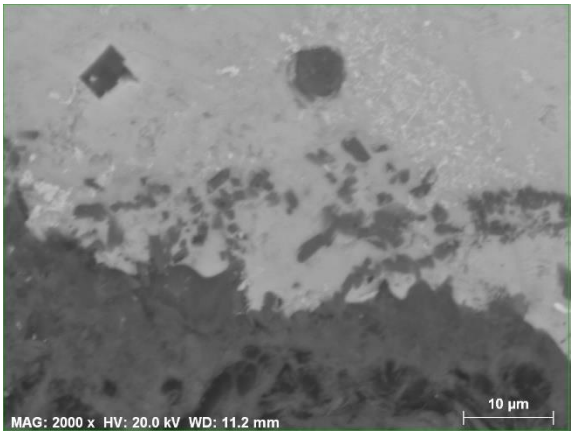

SCV 24Ci3386 green

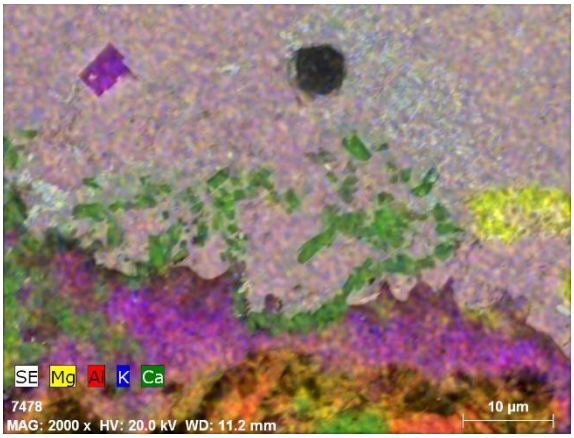

SCV 24Ci3386 green – EDS map

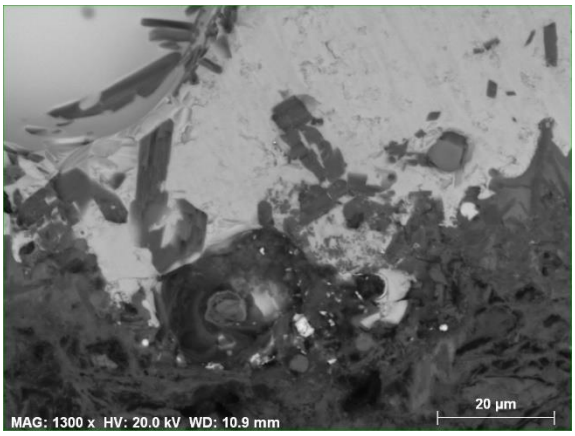

SCV 24Ci3386 amber

SCV 24Ci3386 amber – EDS map

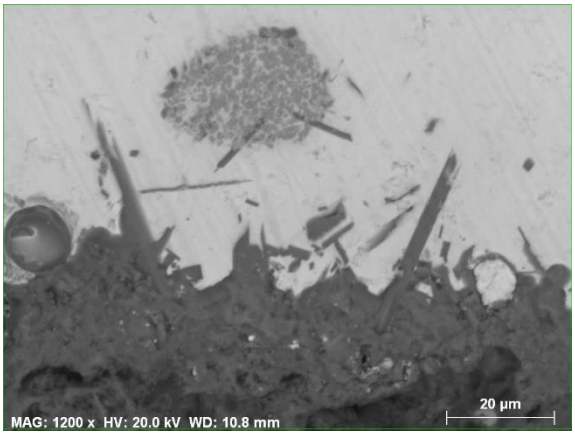

SCV 24Ci3386 brown

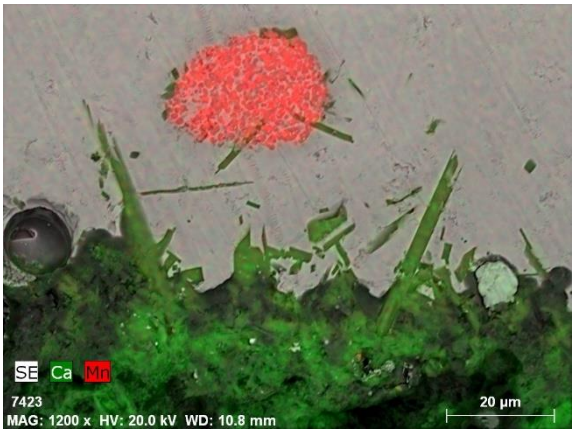

SCV 24Ci3386 brown – EDS map

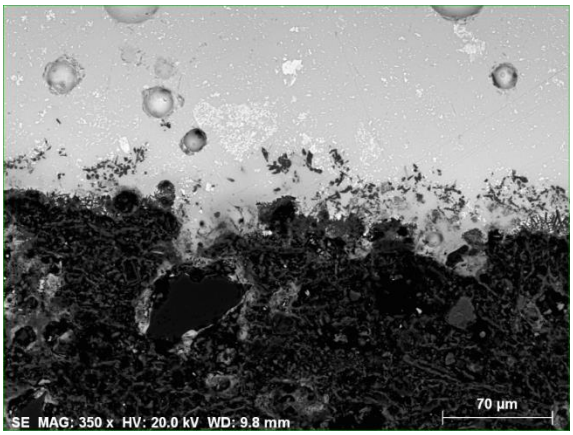

SCV 27i3426 white

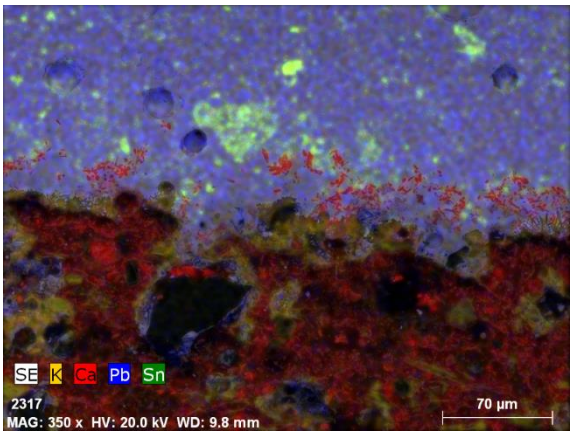

SCV 27i3426 white – EDS map

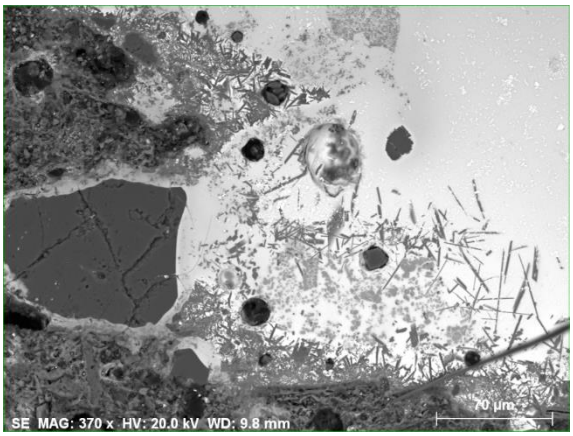

SCV 27i3426 brown

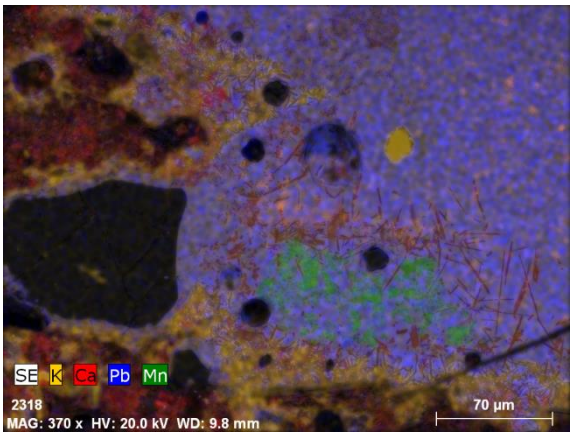

SCV 27i3426 brown – EDS map

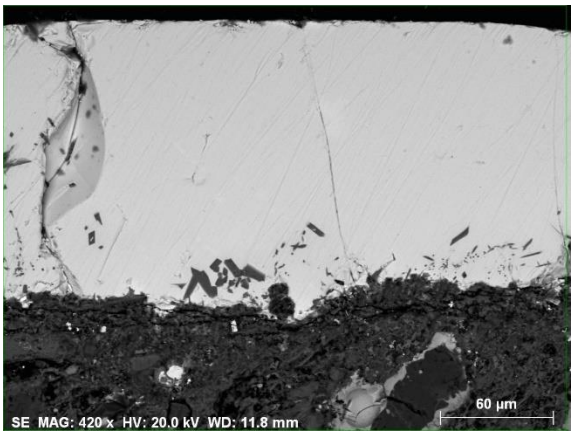

SCV 33Bi3839 amber

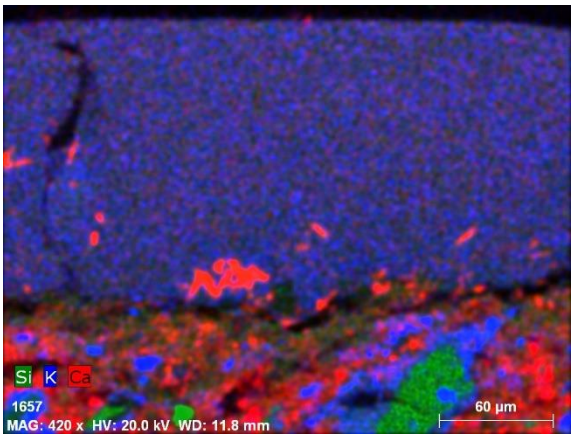

SCV 33Bi3839 amber – EDS map

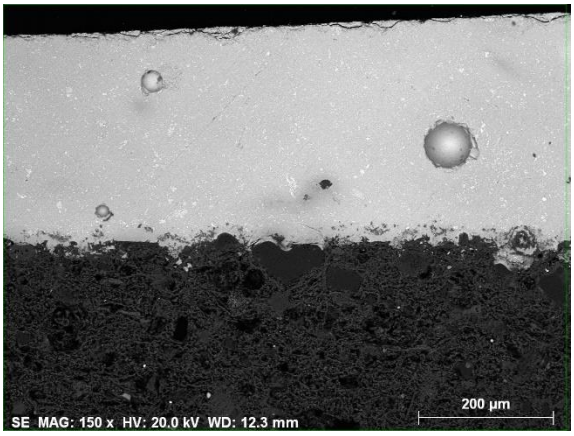

SCV 33Bi3839 blue

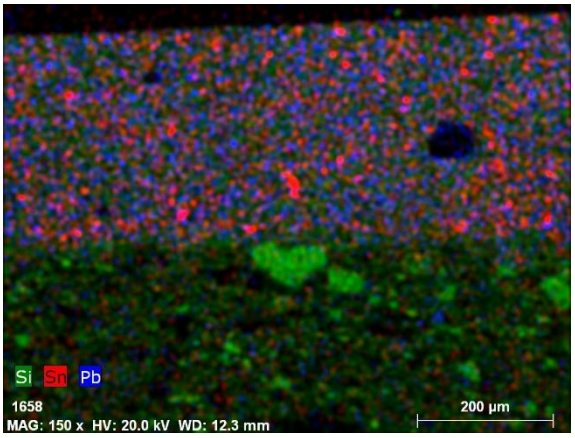

SCV 33Bi3839 blue – EDS map

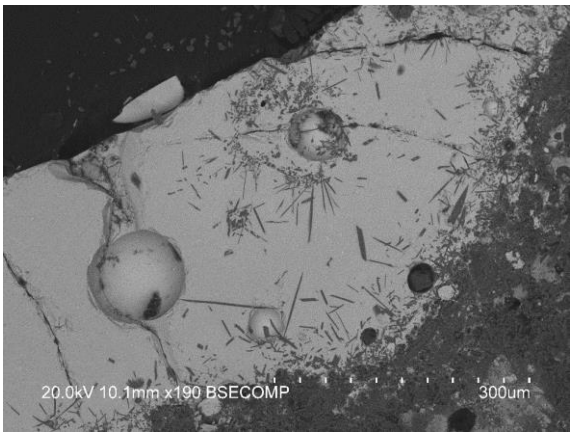

SCV 33Bi3839 - brown

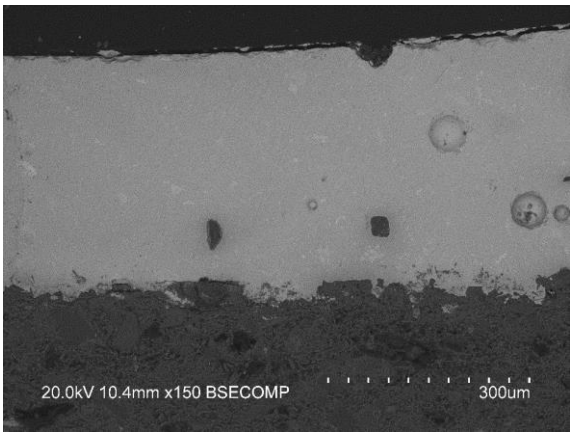

SCV 33Bi3839 - white

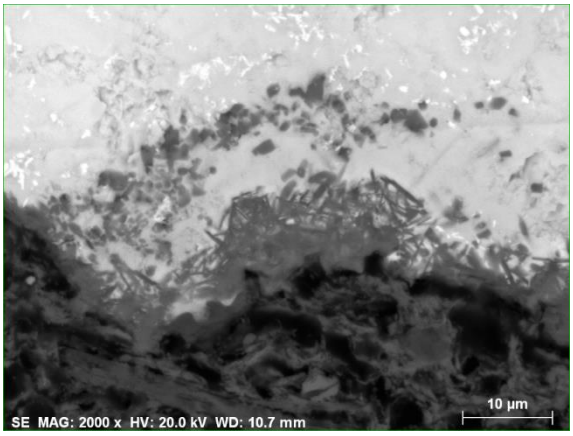

SCV 34Ai4057 white

SCV 34Ai4057 white – EDS map

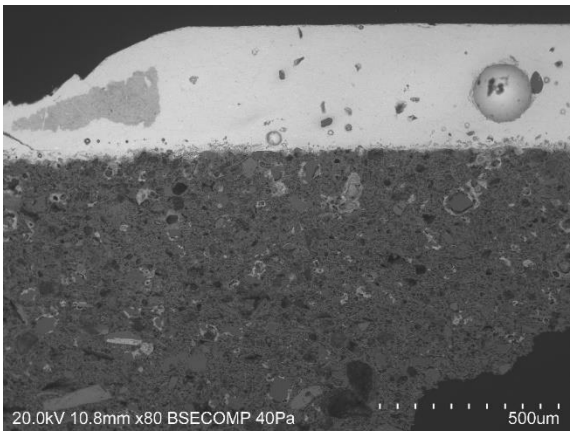

SCV 34Ai4057 blue

SCV 34Ai4057 blue – EDS map

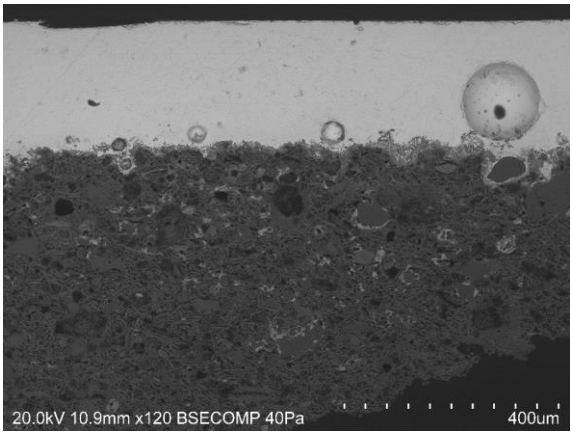

SCV 34Ai4057 green

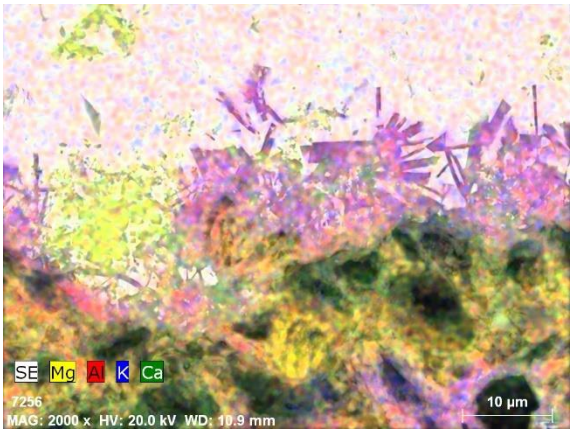

SCV 34Ai4057 green – EDS map

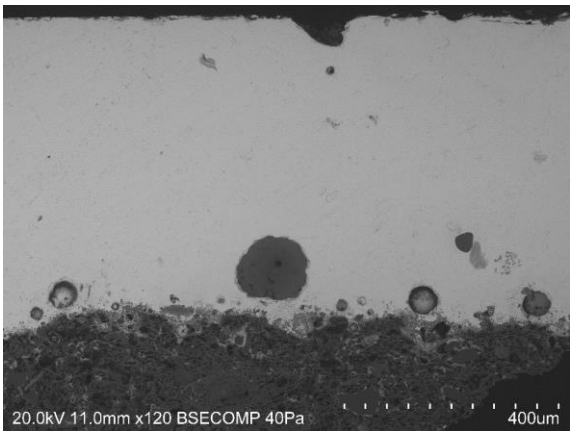

SCV 34Ai4057 amber

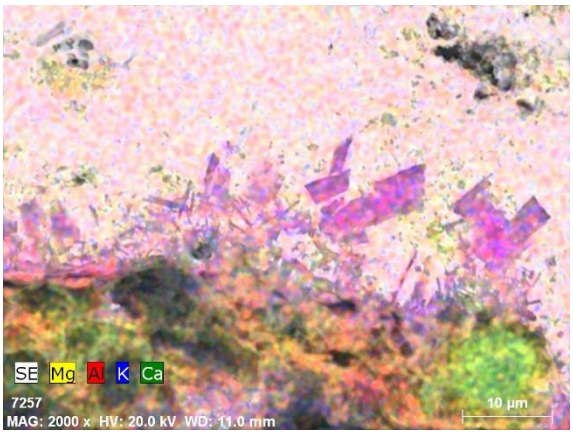

SCV 34Ai4057 green – EDS map

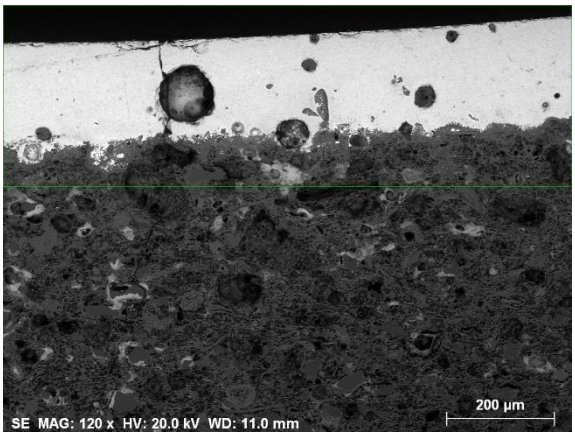

SCV 34Ci4065 green

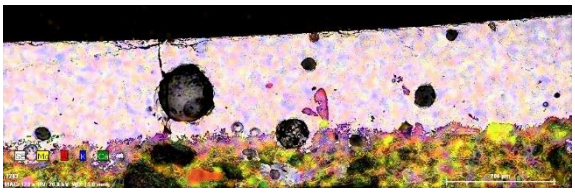

SCV 34Ci4065 green – EDS map

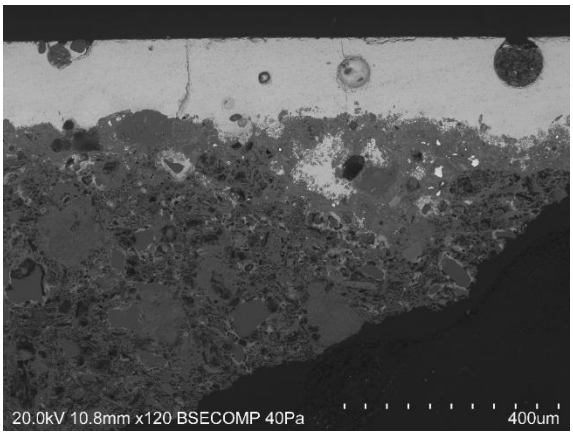

SCV 34Ci4065 amber

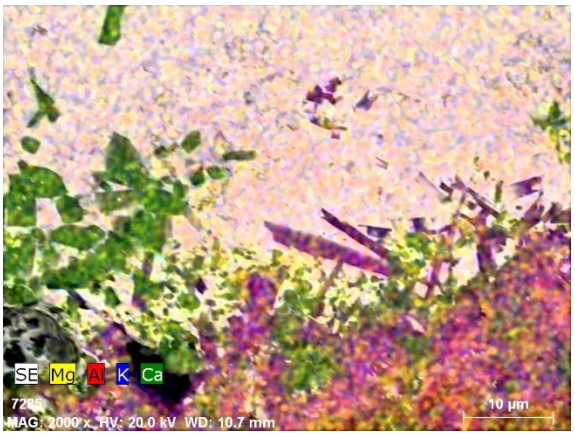

SCV 34Ci4065 amber – EDS map

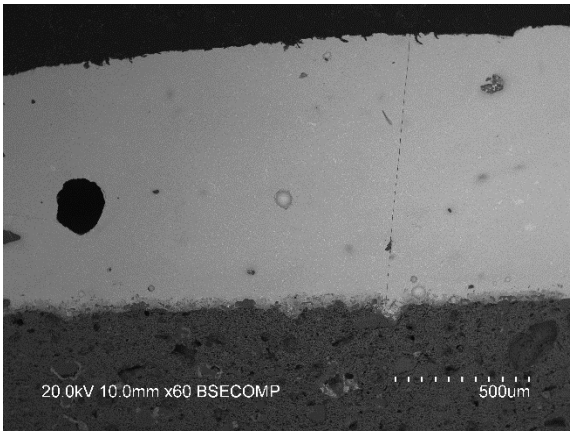

SCV 45M4260 - white

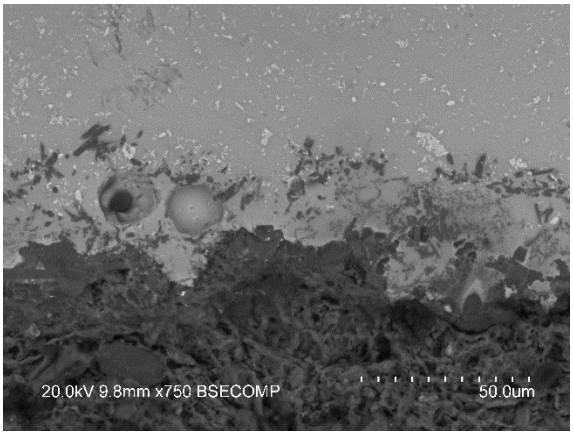

SCV 45M4260 – white (detail)

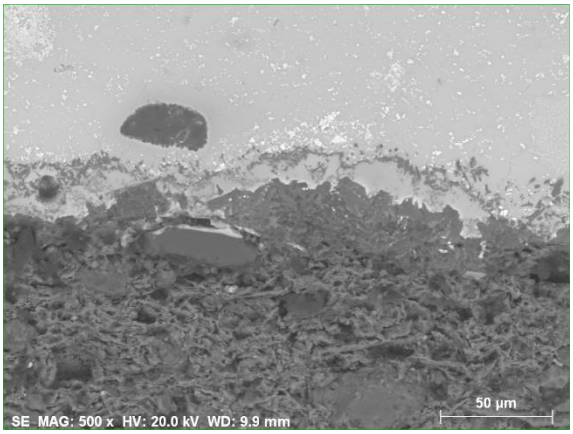

SCV 45M4260 white

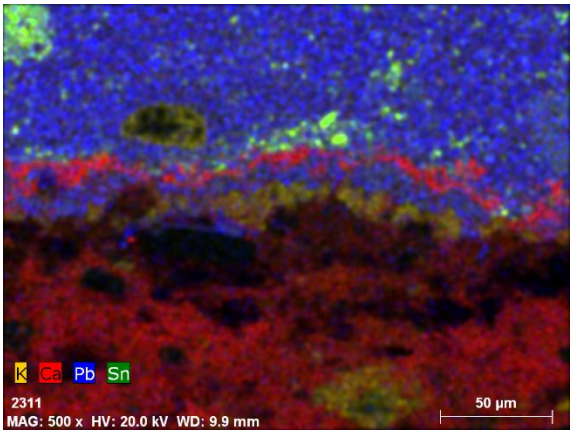

SCV 45M4260 white – EDS map

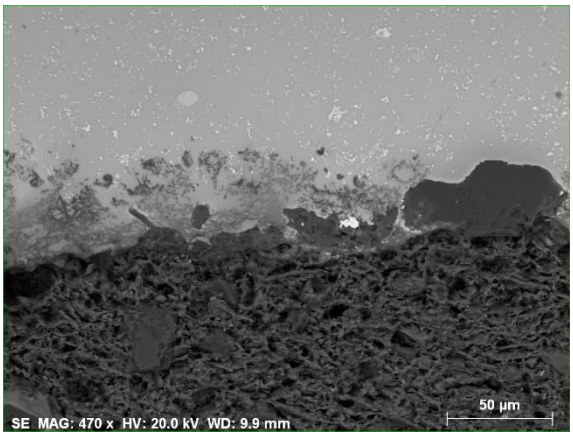

SCV 45M4260 blue

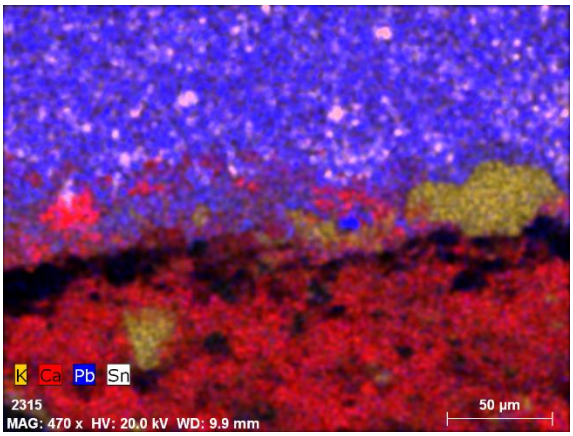

SCV 45M4260 blue – EDS map

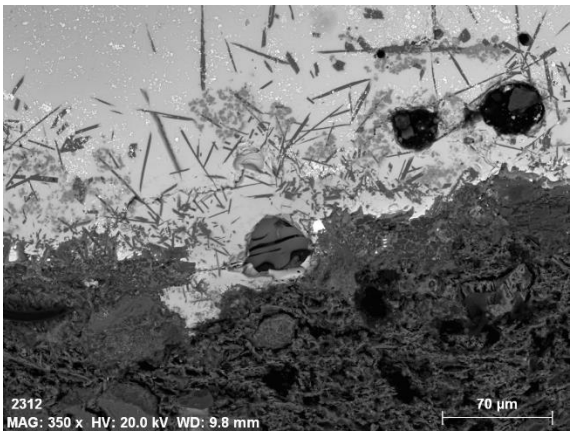

SCV 45M4260 brown

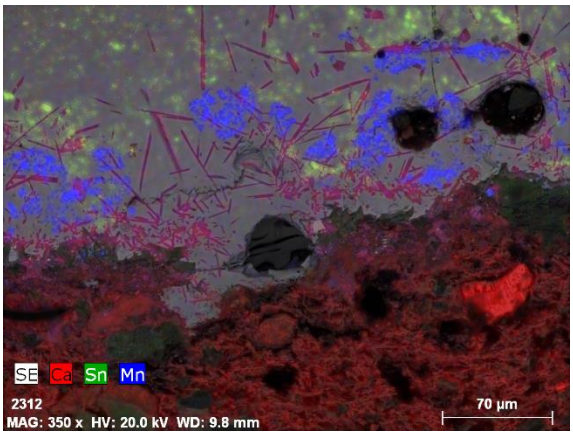

SCV 45M4260 brown – EDS map

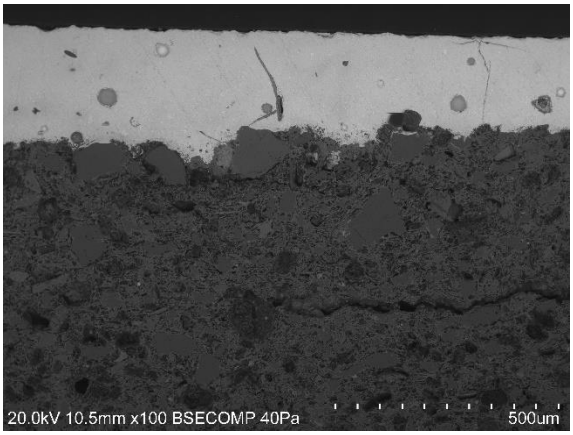

SCV 47Ai4284 blue

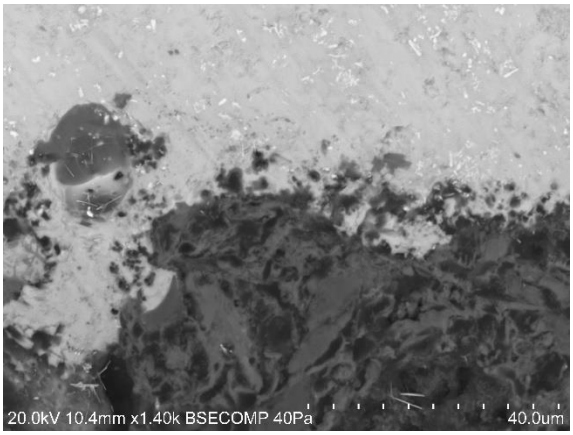

SCV 47Ai4284 blue (detail)

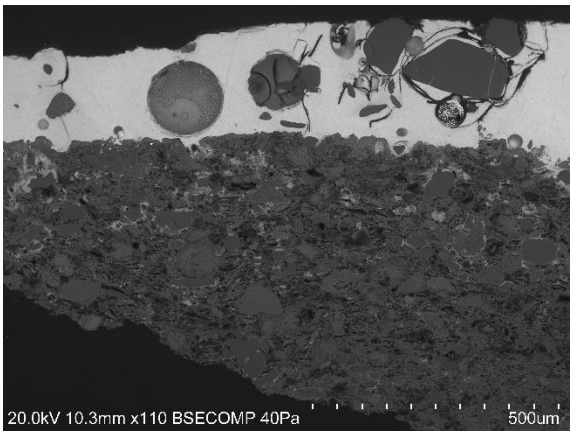

SCV 47Ai4284 green

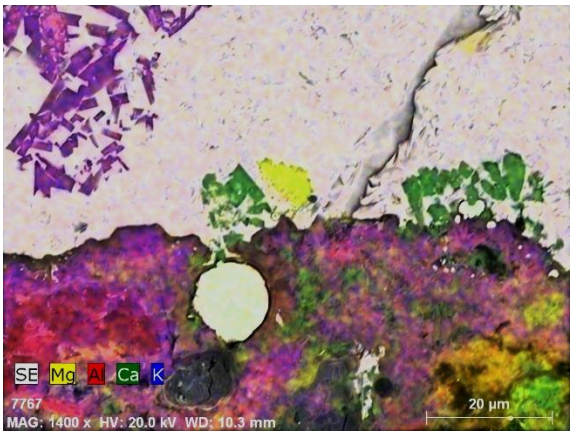

SCV 47Ai4284 green – EDS map

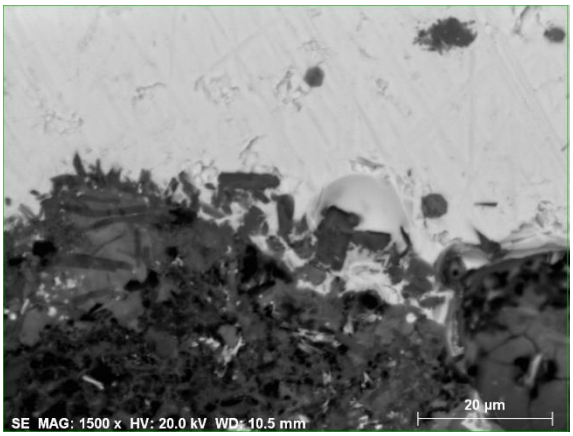

SCV 47Ai4284 amber

SCV 47Ai4284 amber – EDS map

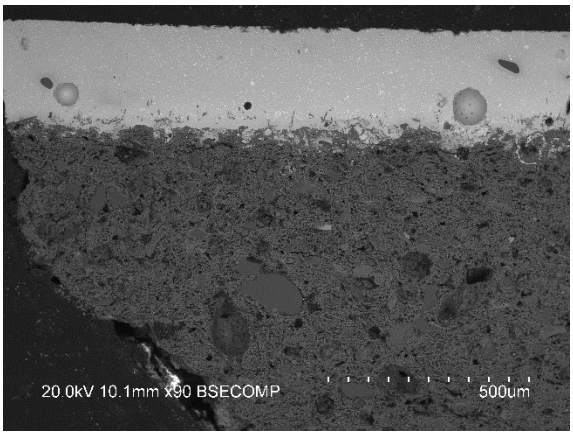

SCV 86i4886 blue

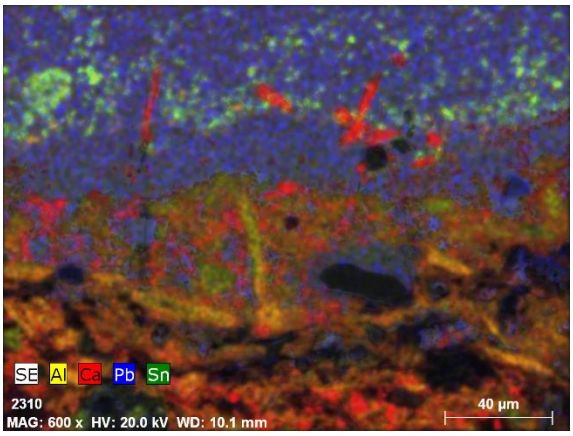

SCV 86i4886 blue – EDS map

VII. 2. National Palace of Sintra

PNS – Flat tiles

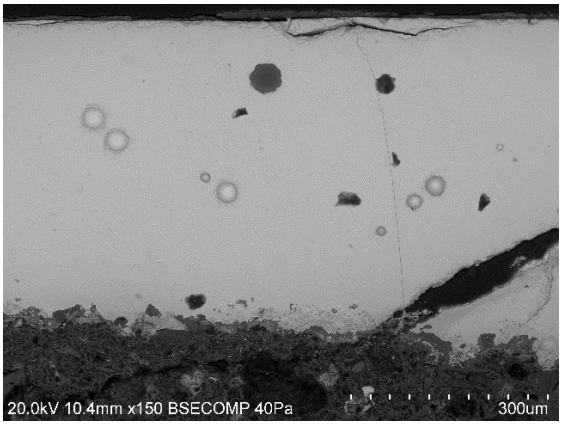

PNS 01 – Blue

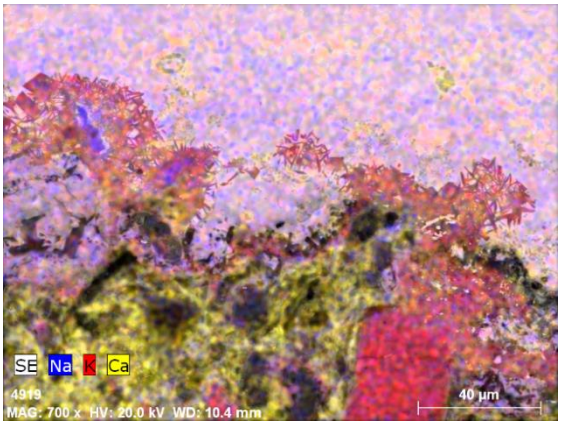

PNS 01 – Blue – EDS map of the interface

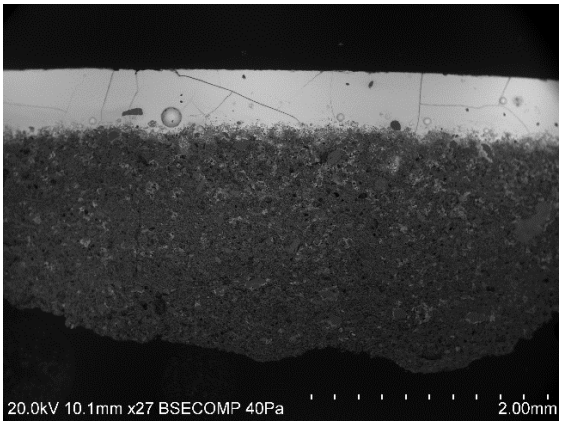

PNS 02 – Green

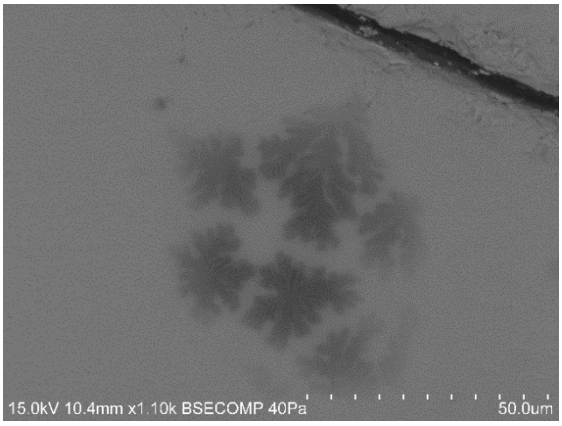

PNS 02 – Green – dendritic inclusion

PNS - *Cuerda seca* tiles

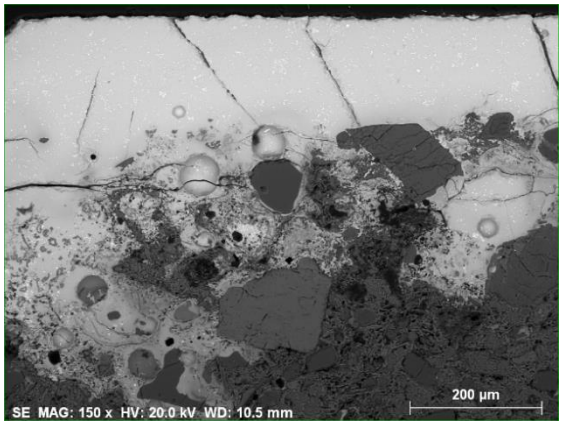

PNS 06 - blue

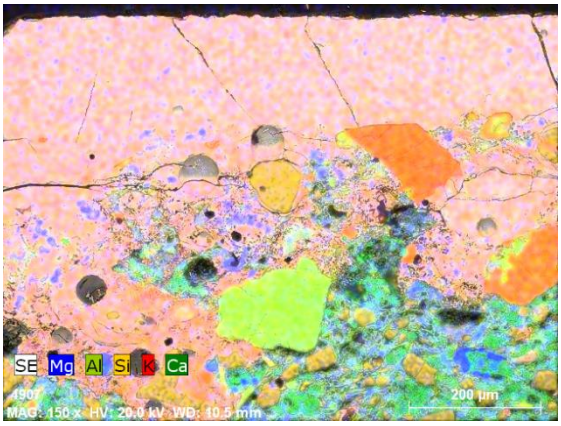

PNS 06 – blue – EDS map of the interface

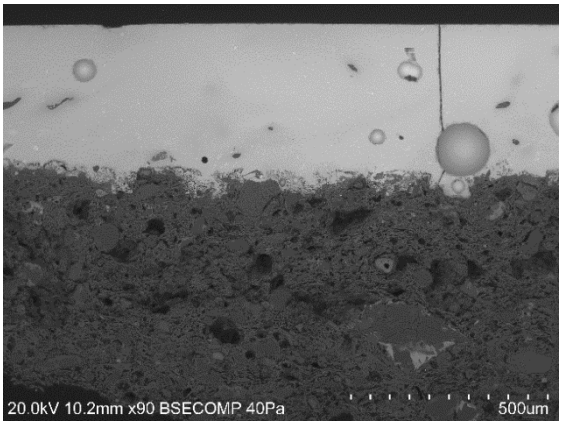

PNS 12 - white

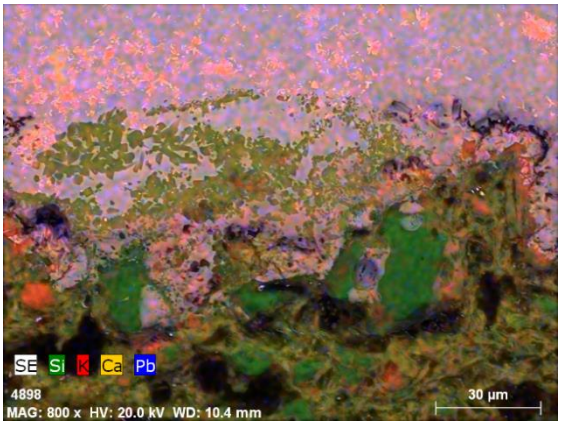

PNS 12 – white – EDS map of the interface

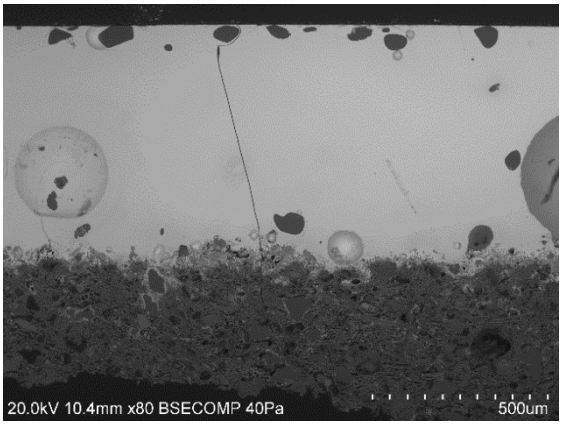

PNS 12 - green

PNS 12 – green – EDS map

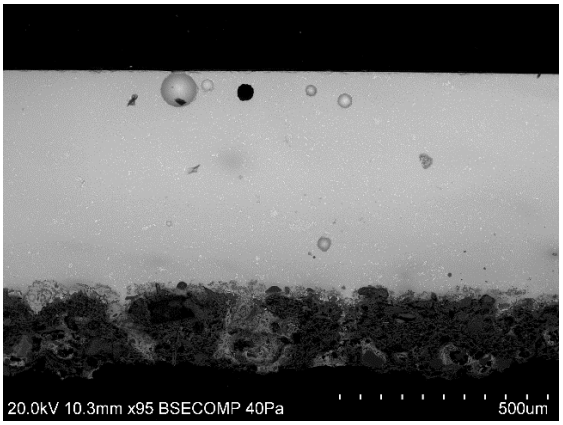

PNS 19 - white

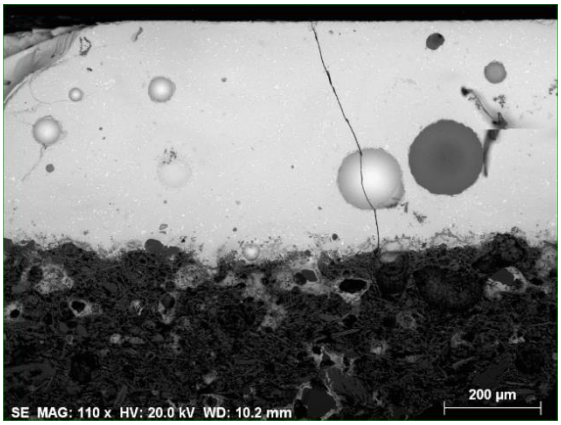

PNS 19 – blue

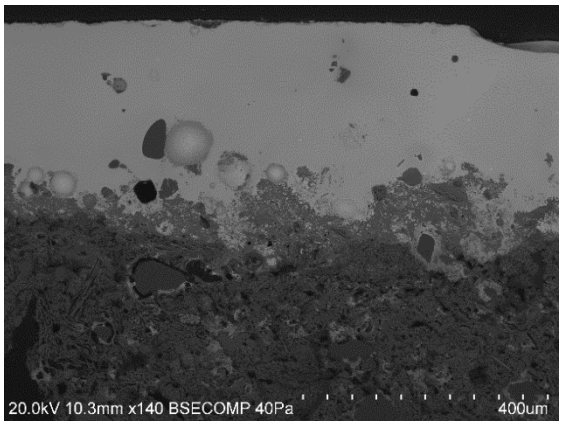

PNS 19 – green

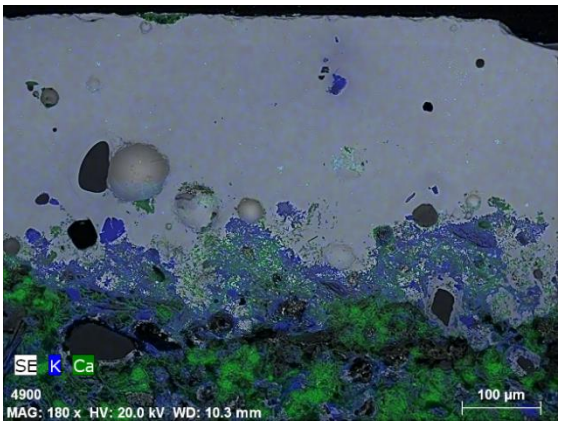

PNS 19 – green – EDS map

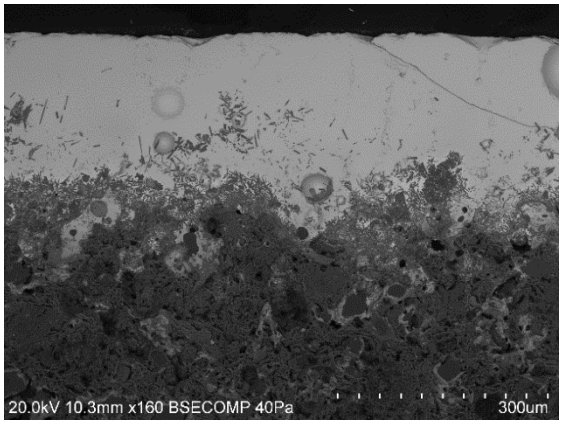

PNS 19 – brown

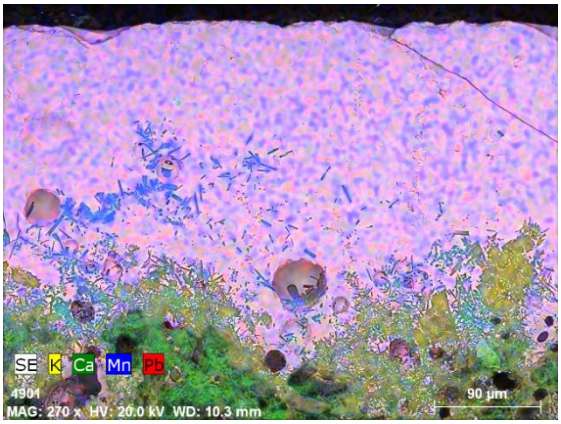

PNS 19 – brown – EDS map

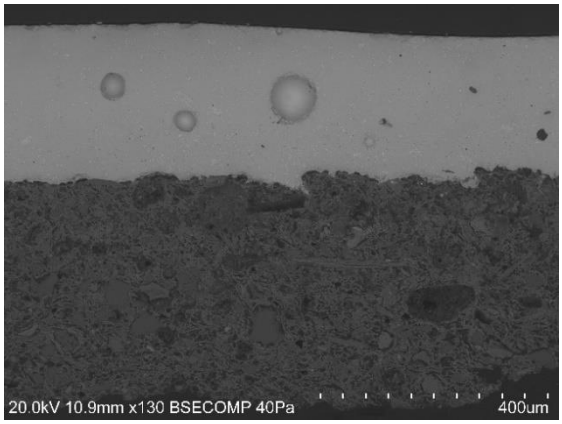

PNS 23 – white

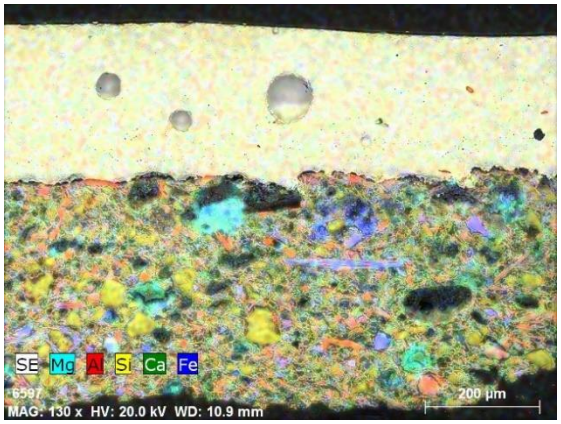

PNS 23 – white – EDS map

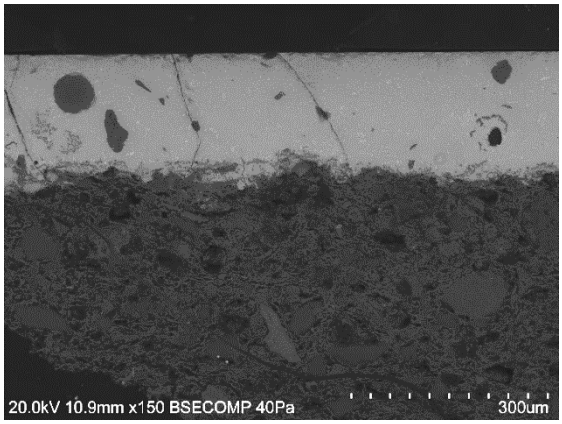

PNS 23 – blue

PNS 23 – blue – EDS map

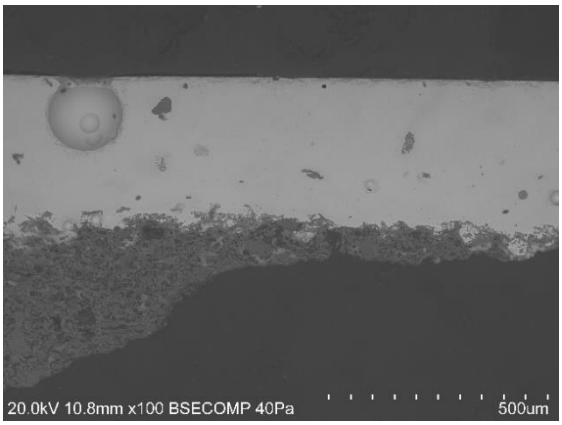

PNS 23 - green

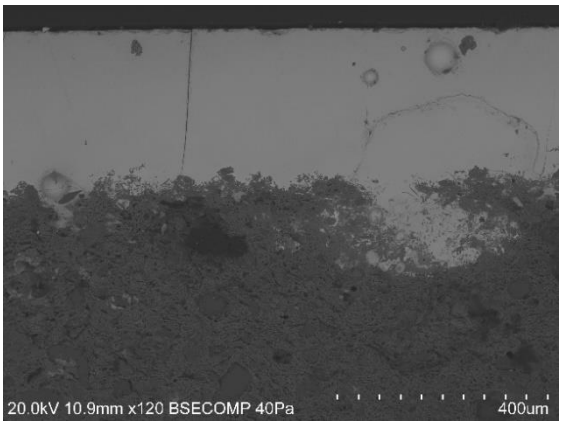

PNS 23 - brown

PNS - *Arista* tiles

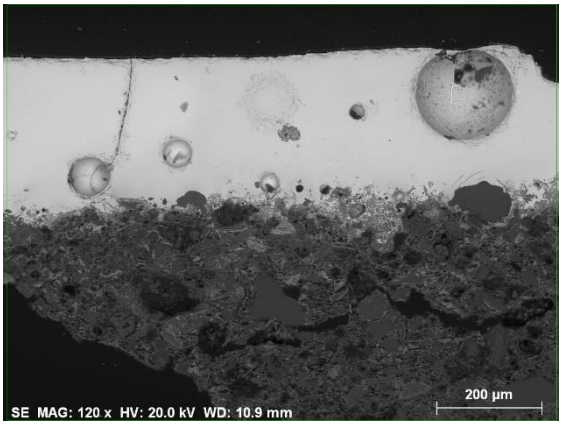

PNS 22 – brown

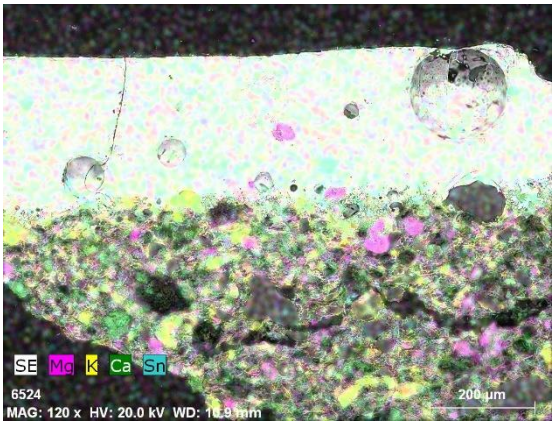

PNS 22 – brown – EDS map

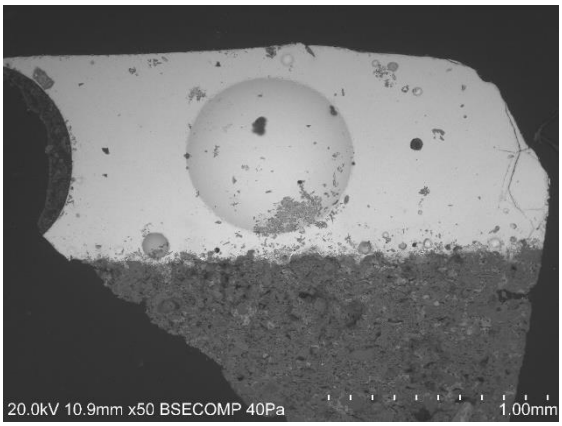

PNS 25 – amber

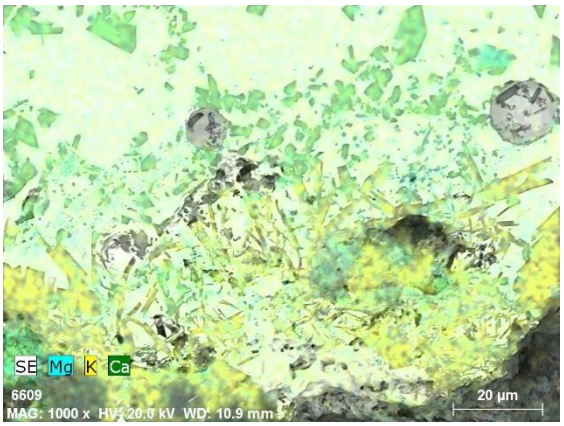

PNS 25 – amber – EDS map of the interface

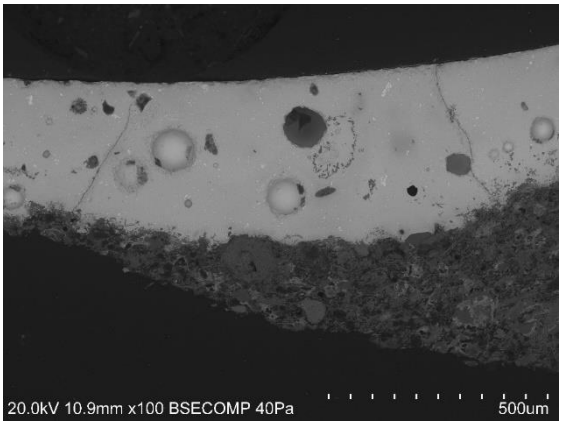

PNS 26 – white

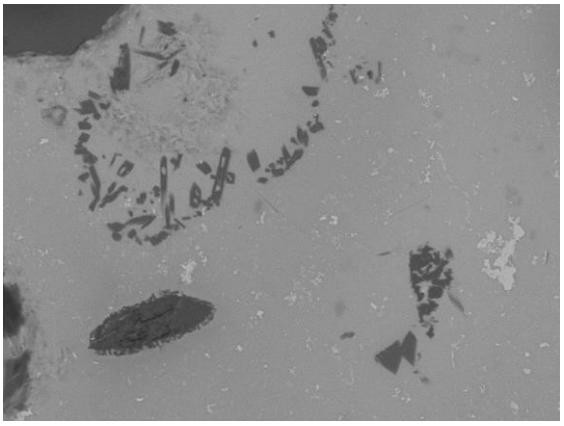
PNS 26 – white – detail

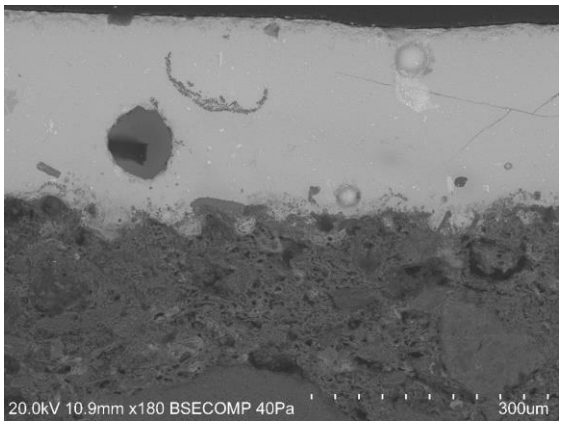

PNS 26 – blue

PNS 26 – blue – EDS map

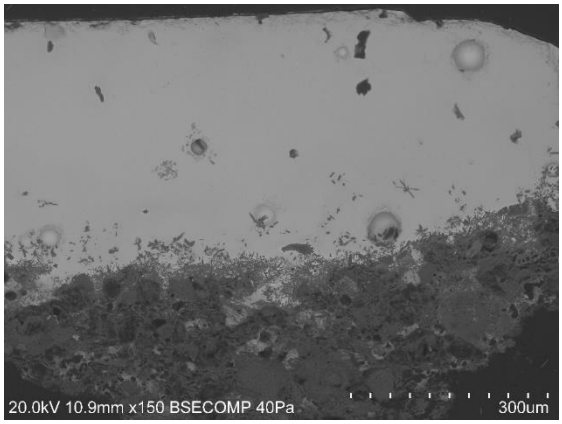

PNS 26 – green

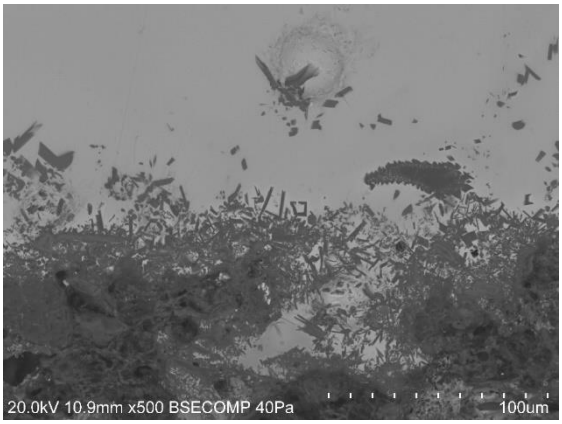

PNS 26 – green – interface

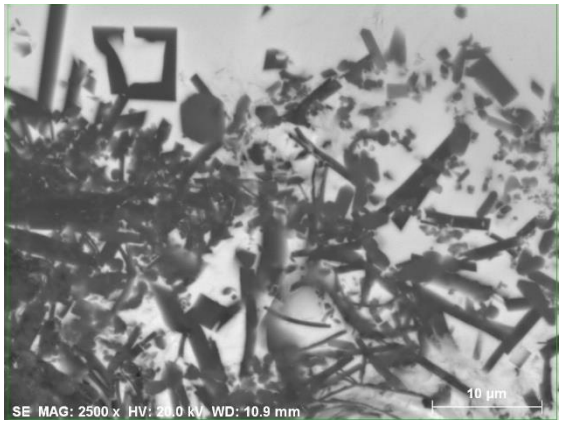

PNS 26 – green – interface detail

PNS 26 – green – interface detail (EDS map)

PNS – Relief tiles

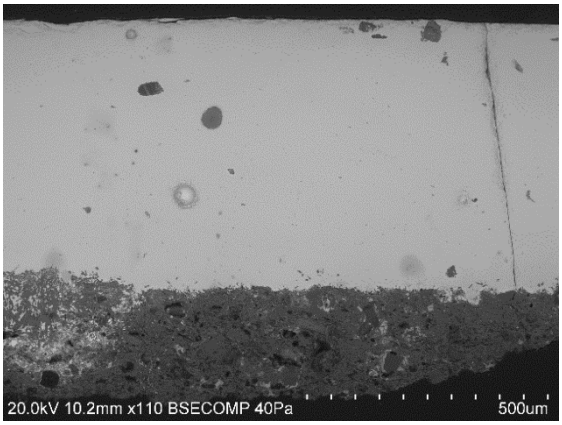

PNS 07 – green

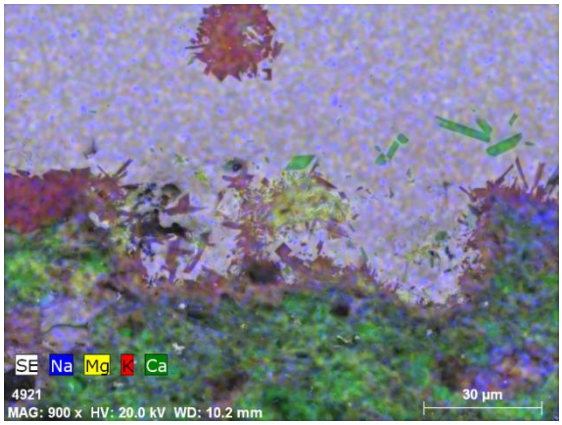

PNS 07 – green – EDS map of the interface

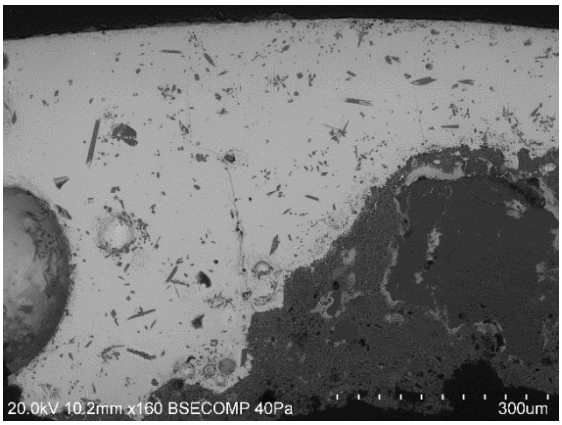

PNS 07 - brown

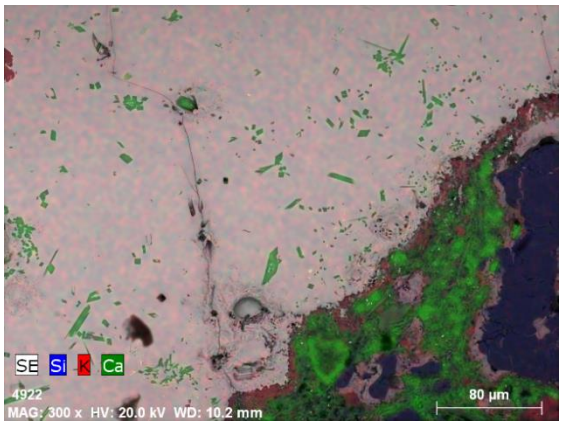

PNS 07 – brown – EDS map of the interface

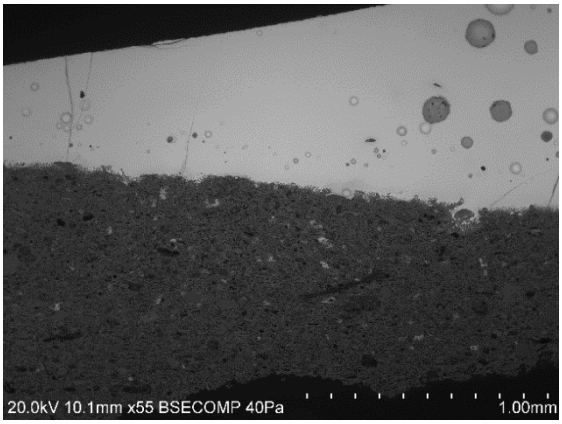

PNS 09 – white

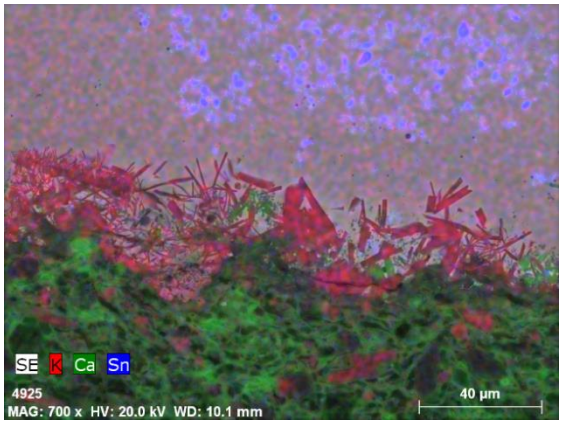

PNS 09 – white – EDS map of the interface

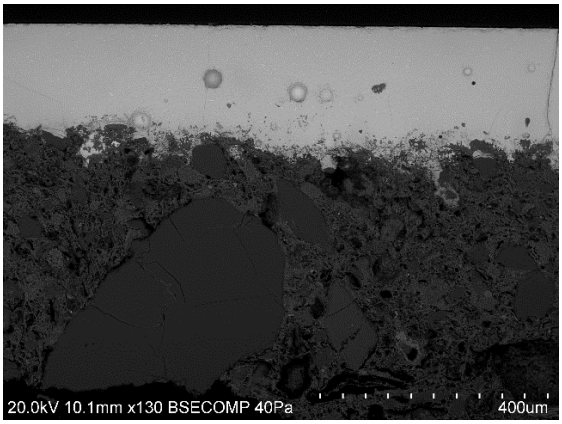

PNS 09 – blue

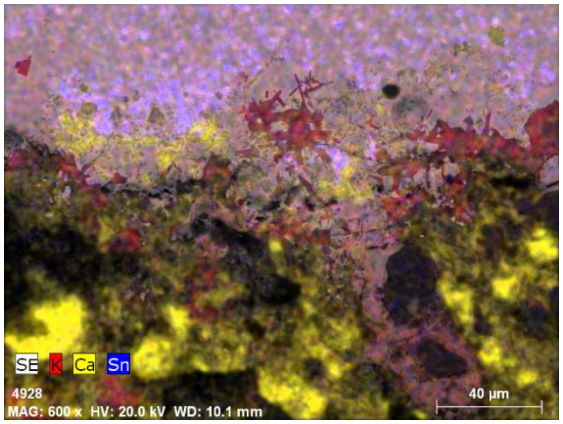

PNS 09 – blue – EDS map of the interface

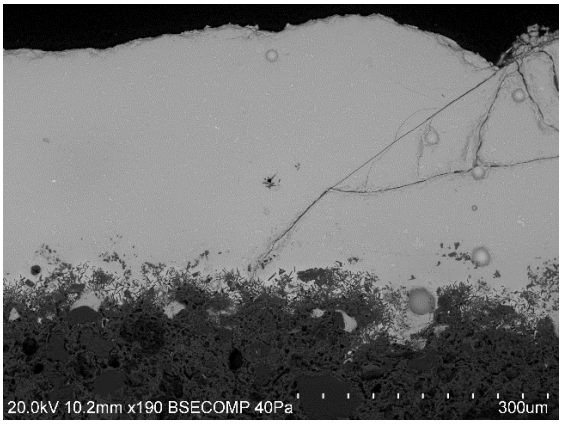

PNS 09 – green

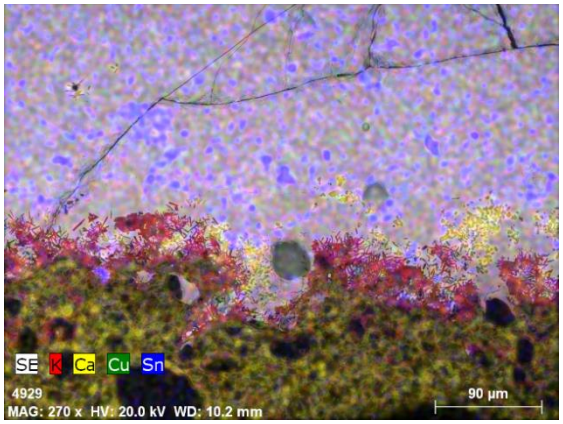

PNS 09 – green – EDS map of the interface

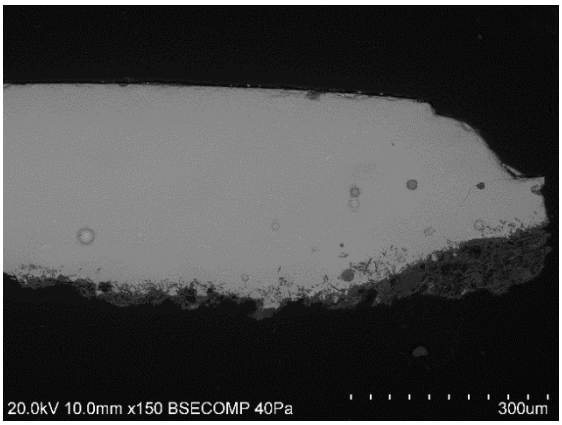

PNS 09 – brown

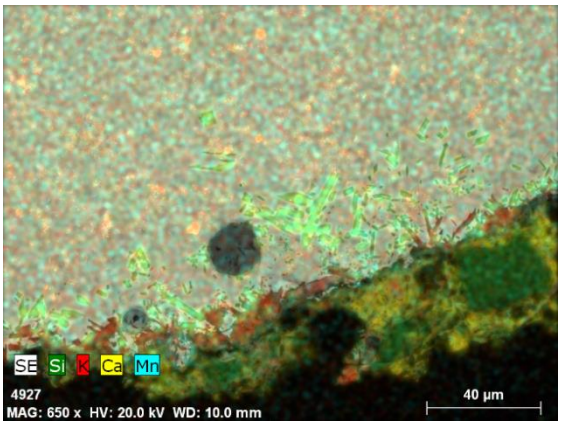

PNS 09 – brown – EDS map of the interface

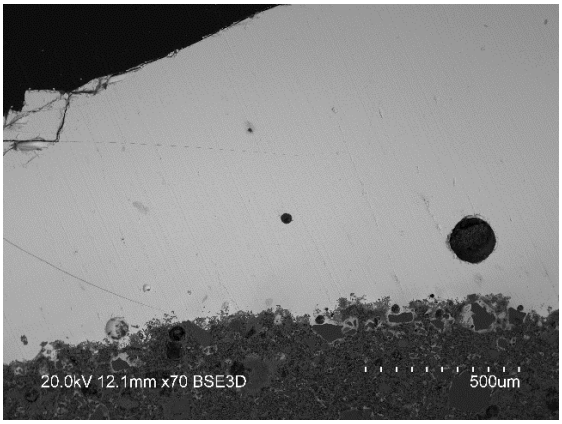

PNS 16 – green

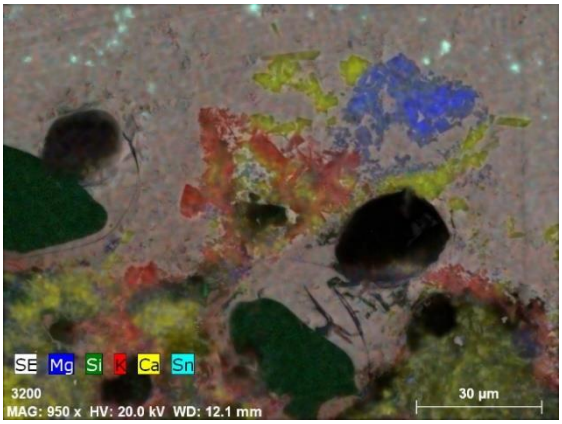

PNS 16 – green – EDS map of the interface

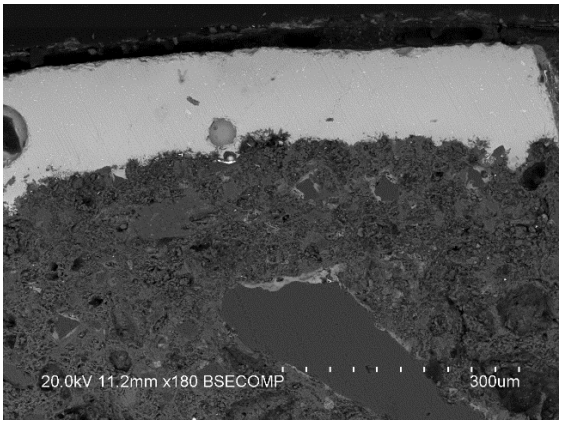

PNS 18 – brown

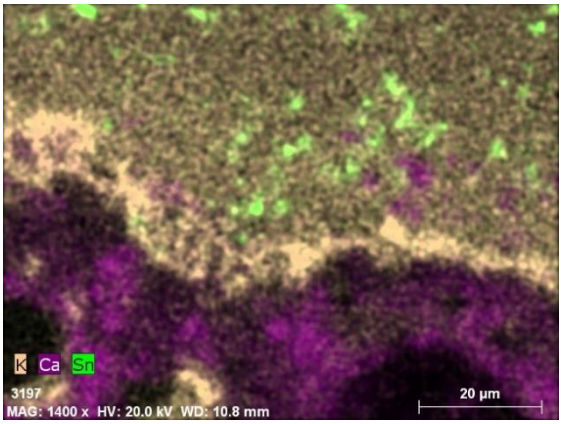

PNS 18 – brown – EDS map of the interface

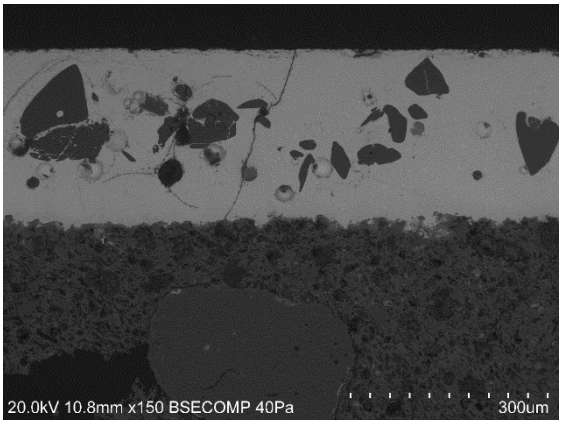

PNS 30 – white

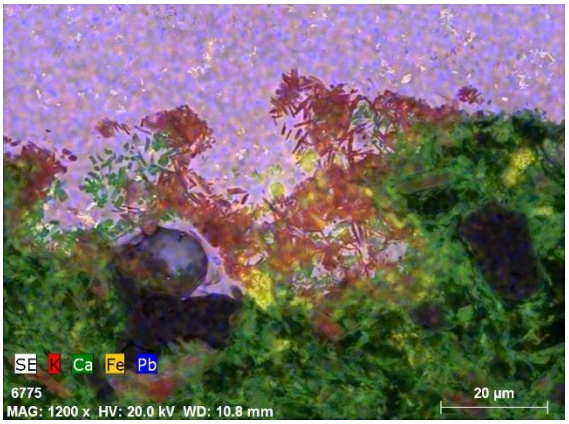

PNS 30 – white – EDS map of the interface

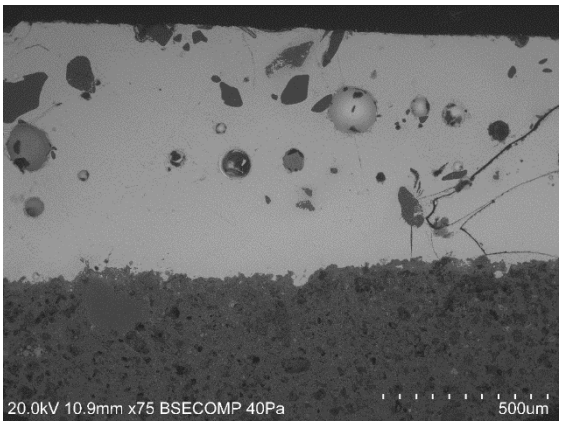

PNS 30 – green

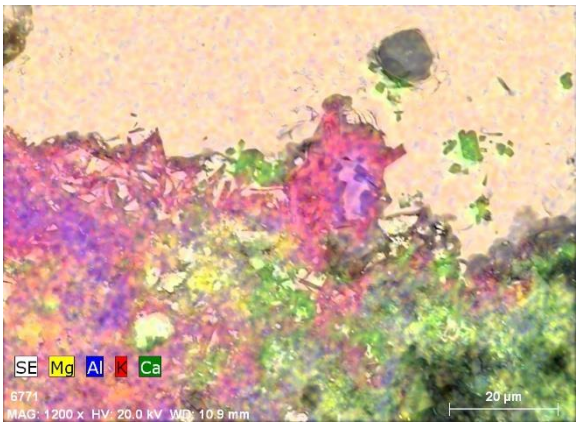

PNS 30 – green – EDS map of the interface

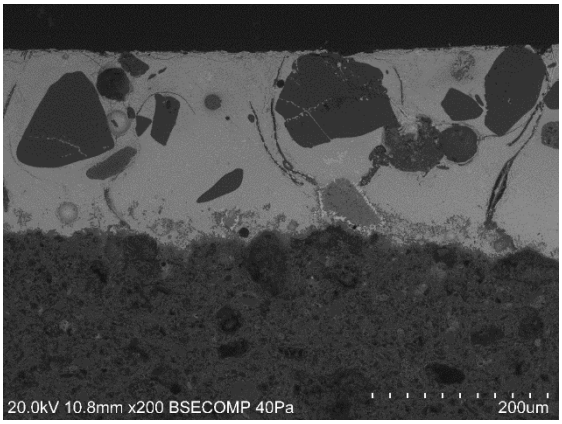

PNS 30 – brown

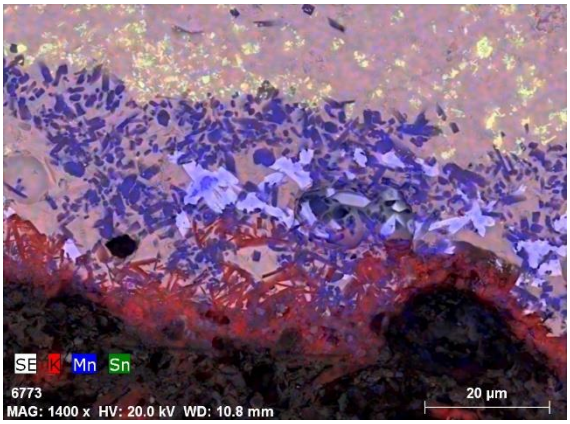

PNS 30 – brown – EDS map of the interface

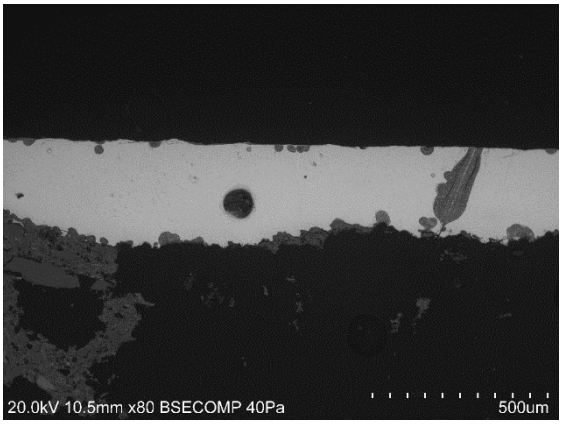

PNS 31 – white

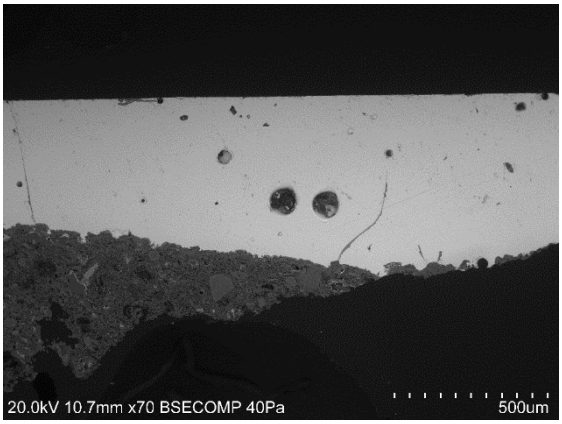

PNS 31 – brown

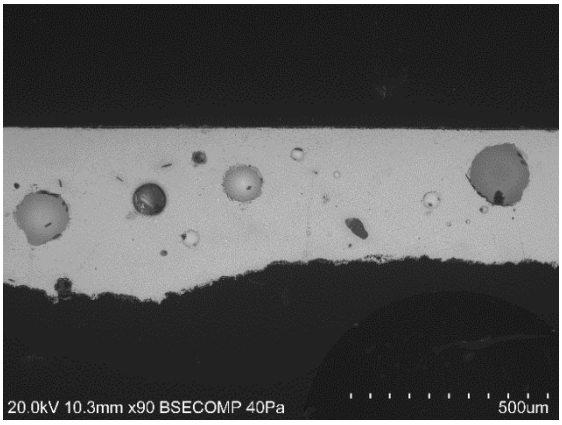

PNS 32 - white

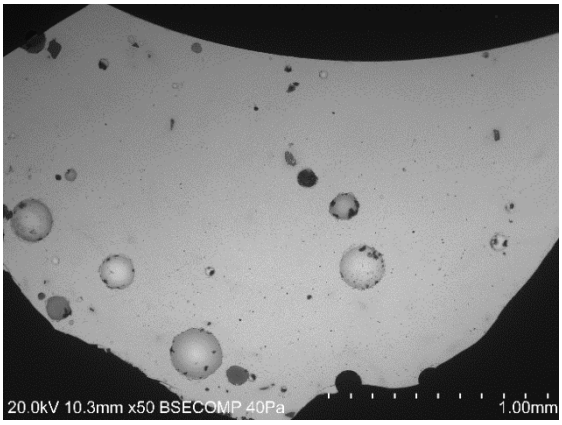

PNS 32 – blue

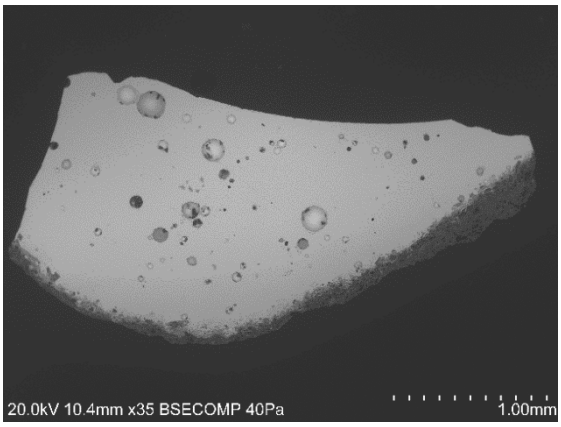

PNS 33 – green

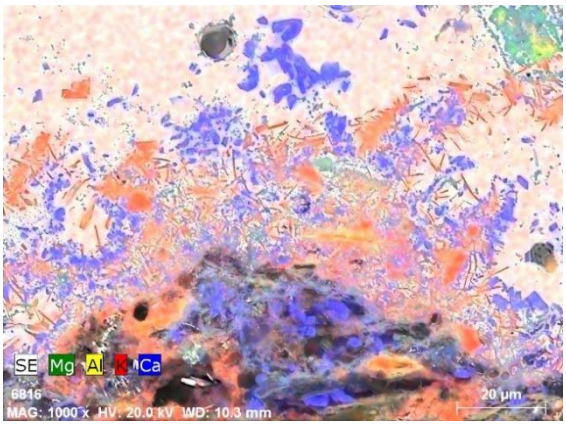

PNS 33 - green - EDS map of the interface

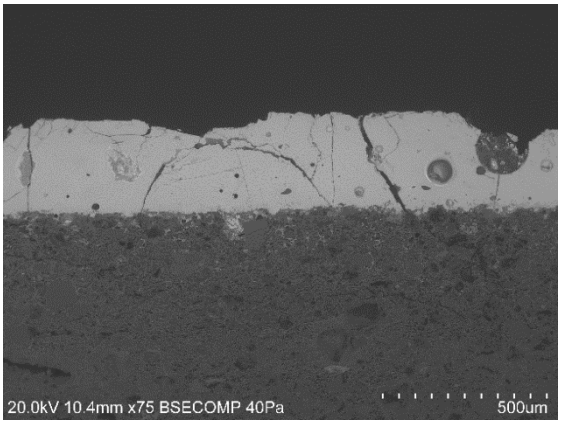

PNS 33 – brown

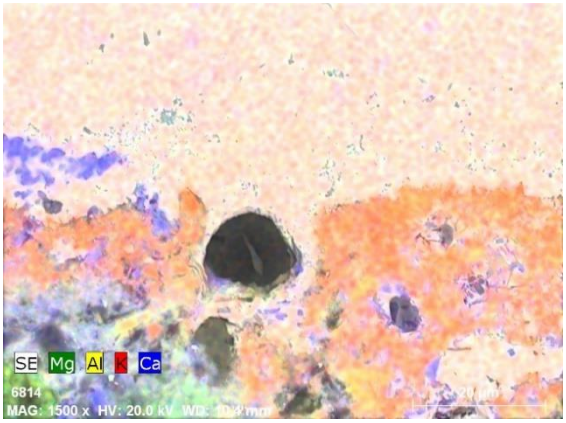

PNS 33 – brown – EDS map of the interface

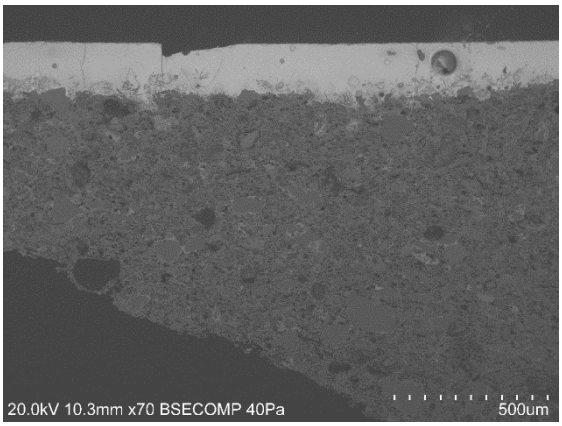

PNS 34 – white

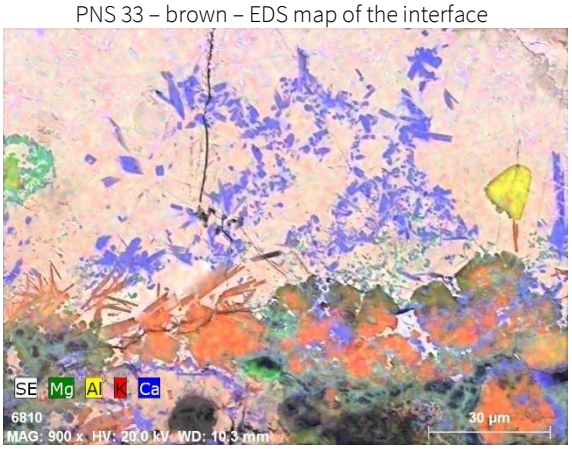

PNS 34 – white – EDS map of the interface

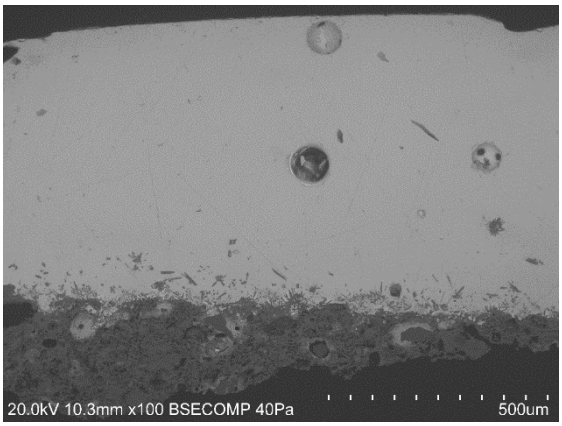

PNS 34 – green

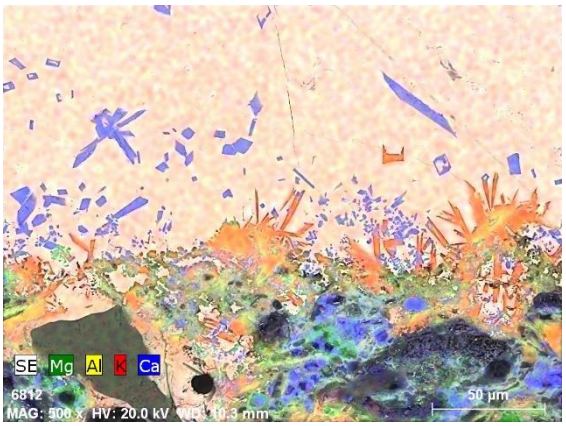

PNS 34 – green – EDS map of the interface

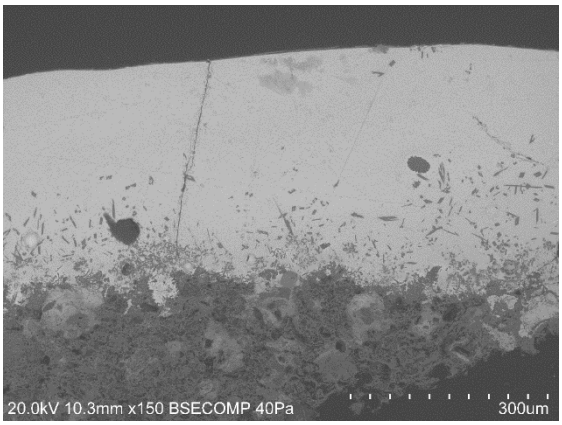

PNS 34 – brown

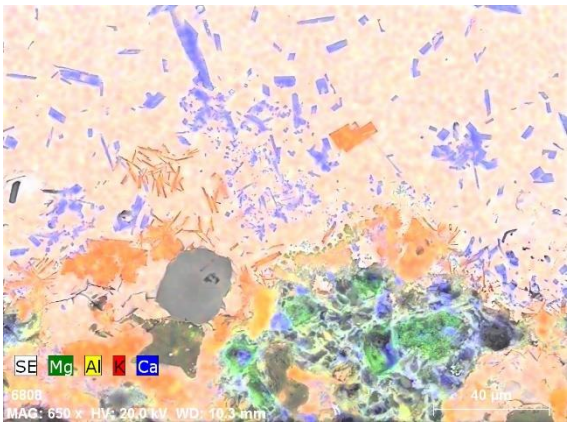

PNS 34 – brown – EDS map of the interface

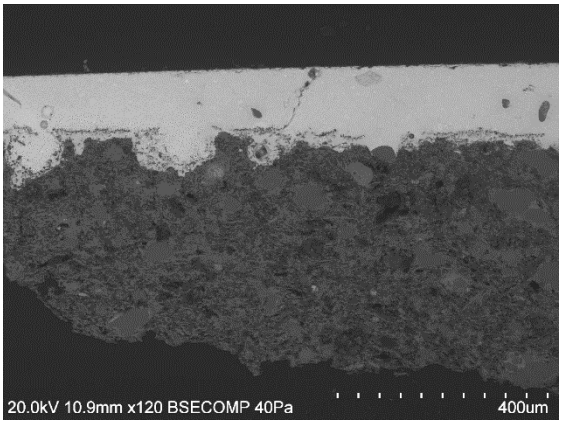

PNS 35 – white

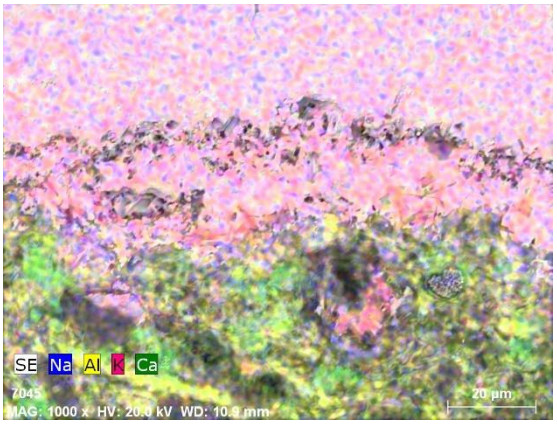

PNS 35 – white – EDS map of the interface

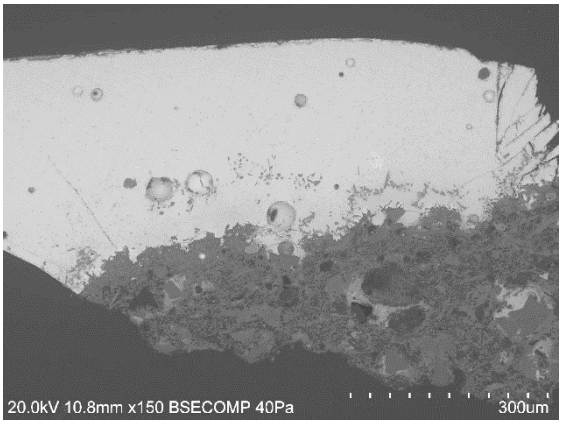

PNS 35 – green

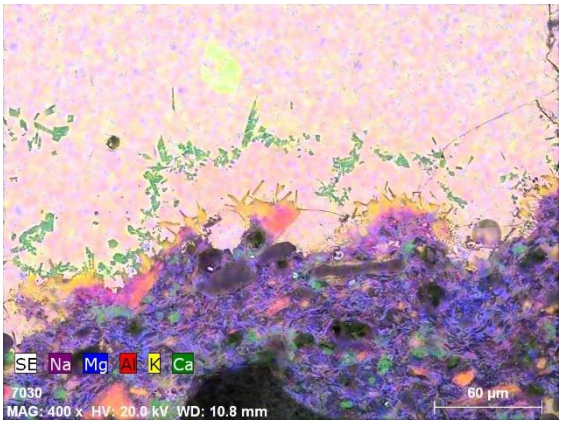

PNS 35 - green – EDS map of the interface

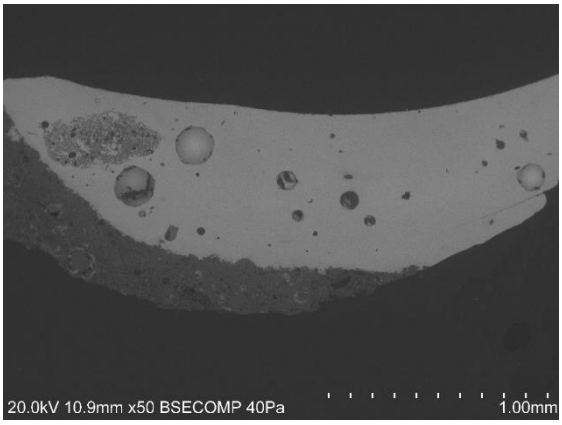

PNS 36 – white

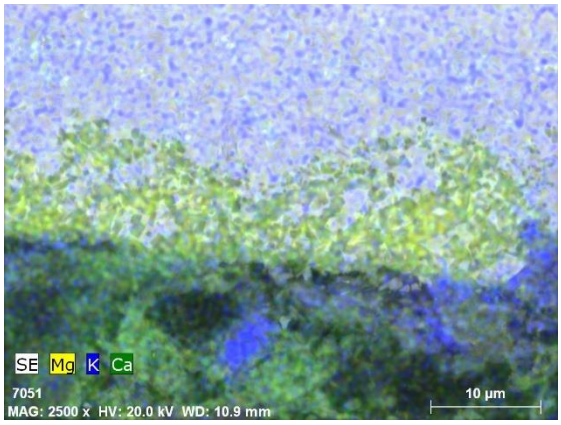

PNS 36 – white – EDS map of the interface

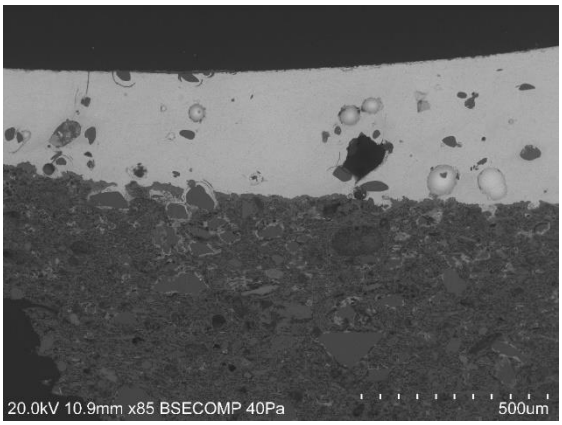

PNS 36 - green

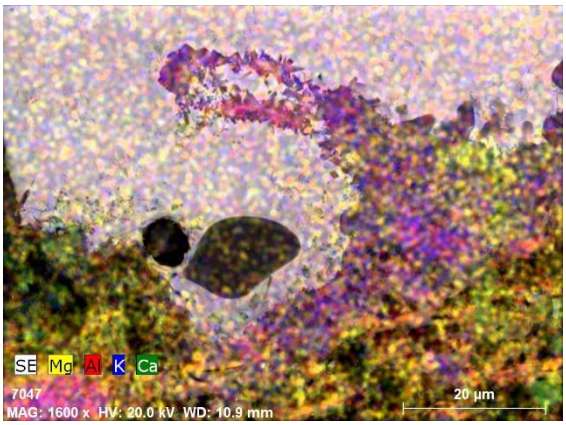

PNS 36 – green – EDS map of the interface

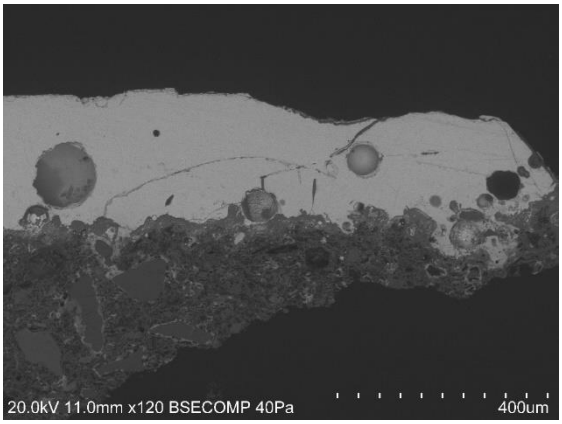

PNS 36 – brown

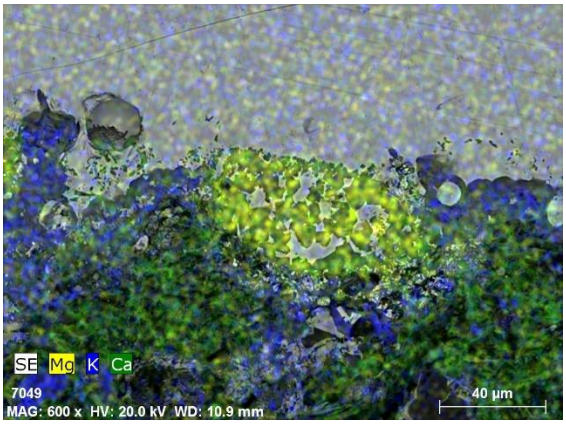

PNS 36 – brown - EDS map of the interface

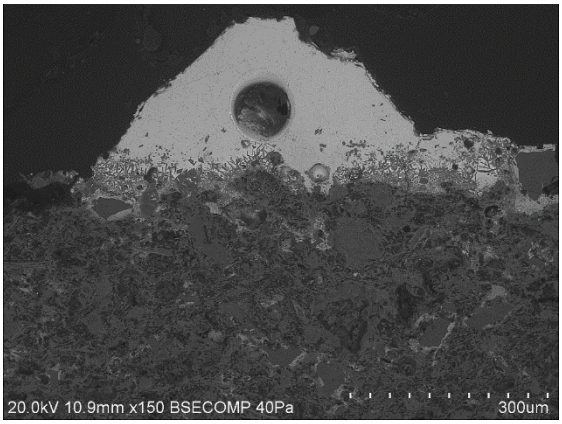

PNS 37 - green

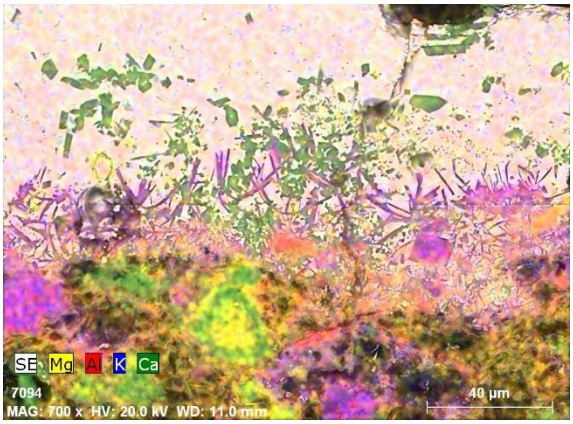

PNS 37 – green – map of the interface

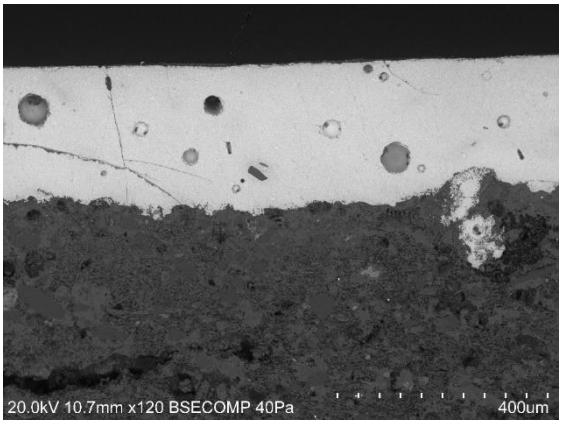

PNS 38 – white

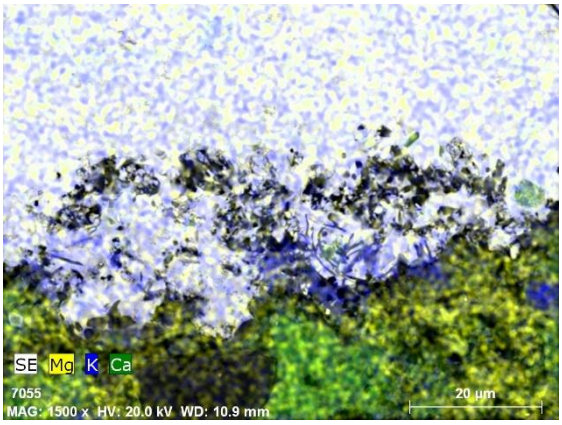

PNS 38 – white – map of the interface

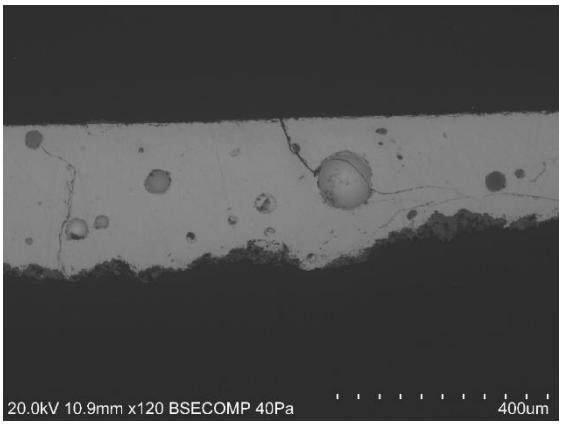

PNS 38 – blue

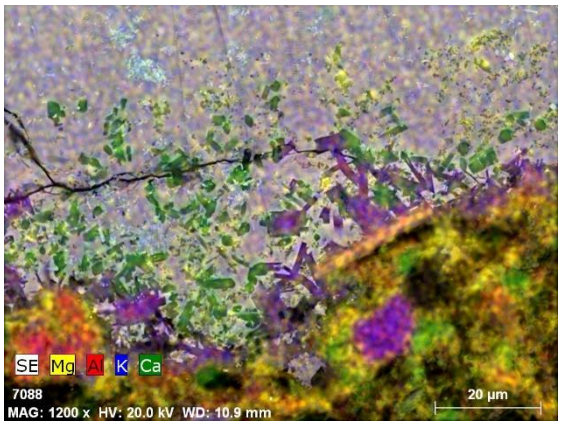

PNS 38 – blue – map of the interface

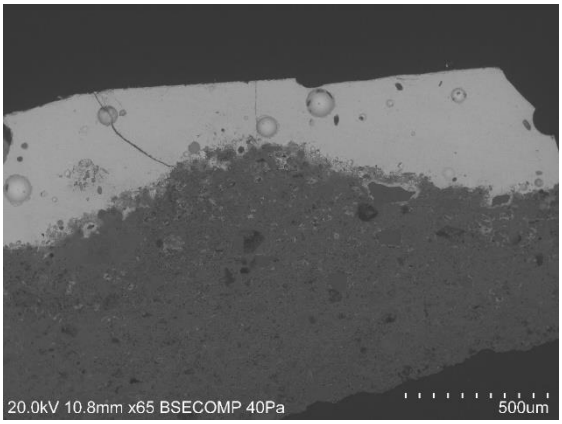

PNS 38 – green

PNS 38 – green – map of the interface

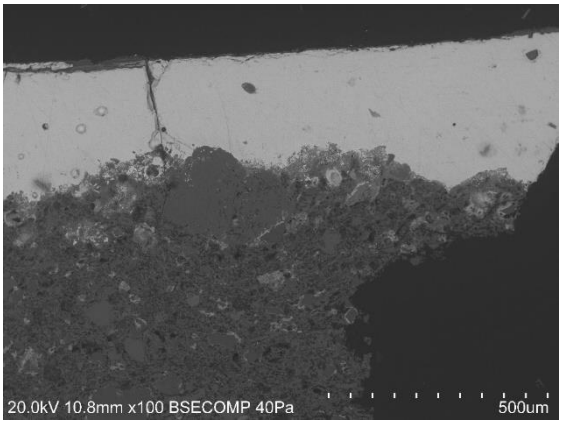

PNS 38 – amber

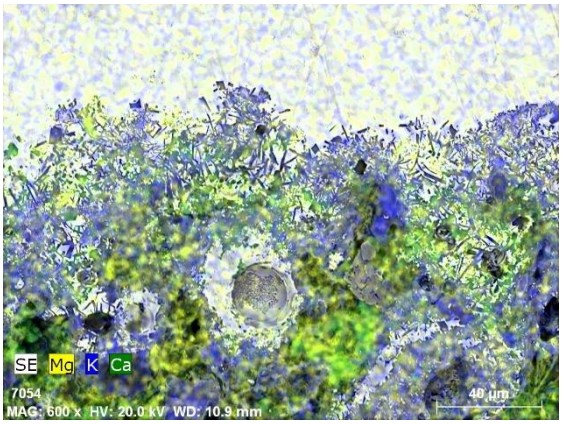

PNS 38 – amber – map of the interface

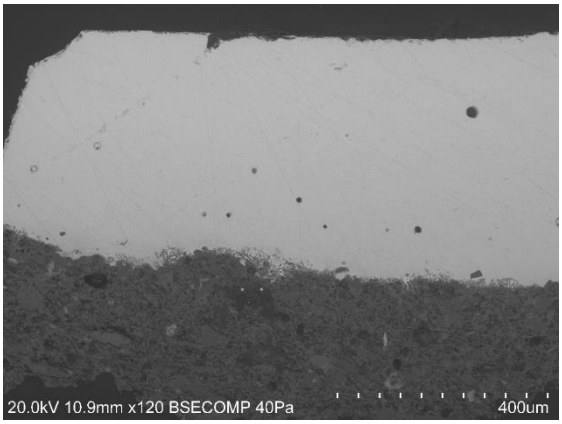

PNS 38 – brown

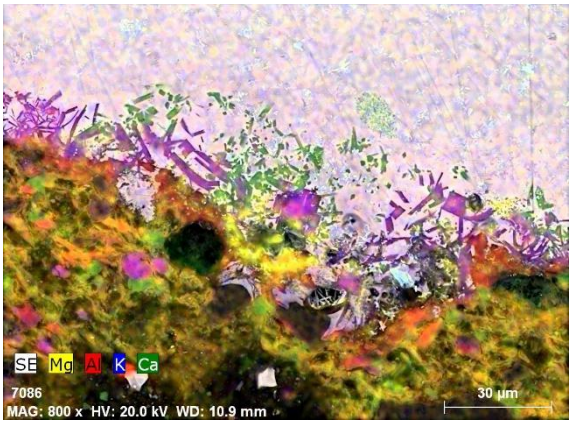

PNS 38 – brown – EDS map of the interface

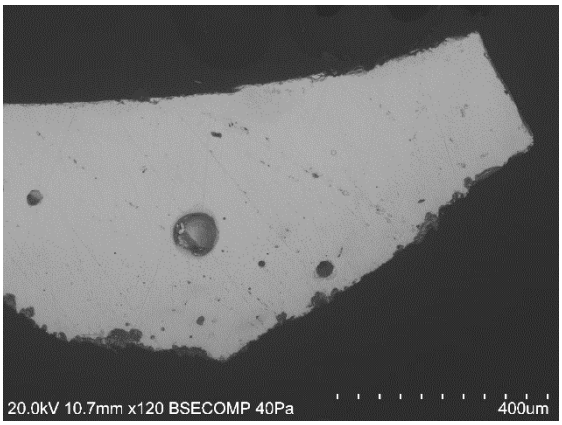

PNS 39 – white

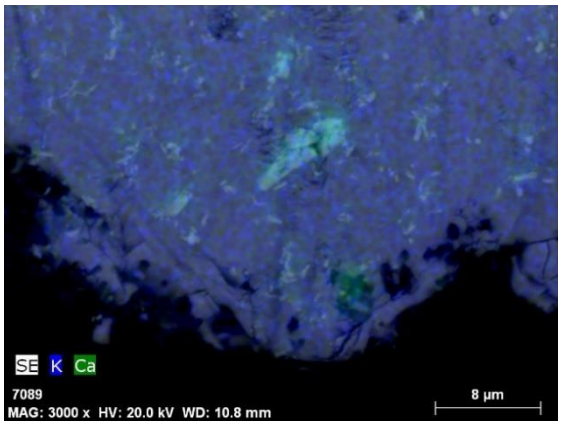

PNS 39 – white – map of the interface

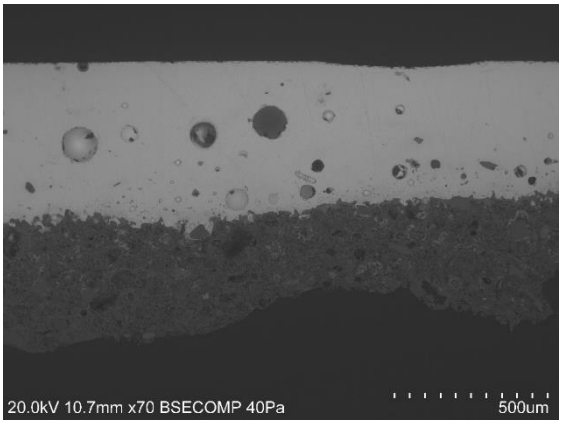

PNS 39 – blue

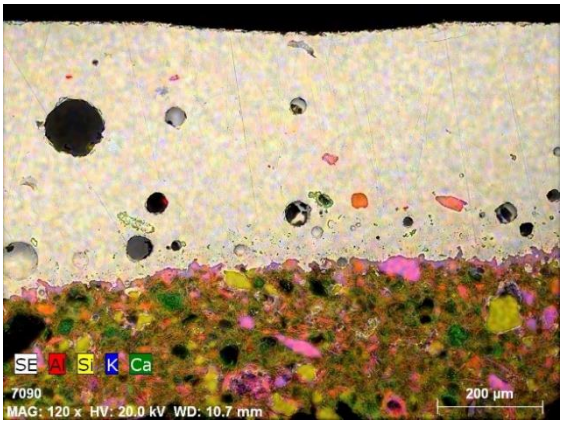

PNS 39 – blue – map of the interface

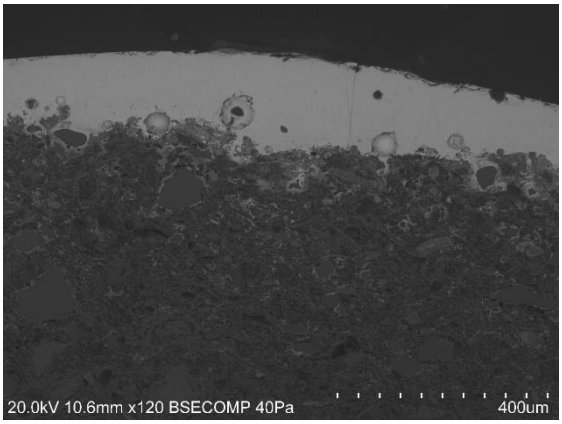

PNS 39 – amber

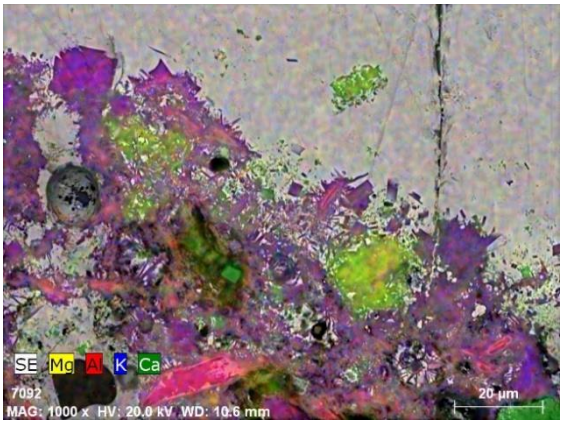

PNS 39 – amber– map of the interface

VII. 3. Instituto Valencia de Don Juan, Madrid

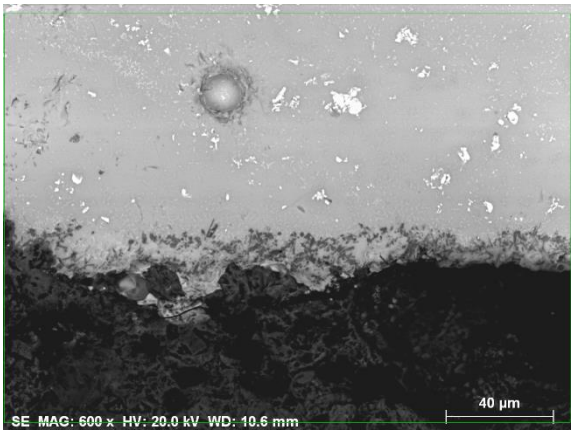

IVDJ-S 3561 turquoise

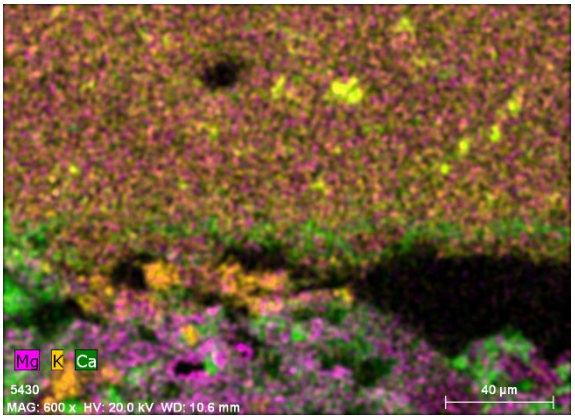

IVDJ-S 3561 turquoise – EDS map

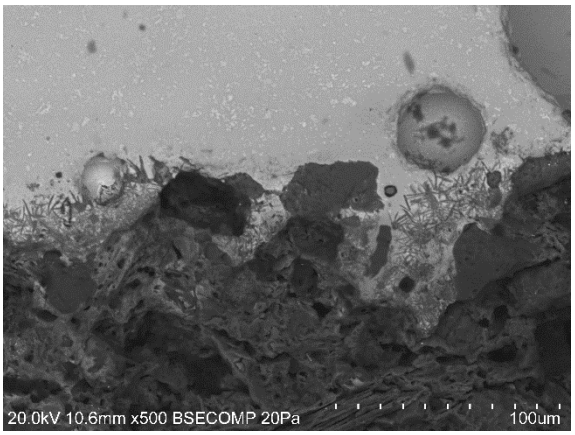

IVDJ-S 3561 white

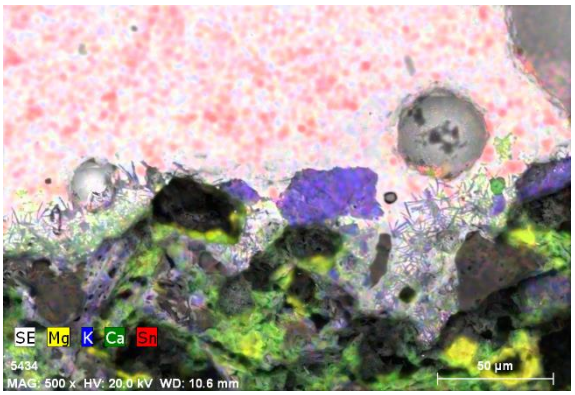

IVDJ-S 3561 white – EDS map

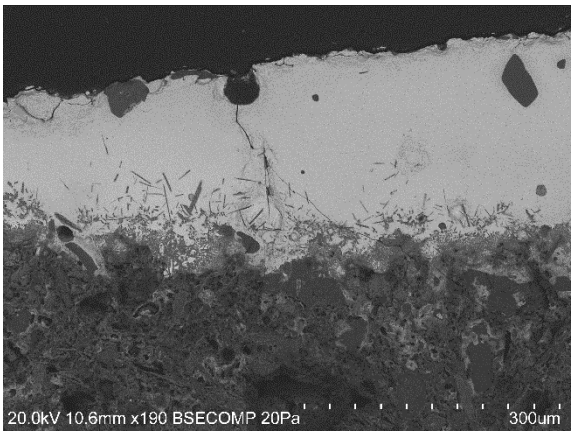

IVDJ-S 4127 brown

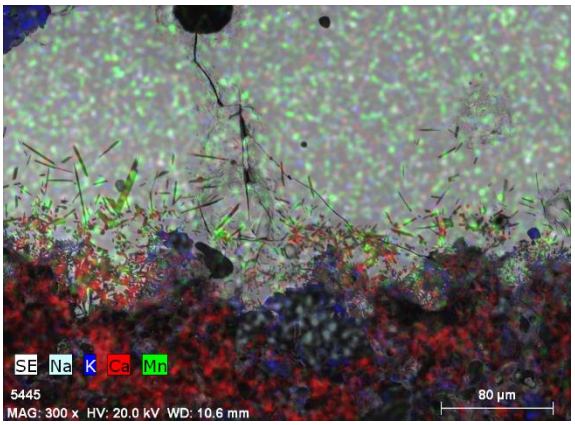

IVDJ-S 4127 brown – EDS map of the interface

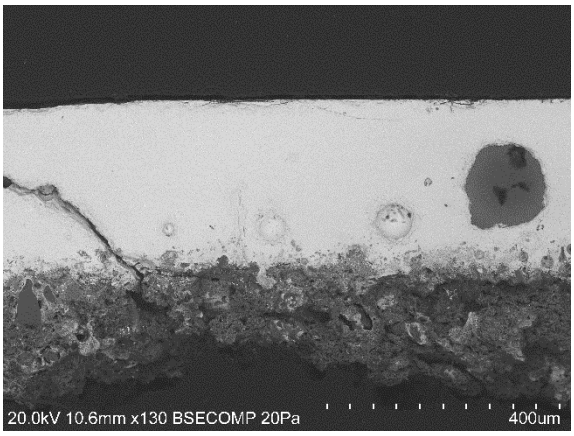

IVDJ-S 4127 blue

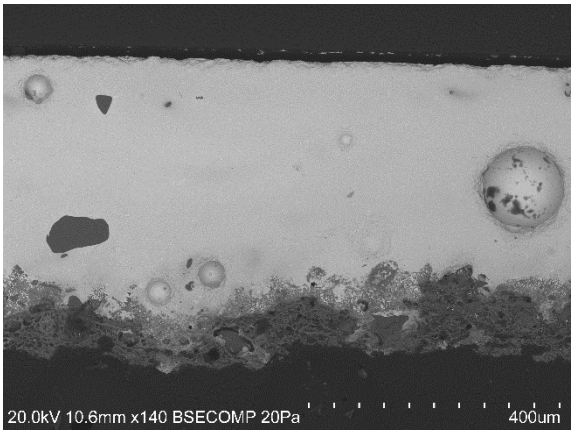

IVDJ-S 4127 white

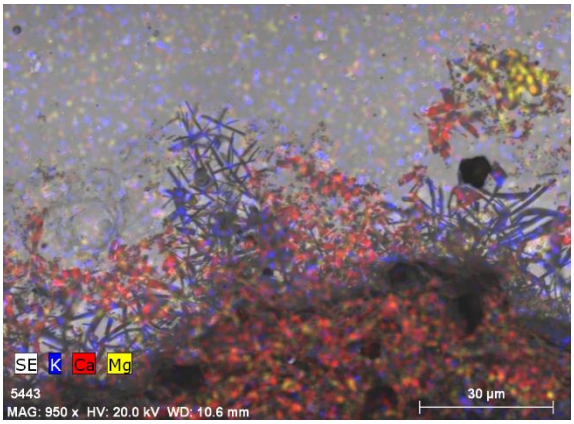

IVDJ-S 4127 white – EDS map of the interface

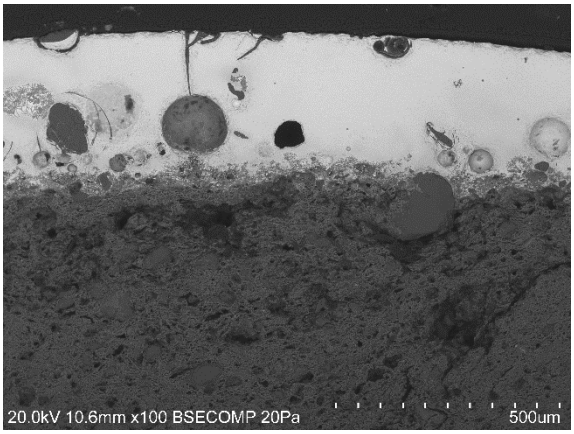

IVDJ-S XV green

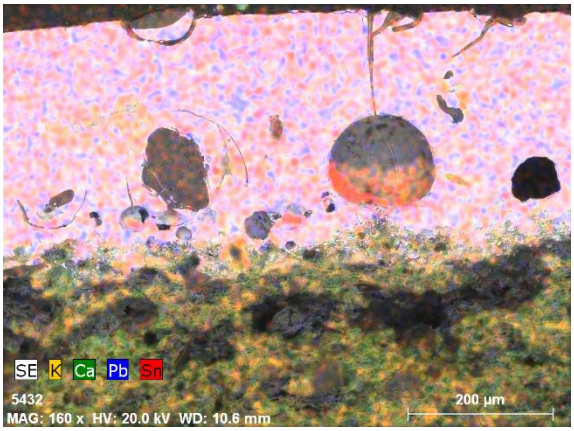

IVDJ-S XV green – EDS map

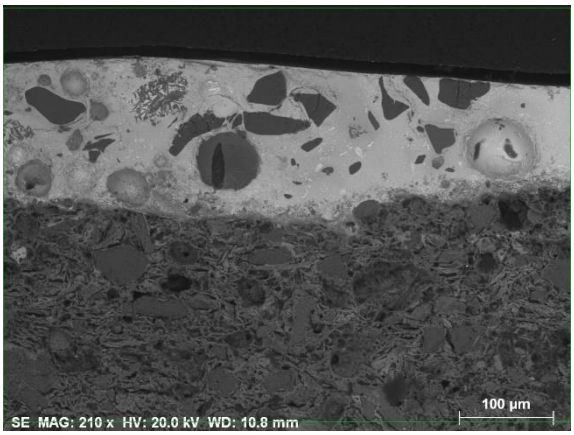

IVDJ-T 96 blue

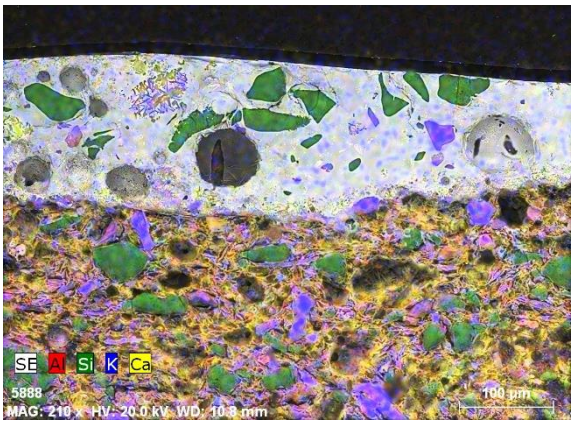

IVDJ-T 96 blue – EDS map

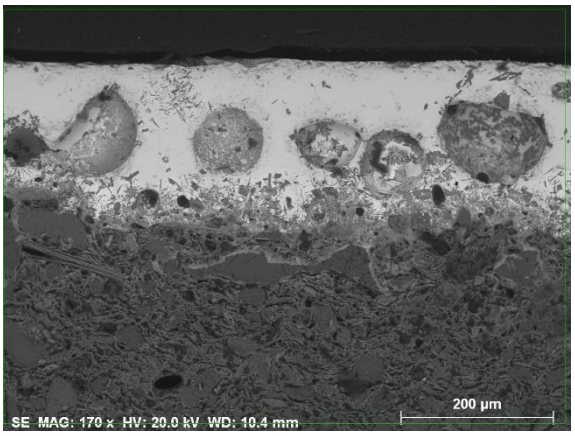

IVDJ-T 96 amber

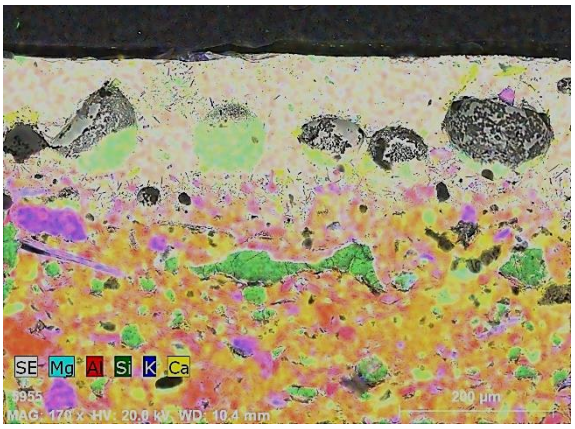

IVDJ-T 96 amber – EDS map

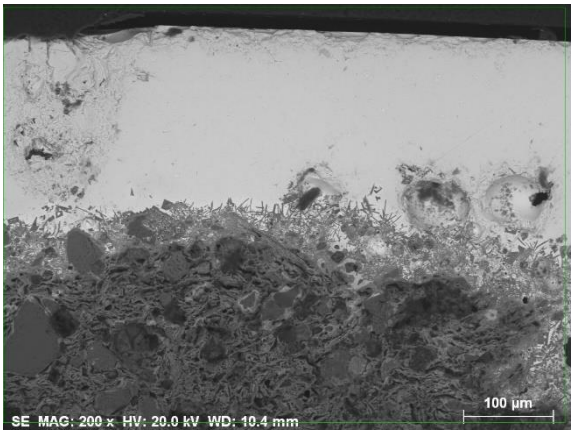

IVDJ-T 96 green

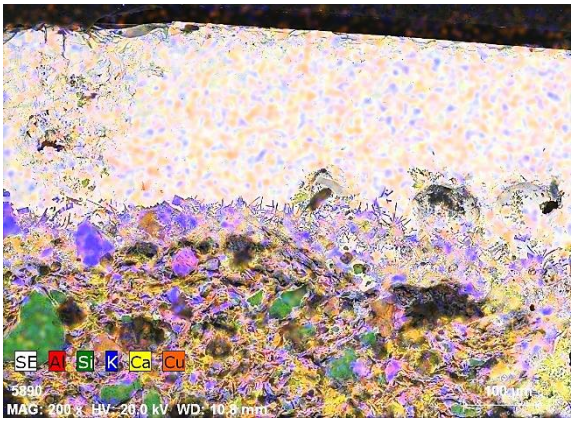

IVDJ-T 96 green – EDS map

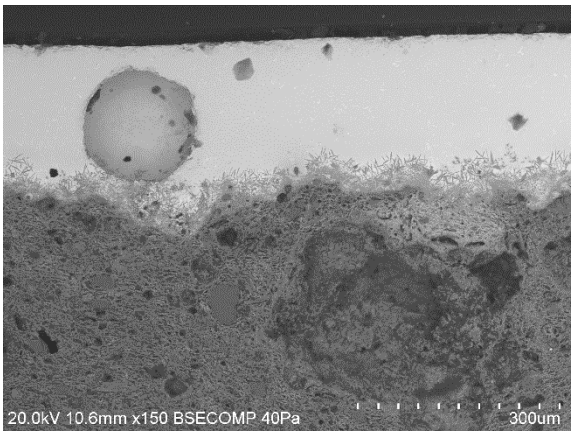

IVDJ-T 3683 brown

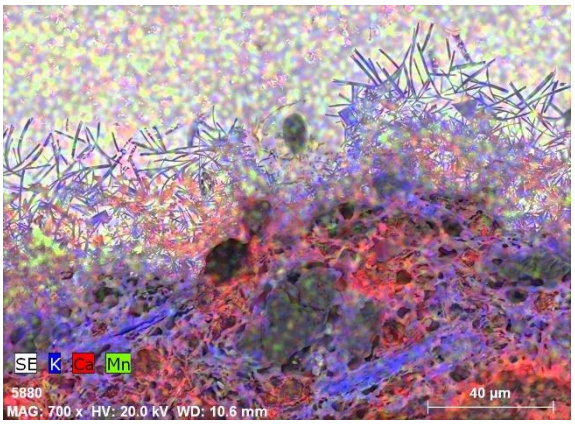

IVDJ-T 2683 brown – EDS map of the interface

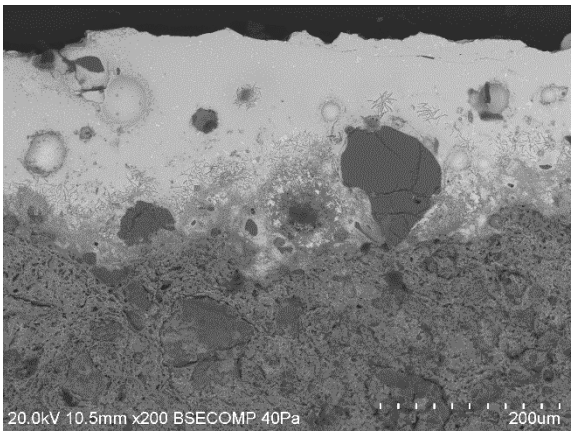

IVDJ-T 3683 blue

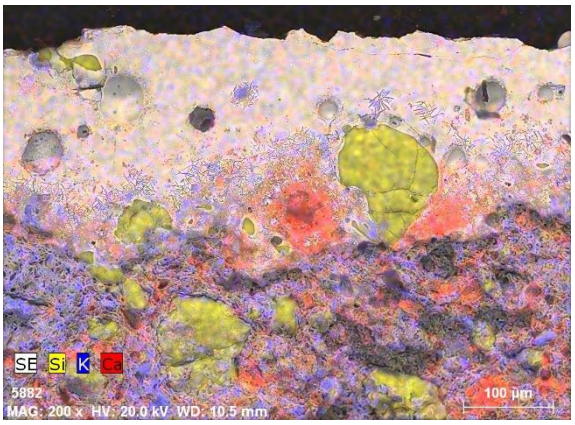

IVDJ-T 3683 blue – EDS map of the interface

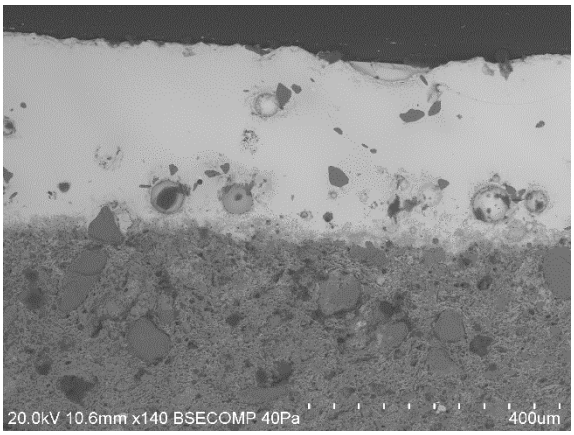

IVDJ-T 3683 white

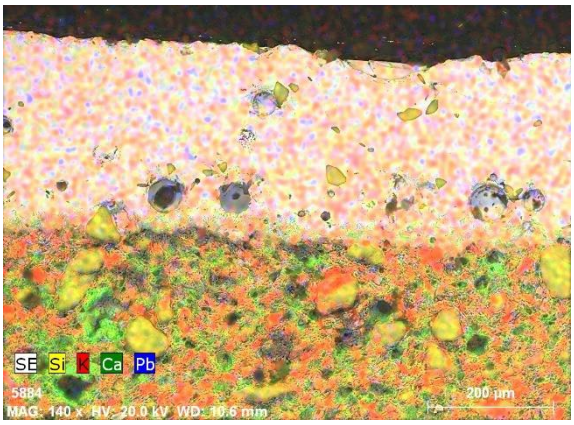

IVDJ-T 3683 white – EDS map

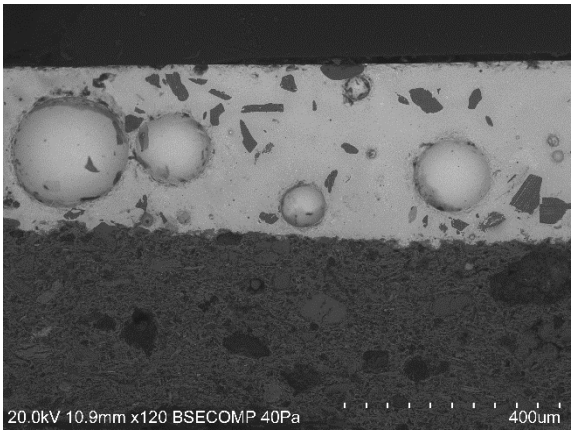

IVDJ-T 4095 blue

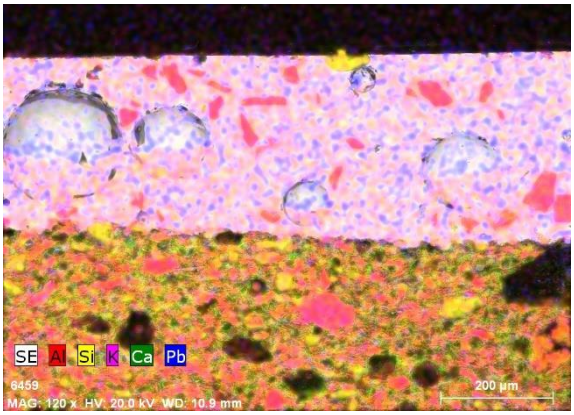

IVDJ-T 4095 blue – EDS map

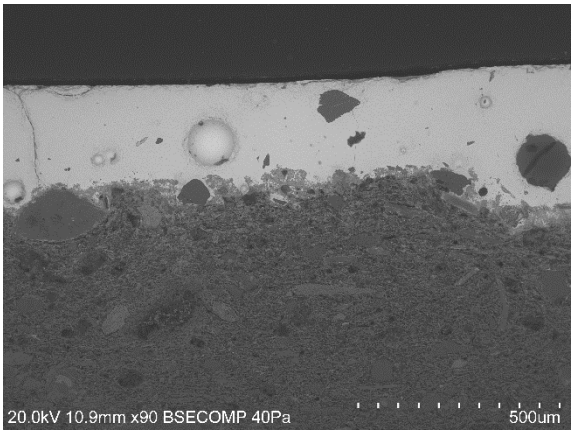

IVDJ-T amber

VII.4. MUSEO DE CERÁMICA Y ARTES SUNTUÁRIAS GONZÁLEZ MARTÍ, VALENCIA

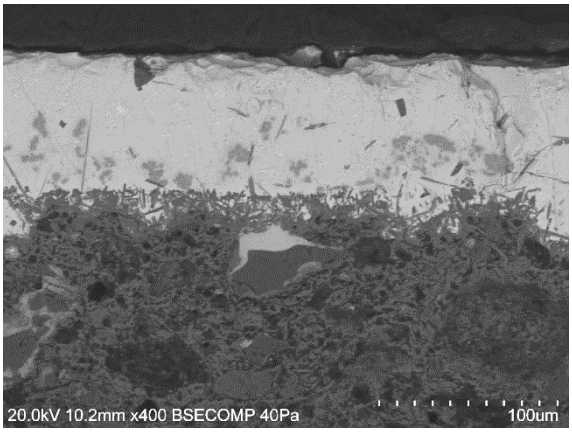

MCV 1.1R Brown

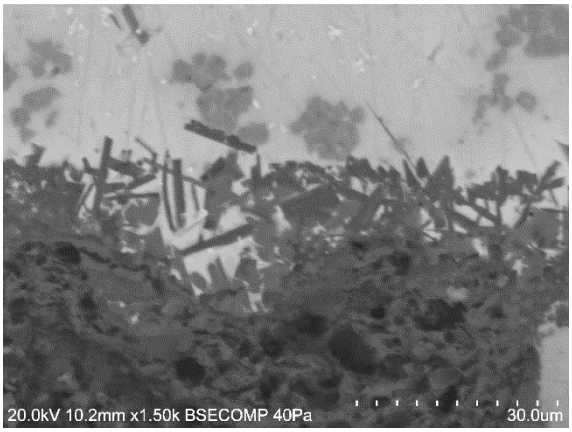

MCV 1.1R Brown – detail of the interface

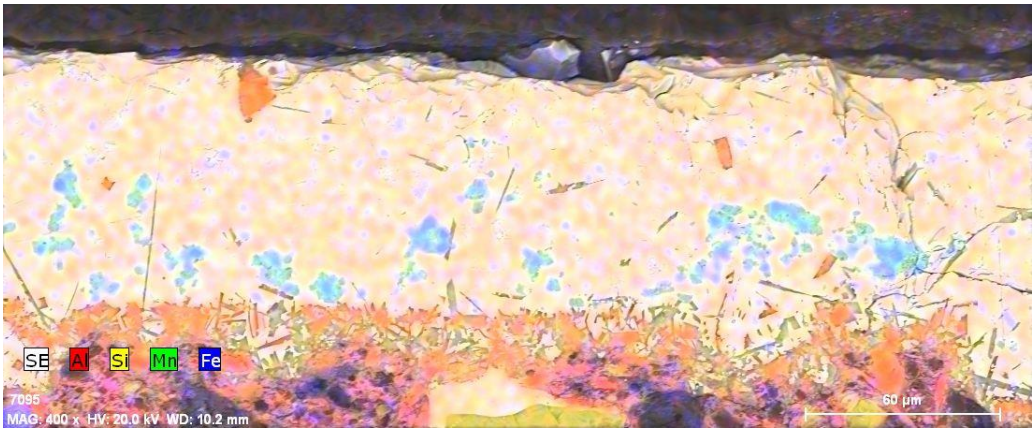

MCV 1.1R – Brown – EDS map

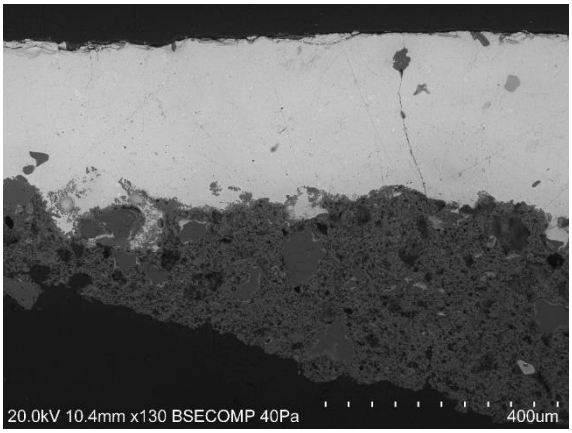

MCV 2.1T – White

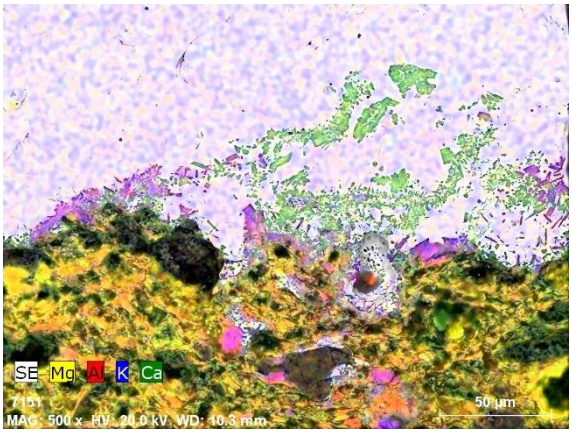

MCV 2.1T – White – EDS map of the interface

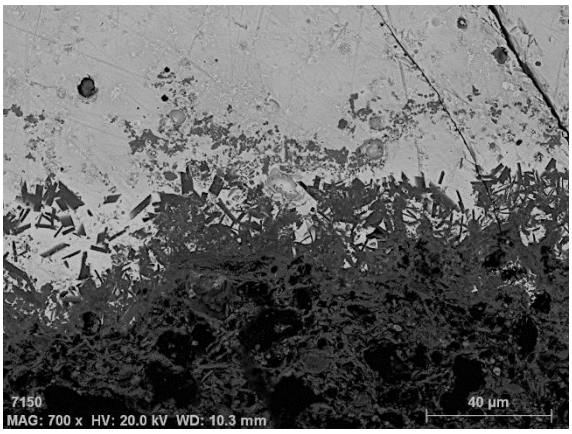

MCV 2.1T – Blue

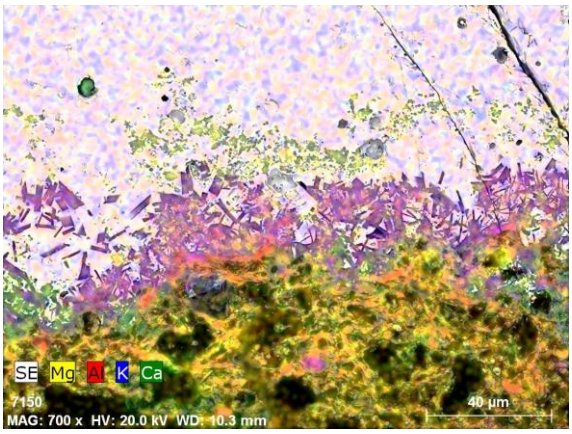

MCV 2.1T – Blue – EDS map of the interface

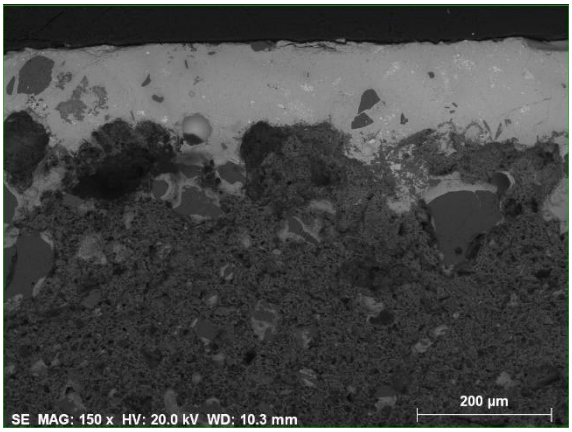

MCV 3.1R – White

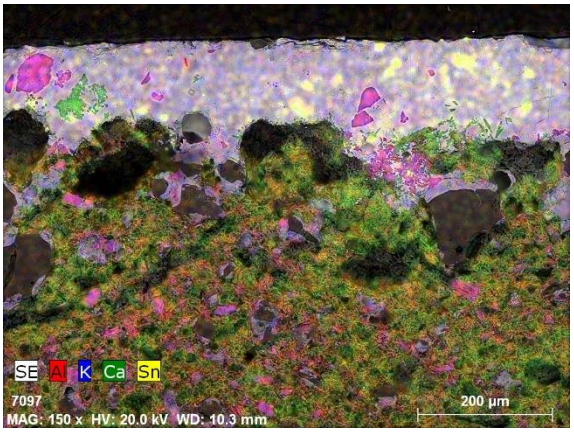

MCV 3.1R – White – EDS map

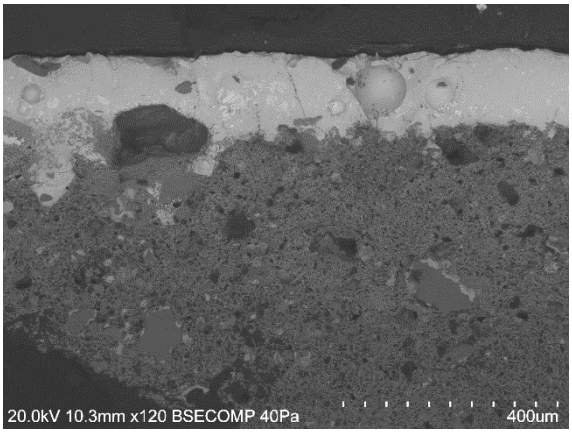

MCV 3.1R – Blue

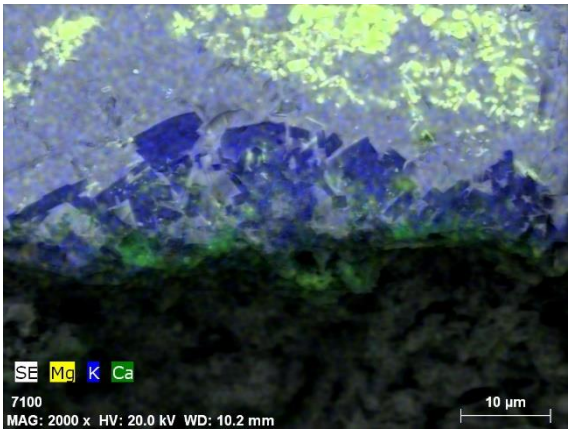

MCV 3.1R – Blue – EDS map of the interface

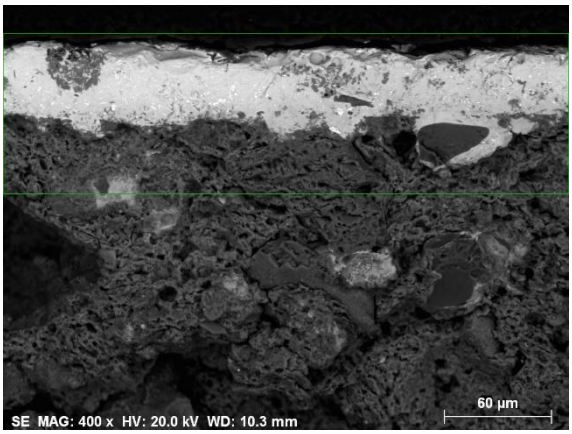

MCV 4.1G – White

MCV 4.1G – White – EDS map

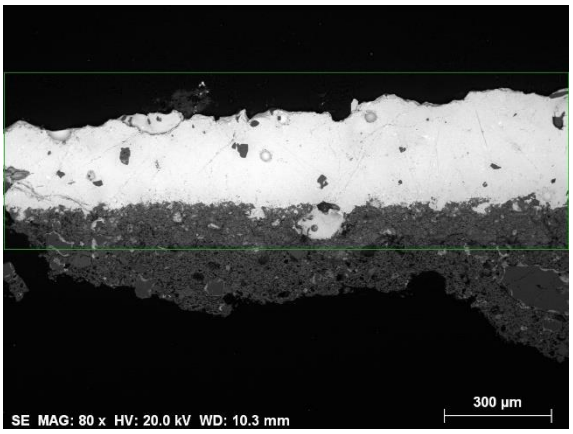

MCV 4.1G – Blue

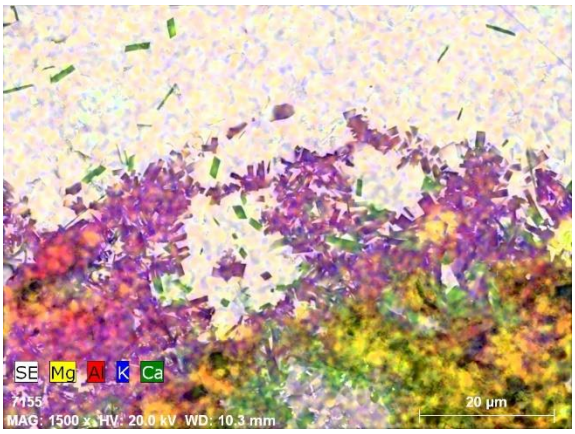

MCV 4.1G – Blue – EDS map of the interface

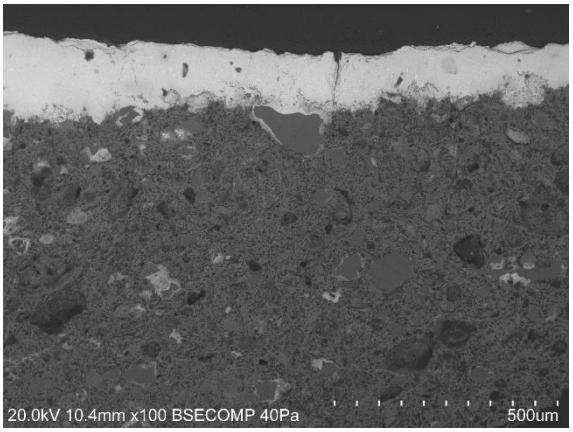

MCV 4.1ML – White

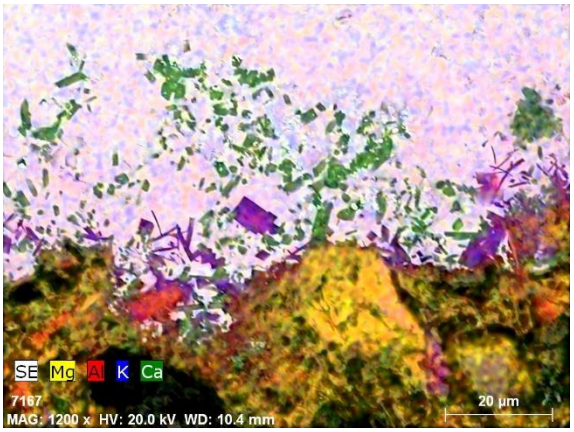

MCV 4.1ML – White – EDS map of the interface

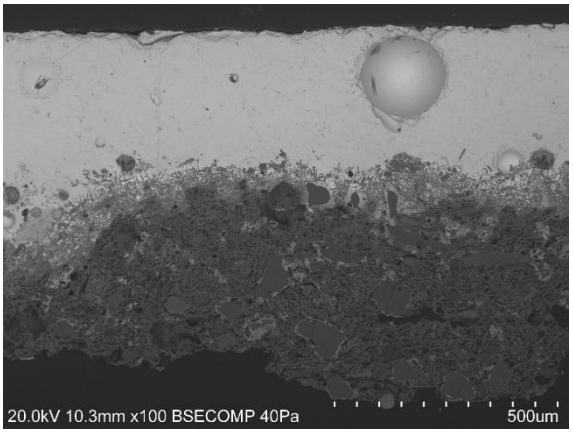

MCV 4.1ML – Green

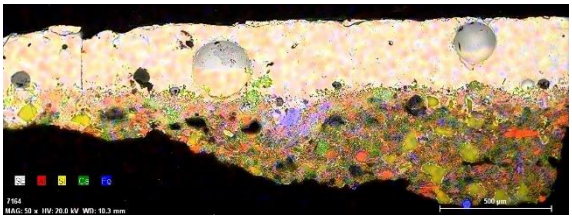
MCV 4.1ML – Green – EDS map

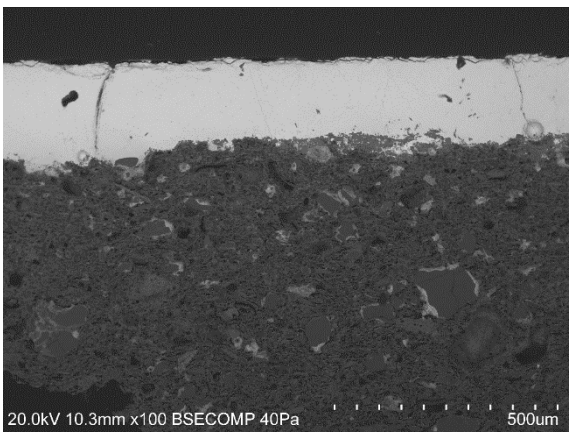

MCV 4.1ML – Amber

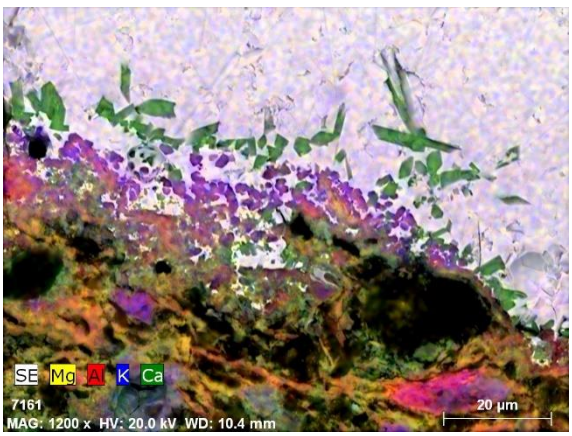

MCV 4.1ML – Amber – EDS map of the interface

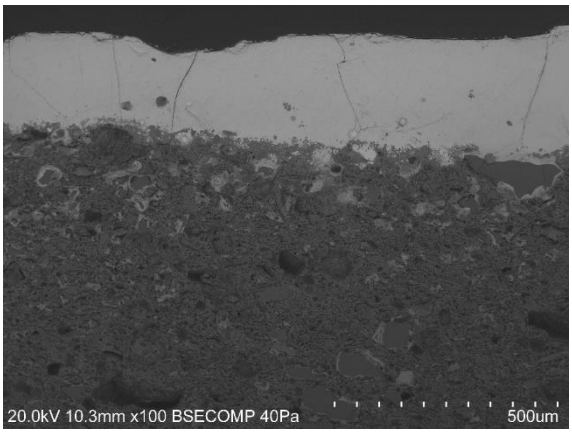

MCV 4.1ML – Brown

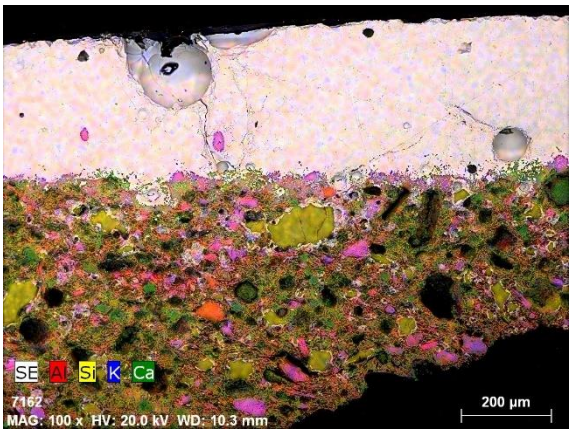

MCV 4.1ML – Brown – EDS map

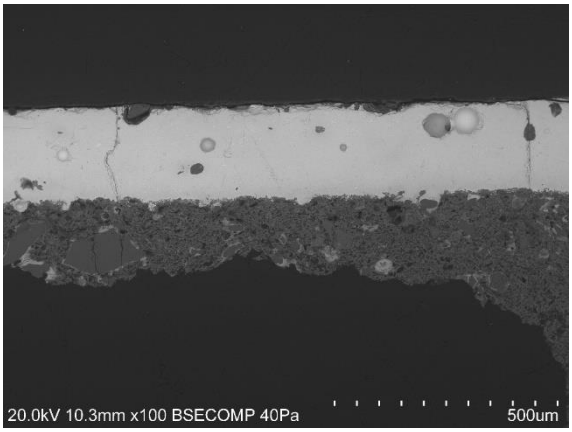

MCV 4.2G – White

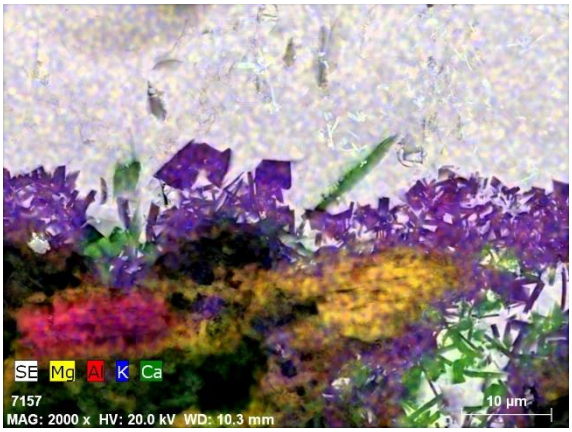

MCV 4.2G – White – EDS map of the interface

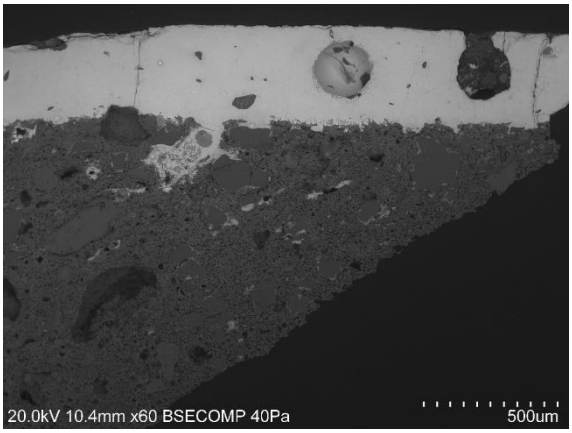

MCV 4.2G – Blue

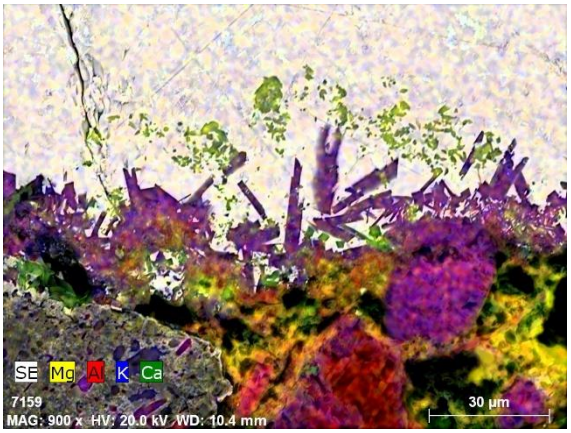

MCV 4.2G – Blue – EDS map of the interface

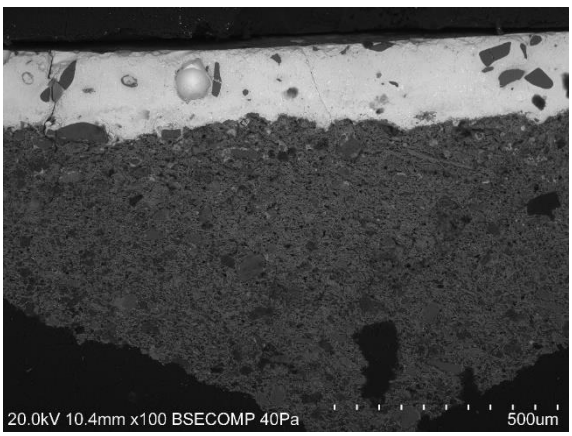

MCV 5.1R – White

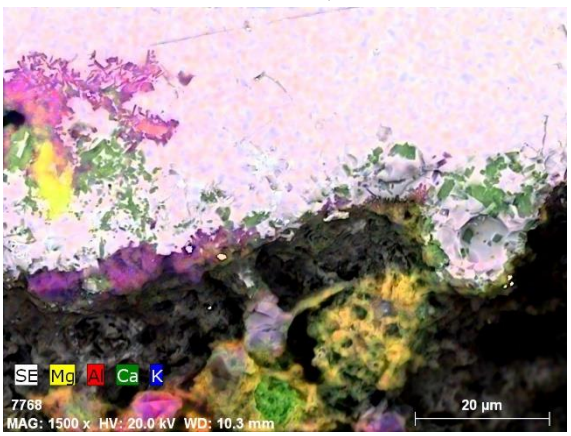

MCV 5.1R – White – EDS map of the interface

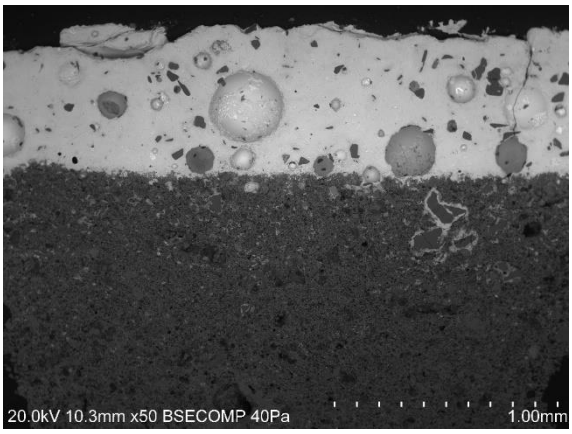

MCV 5.1R – Blue

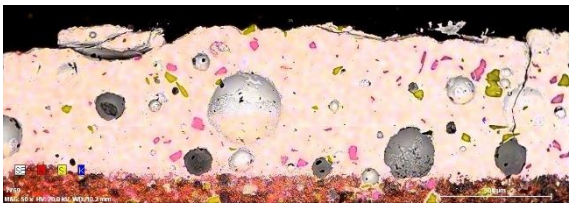

MCV 5.1R – Blue – EDS map

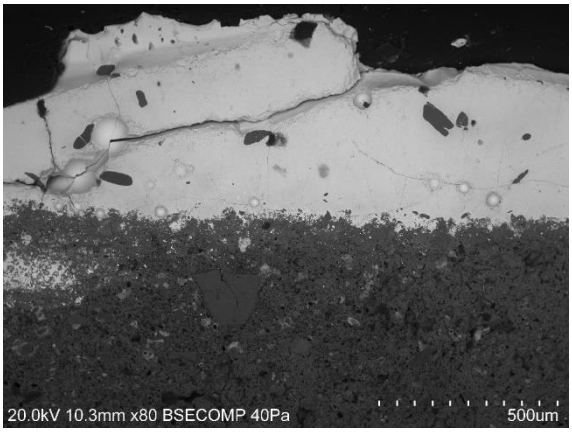

MCV 5.1R – Green

MCV 5.1R – Green – EDS map of the interface

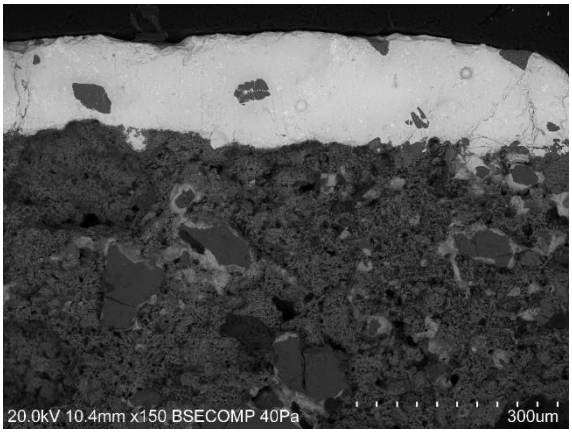

MCV 6.1C – White

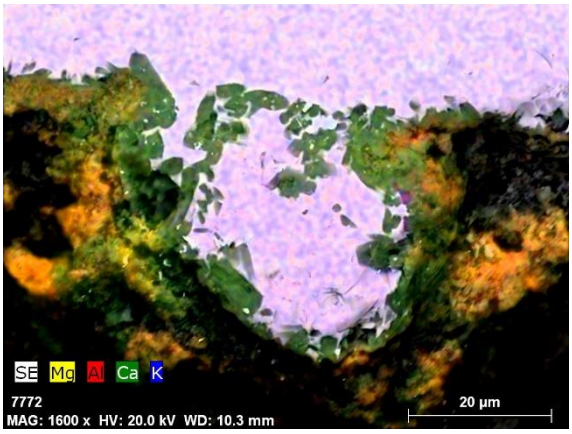

MCV 6.1C – White – EDS map of the interface

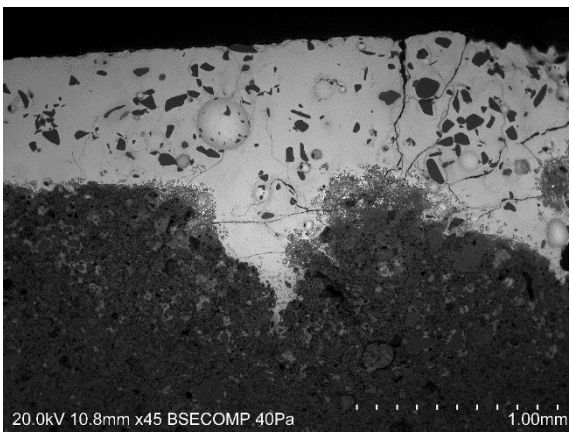

MCV 6.1C – Green

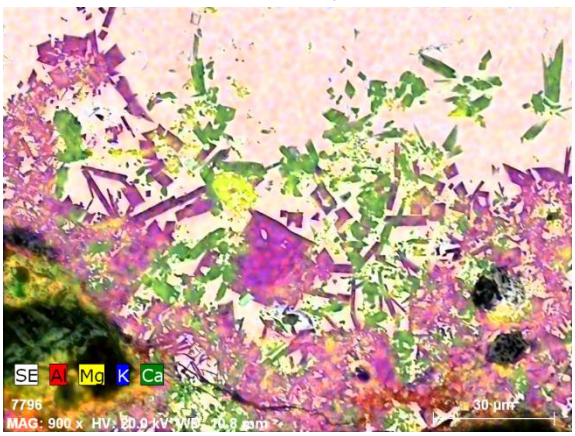

MCV 6.1C – Green – EDS map of the interface

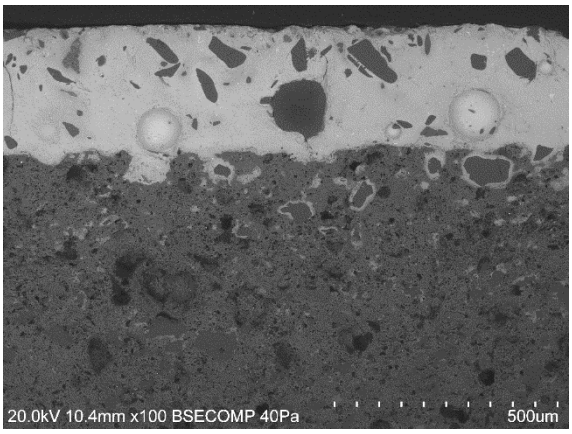

MCV 7.1C – White

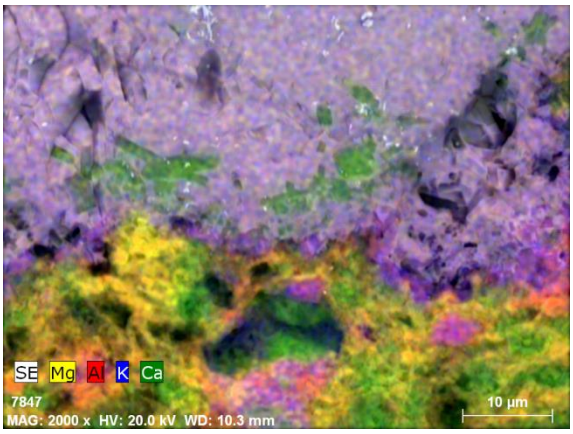

MCV 7.1C – White – EDS map of the interface

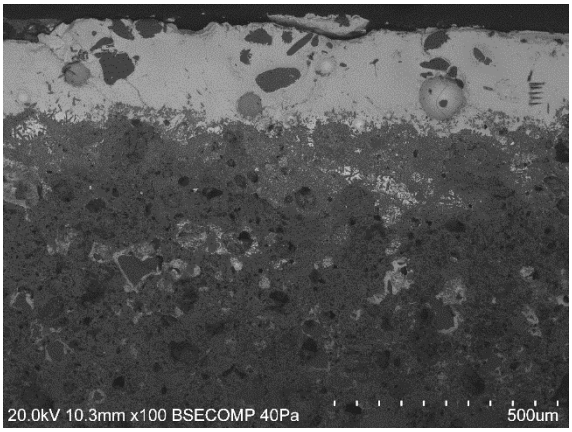

MCV 7.1C – Green

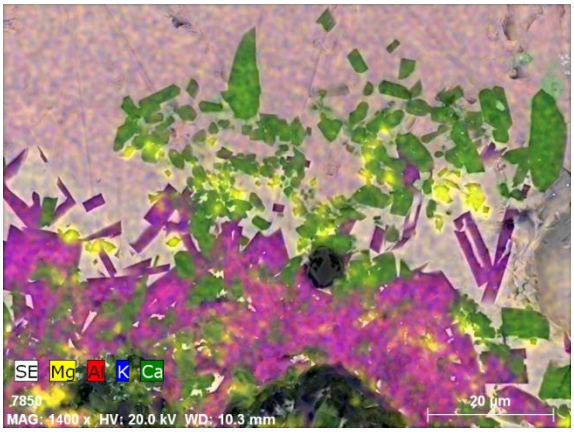

MCV 7.1C – Green – EDS map of the interface

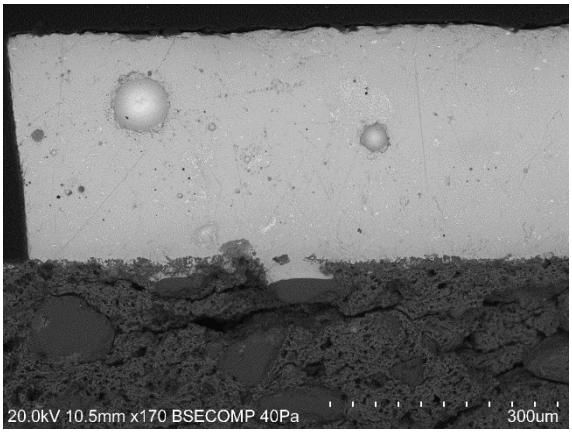

MCV 8.1G – Blue

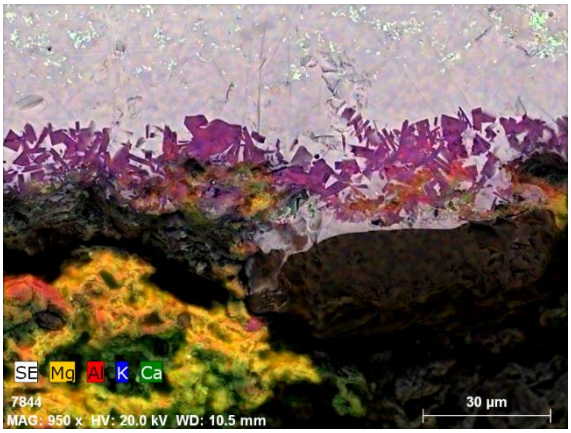

MCV 8.1G – Blue – EDS map of the interface

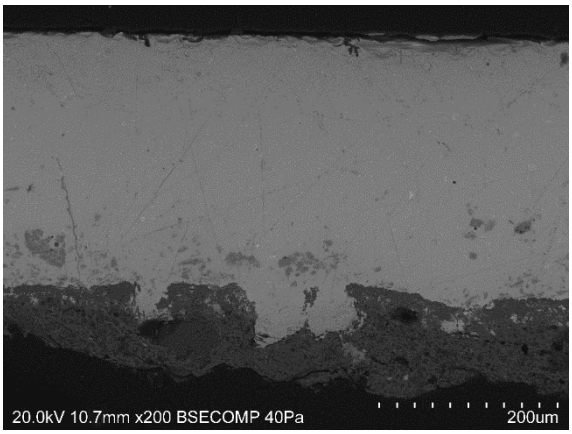

MCV 8.1G – Brown

MCV 8.1G – Brown – EDS map of the interface

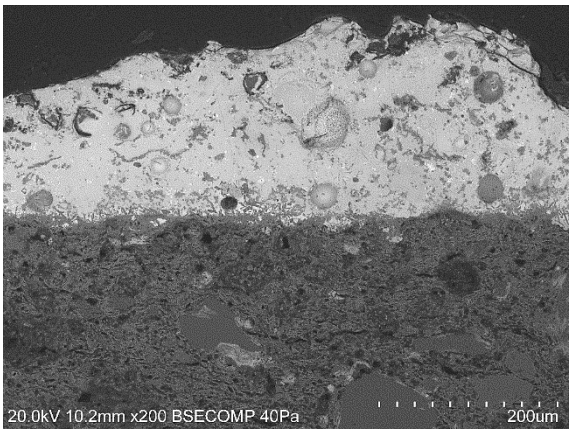

MCV 8.2C – Blue

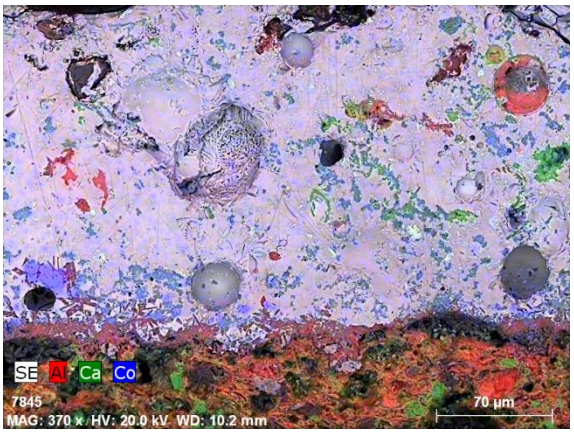

MCV 8.2C – Blue – EDS map

VII.5. CASA DE PILATOS, SEVILLE

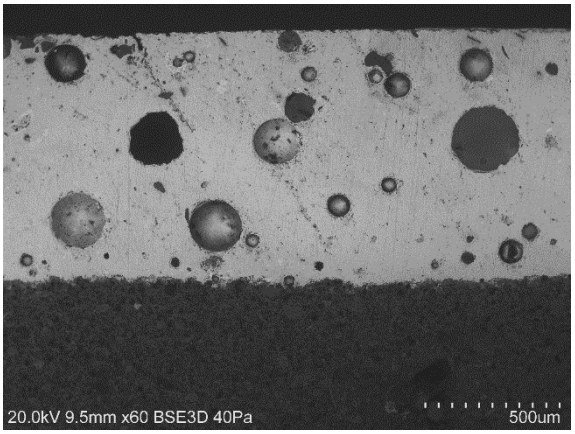

CPS 01 blue

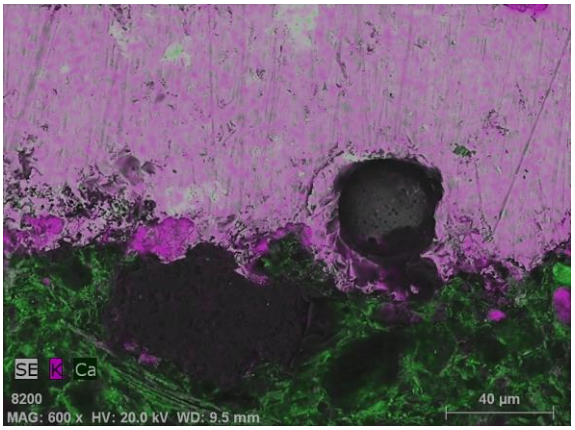

CPS 01 blue – EDS map of the interface

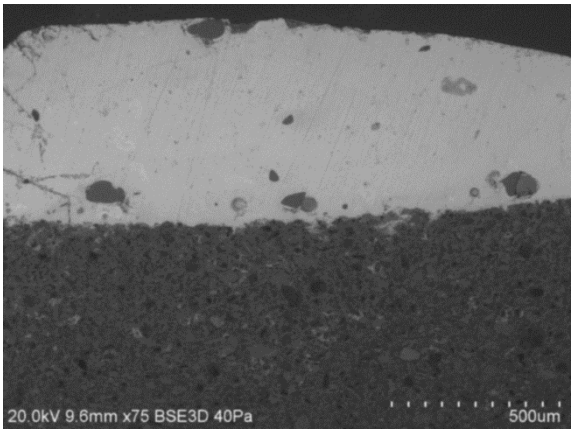

CPS 01 brown

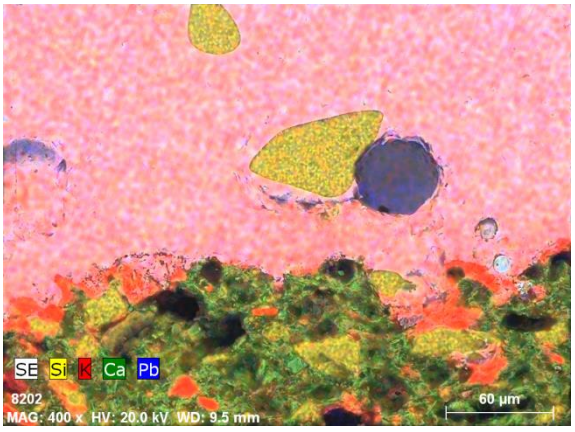

CPS 01 brown – EDS map of the interface

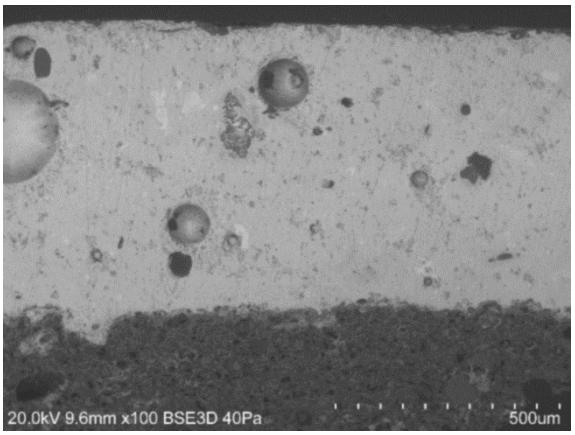

CPS 01 white

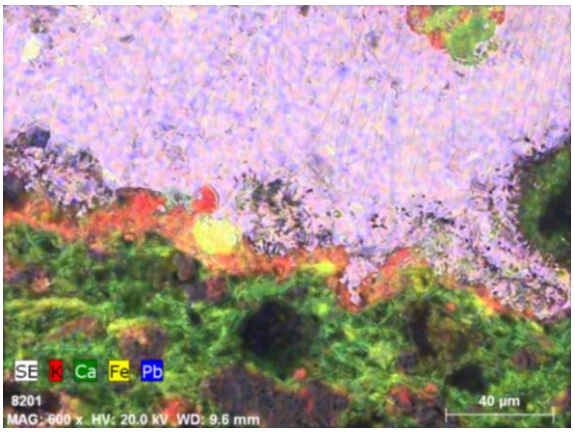

CPS 01 white – EDS map of the interface

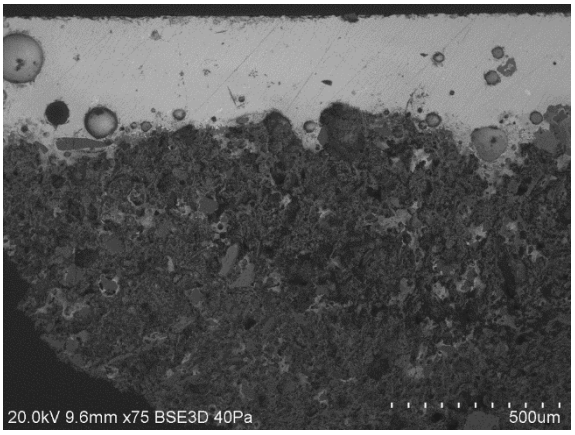

CPS 02 green

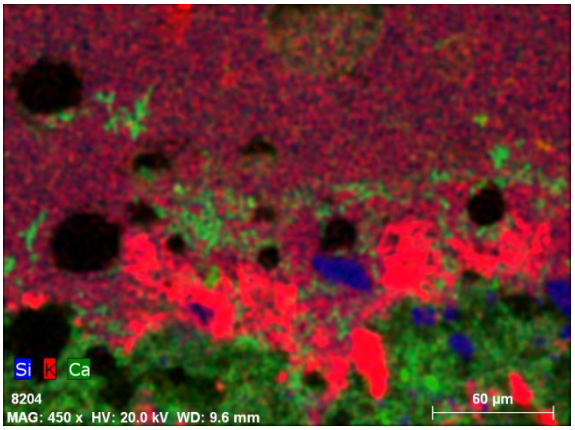

CPS 02 green – EDS map of the interface

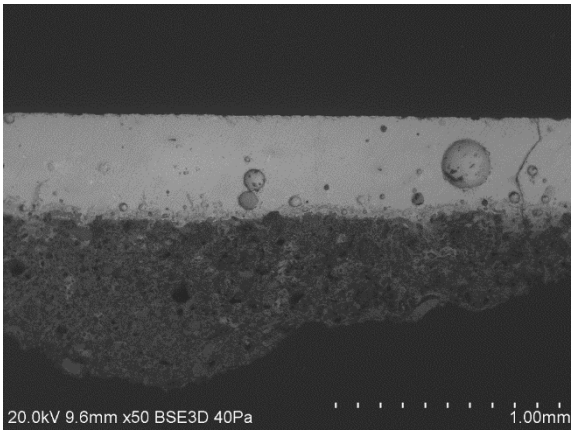

CPS 02 white

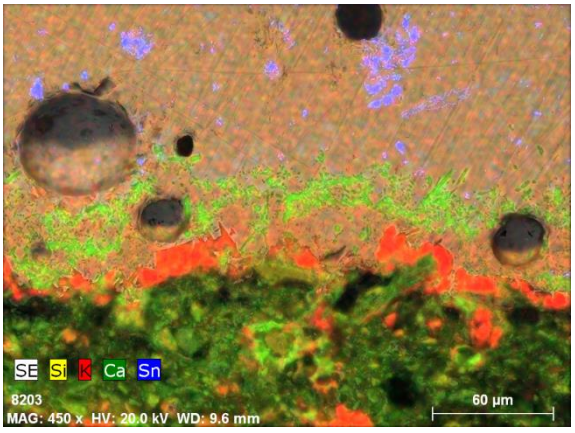

CPS 02 white – EDS map of the interface

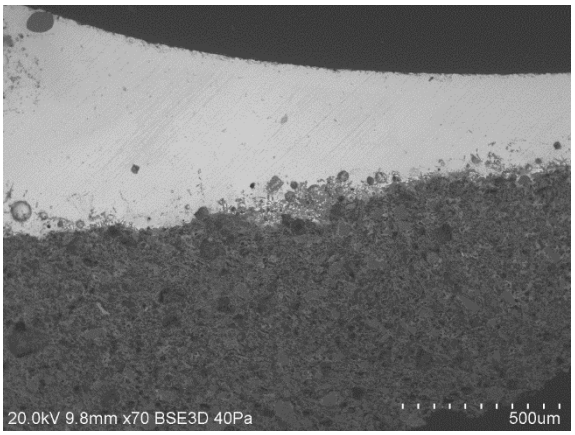

CPS 02 amber

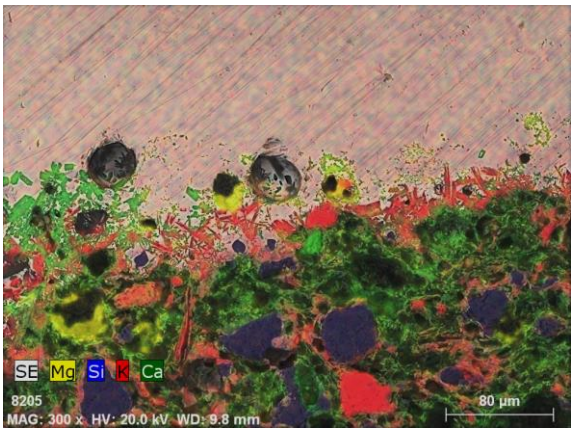

CPS 02 amber – EDS map of the interface

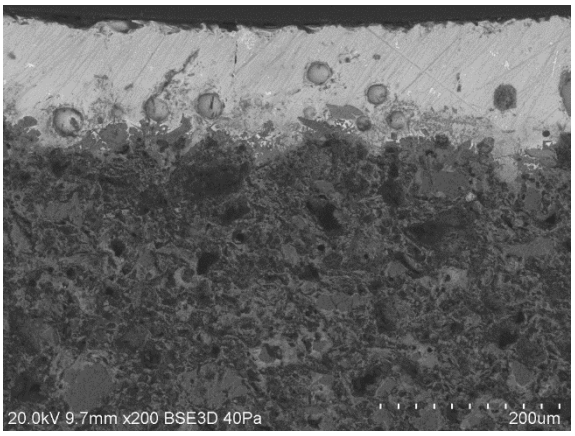

CPS 02 blue

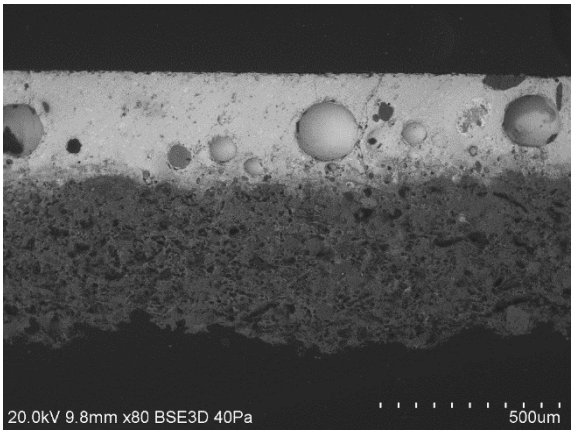

CPS 03 blue

CPS 03 blue – EDS map

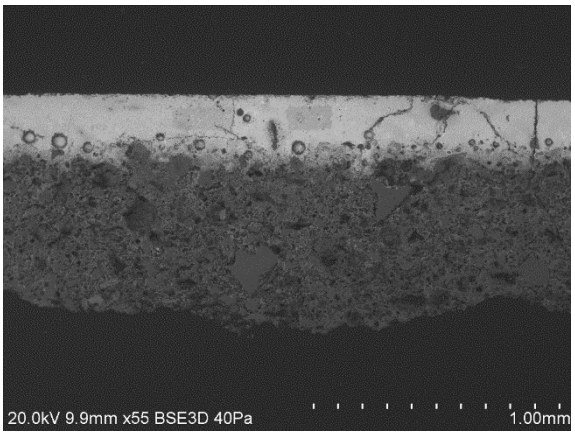

CPS 03 white

CPS 03 white – EDS map

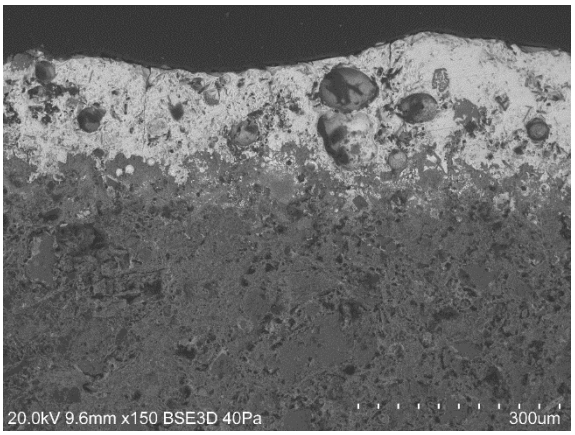

CPS 04 green

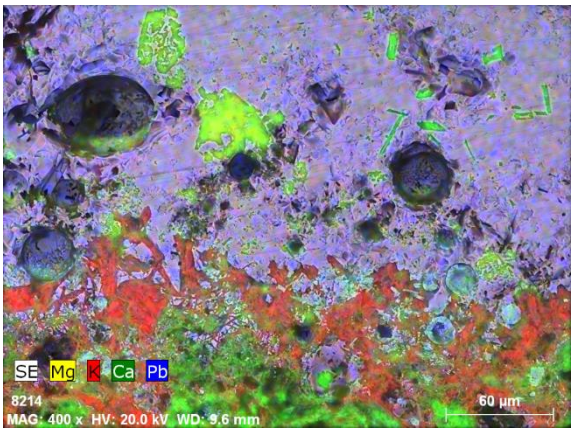

CPS 04 green – EDS map of the interface

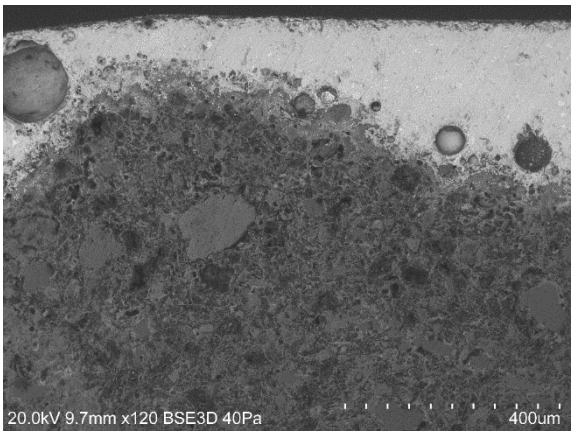

CPS 04 blue

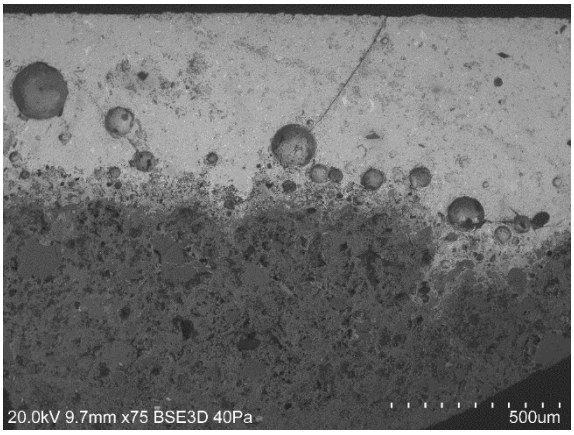

CPS 04 white

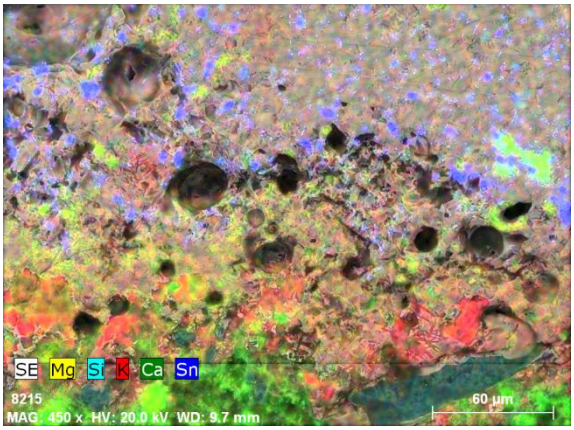

CPS 04 white – EDS map of the interface

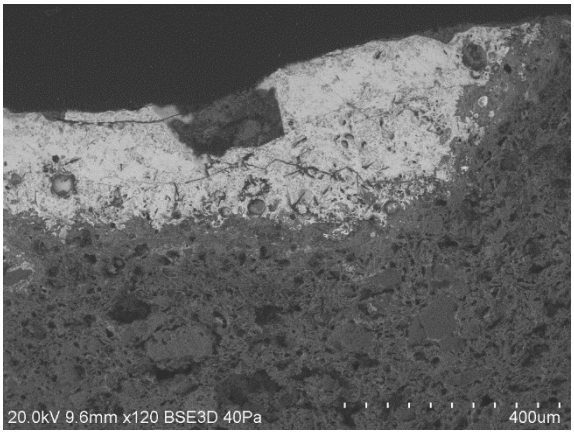

CPS 04 brown

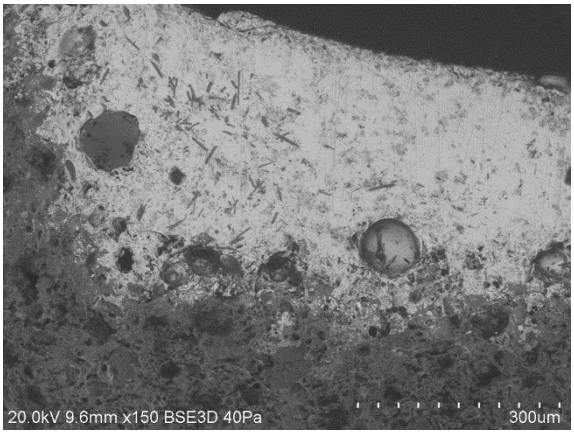

CPS 04 amber

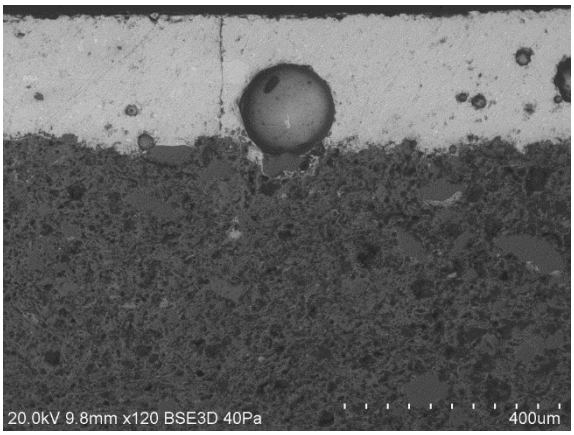

CPS 05 white

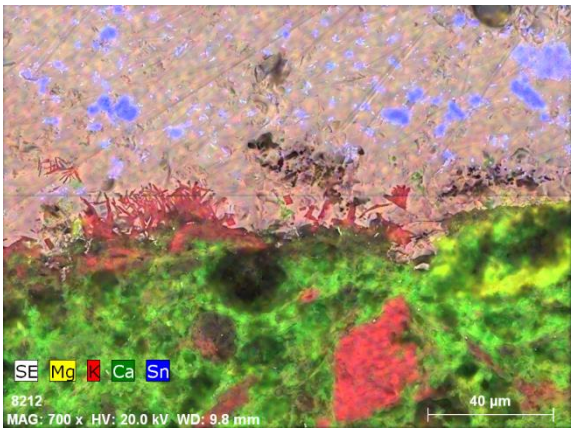

CPS 05 white – EDS map of the interface

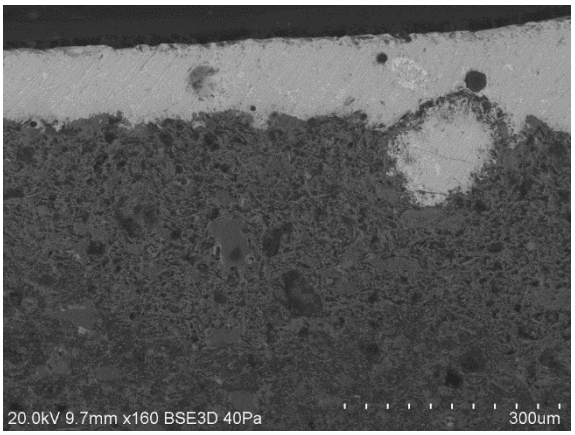

CPS 05 blue

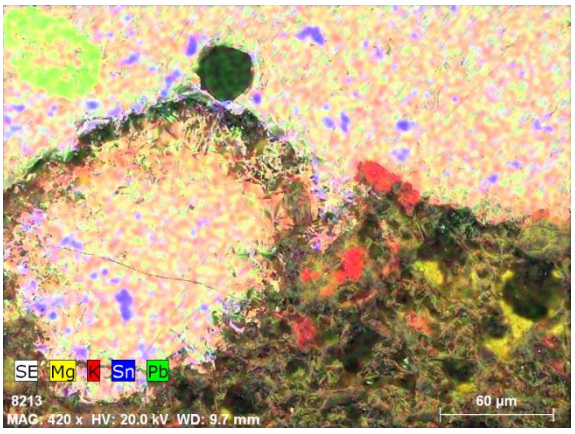

CPS 05 blue – EDS map of the interface

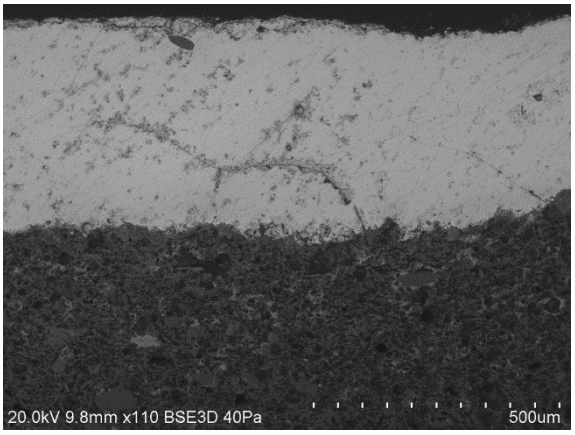

CPS 05 amber

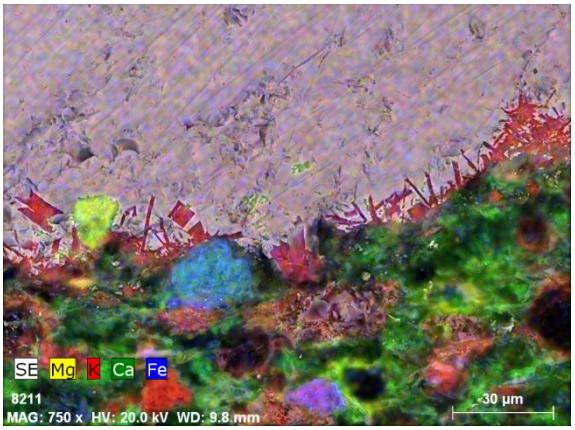

CPS 05 amber – EDS map of the interface

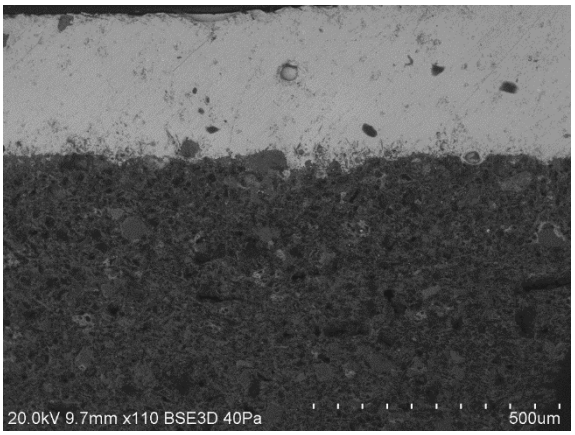

CPS 05 brown

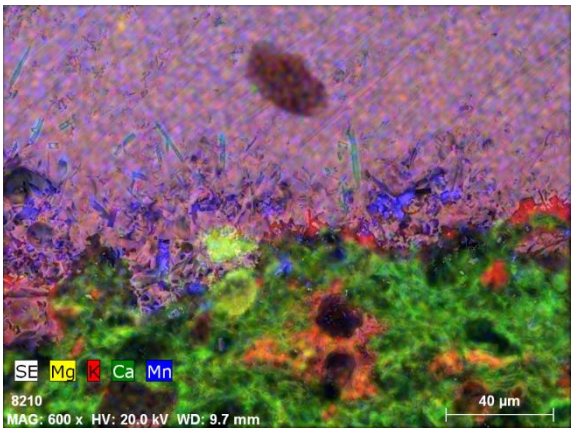

CPS 05 brown – EDS map of the interface

APPENDIX VIII

SEMI-QUANTIFICATION RESULTS OBTAINED FROM THE μ-XRD ANALYSIS

Table VIII.1. Semi-quantification results obtained from the μ-XRD analysis

	Quartz	Calcite	Gehlenite	Diopside	Hematite	Plagioclase	Wollastonite
	01-078-2315	01-072-1652	01-074-1607	01-075-0945	01-085-0595	01-075-1142	01-072-2284
CPS 01	++	+	+	+		+	
CPS 02	+++	+	+	+	+	+	
CPS 03	++	+	+	+	+	+	
CPS 04	++	++	+	+	+	+	
CPS 05	++	++	+	+	+	+	
MCV 1-1R	++	+	+++	+			
MCV 2-1T	++	++	++	+			
MCV 3-1R	+	+++	++	+			
MCV 4-1G	+	++++	+	+			
MCV 4-1ML	++	+	+	++		+	
MCV 4-2G	+	++++	+	+	+		
MCV 5-1R	++	++	++	+			
MCV 6-1C	++	++	++	+	+		
MCV 7-1C	++	++	+++	+	+		
MCV 8-1G	+++		+	+	+	+	
MCV 8-2C	+++	+	+	+		++	
MCV 8-3G	+	++	++	+	+		
MCV 9-1Ag	++	+	++	+	+		
MCV 9-2Ap	+++	++	++	+			
MCV 10-1	+++	++	+	+	+		
MCV 10-2	++	++	+	+	+	+	
MCV 10-3	++	+	++	+	+	+	
MCV M62	++	+++	++				
PNS 06	++	++++				+	
PNS 07	++	++	+	++	+	+	
PNS 08	++	++	+	+		+	
PNS 10	++	++	+	+	+	+	
PNS 17	+	++++	+		+	+	
PNS 20	+++	+	+	+	+	+	
PNS 21	+++	+	+	+		+	
PNS 22	++	++	+			+	
PNS 23	+++	+	+	+	+	+	
PNS 24	++	+	++		+	+	
PNS 25	++++	+	+	+		+	
PNS 26	++	++++	+		+	+	
PNS 27	+++	+	+	+	+		
PNS 28	+	+	++	++	+		
PNS 29	++++	+	+		+	+	
PNS 30	++	+	++	+	+	+	
PNS 31	++	++	++	+			
PNS 32	++	+	++	+	+	+	
PNS 33	++	+	+	+	+	+	
PNS 34	++	+	++	++	+	+	
PNS 35	++	+	+	++	+	+	
PNS 36	++	+	+	+	+	+	
PNS 37	++	+	+	+	+	+	
PNS 38	++	+	+	++	+	+	
PNS 39	+	++	+	+	+	+	

Table VIII.1. (Cont.) Semi-quantification results obtained from the μ-XRD analysis

	Quartz	Calcite	Gehlenite	Diopside	Hematite	Sanidine	Plagioclase	Wollastonite
	01-078-2315	01-072-1652	01-074-1607	01-075-0945	01-085-0595	01-089-1455	01-075-1142	01-072-2284
SCV 4i365	++	+		++	+	+	+	
SCV 6Ai1152	++	+	+	++	+		+	
SCV 9F1501	++	+	+	++	+	+	+	
SCV 9i469	++	+	++	++	+		+	
SCV 10EF175	++++	+	+	+	+			
SCV 18Ai2914	++	+	+	++	+		+	
SCV 20i2989	+++	+		+	+		+	
SCV 21AM3076	+++	+	+	+	+	+	+	
SCV 24Ci3386	++	++	+	+	+	+	+	
SCV 27i3426	++++	+	+		+		+	
SCV 33Bi3839	+++	+	+	++	+		+	
SCV 33Bi3841	+++			++	+		+	
SCV 33Bi3870	++++		+	+	+			
SCV 34Bi4060	++		+	+	+	+	+	
SCV 34Ei4068	++	+	+	++	+		++	
SCV 34FM4072	++		+	+++	+			
SCV 35Hi7790	+++	+	+	+	+		+	
SCV 45M4260	++	++	+	++	+		+	
SCV 47Ai4284	++	++		+	+		++	
SCV 49-4i4327	++	+	+	++	+		++	
SCV 49-15F4338	+	+	+	++	+	++	++	
SCV 50-7F4348	++	+	+	+	+		++	
SCV 50-11M4352	++	++	+				++	
SCV 51-1M4361	++	+	+	+	+		++	
SCV 60Bi4569	+++		+	+	+	+	+	
SCV 80F4745	++	+	+	+	+	+		++
SCV 87M7985	++++			+			++	
SCV SPF8435	+++		+	++			++	
SCV SPM8434	++		+	+			++	
IVDJ-S 3589	++	++	+	+	+	+	+	
IVDJ-S 3601	++	++	+	+	+		+	
IVDJ-S 3774	+	++++	+	+			+	
IVDJ-S 4098	+	+++	+	+			+	
IVDJ-S 4127	+	++++	+	+	+		+	
IVDJ-S 4134	++	+	+	+	+	++	+	

Legend:

+ (< 20%) | ++ (20% > 40%) | +++ (40% > 60%) | ++++ (60% > 80%) | +++++ (80% > 100%)

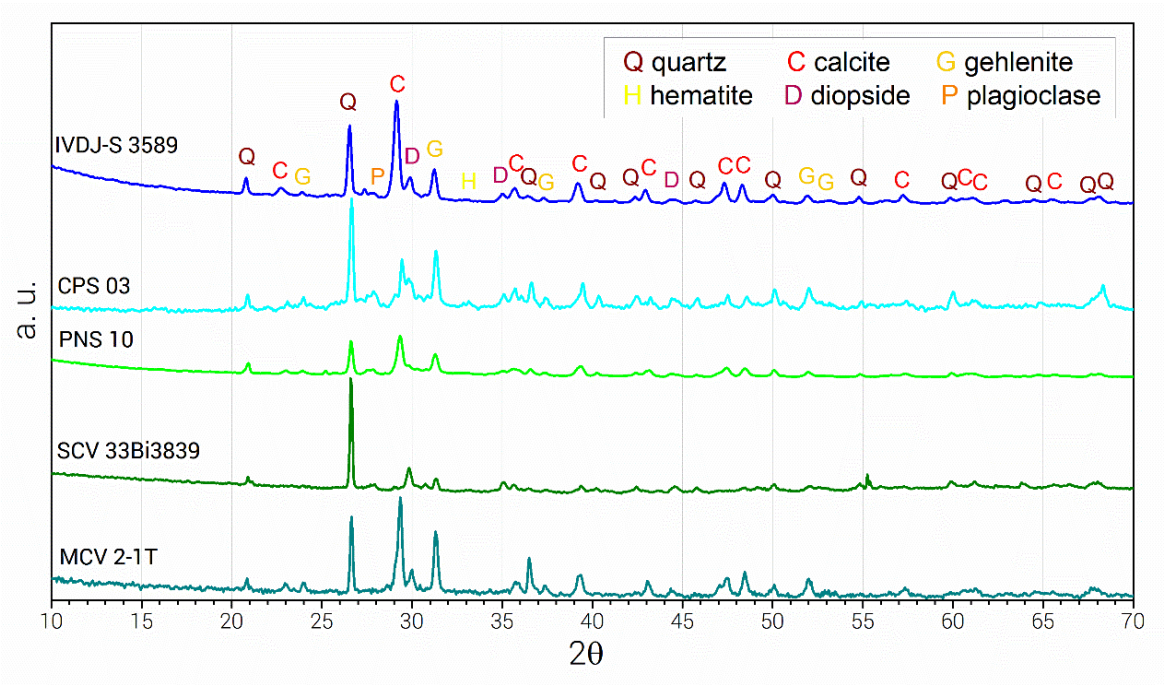

Figure VIII.1. Diffractograms of five samples representing each studied collection

APPENDIX IX
SYNCHROTRON μ-XRD RESULTS

IVDJ-T 96 – blue
Ceramic body

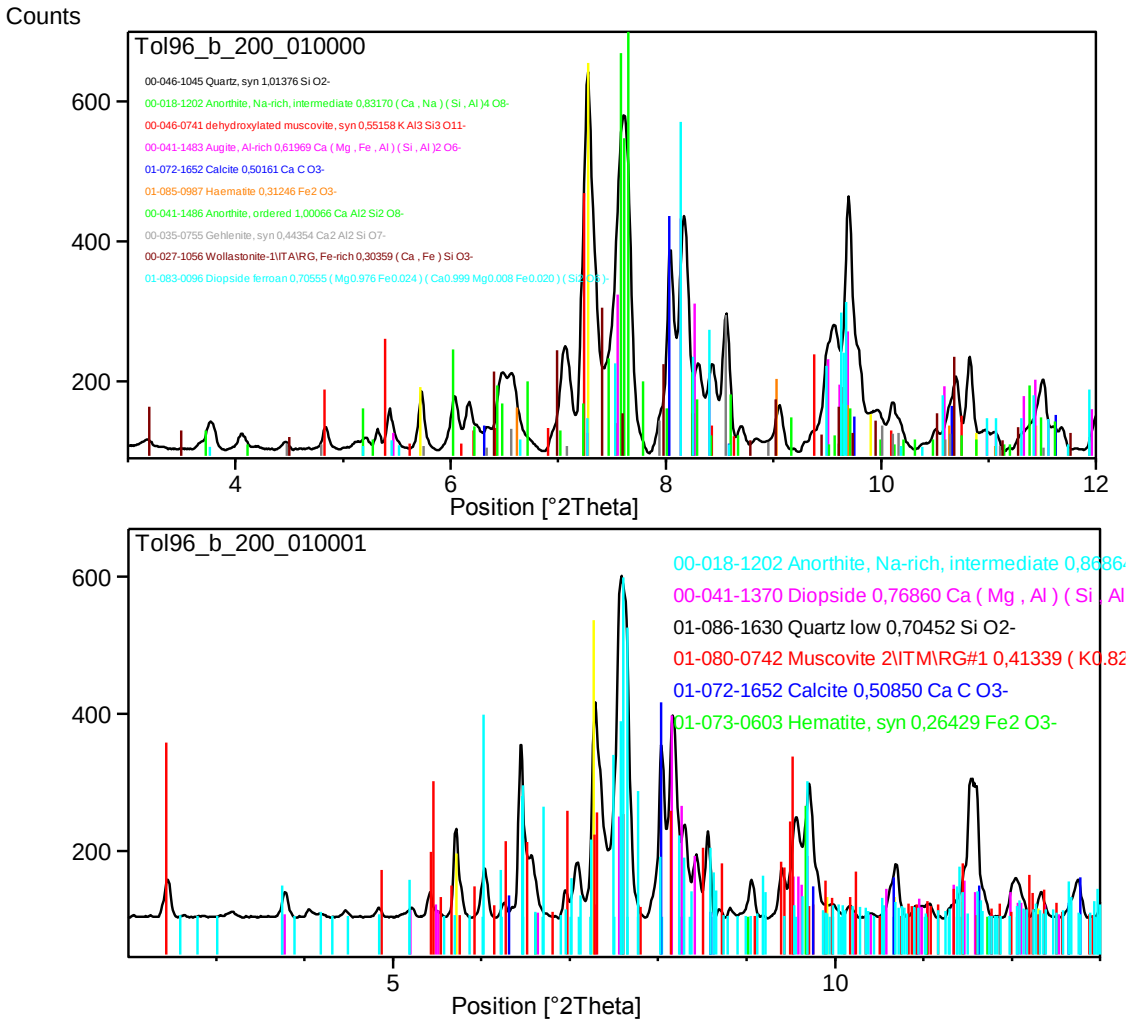

Glaze

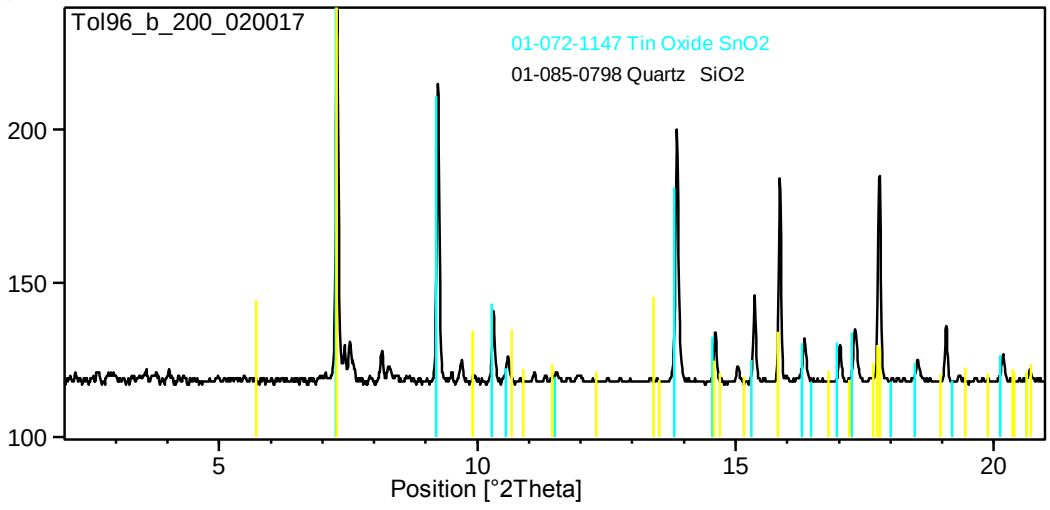

IVDJ-T 4095 – blue

Ceramic body

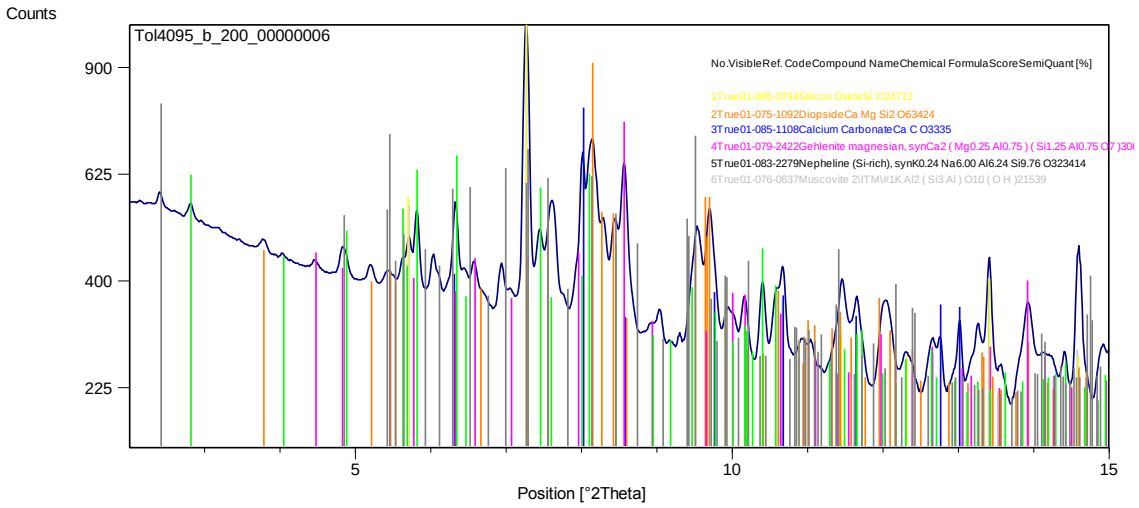

Interface

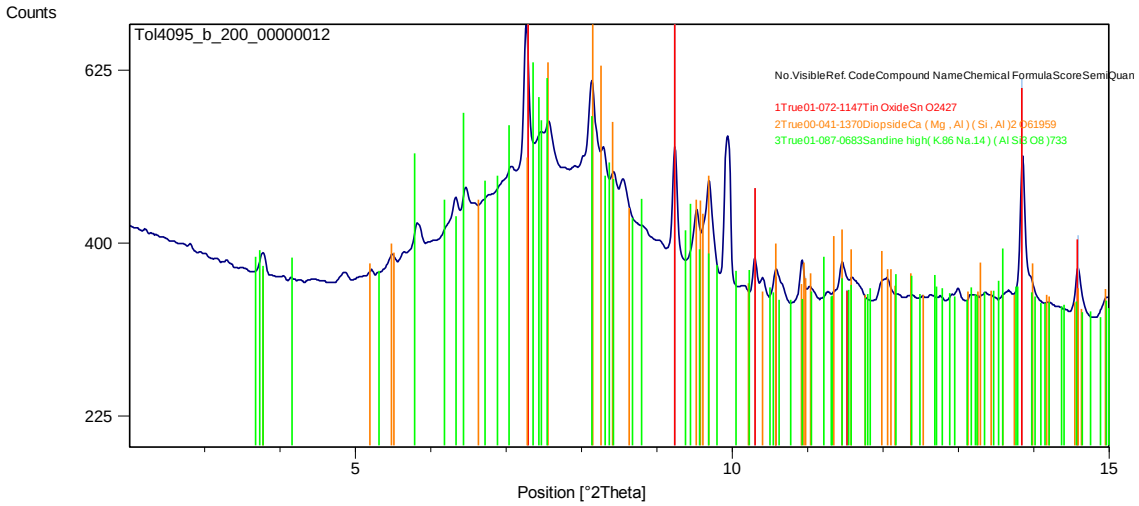

IVDJ-T 3944 – green

Ceramic body

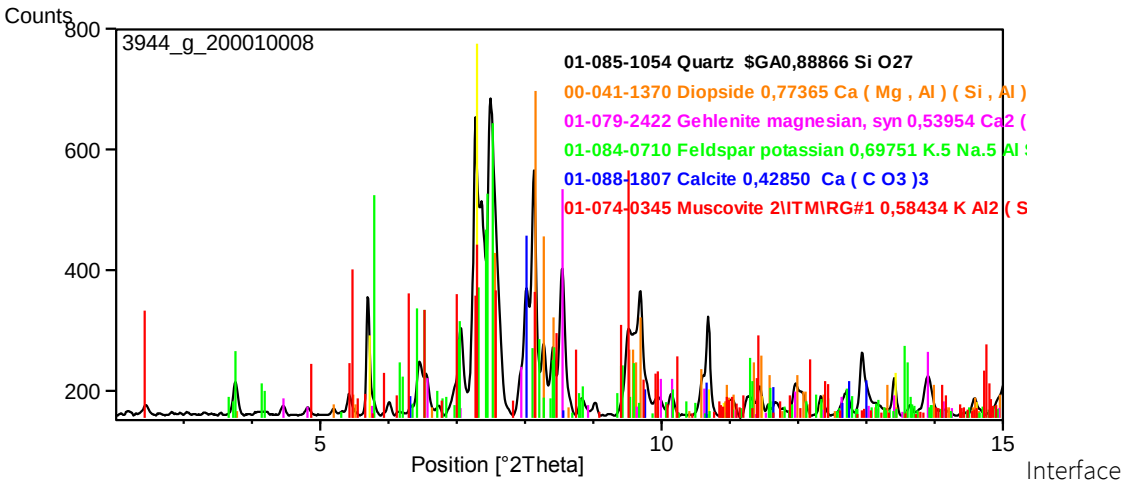

Interface

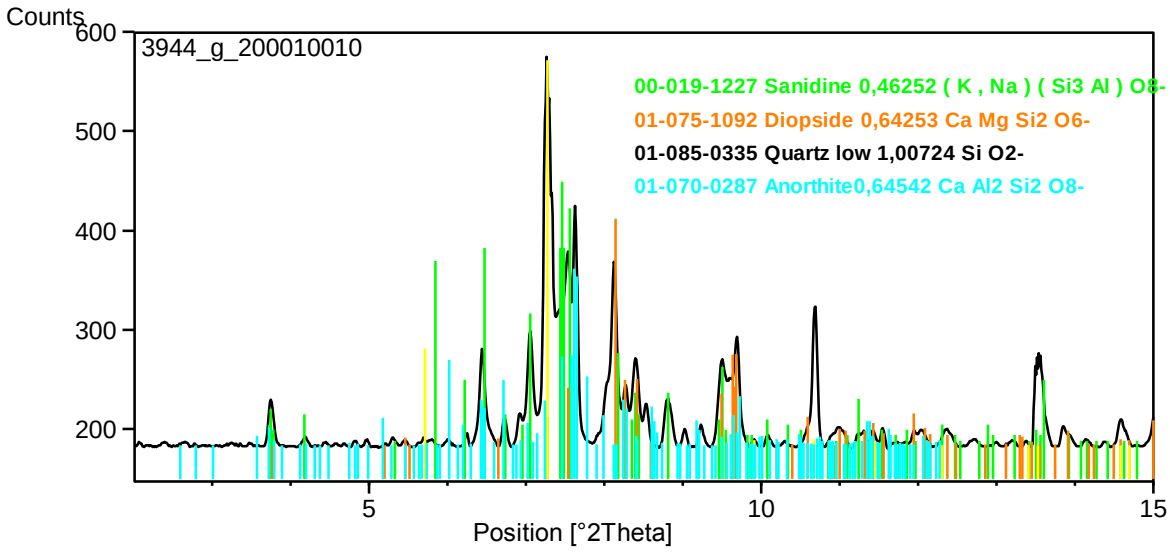

Glaze

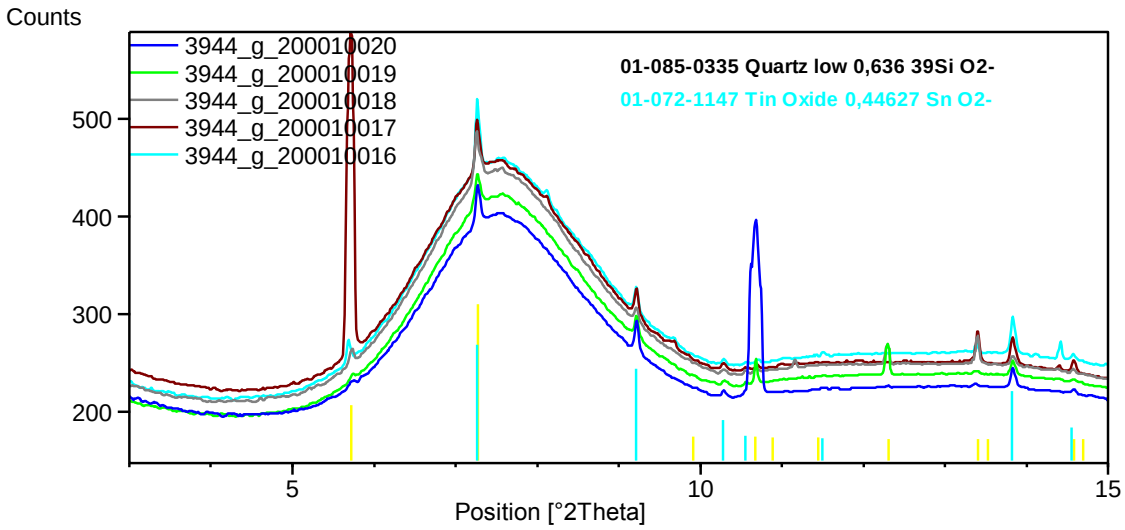

IVDJ-S XV – green

Ceramic body

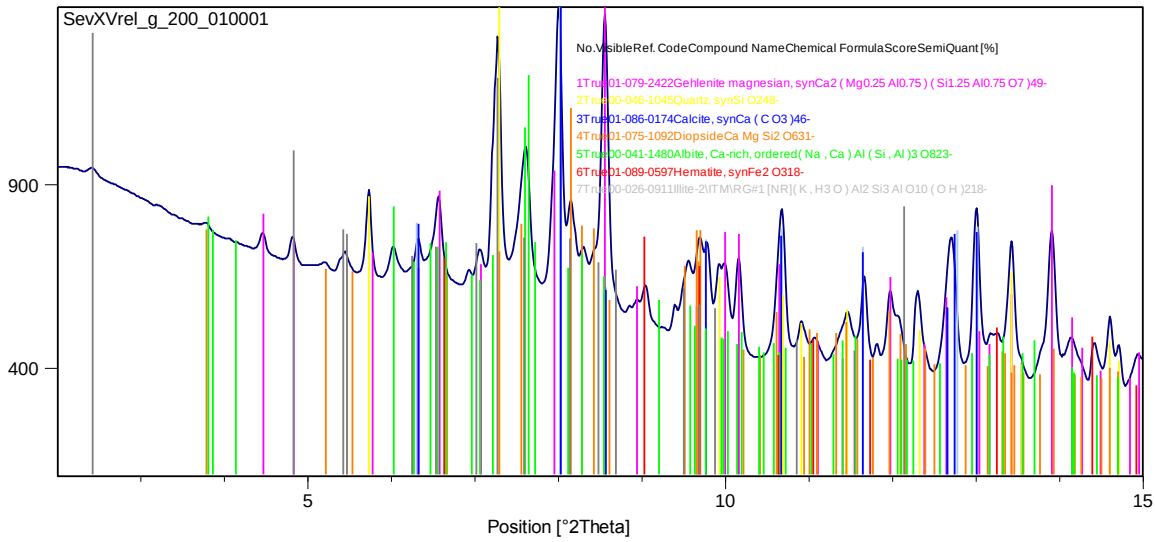

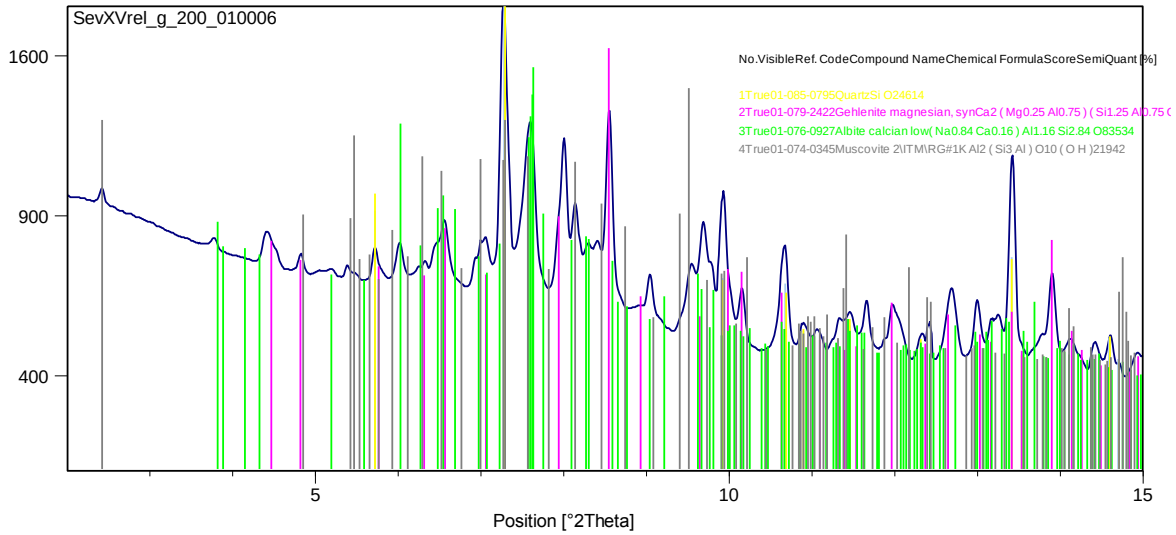

IVDJ-S 3561 – turquoise

Ceramic body

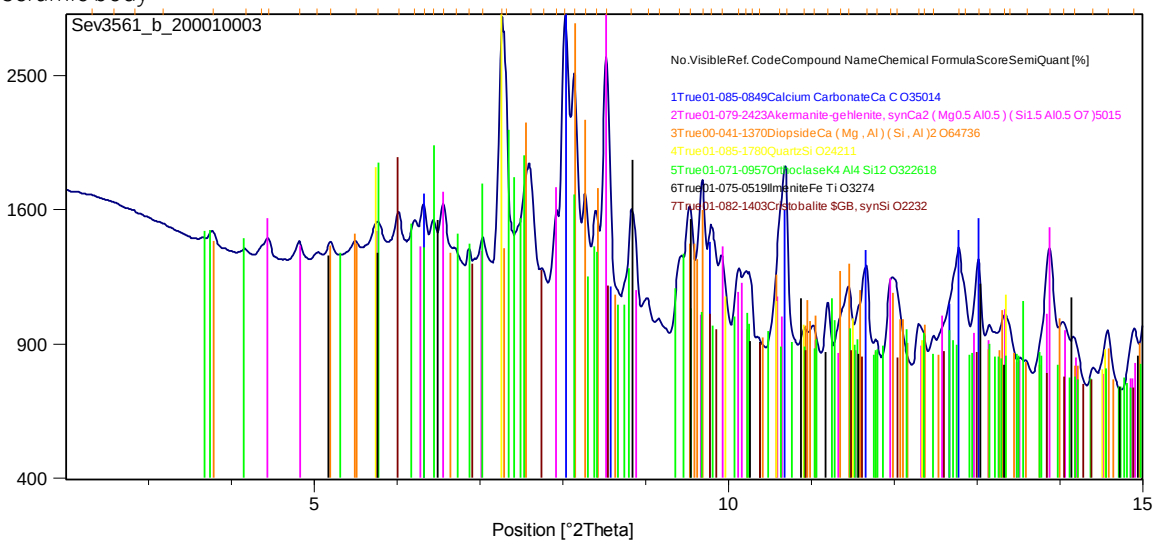

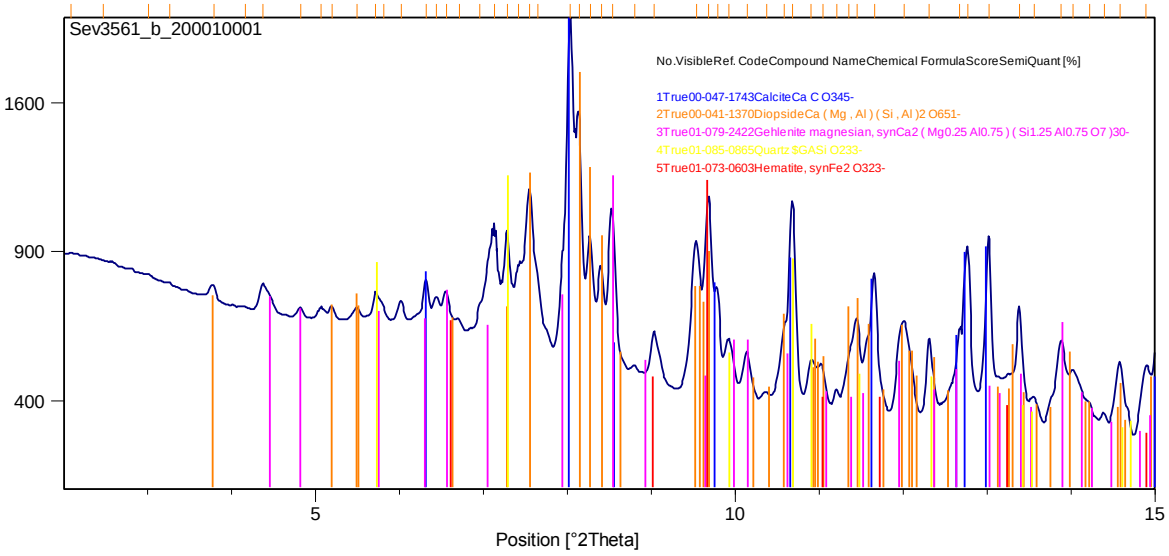

Glaze

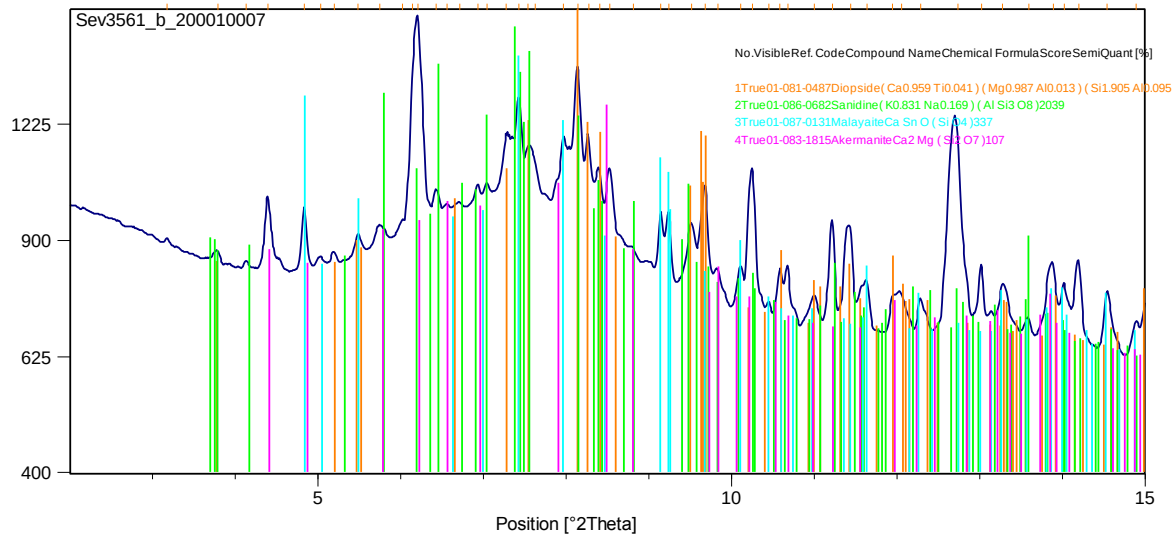

PNS 16 – green

Ceramic body

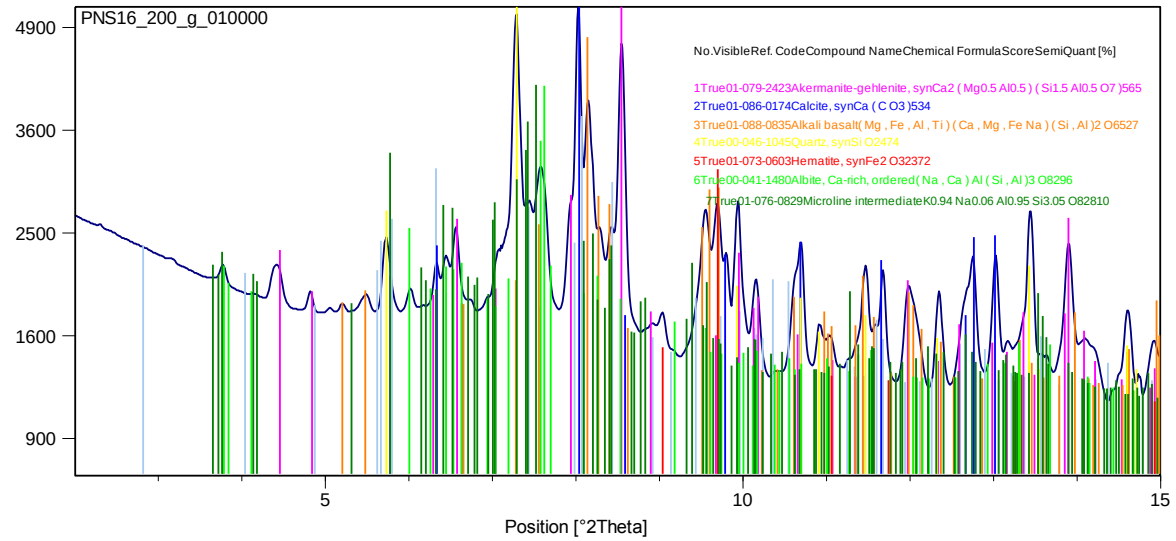

Interface

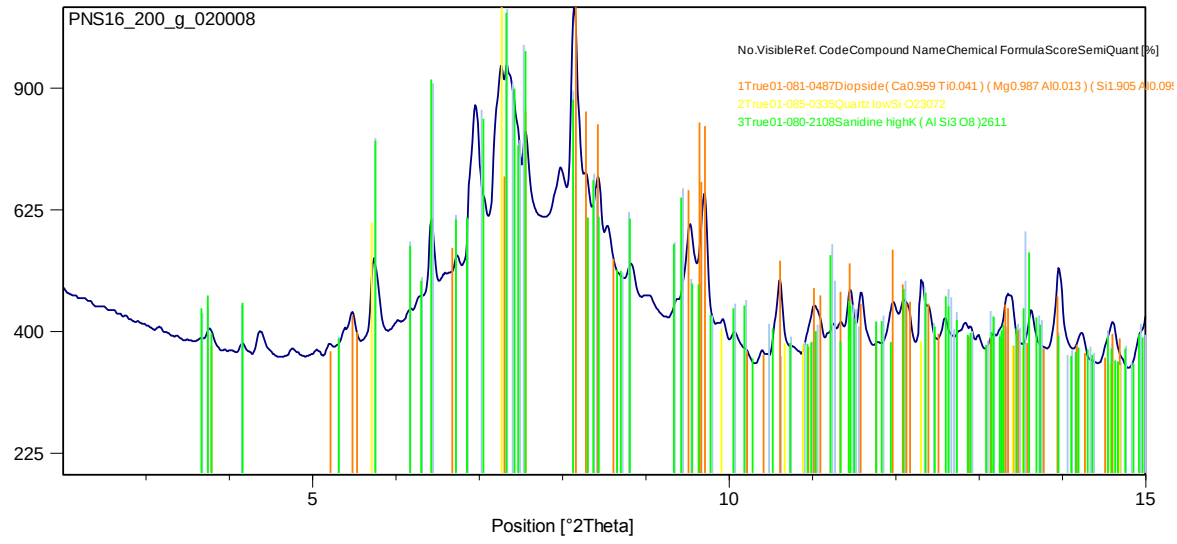

APPENDIX X
UNDERGLAZE DECORATION TESTS

INTRODUCTION

During the course of the Az-Med Project, an experiment was performed to test the diffusion of three pigments through the tin-opacified glaze – cobalt blue, manganese brown and copper green – with different variables. This experiment took as a starting point the observations and analyses of the underglaze-decorated Valencian tiles and the PNS 30 sample.

Contrarily to what was observed regarding the cobalt and the manganese pigments, the green glaze of sample PNS30 did not show any particular concentration of copper immediately above the glaze-ceramic interface. Therefore, there is no clear evidence of a green underglaze decoration, so one of the aims of this experiment was to test the behavior of the copper green pigment when applied underglaze.

This report states the results obtained so far, taking into account that this is a work in progress and an analytical study is still to be made. The experimental work was performed by Francisca Pulido Valente, under the supervision of Susana Coentro and Solange Muralha.

EXPERIMENTAL PROCEDURE

Three experimental samples were prepared for each colour, with the pigment being applied in different stages of the process, as indicated in *Table X.1*.

Cobalt oxide (CoO), manganese oxide (MnO), copper oxide (CuO) and iron oxide (Fe_2O_3) were used as pigments. A calcareous commercial clay (©Barracha) was used for the ceramic body. The white glaze was applied as a frit, which was previously prepared from a recipe similar to the analytical results obtained from the historical glazes (*Table X.2*).

Biscuit-firing took place at 800 °C and the final firing at 1000 °C. The firing cycles are represented in *Figure X.1*.

Table X.1. Experimental design for the three different procedures (A, B and C) used for each pigment.

	Raw clay	Painting	Biscuit firing (800 °C)	Painting	Glazing (frit)	Final firing (1000 °C)
A	●	●	● →		●	●
B	● →		●	●	●	●
C	●	● →			●	●

Table X.2. White glaze recipe presented as oxides in wt.%.

	SiO_2	PbO	SnO_2	Na_2O	K_2O
wt.%	45	45	5	3	2

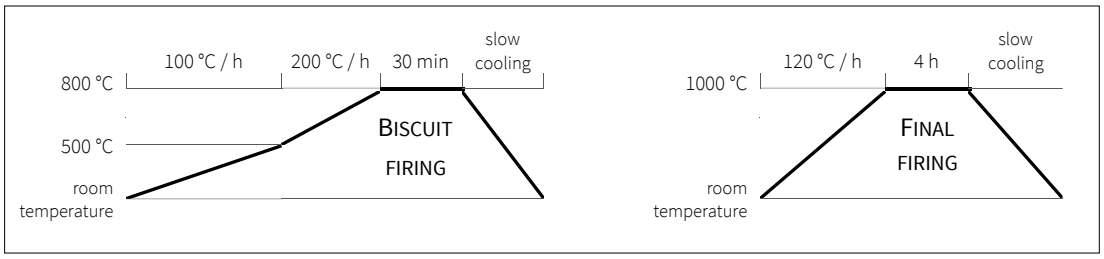

Figure X.1. Firing cycles for the biscuit firing and the final one.

PRELIMINARY RESULTS

This experience has shown that all the used pigments diffuse through the glaze up to its surface, regardless of the number of firings or the methodology employed (*Figure X.2*). Cobalt and manganese showed the most successful results, considering the homogeneity of the final colour. The iron oxide did not always diffuse homogeneously, and the copper oxide shows a considerable spreading of the green colour. No remarkable differences were observed among the different methodologies.

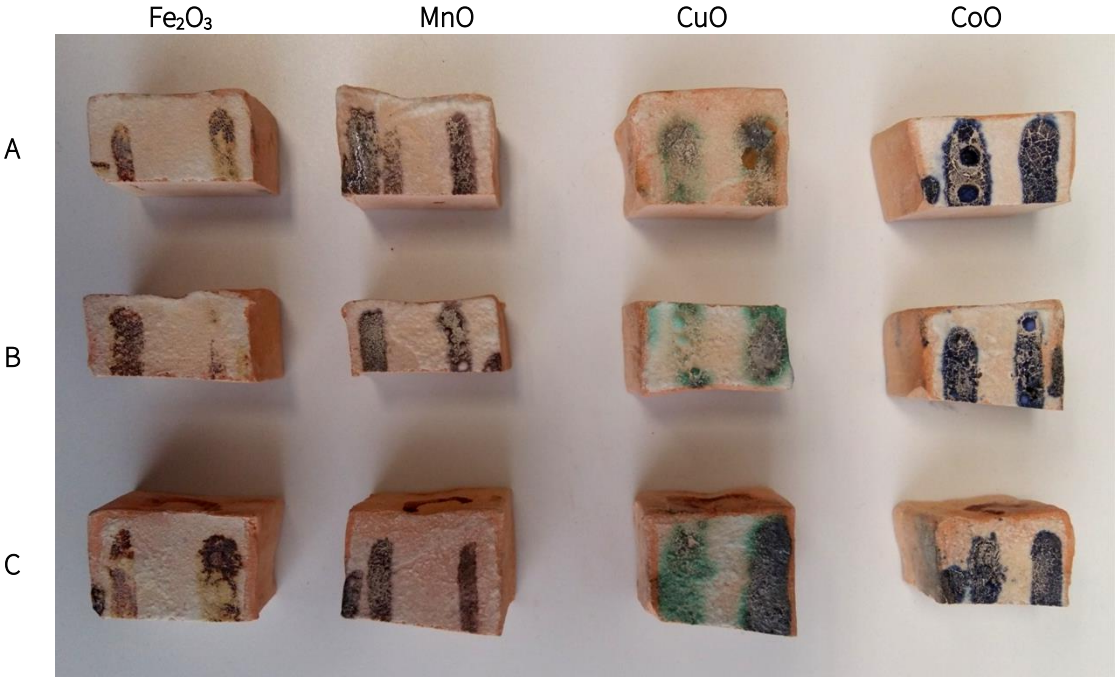

Figure X.2. Samples from the first test. The letters A, B and C correspond to the procedures illustrated in *Table XI.1*.

However, the glaze resulted in a very thin layer. Another test was performed with a larger amount of glaze frit to assess the diffusion of the pigment – this time only with cobalt blue – through a thicker glaze. Again, the three methodologies (A, B and C) resulted in clear blue lines on the glaze surface, without remarkable differences among them (*Figure X.3*).

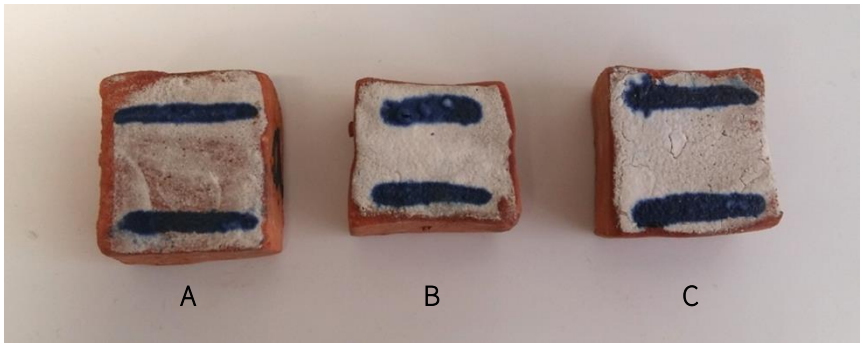

Figure X.3. Samples from the second test with a thicker glaze. The letters A, B and C correspond to the procedures illustrated in *Table XI.1*.

FUTURE WORK

The experimental process is being optimized to achieve a result similar to the original historic tiles in what regards glaze thickness and shine. More tests must be performed to assess the behaviour of the four colours (cobalt blue, copper green, iron amber and manganese brown) in both homogenous fritted glazes and inclusions-containing ones.

The chemical analysis of cross-sections of the samples will take place to map the diffusion of the pigment up to the glaze surface, as well as to identify – if applicable – colour-related compounds that form above the glaze-ceramic body interface.